Universitätsklinikum Hamburg-Eppendorf
Universitäres Herzzentrum
Abteilung für Herz- und Gefäßchirurgie

Immunmodulation von pluripotenten Stammzellen für die Regenerative Medizin

Kumulative Dissertation

zur Erlangung des Doktorgrades der
Naturwissenschaften (Dr. rer. nat.) an der Fakultät für
Mathematik, Informatik und Naturwissenschaften der
Universität Hamburg

vorgelegt von
Xiaomeng Hu

Hamburg 2020

1. Gutachterin: Prof. Dr. Sonja Schrepfer

2. Gutachter: Prof. Dr. Friedrich Koch-Nolte

Tag der Disputation: 9. Dezember 2020

Diese Doktorarbeit wurde von März 2014 bis Oktober 2019 am Institut für Herz- und Gefäßchirurgie (Institutsdirektor: Prof. Dr. Dr. Hermann Reichenspurner) unter der Leitung von Prof. Dr. Sonja Schrepfer erarbeitet.

Inhaltsverzeichnis

Inhaltsverzeichnis…………………………………………………………………… 1

Abkürzungsverzeichnis……………………………………………………………. 3

Abbildungsverzeichnis…………………………………………………………….. 6

Zusammenfassung…………………………………………………………………. 7

Abstract………………………………………………………………………………. 8

1. Einleitung…………………………………………………………………………… 9

1.1. Stammzellen als Zelltherapie………………………………………………… 9

1.1.1. Embryonale Stammzellen (ES-Zellen)……………………………… 9

1.1.2. Somatischer Zellkerntransfer (SCNT)……………………………….. 10

1.1.3. Induzierte pluripotente Stammzellen (iPS-Zellen)……………….... 10

1.2. Das Immunsystem…………………………………………………………….. 12

1.2.1. Major Histocompatibility Complex (MHC)…………………………… 13

1.2.2. Minor Histokompatibilitätsantigene (miHA)………………………… 15

1.2.3. Fetomaternale Toleranz……………………………………………..... 15

1.3. Genmodifizierung……………………………………………………………… 18

1.3.1. Lentivirale Überexpression………………………………………….... 18

1.3.2. Engineering mit der CRIPSR/Cas9 Technologie…………………… 18

1.4. Mitochondrien………………………………………………………………….. 21

1.5. Zielsetzung……………………………………………………………………… 24

2. Publikationen……………………………………………………………………….. 25

2.1 Hypoimmunogenic derivatives of induced pluripotent stem cells evade immune rejection in fully immunocompetent allogeneic recipients………. 25

2.2 De novo mutations in mitochondrial DNA of iPSCs produce immunogenic neoepitopes in mice and humans……………………………. 60

3. Diskussion………………………………………………………………………….. 92

3.1. Die Immunogenität von iPS-Zellen…………………………………………... 93

3.2. Die hypoimmunogene Stammzelle……………………………………….. 96

3.3. Risiken und Nebenwirkungen……………………………………………... 99

3.4. Strategien zur Generierung von hypoimmunogenen Zellen……………….. 101
    3.4.1. Modifizierung von MHC I……………………………………………. 101
    3.4.2. Modifizierung von MHC II…………………………………………… 103
    3.4.3. Weitere Strategien…………………………………………………… 104
3.5. Ausblick…………………………………………………………………….. 106

4. Referenz……………………………………………………………………… 107

Autorenschaft Beitrag……………………………………………………….. 117
Lebenslauf…………………………………………………………………….. 119
Eidesstattliche Erklärung…………………………………………………… 123
Danksagung…………………………………………………………………… 124

Abkürzungsverzeichnis

AP1903	Rimiducid
AP20187	B/B Homodimerizer ($C_{82}H_{107}N_5O_{20}$)
ATP	Adenosintriphosphat
B2M/B2m	Beta-2 microglobulin
BALB/c	Bagg albino mice
C	Zelsius
C57BL/6	C57 black 6 mice
Cas9	CRISPR-assoziiertes Protein 9
CIITA/Ciita	Class II Major Histocompatibility Complex Transactivator
CCL21/Ccl21	CC-chemokine ligand 21
CCL22	CC-chemokine ligand 22
CD/Cd	cluster of differentiation
CEA	Carcinoembryonic antigen
c-Myc	cellular Myelocytomatosis
CO_2	Kohlenstoffdioxid
CRISPR	Clustered Regularly Interspaced Short Palindromic Repeats
crRNA	CRISPR-RNA
CTLA4	cytotoxic T-lymphocyte-associated protein 4
DNA	Desoxyribonukleinsäure
ESC	Embryonale Stammzellen
FASL	Fas ligand
GFP	Grün fluoreszierendes Protein
GvH	Graft-Versus-Host
GvL	Graft-versus-Leukemia
H2-M3	Histocompatibility 2, M region locus 3
HDR	homology-directed repair
hiPSCs	humane induziert pluripotente Stammzelle
HLA	Humane Leukozytenantigen
HSCT	hämatopoetischer Stammzellen
iCasp9	induzierbaren Caspase 9
IDO	Indoleamine-2,3-dioxygenase

ILT2	Ig-Like Transcript 2
iPSC	induziert pluripotente Stammzellen
IgM	Immunoglobulin M
kb	Kilobasen
Klf4	Krüppel-like factor 4
KIR2DL4	Killer cell immunoglobulin-like receptor two Ig domains and long cytoplasmic tail 4
KO	Knockout
Lin28	cell lineage abnormal 28
Mfge8	Milk fat globule-EGF factor 8 protein
MHC	Haupthistokompatibilitätskomplex
miHA	Nebenhistokompatibilitätskomplex
miPSC	murine induziert pluripotente Stammzellen
mRNA	Boten-RNA (engl. Messenger RNA)
mtDNA	mitochondrielle DANN
Nanog	Homöoboxprotein, Ableitung von Tír na nÓg
NHEJ	Non-homologous end joining
NKG2A	NK group 2 member A
NK-Zellen	Natürliche Killerzellen
Oct4	Oktamer-bindender Transkriptionsfaktor
PAM	protospacer adjacent motif
PDL1/ Pdl1	programmed cell death ligand 1
PSC	pluripotente Stammzellen
RFX5	Regulatory Factor X5
RFXANK	Regulatory Factor X Associated Ankyrin Containing Protein
RFXAP	Regulatory Factor X Associated Protein
RNA	Ribonukleinsäure
ROS	reaktive Sauerstoffspezies
SCNT	Somatischer Zellkerntransfer (engl. somatic cell nuclear transfer)
SERPINB9	Serpin Family B Member 9
SIRPa	Signal regulatory protein alpha
SNP	Einzelnukleotid-Polymorphismus (engl. Single nucleotide polymorphismus)

Sox2	geschlechtsbestimmende Region Y- Box 2 (engl. sex determining region Y (SRY)- box 2)
S-Phase	Synthesephase
Spi6	Serine protease inhibitor 6
TALEN	TAL-Effektor-Nukleasen
TAP2	Transporter 2, ATP Binding Cassette Subfamily B Member
Tg	transgene
TGFβ	transforming growth factor beta
Th-1	Type 1 helper T-cells
Th-2	Type 2 helper T-cells
tracrRNA	Trans-activating crRNA
Tregs	regulatorische T-Zellen
WT	Wildtyp
ZFN	Zinkfinger Nukleasen

Abbildungsverzeichnis

Abbildung 1.1 Die schematische Struktur von MHC Klasse I und Klasse II Molekülen………………………………………………………… 14
Abbildung 1.2 Das Cas9-Protein…………………………………………………. 19
Abbildung 1.3 Nuklease induzierte Reparaturmechanismen von DNA-Doppelstrangbrüchen…………………………………………….. 20
Abbildung 1.4 Die humane mtDNA……………………………………………. 21
Abbildung 3.1 Die Immunaktivierung durch Immunzellen einer unmodifizierten iPSC versus der hypoimmunogenen iPSC…………. 97
Abbildung 3.2 Mechanismen zur Unterdrückung der Immunaktivierung….. 105

Zusammenfassung

Pluripotente Stammzellen besitzen die Fähigkeit, sich in alle Zellarten zu differenzieren, und ermöglichen somit auf neue Art und Weise humane Krankheiten zu behandeln. Während die Anwendung von embryonalen Stammzellen (ESCs) ethische Fragen aufwirft, bieten induzierte pluripotente Stammzellen (iPSCs) die Chance und neue Einblicke auf die Herstellung autologer Zellprodukte. Diese sind genetisch identisch zur Ausgangszelle und verhindern somit eine mögliche Abstoßung der Zellimplantate. Die Generierung Patienten-spezifischer iPSCs ist jedoch mit hohen Kosten verbunden und für akute Krankheiten, wie nach einem Myokardinfarkt, nicht anwendbar. In unserer Arbeit haben wir mittels Maus und humanen iPSCs untersucht wie anfällig die Zellen durch Re-Programmierung und Differenzierung für mitochondriale Mutationen sind. Alle untersuchte Zellinien haben mitochondriale Mutationen entwickelt, die in vivo in einigen Transplantationsmodellen zur Abstoßung geführt haben.

Unser Ziel ist es iPSCs so zu modulieren, dass sie als hypoimmunogene Stammzellen für eine universelle Transplantation (allogen) ohne die zusätzliche Gabe von Immunsuppressiva, anwendbar sind. Dafür wurden zunächst bei murinen iPSCs einer C57BL/6 Maus die Oberflächenmoleküle B2m und Ciita durch die CRISPR-Cas9 Technologie ausgeknockt und Cd47 lentiviral überexprimiert. Sowohl bei *in vivo* als auch *in vitro* Experimenten zeigten die transplantierten Zellen ein 100%iges Überleben im allogenen Setting. Basierend auf diesen Ergebnissen wurden dieselben Verfahren mit den gleichen Modulierungen in humanen iPSCs durchgeführt. Modifizierte humane iPSCs zeigten *in vivo*, im humanisierten Mausmodell, ein Langzeitüberleben ohne Abstoßung der transplantierten Zellen. Da undifferenzierte Stammzellen das Potential einer Teratombildung besitzen, werden für klinische Anwendungen die gewünschten Zelltypen vor der Transplantation *ex vivo* generiert. So wurden murine und humane hypoimmunogene iPSCs erfolgreich in Zellen der mesodermalen Linie (Herzmuskelzellen, Endothelzellen, und glatten Muskelzellen) differenziert und transplantiert, und zeigten ebenfalls ein 100%iges Überleben im allogenen Modell. Diese Arbeit liefert Ergebnisse für die Generierung einer hypoimmunogenen Zelllinie und bietet somit eine Grundlage für ihre möglichen Anwendungen in der klinischen Stammzelltherapie.

Abstract

Pluripotent stem cells have the ability to differentiate into all cell types and thus enable a new strategy of treating human diseases. While the use of embryonic stem cells (ESCs) still raises ethical questions, induced pluripotent stem cells (iPSCs) offer the opportunity to produce autologous cell products. These are genetically identical to the donor and not affected by possible rejections after transplantation. The generation of patient-specific iPSCs is, however, associated with high costs and cannot be used for acute diseases, such as after a myocardial infarction. Furthermore, iPSCs were thought to be beneficial and suitable for autologous transplantation; however, our work demonstrated that iPSCs have a high likelihood to develop mitochondrial mutations which can lead to rejection of the cells even when transplanted autologous.

We then aimed to modulate iPSCs to become hypoimmunogenic to make them suitable for universal transplantations without the additional administration of immunosuppressive drugs. For this purpose, mouse iPSCs with a C57BL/6 background underwent knockout of the surface molecules B2m and Ciita using the CRISPR-Cas9 technology and transduced lentivirally to overexpress Cd47. Both *in vivo* and *in vitro* experiments showed 100% survival of the modulated cells in an allogeneic setting. Based on these results, the same methods and modulations were used to create human hypoimmune iPSCs, which also showed complete long-term survival *in vivo* in the humanized mouse model. Since undifferentiated stem cells have the potential to form teratoma, differentiated cells were generated for clinical applications. Mouse and human hypoimmunogenic iPSCs were successfully differentiated into the mesodermal lineage (cardiac, endothelial and smooth muscle cells) and transplanted into allogeneic models. All cells showed 100% survival. This work provides results for the generation of a hypoimmunogenic cell line and advances a foundation for its applications in clinical stem cell therapy.

1. Einleitung

1.1. Stammzellen als Zelltherapie

Das größte Problem bei Organtransplantationen ist der Mangel an Spenderorganen (Patel and Abt, 2019). Eine mögliche Alternative zur Organtransplantation bietet die Stammzelltherapie. Das Ziel ist dabei, das geschädigte Gewebe zu reparieren oder zu ersetzen. Es werden also differenzierte Zellprodukte aus Stammzellen benötigt, die für eine Zelltherapie bereitstehen. Dennoch sind sich Wissenschaftler weltweit noch nicht einig, wie Stammzellen für klinische Anwendungen eingesetzt werden können. Adulte Stammzellen sind multipotent und können sich somit nur in Zellen innerhalb ihrer eigenen Keimbahn differenzieren. Die Behandlung von Herzerkrankungen mit Stammzellen aus dem Knochenmark zeigte nahezu keinerlei Effekt nach einem akuten Herzinfarkt oder bei der chronischen Kardiomyopathie (van der Bogt et al., 2009). Vielversprechender sind pluripotente Stammzellen: Sie sind in der Lage sich in alle Zelltypen zu differenzieren und können somit in der Stammzelltherapie im großem Spektrum eingesetzt werden. Die Differenzierung kann *ex vivo* erfolgen, so dass das Verfahren überwacht werden kann und nur die gewünschte Zellpopulation eingesetzt wird. Undifferenzierte Stammzellen sollten aufgrund ihres Potenzials der Teratombildung vermieden werden (Doss and Sachinidis, 2019).

1.1.1. Embryonale Stammzellen (ES-Zellen)

Im Jahr 1981 wurde zum ersten Mal die Isolierung und *in vitro* Kultivierung von murinen ES-Zellen beschrieben (Evans and Kaufman, 1981; Martin, 1981) und später im Jahr 1998 auch von humanen ES-Zellen (Thomson et al., 1998). Embryonale Stammzellen werden aus dem Embryoblast, ein frühes Stadium einer befruchteten Eizelle, gewonnen. Diese Zellen sind pluripotent und besitzen die Fähigkeit, sich in Zellen der drei Keimblätter Ektoderm, Mesoderm und Endoderm zu differenzieren. Obwohl die Idee der Stammzelltherapie bereits mit der Beschreibung der ersten humanen embryonalen Stammzellen beschrieben wurde ist die Generierung dieser Zellen mit ethischen Bedenken verknüpft und streng kontrolliert. Dennoch werden embryonale

Stammzellen in der Forschung eingesetzt, um ihr Potenzial in der Stammzelltherapie zu untersuchen.

Anfänglich wurde vermutet, dass ES-Zellen immunprivilegiert seien, weil sie eine sehr niedrige Expression an MHC I aufweisen (Drukker et al., 2002). Dies wurde jedoch schnell widerlegt, da die ES-Zellen nach *in vivo* Transplantationen abgestoßen wurden. Außerdem wurde die Geschwindigkeit der Abstoßung nach wiederholter Transplantation schneller, was auf eine Aktivierung des adaptiven Immunsystems hindeutet (Deuse et al., 2011). Obwohl die MHC Oberflächenmoleküle nur niedrig exprimiert sind, scheinen sie auszureichen, um das Immunsystem zu aktivieren und eine Abstoßungsreaktion auszulösen.

1.1.2. Somatischer Zellkerntransfer (SCNT)

Um Abstoßungsreaktionen zu vermeiden, wurde die Generierung von autologen ES-Zellen in Betracht gezogen. Bei dem somatischen Zellkerntransfer (engl. somatic cell nuclear transfer; SCNT) wird ein Zellkern in eine kernlose ES-Zelle transferiert. Die daraus resultierende pluripotente Stammzelle beinhaltet die identische genetische Information wie der Zellkernspender. Diese Methode wurde zuerst in der Maus etabliert und später im Jahr 2013 wurde die erste humane SCNT generiert (Tachibana et al., 2013). Dennoch beinhalten SCNT-Zellen allogene mtDNA aus der Oozyte, die eine Abstoßungsreaktion durch die Minor Histokompatibilitätsantigene (miHA) auslösen kann (Deuse et al., 2015). Somit bleibt ein Risiko vorhanden, dass aus SCNT differenzierte Zelltransplantate abgestoßen werden.

1.1.3. Induzierte pluripotente Stammzellen (iPS-Zellen)

Induzierte pluripotente Stammzellen (iPS-Zellen) wurden zum ersten Mal im Jahr 2006 von Yamanaka und seinem Team beschrieben (Takahashi et al., 2007). Somatische Zellen, wie zum Beispiel Fibroblasten, werden durch eine *in vitro* Reprogrammierung durch die Expression von einer Kombination aus spezifischen Transkriptionsfaktoren (Oct4, Sox2, c-Myc, Klf4, Nanog und Lin28) wieder pluripotent (Aasen et al., 2008;

Takahashi et al., 2007; Yu et al., 2007). Der größte Vorteil hierbei ist die Generierung von patientenspezifischen iPS-Zellen, die genetisch identisch zur Ausgangszelle sind und somit nicht vom syngenen Empfänger abgestoßen werden.

iPS-Zellen ähneln embryonalen Stammzellen in vielen Eigenschaften, jedoch ist bis heute umstritten, ob sie sich identisch verhalten (Yu and Thomson, 2008). Viele Studien beschreiben jedoch eine Abstoßung von iPS-Zellen nach einer syngenen Transplantation (Zhao et al., 2011). Zudem ist die Generierung patienten-spezifischer iPS-Zellen sehr kostspielig. Eine Garantie für die erfolgreiche Reprogrammierung ist nicht gewährleistet und die Qualität der Zellen ist stark vom Alter des Patienten abhängig (Medvedev et al., 2010). Für die Generierung, Validierung, Differenzierung und Purifizierung der Zellen wird viel Zeit benötigt, wodurch ihr Einsatz bei akuten Erkrankungen, wie z.B. nach einem Myokardinfarkt, nicht möglich ist.

1.2. Das Immunsystem

Das Immunsystem stellt einen komplexen Abwehrmechanismus dar, der den eigenen Organismus vor körperfremden Substanzen und Pathogenen schützt. Außerdem ist es in der Lage, körpereigene Zellen zu erkennen und fehlerhafte auszusortieren.

Es kann grundsätzlich zwischen zwei verschiedenen Mechanismen der Immunabwehr unterschieden werden: der angeborenen und der adaptiven Immunabwehr, welche stets zusammenarbeiten und sich gegenseitig ergänzen (Borghans et al., 1999). Die angeborene Immunabwehr ist unspezifisch. Die Grundlage dafür bilden die Phagozyten, wie Makrophagen und Granulozyten, welche in der Lage sind, körperfremde Substanzen unspezifisch zu erkennen und sie durch Phagozytose zu eliminieren. Desweiteren sind NK-Zellen ebenfalls in der Lage, abnormale Zellen zu erkennen und sie gezielt abzutöten. Dagegen ist die adaptive Immunabwehr von hoher Spezifität gezeichnet und entwickelt sich im Laufe der Jahre. Sie ist in der Lage, ein immunologisches Gedächtnis auszubilden, indem die Antigene körperfremder Strukturen erkannt werden und gezielt zelluläre Abwehrmechanismen gegen sie aktiviert und Antikörper gebildet werden. Dabei spielen die T- und B-Lymphozyten eine große Rolle, wobei die T-Lymphozyten die Grundlage für die zellvermittelte Immunantwort bilden, während die B-Lymphozyten für die humorale Immunantwort verantwortlich sind. Beide Zellarten besitzen Rezeptoren auf ihrer Zelloberfläche, welche hochspezifisch Antigene erkennen und entsprechend auf diese reagieren können.

Nach einer primären spezifischen Immunantwort treten einige Lymphozyten in einen rezirkulierenden Status über und bleiben als Gedächtniszellen im Organismus erhalten. Bei einem erneuten Kontakt mit demselben Antigen kann die Immunreaktion viel schneller und effektiver ablaufen, was auch als Booster-Effekt beschrieben wird (Mackay et al., 1990).

Die Bildung und Reifung von B- und T-Lymphozyten finden in den primären lymphatischen Organen statt; dazu gehören der Thymus und das Knochenmark. Die Lymphozyten wandern daraufhin in die sekundären lymphatischen Organe, wo der

Antigenkontakt und die klonale Vermehrung stattfinden. Zu den sekundären lymphatischen Organen gehören die Milz oder auch die Lymphknoten.

1.2.1. Haupthistokompatibilitätskomplex (MHC)

Der Haupthistokompatibilitätskomplex (MHC von engl. Major Histocompatibility Complex) umfasst eine Reihe von Genen, die für Zelloberflächenproteine codieren, welche für die Immunerkennung bei allen Wirbeltieren auftreten. Die exprimierten Antigene werden vom körpereigenen Immunsystem als zugehörig erkannt und sind somit vom Immunsystem geschützt. Die MHCs gehören zur Immunglobulin-Superfamilie.

Die MHC-Proteinkomplexe können in die Klassen I und II unterteilt werden (Kelley et al., 2005) MHC-Proteinkomplexe der Klasse I werden auf der Oberfläche nahezu aller kernhaltigen Zellen exprimiert und haben die Aufgabe der Präsentation von intrazellulären Antigenen für zytotoxische T-Zellen. Zudem dienen sie zur Selbstmarkierung körpereigener Zellen, um sie vor einer Zerstörung durch zytotoxische Zellen, wie NK-Zellen, zu schützen (Karre, 2002). Die Struktur von MHC Klasse I Molekülen besteht aus einer schweren, polymorphen α-Kette mit drei Immunglobulin-ähnlichen Abschnitten, unterteilt in die Domänen $\alpha1$, $\alpha2$ und $\alpha3$, und einer monomorphen $\beta2$-Mikroglobulin Domäne. MHC-Proteinmoleküle der Klasse II findet man auf B-Zellen und anderen antigenpräsentierenden Zellen (APC). Sie haben die Funktion, extrazelluläre Antigene den T-Helferzellen zu präsentieren und somit eine zelluläre oder humorale Immunantwort zu induzieren (Muhlethaler-Mottet et al., 1997). Sie bestehen aus einer polymorphen α-Kette und einer polymorphen β-Kette mit jeweils zwei extrazellulären Domänen.

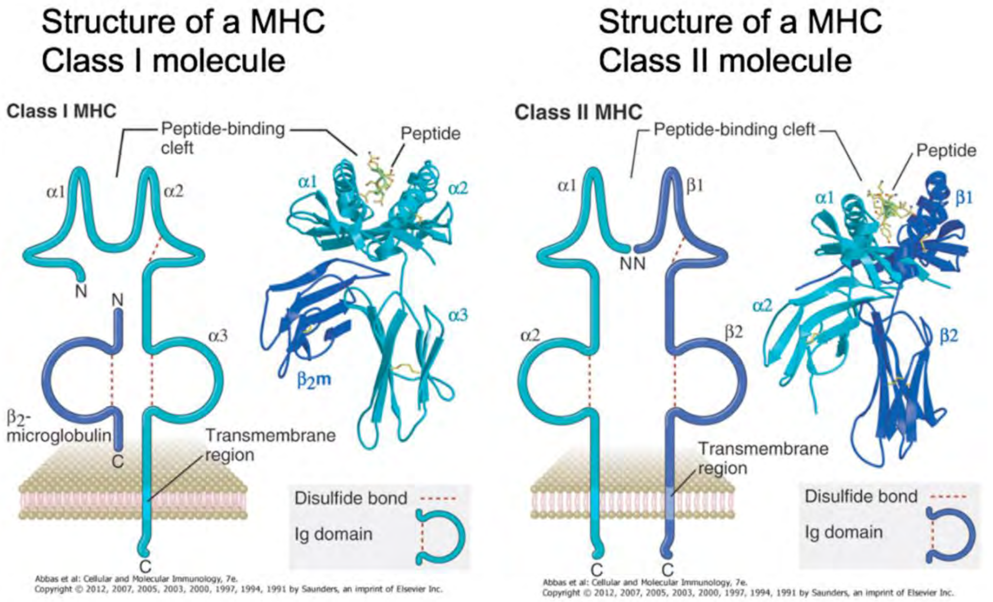
Structure of a MHC Class I molecule

Structure of a MHC Class II molecule

Class I MHC
Peptide-binding cleft
Peptide
α1
α2
N
N
α3
β2m
β2-microglobulin
C
Transmembrane region
C
Disulfide bond
Ig domain
Class II MHC
Peptide-binding cleft
Peptide
α1
β1
NN
α2
β2
Transmembrane region
C
C
Disulfide bond
Ig domain

Abbas et al: Cellular and Molecular Immunology, 7e.
Copyright © 2012, 2007, 2005, 2003, 2000, 1997, 1994, 1991 by Saunders, an imprint of Elsevier Inc.

Abbildung 1.1: Die schematische Struktur von MHC Klasse I und Klasse II Molekülen. Links: MHC Klasse I Molekül, bestehend aus einer polymorphen α-Kette mit drei Immunglobulin-ähnlichen Abschnitten und einer monomorphen β2-Mikroglobulin Domäne. Rechts MHC Klasse II Molekül, bestehend aus einer polymorphen α-Kette und einer polymorphen β-Kette mit jeweils zwei extrazellulären Domänen (Abbas et al., 2012).

Bei der Maus werden MHC-Proteinkomplexe als H-2-Complex bezeichnet und werden von Genen des Haupthistokompatibilitätskomplexes, die auf dem Chromosom 17 lokalisiert sind, codiert. Beim Menschen werden sie als HLA-System (HLA von engl. Human Leucocyte Antigen) bezeichnet und ihre Gene sind auf dem p-Arm des Chromosoms 6 lokalisiert und enthalten zahlreiche eng gekoppelte Genloci mit multiple Anllelen. Ein extremer genetischer Polymorphismus führt zu einer großen Anzahl verschiedener HLA-Phänotypen. Dabei werden bei HLA-I die Isotypen HLA-A, HLA-B und HLA-C und bei HLA-II die Isotypen HLA-DR, HLA-DQ und HLA-DP unterschieden. Die Domäne β2-Mikroglobulin wird als einziges auf dem Chromosom 15 codiert und ist monomorph.

In der Transplantationsmedizin tragen die HLAs erheblich zur Abstoßung des Transplantates bei. Die fremden HLA-Antigene werden von körpereigenen Lymphozyten erkannt und als Folge wird im Körper des Empfängers eine Alloreaktion ausgelöst, welche die akute Abstoßung darstellt (Murphy et al., 2012; Sijpkens et al., 1999). Außerdem kann es zur Bildung von präformierten Antikörpern beim Empfänger gegen die HLA-Antigene der Spender durch Bluttransfusionen, Schwangerschaften oder vorherige Transplantationen kommen (Terasaki, 2003). Dies kann durch ein HLA-Crossmatch vor der Transplantation bestimmt werden. Vorsensibilisierte Patienten mit HLA-Antikörper der Klasse I und II gegen die Antigene der Spender zeigen ein erhöhtes Risiko für Transplantatrejektion (Susal et al., 2009).

1.2.2. Minor Histokompatibilitätsantigene (miHA)

Die Transplantatabstoßung durch die Minor Histokompatibilitätsantigene (miHA) wurde bereits vor 60 Jahren zum ersten Mal beschrieben. Damals wurde eine Abstoßung allogener Hauttransplantate zwischen MHC-identen Mäusen festgestellt (Snell, 1948). In der Transplantation ist sie häufig die Ursache für Graft-Versus-Host (GvH) oder Graft-versus-Leukemia (GvL) Reaktionen, die in bis zu 40% der Fälle nach einer allogenen Transplantation von hämatopoetischer Stammzellen (HSCT) auftreten, trotz HLA-Übereinstimmung mit dem Spender (Bortin et al., 1991). Nach einer T-Zell-Depletion wurde das GvH-Risiko nach einer Transplantation signifikant reduziert (Hale et al., 1988). Die erhöhte Inzidenz von GvH und GvL Reaktionen konnte somit mit T-Zellen in Zusammenhang gebracht werden. Ein Drittel aller beschriebenen miHA sind auf das H-Y Antigen zurückzuführen (Hirayama et al., 2012), welches auf dem Y-Chromosom codiert ist und dementsprechend nur beim männlichen Geschlecht auftritt.

Als miHA werden kurze prozessierte Peptidsequenzen bezeichnet, die in der Antigenbindungsfurche eines passenden MHC Klasse I Moleküls gebunden und in der Lage sind, eine alloreaktive T-Zell Reaktion auszulösen. Die Generierung der miHA erfolgt durch die polymorphen Regionen und ist unabhängig von den MHC-Merkmalen.

1.2.3. Fetomaternale Toleranz

Als Immuntoleranz werden Vorgänge beschrieben, die zur Vermeidung einer Immunreaktion gegen ein fremdes Antigen führen. Ein Beispiel aus der Natur bietet die fetomaternale Toleranz: Während der Schwangerschaft generiert der Fetus, dessen genetisches Material aus einer Kombination der maternalen und paternalen

DNA besteht, eine immunotolerante Umgebung, welche ihn vor dem maternalen Immunsystem schützt (Guleria and Sayegh, 2007). Einige Mechanismen davon sind bereits gut erforscht (Arck and Hecher, 2013). Oft sind jedoch die individuellen Rollen von einzelnen Enzymen und Molekülen noch unklar.

Die Syncytiotrophoblasten, welche das Interface zwischen dem maternalen Blutsystem und fetalem Gewebe bilden (Vento-Tormo et al., 2018), weisen eine sehr niedrige Expression von MHC-I und MHC-II Oberflächenmolekülen auf. MHC-I und MHC-II spielen die größte Rolle bei der Erkennung von Fremdantigenen. In mehreren Studien wurde beobachtet, dass eine verminderte MHC-I Expression zu einer stark verminderten Aktivierung von zytotoxischen T-Zellen beiträgt. Durch das Fehlen von MHC-II ist die Antigenpräsentation und somit die Aktivierung der CD4+ T-Zellen nicht mehr möglich (Clark et al., 2010; Guleria and Sayegh, 2007; Rapacz-Leonard et al., 2014).

Studien belegen zudem, dass eine Schwangerschaft mit einer erhöhten Frequenz von regulatorischen $CD25^{hi}CD4^{+}$T-Zellen (Tregs) einhergeht und die Zellen somit eine wichtige Rolle in der fetomaternalen Toleranz einnehmen (Aluvihare et al., 2004). Das Fehlen von Tregs kann im Mausmodell in einer Fehlgeburt enden und führt zur Akkumulation von Th-1 Zellen in der Dezidua, die gegen die paternalen Antigene gerichtet sind (Zenclussen et al., 2005).

Das Enzym Indoleamine-2,3-dioxygenase (IDO) spaltet Tryptophan, eine essenzielle Aminosäure, welche für die T-Zell Proliferation benötigt wird, in N-formyl-L-kynurenine. Dieses Protein wird während der Schwangerschaft hochreguliert und scheint durch den beschriebenen Mechanismus die T-Zellproliferation der Mutter zu verhindern, indem Tryptophan aus der Serotonin-Synthese entzogen wird. Die Inhibierung von IDO in dem ersten Trimester der Schwangerschaft bei der Maus führte zu einer T-Zell basierten Abstoßung der Feten durch die maternalen T-Zellen (Spinelli et al., 2019).

Die Syncytiotrophoblasten zeigen zudem eine hohe Expression von HLA-G und HLA-E, welche eine immunregulatorische Funktion haben, durch ihre Bindung zu den zytotoxischen T-Zellen und NK-Zellen. Zusätzliche Moleküle, wie CCL22 oder CEA scheinen lokal regulatorische T-Zellen anzuziehen, um die Aktivierung des Immunsystems zu unterdrücken (Finkenzeller et al., 2000; Guleria and Sayegh, 2007).

Außerdem zeigen Syncytiotrophoblasten eine Überexpression des immunregulatorischen Proteins CD47, welches als „don’t-eat-me“ Signal bekannt ist und den Fetus vor dem maternalen Immunsystem schützt (Mawby et al., 1994). Dabei bindet CD47 an seinen Ligand SIRPa, der vor allem auf Makrophagen exprimiert ist, um den Vorgang der Phagozytose zu unterdrücken.

1.3. Genmodifizierung

Als Genmodifizierung werden Methoden und Verfahren bezeichnet, die gezielte Eingriffe in das Erbgut und somit auch auf die biochemischen Steuervorgänge von Lebewesen ermöglichen. Dies umfasst Techniken von viralen Vektoren als Transportvehikel, die zusätzliche Gene in das Genom einschleusen, bis hin zu der CRISPR/Cas9 Technologie, die aufgrund ihrer einfachen Anwendung und Effizienz viele Aspekte der Genmodifizierung revolutioniert hat. Andere Methoden wie die Zinkfinger Nukleasen (ZFN) und TAL-Effektor-Nukleasen (TALEN) sind in ihrer Konstruktion und Herstellung sehr aufwendig und wurden inzwischen fast komplett durch die CRIPSR/Cas9 Technologie ersetzt (Boch, 2011; Kim et al., 1996).

1.3.1. Lentivirale Überexpression

Zur Überexpression von bestimmten Genen werden oft virale Vektoren eingesetzt. Dieser Prozess wird als Transduktion bezeichnet. Die gewünschte DNA Sequenz wird dabei in das Genom des Virus kloniert. Dabei werden Viren verwendet, die nicht mehr replikationskompetent sind. Die DNA wird per Zufall ins Genom der Zielzelle eingebaut. Die Selektion erfolgt meistens durch ein Antibiotikumsresistenzgen, welches im Vektor integriert wurde (Blesch, 2004).

1.3.2. Engineering mit der CRIPSR/Cas9 Technologie

Die CRISPR/Cas9 Technologie leitet sich von einem Mechanismus ab, mit dem sich Bakterien vor eindringenden Viren schützen (Jinek et al., 2012). Dabei spalten die Cas-Proteine die DNA der Viren in kleine Fragmente auf und fügen diese als „Spacer“ im CRISPR-Abschnitt des Bakterien-Erbguts ein. Die Zelle transkribiert die CRISPR-Abschnitte in ein RNA Molekül (CRISPR-RNA, crRNA), welches zusammen mit der Tracr-RNA an das Enzym Cas9 bindet. Kommt es erneut zu einem Virenbefall, kann das Enzym CRISPR/Cas9 das DNA-Virus erkennen und es durch gezieltes Fragmentieren unschädlich machen.

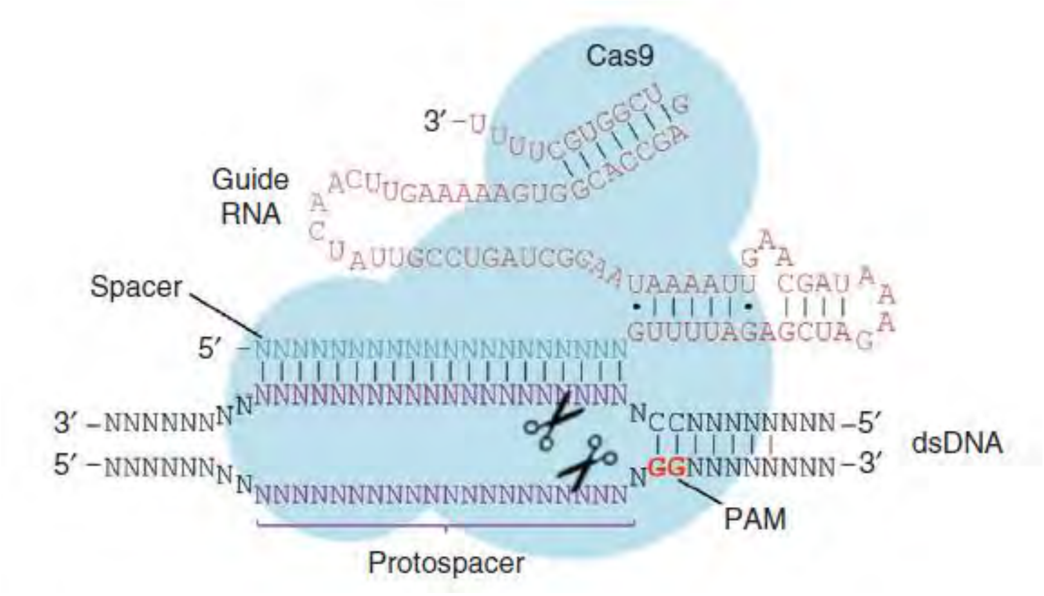

Cas9
3′-UUUUCGUGGCU G
ACCGA
Guide RNA
ACUUGAAAAAGUGGCACCGA
A C U AUUGCCUGAUCGGAA
Spacer
UAAAAUU CGAU
GA A
AAA
GUUUUAGAGCUA G
5′-NNNNNNNNNNNNNNNNNNNNNN
3′-NNNNNNN NNNNNNNNNNNNNNNNNNNNNNN
NCCNNNNNNNN-5′
5′-NNNNNNN NNNNNNNNNNNNNNNNNNNNNNN
NGGNNNNNNNN-3′
dsDNA
PAM
Protospacer

Abbildung 1.2: Das Cas9-Protein. Die GuideRNA hat eine Spacer-Sequenz und geht komplementäre Basenpaarungen mit der Ziel-DNA ein. Das Nukleotid "G" vor Beginn des Spacers ist wichtig für die Erkennung durch den Promotor. Dem Protospacer in der Zielsequenz folgt PAM. Die katalytischen Einheiten schneiden jeweils einen der gegenüberliegenden DNA-Stränge (Mali et al., 2013).

Für die Gentechnik kann die CRISPR-RNA Sequenz beliebig ausgetauscht werden. Im Jahr 2013 wurde erstmals das CRISPR/Cas9 System gezielt für genomische Modifikationen in Mauszellen und humanen Zellen eingesetzt. Dabei wurden die Zellen mit einem Vektorkonstrukt aus Genen für die Tracr-RNA, CrRNA und Cas9 aus dem Bakterium *Streptococcus pyogenes* transfiziert und erfolgreich multiple Doppelstrangbrüche erzeugt (Cong et al., 2013). Die Selektion transfizierter Zellen erfolgt mithilfe einer Koexpression von GFP oder einem Antibiotikaresistenzgen. Das Screening der positiven Klone kann demnach anschließend mit der Durchflusszytometrie oder Antibiotikaselektion durchgeführt werden.

Mit der crRNA lässt sich die genaue Stelle bestimmen, wo CRISPR/Cas9 die DNA durchtrennt und im Zuge der anschließenden Reparatur einzelne DNA-Bausteine ausschneidet, austauscht oder auch neu einfügt. DNA-Doppelstrangbrüche werden vom zelleigenen Reparaturmechanismus beseitigt. Dabei wird zwischen der Non-homologous end joining (NHEJ) und der homology-directed repair (HDR) unterschieden. NHEJ ist weniger präzise und eher ein „Notfall-Reparaturmechanismus“ der Zelle. Sie kann zur Bildung von Indels, kleinen Insertionen oder Deletionen, führen und kommt in allen Zellzyklusphasen vor (Lieber, 2008). Indels als Folge der NHEJ-Reparatur können zu Basenaustausch oder Leseraster-Verschiebungen führen, die jedoch nicht zwingend zu einem Gen-Knockout führen müssen.

Der Reparaturmechanismus HDR ist dagegen zwar präziser, jedoch wird ein DNA-Template benötigt. Außerdem ist der Prozess zellzyklusabhängig und hat die höchste Aktivität in der frühen S-Phase (Capecchi, 2005; Cui et al., 2011). Für Insertionen wird neben den CRISPR-Konstrukten ein DNA Template kotransfiziert, das bei der HDR als Vorlage genutzt werden kann.

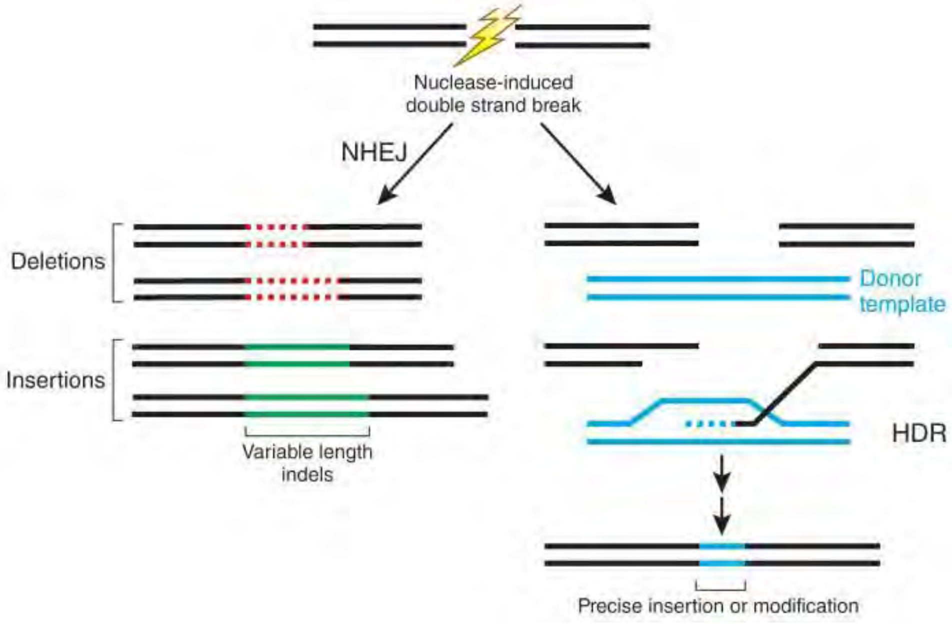
Nuclease-induced double strand break
NHEJ
Deletions
Insertions
Variable length indels
Donor template
HDR
Precise insertion or modification

Abbildung 1.3: Nuklease induzierte Reparaturmechanismen von DNA-Doppelstrangbrüchen Non-homologous end joining (NHEJ) ist ein fehleranfälliger endogener Reparaturmechanismus, der zu Insertionen oder Deletionen führen kann. Homology-directed repair (HDR) ist ein präziser DNA-Reparaturmechanismus, der ein Donor Template benötigt (Sander and Joung, 2014).

1.4. Mitochondrien

Mitochondrien sind Organellen, die ausschließlich in eukaryotischen Zellen vorkommen und als „Kraftwerke“ der Zelle fungieren. Sie besitzen eine Doppelmembran und eine eigene Erbsubstanz, die mitochondriale DNA, welche zum ersten Mal im Jahr 1963 von Margit und Sylvan Nass (Nass and Nass, 1963) beschrieben wurde. Sie ist zirkulär organisiert und besteht aus einem zu einem Ring geschlossenen DNA-Doppelstrang. Bei Säugetieren hat die mtDNA eine Größe von etwa 16,5 Kilobasen und exprimiert 13 mRNAs, welche alle für die Codierung von Protein-Untereinheiten der Atmungsketten zuständig sind (Taanman, 1999). Die Vererbung der mtDNA ist stets maternal über die Eizelle.

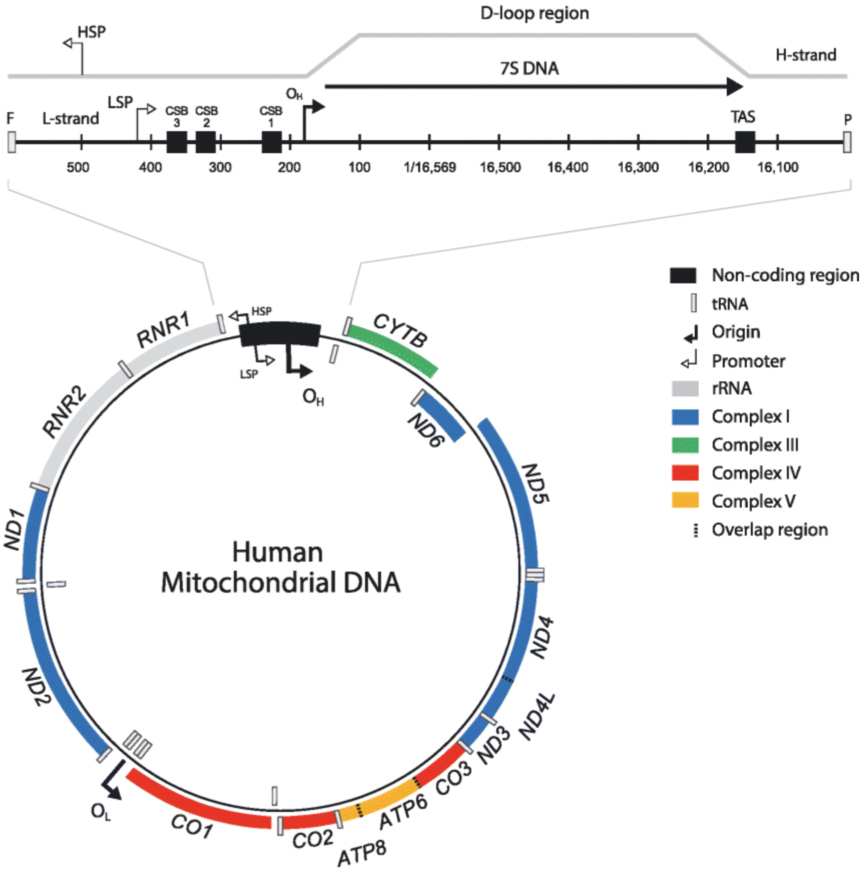
D-loop region
HSP
H-strand
7S DNA
O_H
LSP
F
L-strand
CSB 3
CSB 2
CSB 1
TAS
P
500
400
300
200
100
1/16,569
16,500
16,400
16,300
16,200
16,100
Non-coding region
tRNA
Origin
Promoter
rRNA
Complex I
Complex III
Complex IV
Complex V
Overlap region
HSP
LSP
O_H
RNR1
RNR2
CYTB
ND6
ND5
ND1
Human
Mitochondrial DNA
ND4
ND2
ND4L
ND3
CO3
ATP6
ATP8
CO2
CO1
O_L

Abbildung 1.4: Die humane mtDNA. Elf mRNAs codieren für 13 Polypeptide (Gammage and Frezza, 2019)

Mitochondrien befinden sich in nahezu allen Zellen. Ihre Anzahl wird dem Energiebedarf der Zelle angepasst und steigert sich bei hohem Energieverbrauch. In den Kardiomyozyten nehmen sie ca. 30% des Zellvolumens ein (Piquereau et al., 2013). Zu ihren Aufgaben gehört vor allem die Generierung von ATP durch die oxidative Phosphorylierung. Außerdem sind sie an Reaktionen des Citratzyklus und der Beta-Oxidation beteiligt. Ebenfalls sind sie der Ort für die Generierung von Eisen-Schwefel-Clustern und für die intrazelluläre Speicherung von Kalium. Zudem sind sie an der Regulation des programmierten Zelltods beteiligt und produzieren reaktive Sauerstoffspezies (ROS), die der Signaltransduktion dienen.

In den Mitochondrien findet mehr als 90 % der benötigten Energiegewinnung zur Aufrechterhaltung der Lebensfunktionen einer Zelle statt. Mitochondriale Dysfunktionen haben demnach eine starke Auswirkung auf die Funktion und das Wachstum einer Zelle (Shoffner et al., 1989).

Die Mutationsrate der mitochondrialen DNA ist im Vergleich zur genomischen DNA deutlich erhöht, da unter anderem unzureichende Reparaturmechanismen für mitochondriale DNA-Schäden existieren (Shigenaga et al., 1994). Ein Einzelnukleotid-Polymorphismus (engl. single-nucleotide polymorphismus, SNP), was eine Variation eines einzelnen Basenpaares in der DNA beschreibt, könnte in der mtDNA über die Zeit akkumulieren. Diese genetischen Varianten sind meistens geerbt und können auch vererbt werden. Häufig entstehen SNPs auch durch Spontanmutationen und können sowohl in den Introns als auch in den Exons auftreten. In den Exons werden zwischen synonyme SNPs und nicht-synonyme SNPs unterschieden: Synonyme SNPs haben zwar eine Punktmutation, jedoch bleibt die davon abgeleiteten Aminosäuresequenz unverändert. Bei nicht-synonymen SNPs kommt es durch den Austausch des Nukleotids zu einem Aminosäurewechsel, welcher somit Auswirkungen auf die Gen-Transkription und die damit verbundene Translation hat.

Mutationen in mitochondrialen Genen sind meist heteroplasmatisch. Als Heteroplasmie wird das Auftreten von Mitochondrien mit unterschiedlichen mtDNA Sequenzen innerhalb einer Zelle bezeichnet. Die unterschiedlichen Varianten sind meistens auf eine Mutation, wie zum Beispiel Replikationsfehler, zurückzuführen (Stewart and Chinnery, 2015). Der Prozentanteil von Heteroplasmie kann in unterschiedlichen Gewebeproben variieren und durch eine mtDNA Sequenzierung bestimmt werden.

1.5. Zielsetzung

Das Ziel der vorliegenden Arbeit war die Entwicklung neuer Strategien für die Zelltransplantation als Therapieoption in der klinischen Anwendung. Hierfür war es zunächst erforderlich, die unterschiedlichen Stammzelltypen auf ihre Immunogenität zu untersuchen und Mechanismen zu erforschen, die zur Zellabstoßung führen. Durch Modulationen mithilfe der CRISPR/Cas9 Technologie an murinen und humanen iPS-Zellen wurden die Oberflächenmoleküle MHCI und MHCII inaktiviert und das tolerogene Molekül CD47 überexprimiert. Diese „hypoimmunogenen“ iPS-Zellen wurden anschließend in Zellderivate der mesodermalen Linien differenziert und durch unterschiedliche *in vivo* und *in vitro* Methoden erneut auf ihre Immunogenität untersucht.

2. Publikationen

2.1 Hypoimmunogenic derivatives of induced pluripotent stem cells evade immune rejection in fully immunocompetent allogeneic recipients

In diesem Kapitel wird die Publikation „Hypoimmunogenic derivatives of induced pluripotent stem cells evade immune rejection in fully immunocompetent allogeneic recipients“ vorgestellt, welche im Jahr 2019 in Nature Biotechnology publiziert wurde. Mein Anteil der Publikation beinhaltet die Durchführung von allen immunologischen sowie molekularbiologischen Experimenten, die Zelldifferenzierung und Zellkultur, sowie *In-vivo* Imaging Studien und Datenanalysen. Meine Mitwirkung an dem Paper resultierte in einer Erstautorenschaft.

Titel: Hypoimmunogenic derivatives of induced pluripotent stem cells evade immune rejection in fully immunocompetent allogeneic recipients

Autoren: Xiaomeng Hu*, Tobias Deuse*, Alessia Gravina, Dong Wang, Grigol Tediashvili, Chandrav De, William O. Thayer, Angela Wahl, J. Victor Garcia, Hermann Reichenspurner, Mark M. Davis, Lewis L. Lanier, Sonja Schrepfer
*geteilte Erstautorenschaft

Journal: Nature Biotechnology,

DOI: 10.1038/s41587-019-0016-3

LETTERS
https://doi.org/10.1038/s41587-019-0016-3

nature biotechnology

Hypoimmunogenic derivatives of induced pluripotent stem cells evade immune rejection in fully immunocompetent allogeneic recipients

Tobias Deuse[1,7], Xiaomeng Hu[1,2,3,7], Alessia Gravina[1], Dong Wang[1,2], Grigol Tediashvili[1,2,3], Chandrav De[4], William O. Thayer[4], Angela Wahl[4], J. Victor Garcia[4], Hermann Reichenspurner[2,3], Mark M. Davis[5], Lewis L. Lanier[6] and Sonja Schrepfer[1*]

Autologous induced pluripotent stem cells (iPSCs) constitute an unlimited cell source for patient-specific cell-based organ repair strategies. However, their generation and subsequent differentiation into specific cells or tissues entail cell line-specific manufacturing challenges and form a lengthy process that precludes acute treatment modalities. These shortcomings could be overcome by using prefabricated allogeneic cell or tissue products, but the vigorous immune response against histo-incompatible cells has prevented the successful implementation of this approach. Here we show that both mouse and human iPSCs lose their immunogenicity when major histocompatibility complex (MHC) class I and II genes are inactivated and CD47 is over-expressed. These hypoimmunogenic iPSCs retain their pluripotent stem cell potential and differentiation capacity. Endothelial cells, smooth muscle cells, and cardiomyocytes derived from hypoimmunogenic mouse or human iPSCs reliably evade immune rejection in fully MHC-mismatched allogeneic recipients and survive long-term without the use of immunosuppression. These findings suggest that hypoimmunogenic cell grafts can be engineered for universal transplantation.

Treatment of heart disease with adult multipotent, bone marrow-derived stem cells has shown marginal efficacy in patients with acute myocardial infarction[1] or chronic ischemic cardiomyopathy[2,3]. This has been attributed to the limited plasticity of adult hematopoietic stem cells, which do not differentiate into cardiomyocytes and thus cannot replace contractile elements[4]. Pluripotent stem cells are more promising cell sources for regenerative strategies as they can produce an unlimited amount of progeny cells that can be differentiated into functional tissue cells. Although reprogramming technology allows the generation of autologous iPSCs for patient-specific treatments, this is laborious, costly, associated with uncertain quality and efficacy of individual cell products and is only practical for chronic diseases[5–7]. Thus, most regenerative approaches relying on autologous iPSC generation have been abandoned. Allogeneic cell therapies targeting large patient populations could be more economically feasible[8,9], but are subject to forceful immune rejection[10]. The use of allogeneic iPSC- or embryonic stem cell (ESC)-based products would require strong immunosuppression.

We envisioned engineering hypoimmunogenic pluripotent stem cells as a source for universally compatible cell or tissue grafts not requiring any immunosuppression. During pregnancy, the maternal immune system is tolerant of allogeneic paternal antigens although it would reject cells from the baby later in life[11]. We examined syncytiotrophoblast cells, which form the interface between maternal blood and fetal tissue, and found low MHC class I and II expression (Supplementary Fig. 1) as well as strong expression of CD47, a ubiquitous membrane protein that can interact with several cell surface receptors to inhibit phagocytosis[12]. We used this knowledge to design hypoimmunogenic mouse iPSCs (miPSCs).

C57BL/6 wild type (WT) miPSCs[13] give rise to classical teratomas with ectodermal, mesodermal and endodermal features in SCID-beige mice (Supplementary Fig. 2). To achieve hypoimmunogenicity, these miPSCs underwent a threestep gene-editing process (Supplementary Fig. 3a). First, CRISPR guide RNAs targeting the coding sequence of the mouse β2-microglobulin (*B2m*) gene were ligated into vectors containing the Cas9 expression cassette and subsequently transfected into miPSCs. B2m is a structural component of MHC class I. Second, $B2m^{-/-}$ miPSCs were transfected with a CRISPR–Cas9 vector targeting *Ciita*, the master regulator of MHC class II molecules[14]. Third, the *Cd47* gene sequence was synthesized and cloned into a lentivirus with blasticidin resistance, which was used to transduce $B2m^{-/-}Ciita^{-/-}$ miPSC clones followed by antibiotic selection and expansion of $B2m^{-/-}Ciita^{-/-}$ *Cd47* transgene (tg)-expressing miPSCs. WT miPSCs had interferon-γ (IFN-γ)-inducible MHC class I surface expression, low but detectable MHC class II expression and negligible Cd47 expression (Supplementary Fig. 3b–d). We confirmed that the miPSC lines we generated lacked MHC class I and II expression, and overexpressed Cd47 roughly 4.5-fold in flow cytometry. All three lines maintained their expression of pluripotency genes (Supplementary Fig. 3e–h).

Next, we transplanted WT miPSCs or engineered miPSCs into syngeneic C57BL/6 ($H2^b$) and allogeneic ($H2^d$) BALB/c recipients without immunosuppression. As expected, WT miPSCs showed

---

[1] Department of Surgery, Division of Cardiothoracic Surgery, Transplant and Stem Cell Immunobiology-Lab, University of California San Francisco, San Francisco, CA, USA. [2] Department of Cardiovascular Surgery, University Heart Center Hamburg, Hamburg, Germany. [3] Cardiovascular Research Center Hamburg and DZHK (German Center for Cardiovascular Research), Partner Site Hamburg/Kiel/Luebeck, Hamburg, Germany [4] Division of Infectious Diseases, UNC Center for AIDS Research, University of North Carolina School of Medicine, Chapel Hill, NC, USA. [5] Howard Hughes Medical Institute, Institute for Immunity, Transplantation and Infection, and Department of Microbiology and Immunology, Stanford University School of Medicine, Stanford, CA, USA. [6] Department of Microbiology and Immunology and the Parker Institute for Cancer Immunotherapy, University of California San Francisco, San Francisco, California, USA. [7] These authors contributed equally: Tobias Deuse, Xiaomeng Hu. *e-mail: Sonja.Schrepfer@ucsf.edu

100% teratoma growth in syngeneic recipients, but all cell grafts were rejected in allogeneic BALB/c mice (Fig. 1a,b). After 5 days, splenocytes from allogeneic BALB/c recipients showed a strong IFN-γ and a moderate IL-4 response relative to baseline responder cell activity (not shown); syngeneic mice showed no responsiveness (Fig. 1c). Only allogeneic BALB/c recipients mounted a strong IgM antibody response against the WT miPSCs relative to baseline MFI (not shown) (Fig. 1d). Engineered miPSCs developed comparable teratomas to WT miPSCs in syngeneic recipients, with enhanced survival in allogeneic recipients that depended on their level of hypoimmunogenicity and increased with every engineering step (Supplementary Fig. 4a–h). Our final $B2m^{-/-}Ciita^{-/-}$ Cd47 tg miPSC line showed 100% teratoma formation and induced no IFN-γ or antibody responses (Fig. 1e–h).

We further evaluated the contribution of Cd47 overexpression by comparing $B2m^{-/-}Ciita^{-/-}$ miPSCs to $B2m^{-/-}Ciita^{-/-}$ Cd47 tg miPSCs in natural killer (NK) cell toxicity assays. Gene editing did not enhance the expression of stimulatory ligands for the mouse NK cell NKG2D or NKp46 receptors (Supplementary Fig 4i), which are constitutively expressed in the NK cell-sensitive target cell line YAC-1[15]. $B2m^{-/-}Ciita^{-/-}$ miPSCs induced IFN-γ release that was significantly elevated when compared to unchallenged NK cells, but lower than IFN-γ release triggered by YAC-1 (Supplementary Fig. 4j). This suggested that Cd47 overexpression completely prevented any miPSC-induced NK cell IFN-γ release in vitro. To further assess innate miPSC clearance in vivo, a 1:1 mixture of CFSE-labeled WT miPSCs and either $B2m^{-/-}Ciita^{-/-}$ miPSCs or $B2m^{-/-}Ciita^{-/-}$ Cd47 tg miPSCs were injected into the innate immune cell-rich peritoneum of syngeneic C57BL/6 mice (Supplementary Fig 5a). Using a syngeneic host for this assay precluded relevant T cell-mediated cytotoxicity. After 48 h, the peritoneal fluid was aspirated and CFSE-labeled cells were analyzed by flow cytometry. $B2m^{-/-}Ciita^{-/-}$ Cd47 tg miPSCs, but not $B2m^{-/-}Ciita^{-/-}$ miPSCs, were resistant to innate immune clearance and the 1:1 ratio with WT miPSCs could be maintained. We observed the same pattern of cell clearance when mice were pretreated with clodronate to eliminate macrophages (Supplementary Fig. 5b). Notably, a blocking antibody against mouse Cd47 completely abolished the protective effect of Cd47 in macrophage-depleted mice and $B2m^{-/-}Ciita^{-/-}$ Cd47 tg miPSCs were rapidly eliminated (Supplementary Fig. 5c). Collectively, these data suggest an inhibitory effect of Cd47 on NK cells in vivo.

To test whether hypoimmunogenic $B2m^{-/-}Ciita^{-/-}$ Cd47 tg miPSCs could give rise to hypoimmunogenic cardiac tissue, they were differentiated into endothelial cells (miECs), smooth muscle cells (miSMCs) and cardiomyocytes (miCMs) with WT miPSC derivatives serving as controls (Supplementary Fig. 6). All derivatives showed the morphologic appearance, cell marker immunofluorescence and gene expression characteristic of their mature target tissue cell lines, and cultures achieved >90% purity of VE-Cadherin$^+$ miECs, Sma$^+$ miSMCs and troponin I$^+$ miCMs. The expression of MHC class I and II molecules in WT derivatives markedly varied by cell type (Supplementary Fig. 7a–c) but, as expected, miECs had by far the highest expression of IFN-γ induced MHC class I and II, miSMCs had moderate MHC class I and II expression[16] and miCMs had moderate MHC class I but very low MHC class II expression[17]. All $B2m^{-/-}Ciita^{-/-}$ Cd47 tg derivatives appropriately showed a complete lack of MHC class I and II and significantly elevated Cd47 compared to their WT counterparts. None of the $B2m^{-/-}Ciita^{-/-}$ Cd47 tg derivatives showed upregulation of NKG2D or NKp46 ligands (Supplementary Fig 7d,e).

We next assessed the in vivo immunogenicity of WT and hypoimmunogenic miPSCderivatives. miECs, miSMCs or miCMs derived from WT or $B2m^{-/-}Ciita^{-/-}$ Cd47 tg were transplanted intramuscularly into syngeneic C57BL/6 or allogeneic BALB/c mice and adaptive immune responses were assessed after 5 days. All allogeneic recipients mounted a strong cellular IFN-γ response, as well as a strong IgM antibody response against all differentiated WT cell grafts (Supplementary Fig. 8a–c). In contrast, neither of the corresponding $B2m^{-/-}Ciita^{-/-}$ Cd47 tg derivatives showed detectable increases in IFN-γ Elispot frequencies or IgM antibody production (Supplementary Fig. 8d–f). To assess the efficacy of Cd47 to mitigate the susceptibility to innate immune killing, we performed NK cell Elispot assays with antibody-coated magnetic bead-enriched BALB/c NK cells and $B2m^{-/-}Ciita^{-/-}$ or $B2m^{-/-}Ciita^{-/-}$ Cd47tg derivatives (Supplementary Fig. 8g–i). While $B2m^{-/-}Ciita^{-/-}$ derivatives triggered NK cell IFN-γ release, none of the $B2m^{-/-}Ciita^{-/-}$ Cd47 tg derivatives produced IFN-γ spot frequencies significantly exceeding those of unchallenged NK cells. Accordingly, in vivo innate immune assays showed rapid clearance of all $B2m^{-/-}Ciita^{-/-}$ derivatives, but confirmed that none of the $B2m^{-/-}Ciita^{-/-}$ Cd47 tg derivatives showed susceptibility to innate elimination (Supplementary Fig. 8j–l). To confirm an inhibitory effect of Cd47 on NK cells, we next performed real-time in vitro killing assays with confluent miECs and highly purified NK cells. Both allogeneic (BALB/c) and syngeneic (C57BL/6) NK cells rapidly killed $B2m^{-/-}Ciita^{-/-}$ miECs, but not WT and $B2m^{-/-}Ciita^{-/-}$ Cd47 tg miECs (Supplementary Fig. 5d,e). However, antibody blocking of mouse Cd47 resulted in the rapid killing of $B2m^{-/-}Ciita^{-/-}$ Cd47 tg miECs (Supplementary Fig. 5f). The effect of CD47 is species-specific as human NK cells rapidly killed both $B2m^{-/-}Ciita^{-/-}$ and $B2m^{-/-}Ciita^{-/-}$ Cd47 tg miECs (Supplementary Fig. 5g).

We next examined survival of WT and hypoimmunogenic miPSC derivates in vivo. WT and $B2m^{-/-}Ciita^{-/-}$ Cd47 tg derivatives were transduced to express firefly luciferase, and Matrigel plugs containing differentiated cells were transplanted into syngeneic C57BL/6 or allogeneic BALB/c mice. All three WT derivatives showed long-term (50 days) survival in syngeneic C57BL/6 recipients, but were rejected in allogeneic mice (Fig. 1i–k). In contrast, all three $B2m^{-/-}Ciita^{-/-}$ Cd47 tg derivatives showed 100% long-term survival in both syngeneic and allogeneic recipients (Fig. 1l–n).

Matrigel plugs containing WT or $B2m^{-/-}Ciita^{-/-}$ Cd47 tg miECs were transplanted into allogeneic BALB/c recipients (Supplementary Fig. 9a). ECs are the most immunogenic cardiac cell type due to their high expression of MHC class I and II, which allows them to function as antigen-presenting cells. We observed infiltrating immune cells containing mostly T and B lymphocytes, but also some NK cells and macrophages in WT miEC plugs. $B2m^{-/-}Ciita^{-/-}$ Cd47 tg miEC-containing plugs had almost no immune cell infiltration (Supplementary Fig. 9b). In the WT plugs, cytokine arrays on day 10 revealed an inflammatory milieu that included upregulated T helper cell (T_h)-1 cytokines (IFN-γ and IL-2) and T_h-2 cytokines (IL-4, IL-5, IL-10 and IL-13). In contrast, in plugs containing $B2m^{-/-}Ciita^{-/-}$ Cd47 tg miECs, the cytokine milieu was very similar to that of cell-free plugs containing only Matrigel, with no indication of immune activation (Supplementary Fig. 9c). Over time, transplanted $B2m^{-/-}Ciita^{-/-}$ Cd47 tg miECs organized in circular structures and formed primitive vessels that contained erythrocytes (Supplementary Fig. 10a). Similarly transplanted $B2m^{-/-}Ciita^{-/-}$ Cd47 tg miSMCs (Supplementary Fig. 10b) or miCMs (Supplementary Fig. 10c) did not form three-dimensional structures, and their in vivo maturation and integration potential in cardiac tissue remains to be studied.

We next applied our engineering strategy to human iPSCs (hiPSCs) using a human episomal iPSC line derived from CD34$^+$ cord blood that showed a normal human XX karyotype and features of pluripotency (Supplementary Fig. 11a–c,g–h). The gene-editing process included two steps (Fig 2a). First, both the human *B2M* and human *CIITA* genes were simultaneously targeted for CRISPR/Cas9-mediated disruption. Second, these edited hiPSCs were transduced with a lentivirus carrying human CD47 complementary DNA with an EFS promotor and puromycin resistance. Antibiotic-resistant $B2M^{-/-}CIITA^{-/-}$ CD47 tg hiPSC colonies maintained their normal

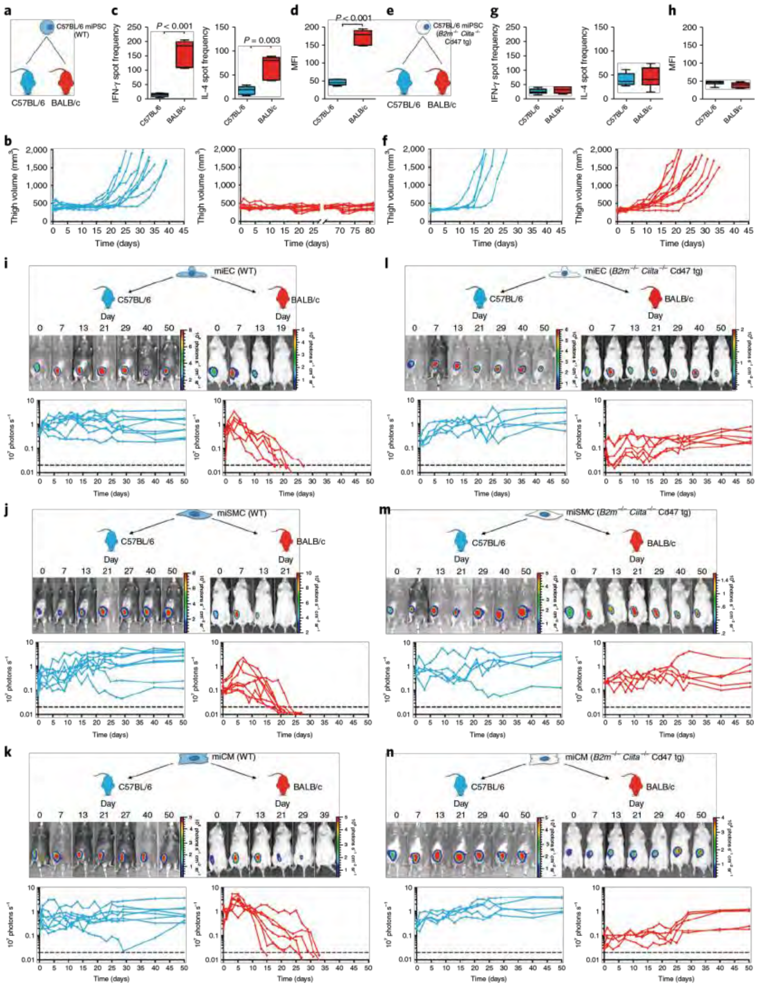

Fig. 1 | Survival of miPSCs and miPSC derivatives. **a**, WT C57BL/6 miPSCs were injected into the thigh muscle of syngeneic C57BL/6 or allogeneic BALB/c mice. **b**, Teratoma formation was observed by measuring the thigh muscle ($n=10$ per group). **c**, IFN-γ and IL-4 enzyme-linked immunospots (Elispots) with splenocytes recovered 5 days after the transplantation (box 25th to 75th percentile with median, whiskers min–max, five animals per group, two-tailed Student's *t*-test). **d**, Mean fluorescence imaging (MFI) of IgM binding to WT miPSCs incubated with recipient serum after 5 days (box 25th to 75th percentile with median, whiskers min–max, six animals per group, two-tailed Student's *t*-test). **e**, $B2m^{-/-}Ciita^{-/-}$ Cd47 tg C57BL/6 miPSCs were transplanted into syngeneic C57BL/6 or allogeneic BALB/c recipients. **f**, Thigh volume C57BL/6 ($n=5$) and BALB/c ($n=11$) animals. The overall percentage of cell grafts that survived and formed teratomas in BALB/c was 100%. **g**, IFN-γ and IL-4 Elispots with splenocytes recovered 5 days after the transplantation and $B2m^{-/-}Ciita^{-/-}$ Cd47 tg miPSCs stimulator cells (box 25th to 75th percentile with median, whiskers min–max, $n=6$ per group, two-tailed Student's *t*-test). **h**, MFI of IgM binding to $B2m^{-/-}Ciita^{-/-}$ Cd47 tg miPSCs incubated with recipient serum after 5 days (box 25th to 75th percentile with median, whiskers min–max, six animals per group, two-tailed Student's *t*-test). **i–n**, Grafts of Fluc^{+} C57BL/6 miPSC derivatives in C57BL/6 or BALB/c recipients were longitudinally followed by bioluminescent imaging (BLI). One representative animal is depicted per group and the BLI values of all animals are plotted. All WT miPSC-derived miECs (**i**, eight animals in C57BL/6 and six animals in BALB/c), miSMCs (**j**, nine animals in C57BL/6 and eight animals in BALB/c) and miCMs (**k**, eight animals in C57BL/6 and seven animals in BALB/c) showed long-term survival in syngeneic C57BL/6 recipients but were rejected in allogeneic BALB/c animals. In contrast, all $B2m^{-/-}Ciita^{-/-}$ Cd47 tg miPSC-derived miECs (**l**, five animals in C57BL/6 and six animals in BALB/c), miSMCs (**m**, five animals in C57BL/6 and five animals in BALB/c) and miCMs (**n**, five animals in C57BL/6 and five animals in BALB/c) showed long-term survival in both syngeneic C57BL/6 and allogeneic BALB/c recipients.

human karyotype and pluripotency (Supplementary Fig. 11d–f,i–j) and successful depletion of HLA I and II surface expression, along with overexpression of CD47, was confirmed by flow cytometry (Fig. 2b). Both WT hiPSCs and $B2M^{-/-}CIITA^{-/-}$ CD47 tg hiPSCs were differentiated into endothelial-like cells (hiECs) and cardiomyocyte-like cells (hiCMs) (Fig. 2c). All derivatives showed the morphologic features and protein expression of the differentiated target cells and lost their pluripotency genes (Supplementary Fig. 12a,b). Cultures showed >95% purity for VE-Cadherin$^+$ hiECs and troponin I$^+$ hiCMs. There were no alterations in the expression of stimulatory NK cell ligands with gene engineering (Supplementary Fig. 12c–i). WT hiECs and hiCMs upregulated IFN-γ induced HLA I expression roughly three- and two-fold, respectively, compared to WT hiPSCs and hiECs also showed roughly 11-fold elevated HLA II (Fig. 2d–e). $B2M^{-/-}CIITA^{-/-}$ CD47 tg hiECs and hiCMs exhibited HLA I and II depletion and significant CD47 upregulation compared to their WT counterparts.

We next performed transplant studies in humanized CD34$^+$ hematopoietic stem cell-engrafted NSG-SGM3 mice[18], which were allogeneic to the hiPSC, hiEC and hiCM grafts. Since no syngeneic controls are available in this humanized mouse model, background measurements were collected in naïve mice. After 5days, recipients of WT hiPSCs (Fig. 2f) showed a high splenocyte IFN-γ spot frequency (Fig. 2g) and elevated IgM levels (Fig. 2h). Recipients of $B2M^{-/-}CIITA^{-/-}$ CD47 tg hiPSCs did not mount any detectable cellular IFN-γ response or antibody response. NK cell activation was assessed using in vitro incubation with human enriched CD56$^+$ NK cells. $B2M^{-/-}CIITA^{-/-}$ hiPSCs resulted in an IFN-γ release reaching roughly one-third of the spot frequency of the highly NK cell susceptible K562 line, whereas $B2M^{-/-}CIITA^{-/-}$ CD47 tg hiPSCs did not provoke any measurable response (Fig. 2i). The allogeneic transplantation of WT hiECs (Fig. 2j) and WT hiCMs (Fig. 2n) resulted in strong systemic IFN-γ reactions (Fig. 2k,o) and IgM antibody increases (Fig. 2l,p) of similar intensity as WT hiPSCs, whereas hypoimmunogenic hiECs and hiCMs did not induce any cellular or humoral immune response. Moreover, in vitro, hypoimmunogenic derivatives did not trigger NK cell activation (Fig. 2m, q) or NK cell killing (Supplementary Fig. 5h). As with the miPSCs, a blocking antibody specific for human CD47 completely abolished NK cell protection of $B2M^{-/-}CIITA^{-/-}$ CD47 tg hiPSCs (Supplementary Fig. 5i).

We also assessed the survival of hiPSCs, as well as their derivatives in allogeneic humanized NSG-SGM3 mice. All cell lines were transduced to express Fluc to enable tracking by BLI. There was no significant difference in HLA-A mismatch between groups (Supplementary Fig. 12j). As expected, all WT hiPSC grafts in Matrigel plugs underwent rejection (Fig. 3a) and all $B2M^{-/-}CIITA^{-/-}$ CD47 tg hiPSCs formed teratomas. Similarly, WT hiECs (Fig. 3b) and WT hiCMs (Fig. 3c) were rejected, although at slightly slower rate than in the corresponding miPSC derivative experiments. This difference may be based on the reduced number, diversity and function of human immune cells in mouse recipients[19], although the triple transgenic NSG-SGM3 mice specifically express human cytokines[20] to minimize these limitations. All $B2M^{-/-}CIITA^{-/-}$ CD47 tg hiEC and hiCM grafts showed long-term survival (50 days) and stable BLI signal levels over time. The hiECs gradually organized into structures resembling primitive vascular structures, which occasionally contained erythrocytes, and the hiCMs acquired a limited polarized architecture (Fig. 3d,e).

hiECs, the most immunogenic derivatives, were further tested in the humanized BLT mouse model. BLT humanized mice are bioengineered by implantation of human fetal liver and thymic tissue under the kidney capsule followed by intravenous transplantation with autologous CD34$^+$ HSCs[21] (Fig. 3f). This allows for T cell maturation in human thymic tissue and permits HLA restricted T cell responses. WT hiEC grafts in Matrigel plugs triggered a roughly 40% stronger IFN-γ response but 40% weaker IgM antibody response than in the previous NSG-SGM3 mice. No measurable immune activation was detected in recipients of $B2M^{-/-}CIITA^{-/-}$ CD47 tg hiEC grafts (Fig. 3g,h). All WT hiEC grafts underwent rapid rejection while four out of five $B2M^{-/-}CIITA^{-/-}$ CD47 tg hiEC grafts achieved survival (Fig. 3i). We assume a non-immune-related reason for the failure of the fifth graft since no immune activation could be detected in this specific recipient. We thus demonstrated that the combination of MHC class I and II depletion and CD47 overexpression renders both mouse and human stem cells, as well as their differentiated derivatives, hypoimmunogenic. In the models studied here, engineered differentiated derivatives achieved long-term survival in fully allogeneic hosts without any immunosuppression and retained basic cell-specific features after transplantation.

The initial concept of hypoimmunogenic pluripotent stem cells was based on an MHC class I knockdown and showed encouraging early results[22]. However, according to the 'missing-self theory', MHC class I-deficient mouse and human PSCs become susceptible to NK

Fig. 2 | Immune response against hiPSC derivatives. a, WT hiPSCs first underwent *B2M* and *CIITA* gene disruption and then CD47 transgene overexpression **b**, Gene editing of hiPSCs was confirmed by flow cytometry (box 25th to 75th percentile with median, whiskers min–max, four independent experiments per graph, analysis of variance (ANOVA) with Bonferroni's post-hoc test). **c**, WT and $B2M^{-/-}CIITA^{-/-}$ CD47 tg hiPSCs were differentiated into both hiECs and hiCMs. **d–e**, The immune phenotype of WT and $B2M^{-/-}CIITA^{-/-}$ CD47 tg hiECs (**d**) and hiCMs (**e**) is shown (box 25th to 75th percentile with median, whiskers min–max, four independent experiments per graph, two-tailed Student's *t*-test). **f**, WT or $B2M^{-/-}CIITA^{-/-}$ CD47 tg hiPSC grafts were injected into allogeneic humanized NSG-SGM3 mice. **g**, IFN-γ Elispots were performed after 5 days (mean ± s.d., $n=7$ per group, two-tailed Student's *t*-test), the background spot frequency in naïve mice is shown (mean ± s.d., four animals per group, two-tailed Student's *t*-test). **h**, MFI of IgM binding to either hiPSC incubated with recipient serum after 5 days (mean ± s.d., five animals per group, two-tailed Student's *t*-test), the background fluorescence in naïve mice is shown (mean ± s.d., three animals per group, Student's *t*-test). **i**, IFN-γ Elispots with human NK cells were performed with $B2M^{-/-}CIITA^{-/-}$ hiPSC or $B2M^{-/-}CIITA^{-/-}$ CD47 tg hiPSC (box 25th to 75th percentile with median, whiskers min–max, six independent experiments, ANOVA with Bonferroni's post-hoc test). **j**, WT or $B2M^{-/-}CIITA^{-/-}$ CD47 tg hiEC grafts were injected into allogeneic humanized NSG-SGM3 mice. **k**, IFN-γ Elispots were performed after 5 days (mean ± s.d., three animals per group, two-tailed Student's *t*-test), the background spot frequency in naïve mice is shown (mean ± s.d., four animals per group, two-tailed Student's *t*-test). **l**, MFI of IgM binding to either hiEC incubated with recipient serum after 5 days (mean ± s.d., three animals per group, two-tailed Student's *t*-test), the background fluorescence in naïve mice is shown (mean ± s.d., three animals per group, Student's *t*-test). **m**, IFN-γ Elispots with human NK cells were performed with $B2M^{-/-}CIITA^{-/-}$ hiECs or $B2M^{-/-}CIITA^{-/-}$ CD47 tg hiECs (box 25th to 75th percentile with median, whiskers min–max, six independent experiments, ANOVA with Bonferroni's post-hoc test). **n**, WT or $B2M^{-/-}CIITA^{-/-}$ CD47 tg hiCM grafts were injected into allogeneic humanized NSG-SGM3 mice. **o**, IFN-γ Elispots were performed after 5 days (mean ± s.d., three animals per group, two-tailed Student's *t*-test), the background spot frequency in naïve mice is shown (mean ± s.d., four animals per group, two-tailed Student's *t*-test). **p**, MFI of IgM binding to either hiCM incubated with recipient serum after 5 days (mean ± s.d., three animals per group, two-tailed Student's *t*-test), the background fluorescence in naïve mice is shown (mean ± s.d., three animals per group, Student's *t*-test). **q**, IFN-γ Elispots with human NK cells were performed with $B2M^{-/-}CIITA^{-/-}$ hiCMs or $B2M^{-/-}CIITA^{-/-}$ CD47 tg hiCMs (box 25th to 75th percentile with median, whiskers min–max, six independent experiments, ANOVA with Bonferroni's post-hoc test).

cell killing[23–25]. Although isolated expression of HLA-E[26] or HLA-G[27] in human pluripotent stem cells has been used to mitigate NK cell cytotoxicity, we observed that CD47 is a very effective non-MHC ligand to silence all innate immune responses. However, cells eluding immune monitoring may pose the long-term risks of uncontrollable malignant transformation or impaired virus clearance, although for the latter alternative mechanisms have been shown[28]. Inducible kill switches could enhance their overall safety.

The ability to generate substantial amounts of cardiac tissue from allogeneic iPSC-derived CMs has been well demonstrated in macaques[29]. However, the amounts of toxic immunosuppressive drugs required to achieve allogeneic cell survival pose a major

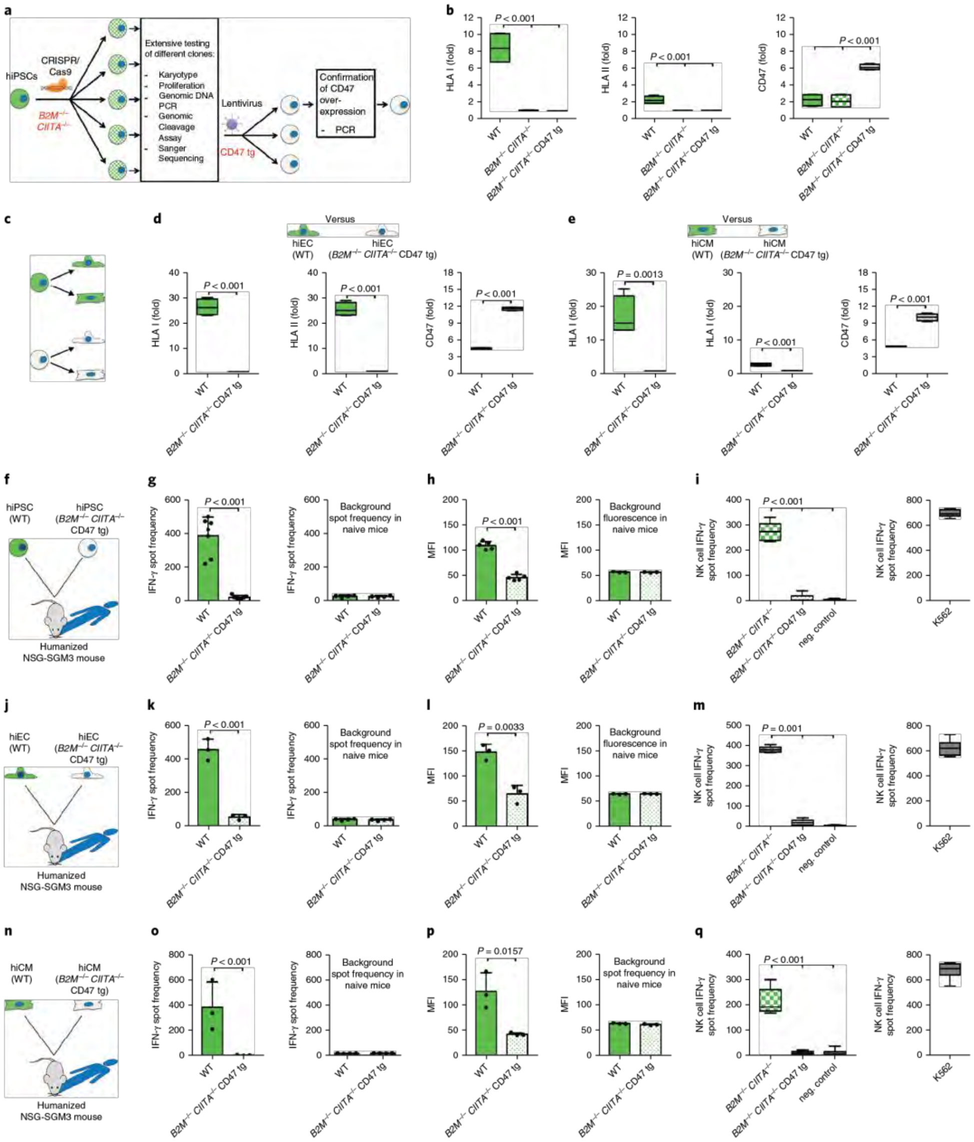

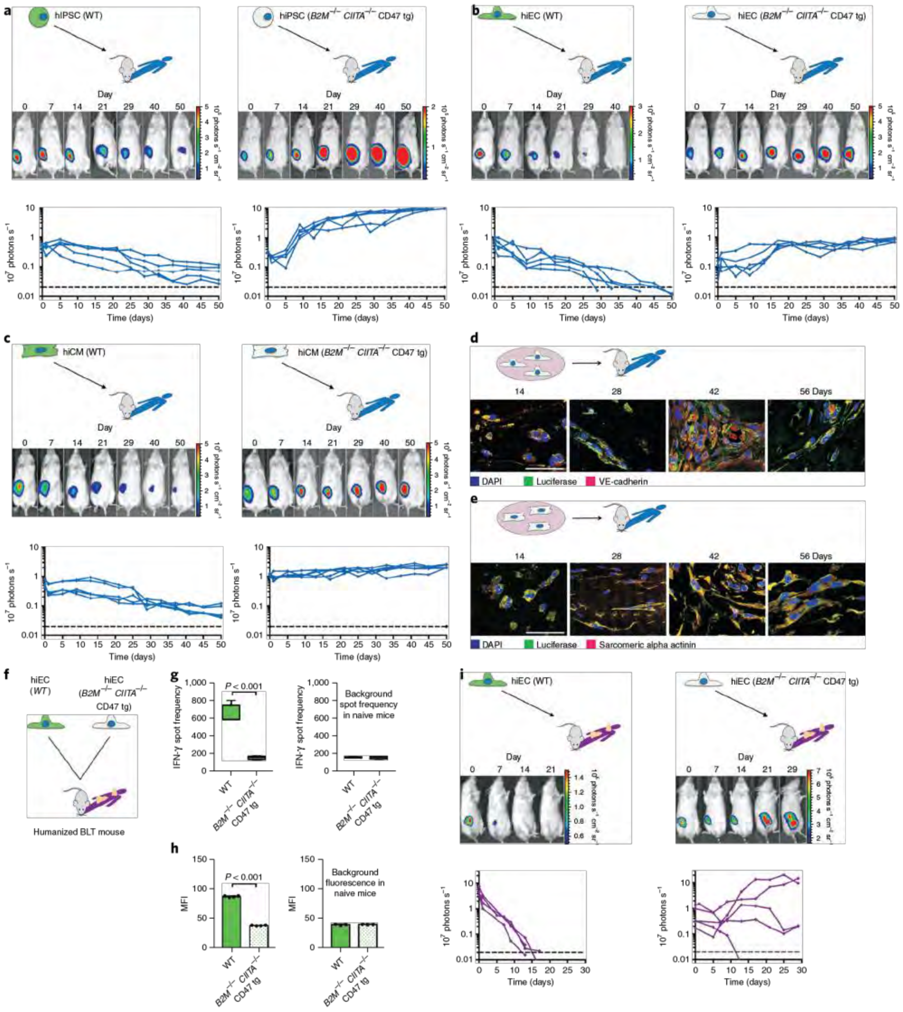

Fig. 3 | Survival of hiPSCs and hiPSC derivatives in allogeneic hosts. Grafts of Fluc$^+$ WT or *B2M*$^{-/-}$*CIITA*$^{-/-}$ CD47 tg hiPSCs, hiECs and hiCMs were transplanted into allogeneic humanized mice (NSG-SGM3 mice in **a**–**e**, BLT mice in **f**–**i**) and were longitudinally followed by BLI. One representative animal is depicted per group and the BLI values of all animals are plotted. **a**, BLI signals over time of WT and *B2M*$^{-/-}$*CIITA*$^{-/-}$ CD47 tg hiPSC grafts ($n=5$ per group). **b**, WT and *B2M*$^{-/-}$*CIITA*$^{-/-}$ CD47 tg hiECs were transplanted as in **a** ($n=5$ per group). **c**, WT and *B2M*$^{-/-}$*CIITA*$^{-/-}$ CD47 tg hiCMs ($n=5$). **d**, *B2M*$^{-/-}$*CIITA*$^{-/-}$ CD47 tg hiECs started to organize into a more complex structure, which included primitive vascular structures (representative pictures of three independent experiments). Scale bar, 50 µm. **e**, The *B2M*$^{-/-}$*CIITA*$^{-/-}$ CD47 tg hiCMs began to organize into a more polarized framework and maintained their sarcomeric alpha-actinin cytoskeletal structure typical of cardiomyocytes (representative pictures of three independent experiments). Scale bar, 50 µm. **f**, WT or *B2M*$^{-/-}$*CIITA*$^{-/-}$ CD47 tg hiECs were transplanted into allogeneic humanized BLT mice. **g**, IFN-γ Elispots were performed after 5 days (box 25th to 75th percentile with median, whiskers min–max, four animals per group, two-tailed Student's *t*-test), the background spot frequency in naïve mice is shown. **h**, MFI of IgM binding to either hiEC incubated with recipient serum after 5 days (mean ± s.d., four animals per group, two-tailed Student's *t*-test), the background fluorescence in naïve mice is shown (mean ± s.d., three animals per group, two-tailed Student's *t*-test). **i**, Grafts of Fluc$^+$ WT or *B2M*$^{-/-}$*CIITA*$^{-/-}$ CD47 tg hiECs were transplanted into allogeneic humanized BLT mice and were longitudinally followed by BLI. All WT hiEC grafts were rejected within roughly 14 days (four animals). Four of the five *B2M*$^{-/-}$*CIITA*$^{-/-}$ CD47 tg hiEC grafts permanently survived, the one failure is believed not to be immune-mediated (five animals).

hurdle for clinical use. Even with fully MHC class I- and II-matched allogeneic iPSC-derived CM grafts, macaque recipients required substantial and highly toxic immunosuppression to prevent cell rejection[29,30]. Thus, the generation of universal hypoimmunogenic iPSCs that can be differentiated into the main components of cardiac tissue and achieve long-term survival in a fully allogeneic recipient without any immunosuppression may help to develop universal cell products to treat heart failure.

Online content

Any methods, additional references, Nature Research reporting summaries, source data, statements of data availability and associated accession codes are available at https://doi.org/10.1038/s41587-019-0016-3.

Received: 23 April 2018; Accepted: 28 December 2018;
Published online: 18 February 2019

References

1. Gyongyosi, M. et al. Meta-analysis of cell-based CaRdiac stUdiEs (ACCRUE) in patients with acute myocardial infarction based on individual patient data. *Circ. Res.* **116**, 1346–1360 (2015).
2. Fisher, S. A., Doree, C., Mathur, A. & Martin-Rendon, E. Meta-analysis of cell therapy trials for patients with heart failure. *Circ. Res.* 116, 1361–1377 (2015).
3. Kandala, J. et al. Meta-analysis of stem cell therapy in chronic ischemic cardiomyopathy. *Am. J. Cardiol.* 112, 217–225 (2013).
4. Fernandez-Aviles, F. et al. Global position paper on cardiovascular regenerative medicine. *Eur. Heart J.* 38, 2532–2546 (2017).
5. Lipsitz, Y. Y., Timmins, N. E. & Zandstra, P. W. Quality cell therapy manufacturing by design. *Nat. Biotechnol.* 34, 393–400 (2016).
6. Blair, N. F. & Barker, R. A. Making it personal: the prospects for autologous pluripotent stem cell-derived therapies. *Regen. Med.* 11, 423–425 (2016).
7. Chakradhar, S. An eye to the future: researchers debate best path for stem cell-derived therapies. *Nat. Med.* 22, 116–119 (2016).
8. Smith, D. M. Assessing commercial opportunities for autologous and allogeneic cell-based products. *Regen. Med.* 7, 721–732 (2012).
9. Lipsitz, Y. Y., Bedford, P., Davies, A. H., Timmins, N. E. & Zandstra, P. W. Achieving efficient manufacturing and quality assurance through synthetic cell therapy design. *Cell. Stem. Cell* 20, 13–17 (2017).
10. van Berlo, J. H. & Molkentin, J. D. An emerging consensus on cardiac regeneration. *Nat. Med.* 20, 1386–1393 (2014).
11. Arck, P. C. & Hecher, K. Fetomaternal immune cross-talk and its consequences for maternal and offsprings health. *Nat. Med.* 19, 548–556 (2013).
12. Jaiswal, S. et al. CD47 is upregulated on circulating hematopoietic stem cells and leukemia cells to avoid phagocytosis. *Cell* 138, 271–285 (2009).
13. Diecke, S. et al. Novel codon-optimized mini-intronic plasmid for efficient, inexpensive, and xeno-free induction of pluripotency. *Sci. Rep.* 5, 8081 (2015).
14. Chang, C. H., Fontes, J. D., Peterlin, M. & Flavell, R. A. Class II transactivator (CIITA) is sufficient for the inducible expression of major histocompatibility complex class II genes. *J. Exp. Med.* 180, 1367–1374 (1994).
15. Elsner, L. et al. The heat shock protein HSP70 promotes mouse NK cell activity against tumors that express inducible NKG2D ligands. *J. Immunol.* 179, 5523–5533 (2007).
16. Maddaluno, M. et al. Murine aortic smooth muscle cells acquire, though fail to present exogenous protein antigens on major histocompatibility complex class II molecules. *Biomed. Res. Int.* 2014, 949845 (2014).
17. Didie, M., Galla, S., Muppala, V., Dressel, R. & Zimmermann, W. H. Immunological properties of murine parthenogenetic stem cell-derived cardiomyocytes and engineered heart muscle. *Front. Immunol.* 8, 955 (2017).
18. Wunderlich, M. et al. AML xenograft efficiency is significantly improved in NOD/SCID-IL2RG mice constitutively expressing human SCF, GM-CSF and IL-3. *Leukemia* 24, 1785–1788 (2010).
19. Shultz, L. D., Ishikawa, F. & Greiner, D. L. Humanized mice in translational biomedical research. *Nat. Rev. Immunol.* 7, 118–130 (2007).
20. Billerbeck, E. et al. Development of human CD4+ FoxP3+ regulatory T cells in human stem cell factor-, granulocyte-macrophage colony-stimulating factor-, and interleukin-3-expressing NOD-SCID IL2Rgamma(null) humanized mice. *Blood* 117, 3076–3086 (2011).
21. Melkus, M. W. et al. Humanized mice mount specific adaptive and innate immune responses to EBV and TSST-1. *Nat. Med.* 12, 1316–1322 (2006).
22. Deuse, T. et al. Human leukocyte antigen I knockdown human embryonic stem cells induce host ignorance and achieve prolonged xenogeneic survival. *Circulation* 124, S3–S9 (2011).
23. Wang, D., Quan, Y., Yan, Q., Morales, J. E. & Wetsel, R. A. Targeted disruption of the beta2-microglobulin gene minimizes the immunogenicity of human embryonic stem cells. *Stem Cells Transl. Med.* 4, 1234–1245 (2015).
24. Dressel, R. et al. Pluripotent stem cells are highly susceptible targets for syngeneic, allogeneic, and xenogeneic natural killer cells. *FASEB J.* 24, 2164–2177 (2010).
25. Kruse, V. et al. Human induced pluripotent stem cells are targets for allogeneic and autologous natural killer (NK) cells and killing is partly mediated by the activating NK Receptor DNAM-1. *PLoS ONE* 10, e0125544 (2015).
26. Gornalusse, G. G. et al. HLA-E-expressing pluripotent stem cells escape allogeneic responses and lysis by NK cells. *Nat. Biotechnol.* 35, 765–772 (2017).
27. Zhao, L., Teklemariam, T. & Hantash, B. M. Heterelogous expression of mutated HLA-G decreases immunogenicity of human embryonic stem cells and their epidermal derivatives. *Stem Cell Res.* 13, 342–354 (2014).
28. Hou, S., Doherty, P. C., Zijlstra, M., Jaenisch, R. & Katz, J. M. Delayed clearance of Sendai virus in mice lacking class I MHC-restricted CD8+ T cells. *J. Immunol.* 149, 1319–1325 (1992).
29. Shiba, Y. et al. Allogeneic transplantation of iPS cell-derived cardiomyocytes regenerates primate hearts. *Nature* 538, 388–391 (2016).
30. Kawamura, T. et al. Cardiomyocytes derived from MHC-homozygous induced pluripotent stem cells exhibit reduced allogeneic immunogenicity in MHC-matched non-human primates. *Stem Cell Rep.* 6, 312–320 (2016).

Acknowledgements

We thank C. Pahrmann for cell culture work, imaging experiments and overall assistance and L. Li for his assistance. The in vivo BLI experiments were performed at the UCSF Pre-clinical Therapeutics Core (A. Fries; with special thanks to B.C. Hann). Special thanks go to J. Wu (Stanford Cardiovascular Institute, Stanford University School of Medicine) for providing the miPSCs and the help of his laboratory with developing the protocol for hiPSC differentiation into cardiomyocytes. We thank J.-F. Garcia-Gomez (City of Hope, Duarte) for the HLA typing of humanized BLT mice. We also thank E. Maltepe and H. Pektas for providing the syncytiotrophoblast cells. D.W. was supported by the Max Kade Foundation. A.W. received funding from the National Institutes of Health (grant AI123010). J.V.G. received funding from the National Institutes of Health (AI111899 and MH108179). The cardiomyocyte research was partly made possible by a grant from the California Institute for Regenerative Medicine (Grant Number DISC1 09984). Research related to cardiomyocyte immunobiology reported in this publication was supported by National Heart, Lung, and Blood Institute of the National Institutes of Health under award number R01HL140236. L.L.L. is an American Cancer Society Professor funded by NIH AI068129 and in part by the Parker Institute for Cancer Immunotherapy. S.S. and T.D. received funding for the cardiomyocyte research from the California Institute for Regenerative Medicine (Grant Number DISC1 09984) and for the immunobiology work from the National Heart, Lung, and Blood Institute of the National Institutes of Health under award number R01HL140236. The contents of this publication are solely the responsibility of the authors and do not necessarily represent the official views of the NIH, CIRM and other agencies of the State of California.

Author contributions

T.D. and S.S. designed the experiments, supervised the project, and wrote the manuscript. X.H. performed the adaptive and innate immunobiology experiments, molecular biology and imaging studies and cell culture work and analyzed the data. A.G. performed imaging studies and analyzed the data. D.W. performed the in vivo and immunofluorescence imaging studies (confocal microscopy) and histopathology. G.T. performed imaging studies and cell injections. C.D. and W.O.T. generated BLT mice and performed the BLT imaging experiments. A.W. and J.V.G. designed and supervised the experiments using BLT mice. W.O.T. and C.D. performed the experiments using BLT mice. H.R., M.M.D. and L.L.L. gave technical support and conceptual advice. All authors contributed to editing the manuscript.

Competing interests

The authors declare no competing interests.

Additional information

Supplementary information is available for this paper at https://doi.org/10.1038/s41587-019-0016-3.

Reprints and permissions information is available at www.nature.com/reprints.

Correspondence and requests for materials should be addressed to S.S.

Publisher's note: Springer Nature remains neutral with regard to jurisdictional claims in published maps and institutional affiliations.

© The Author(s), under exclusive licence to Springer Nature America, Inc. 2019

Methods

Syncytiotrophoblast cells of mouse placenta. On isolated mouse syncytiotrophoblast cells, expression of MHC class I, MHC class II and Cd47 was performed using PCR RNA was isolated with the RNeasy Plus Mini kit (Qiagen) according to the manufacturer's protocol. RT–PCR was performed to generate the cDNA (Applied Biosystems). The following primers were used: mouse MHC class I: 5′-AGTGGTGCTGCAGAGCATTACAA 3′, reverse: 5′-GGTGACTTCACCTTTAGATCTGGG-3′, MHC class II forward: 5′-GATGTGGAAGACCTGCG-3′, reverse 5′-TGCATCTTCTGAGGGGTTTC-3′; mouse Cd47 forward: 5′-GGCGCAAAGCACCGAAGAAATGTT-3′, reverse: 5′-CCATGGCATCGCGCTTATCCATTT-3′. PCRs were performed on Mastercycler nexus (Eppendorf) and the amplification products were visualized by 2% agarose gel electrophoresis (Thermo Fisher).

Derivation of mouse iPSCs. Mouse tail tip fibroblasts of mice were dissociated and isolated with collagenase type IV (Life Technologies) and maintained with Dulbecco's modified Eagle medium (DMEM) containing 10% fetal bovine serum (FBS), 1% glutamine, 4.5 g l^{-1} glucose, 100 U ml^{-1} penicillin, and 100 µg ml^{-1} streptomycin (pen strep) at 37 °C, 20% O_2, and 5% CO_2 in a humidified incubator 1 × 10^6 mouse fibroblasts were then re-programmed using a mini-intronic plasmid carrying sequences of Oct4, Klf4, Sox2 and c-Myc as well as short hairpin RNA against p53 (1 0 12 µM of DNA) using the Neon Transfection system[13]. After transfection, fibroblasts were plated on mitomycin-inhibited CF1 mouse embryonic fibroblasts (MEF, Applied Stemcell) and kept in fibroblast media with the addition of sodium butyrate (0.2 mM) and 50 µg ml^{-1} ascorbic acid. When ESC-like colonies appeared, media was changed to mouse iPSC media containing DMEM + GlutaMax 31966 (Gibco) with 10% heat-inactivated fetal calf sera (FCS hi), 1% MEM-NEAA and 1% pen-strep (all Gibco). With every passage, the iPSCs were sorted for the mouse pluripotency marker SSEA-1 using antibody-coated magnetic bead based cell sorting

Mouse iPSC culture After the MEF feeder cells attached and were 100% confluent, miPSCs were grown on MEF in knockout DMEM 10829 with 15% knockout Serum Replacement, 1% glutamine, 1% MEM-NEAA, 1% pen-strep (all Gibco), 0.2% beta-mercaptoethanol and 100 units LIF (both Millipore). Cells were maintained in 10 cm dishes, medium was changed daily and the cells were passaged every 2–3 days using 0.05% trypsin-EDTA (Gibco). miPSCs were cultured on gelatin (Millipore) without feeders before experiments using the standard media. Cell cultures were regularly screened for mycoplasma infections using the MycoAlert Kit (Lonza).

Pluripotency analysis by RT–PCR and immunofluorescence. miPSC were plated in confocal dishes (MatTek) for immunofluorescence analysis 48h after plating using the miPSC Characterization kit (Applied Stemcell). Briefly, cells were fixed, permeabilized, and stained overnight at 4 °C with the primary antibodies for Sox2, SSEA-1 and Oct4. After several washes the cells were incubated with a secondary antibody and DNA staining solution. Alkaline phosphatase activity assay was performed (Applied Stemcell) Stained cells were imaged using a fluorescent microscope

For RT–PCR, RNA was extracted using the RNeasy Plus Mini Kit (Qiagen). Genomic DNA contamination was removed using the gDNA spin column. cDNA was generated using Applied Biosystems High-Capacity cDNA Reverse Transcription kit. Gene-specific primers of the miPSC Characterization Kit (Applied Stemcell) were used to amplify target sequences. Actin was used as housekeeping gene, which encodes a cellular cytoskeleton protein. PCR reactions were performed on Mastercycler nexus (Eppendorf) and visualized on 2% agarose gels.

Pluripotency analysis by in vivo teratoma assay. Ten million miPSCs were injected intramuscular into the hind limb of immunodeficient SCID-beige mice and teratoma development was observed within 14days. Teratomas were recovered and fixed in 4% paraformaldehyde in PBS, dehydrated, embedded in paraffin, and cut into sections of 5 µm thickness. For histopathology, sections were rehydrated and stained with hematoxylin and eosin (Carl Roth). Images were taken with an inverted light microscope.

Immunofluorescence staining demonstrated differentiation into ectodermal, mesodermal, and endodermal cells using antibodies against brachyury (ab20680, Abcam), cytokeratin 8 (ab 192467) and GFAP (GA5, Cell Signaling). For visualization, secondary antibodies conjugated with Alexa Fluor 555, 488 and 647 (all Invitrogen) were used, respectively Cell nuclei were counterstained with 4,6-diamidino-2-phenylindole (DAPI) and imaging was performed with a Leica SP5 laser confocal microscope (Leica).

Gene editing of mouse iPSCs. miPSCs underwent three gene modification steps. First, CRISPR guides targeting the coding sequence of mouse *B2m* gene were annealed and ligated into vectors containing the Cas9 expression cassette. Transfected miPSCs were dissociated to single cells, expanded to colonies, sequenced and tested for homogeneity. Second, these $B2m^{-/-}$ miPSCs were transfected with vectors containing CRISPR guides targeting *Ciita*. Expanded single cell colonies were sequenced and $B2m^{-/-}Ciita^{-/-}$ clones were identified through the presence of aberrant sequence from the CRISPR cleavage site. Third, the *Cd47* gene sequence was synthesized and the DNA was cloned into a lentiviral with blasticidin resistance $B2m^{-/-}Ciita^{-/-}$ miPSCs were transduced with the resulting lentivirus and grown in the presence of blasticidin. Antibiotic-selected pools were tested for Cd47 overexpression and $B2m^{-/-}Ciita^{-/-}$ Cd47 tg miPSCs were expanded.

Generation of $B2m^{-/-}$ miPSCs. CRIPSR technology was used for disruption of the *B2m* gene. For targeting the coding sequence of mouse *B2m* gene, the CRISPR sequence 5′-TTCGGCTTCCCATTCTCCGG(TGG)-3′ was annealed and ligated into the All-In-One (AIO) vectors containing the Cas9 expression cassette as per the kit's instructions (GeneArt CRISPR Nuclease Vector Kit, Thermo Fisher). miPSC were transfected with the AIO vectors using Neon electroporation with two 1,200 V pulses of 20 ms duration. The transfected iPSC cultures were dissociated to single cells using 0.05% trypsin (Gibco) and then sorted with FACSAria cell sorter (BD Bioscience) for removing doublets and debris by selective gating on forward and side light scatter properties. Single cells were expanded to full-size colonies and tested for CRISPR editing by screening for the presence of the altered sequence from the CRISPR cleavage site. Briefly, the target sequence was amplified via PCR using AmpliTaq Gold Master Mix (Applied Biosystems) and the primers B2m gDNA forward: 5′-CTGGATCAGACATATGTGTTGGGA 3′, reverse: 5′-GCAAAGCAGTTTTAAGTCCACACAG-3′. After cleanup of the obtained PCR product (PureLink Pro 96 PCR Purification Kit, Thermo Fisher), Sanger sequencing was performed. The Ion Personal Genome Machine (PGM) Sequencing was used for the identification of the homogeneity, through sequencing of a PCR amplified 250 base pair region of the *B2m* gene usingprimers B2m gDNA PGM forward: 5′-TTTTCAAAATGTGGGTAGACTTTGG 3′ and reverse: 5′-GGATTTCAATGTGAGGCGGGT-3′. The PCR product was purified as described above and prepared using the Ion PGM Hi-Q Template Kit (Thermo Fisher). Experiments were performed on the Ion PGM System with the Ion 318 Chip Kit v.2 (Thermo Fisher).

Generation of $B2m^{-/-}Ciita^{-/-}$ miPSCs. CRIPSR technology was used for the further disruption of the *Ciita* gene. For targeting the coding sequence of mouse *Ciita* gene, the CRISPR sequence 5'- GGTCCATCTGGTCATAGAGG (CGG)-3′ was annealed and ligated into the All-In-One (AIO) vectors containing the Cas9 expression cassette as per the kit's instructions (GeneArt CRISPR Nuclease Vector Kit, Thermo Fisher). miPSC were transfected with the AIO vectors using the same condition for *B2m* disruption. The transfected miPSC cultures were dissociated to single cells using 0.05% trypsin (Gibco) and then sorted with FACSAria cell sorter (BD Bioscience) for removing doublets and debris by selective gating on forward and side light scatter properties. Single cells were expanded to full-size colonies and tested for CRISPR editing by screening for the presence of an altered sequence from the CRISPR cleavage site Briefly, the target sequence was amplified via PCR using AmpliTaq Gold Master Mix (Applied Biosystems) and the primers Ciita gDNA forward: 5′-CCCCCAGAACGATGAGCTT 3′, reverse: 5′-TGCAGAAGTCCTGAGAAGGCC 3′. After cleanup of the obtained PCR product (PureLink Pro 96 PCR Purification Kit, Thermo Fisher), Sanger sequencing was performed. Using the DNA sequence chromatogram, edited clones were then identified through the presence of altered sequence from the CRISPR cleavage site Indel size was calculated using the TIDE tool. PCR and ICC were performed again to verify the pluripotency status of the cells.

Generation of $B2m^{-/-}Ciita^{-/-}$ Cd47 tg miPSCs. Cd47 transgene overexpression was generated using lentivirus-mediated delivery of a Cd47-expressing vector containing the antibiotic resistance cassette blasticidin. The Cd47 cDNA was synthesized and cloned into the lentiviral plasmid pLenti6/V5 (Thermo Fisher) with a blasticidin resistance Sanger sequencing was performed to verify that no mutation had occurred. Lentivirus generation was performed with a stock titer of 1 × 10^7 TU per ml. The transduction was performed into 2 × 10^5 $B2m^{-/-}Ciita^{-/-}$ miPSCs, grown on blasticidin-resistant MEF cells for 72 h with a MOI ratio of 1:10 followed by antibiotic selection with 12.5 µg ml^{-1} blasticidin for 7 days. Antibiotic-selected pools were tested by RT–quantitative PCR amplification of Cd47 mRNA and flow cytometry detection of Cd47 on the surface of the cells. After the confirmation ofCd47, cells were expanded and validated by running pluripotency assays.

Transduction to express firefly luciferase. iPSCs were transduced to express Fluc. One hundred thousand miPSCs were plated in one gelatin coated six well plates and incubated overnight at 37 °C at 5% CO_2. The next day, media was changed and one vial of Fluc lentiviral particles expressing luciferase II gene under re-engineered EF1a promotor (GenTarget) was added to 1.5 ml media. After 36h, 1 ml of cell media was added. After further 24 h, complete media change was performed. After 2 days, luciferase expression was confirmed by adding D-luciferin (Promega). Signals were quantified with IVIS 200 (Perkin Elmer) in maximum photons s^{-1} cm^{-2} sr^{-1}

Karyotyping. Cell collection, slide preparation and G-banded karyotyping were performed using standard cytogenetics protocols optimized for human pluripotent cells. Cells were incubated with ethidium bromide and colcemid (Gibco) and then trypsinized to detach the cells from the plate The cells were placed in hypotonic solution (0.075 M potassium chloride, 0.559 g KCl in 100 ml water, Millipore), followed by fixation Metaphase cell preparations were stained with Leishman's stain. Karyotype analysis consisted of chromosomes counted in twenty cells with band-by-band analysis of eight cells.

Mice. BALB/c (BALB/cAnNCrl, H2^{d}), C57BL/6 (C57BL/6J, H2^{b}) and SCID beige (CBySmn CB17-Prkdcscid/J) (all 6–12 weeks) were used as recipients for different assays. The number of animals per experimental group is presented in each figure. Mice were purchased from Charles River Laboratories (Sulzfeld) and received humane care in compliance with the Guide for the Principles of Laboratory Animals. Animal experiments were approved by the Hamburg 'Amt für Gesundheit und Verbraucherschutz' or the University of California San Francisco (UCSF) Institutional Animal Care and Use Committee and performed according to local and EU guidelines.

Teratoma assays to study miPSC survival in vivo. Six to eight-week old syngeneic or allogeneic mice were used for transplantation of WT miPSCs or hypoimmunogenic miPSCs. Two million cells were injected in 60 µl saline into the right thigh muscle of the mice. Tumor growth was measured with a caliper every other day until day 30 and from day 30 to day 80 every tenth day They were killed after development of tumors larger than 1.5 cm^{3} or following an observation period of 80 days.

Derivation and characterization of miPSC-derived endothelial cells (miECs). miPSC were plated on gelatin in six-well plates and maintained in mouse iPSC media. After the cells reached 60% confluency, the differentiation was started and media was changed to RPMI-1640 containing 2% B-27 minus Insulin (both Gibco) and 5 µM CHIR-99021 (Selleckchem). On day 2, the media was changed to reduced media: RPMI 1640 containing 2% B-27 minus Insulin (both Gibco) and 2 µM CHIR 99021 (Selleckchem). From day 4 to day 7, cells were exposed to RPMI-1640 EC media. RPMI-1640 containing 2% B-27 minus Insulin plus 50 ng ml^{-1} mouse vascular endothelial growth factor (mVEGF; R&D Systems), 10 ng ml^{-1} mouse fibroblast growth factor basic (mFGFb; R&D Systems), 10 µM Y-27632 (Sigma-Aldrich) and 1 µM SB 431542 (Sigma-Aldrich) Endothelial cell clusters were visible from day 7 and cells were maintained in EGM-2 SingleQuots media (Lonza) plus 10% FCS hi (Gibco), 25 ng ml^{-1} mVEGF, 2 ng ml^{-1} mFGFb, 10 µM Y-27632 (Sigma-Aldrich) and 1 µM SB 431542. The differentiation process was completed after 21 days and undifferentiated cells detached during the differentiation process. For purification, cells went through magnetic-activated cell separation (MACS) purification according the manufacturer's protocol using anti-CD15 mAb-coated magnetic microbeads (Miltenyi) for negative selection.

The highly purified miECs in the flow through were cultured in EGM-2 SingleQuots media plus supplements and 10% FCS hi. TrypLE was used for splitting the cells 1:3 every 3–4 days. Their phenotype was confirmed by immunofluorescence for CD31 (ab28364, Abcam) and VE-Cadherin (sc 6458, Santa Cruz Biotechnology). Briefly, cells were fixed with 4% paraformaldehyde in PBS for 15 min. Cell membranes were permeabilized with Permeabilization solution (ASB-0102, Applied StemCell), followed by Blocking solution (ASB-0103, Applied StemCell) and incubation with the primary antibodies. For visualization, cells were incubated with secondary antibody conjugated with AF488 or AF555 (Invitrogen). After nuclei staining with DAPI, images were obtained and analyzed with a Leica SP5 laser confocal microscope (Leica).

Tube formation assay was performed for miEC characterization: 2.5 × 10^{5} miECs were stained with 5 µM CFSE and 0.1 µg ml^{-1} Hoechst (both Thermo Fisher) for 10 min at room temperature and plated on 10 mg ml^{-1} undiluted Matrigel (356231, Corning) in 24-well plates After 48 h, tube formations were visualized by immunofluorescence. PCR was performed as described above. The following primers were used: VE Cadherin forward: 5′ GGATGCAGAGGCTCACAGAG-3′, reverse: 5′-CTGGCGGTTCACGTTGGACT-3′.

Derivation and characterization of miPSC-derived smooth muscle cells (miSMCs). The resuspended miPSCs were cultivated on six-well, 0.1% gelatin-coated plastic petri dishes (Falcon, Becton–Dickinson) at 2 × 10^{6} cells per well at 37 °C, 5% CO$_2$ in 2 ml of differentiation medium with the presence of 10 µM all-trans-retinoic acid The differentiation medium was made of DMEM, 15% FCS, 2 mM L-glutamine, 1 mM methyl thioglycolate (MTG) (Sigma-Aldrich), 1% non-essential amino acids and pen-strep The culture was continued for 10 days with daily media changes Starting from the 11th day, the differentiation medium was replaced by serum-free culture medium, which was composed of knock-out DMEM, 15% knock-out serum replacement, 2 mM L-glutamine, 1 mM MTG, 1% non-essential amino acids and pen-strep. The cultures were continued for another 10 days with daily change of the serum free medium. For purification, cells were enriched according the manufacturer's protocol using anti-CD15 mAb-coated magnetic microbeads (Miltenyi) for negative selection. The flow-through containing enriched miSMCs were cultured in RMPI-1640 Glutamax plus 20% FCS hi and 1% pen-strep (all Gibco). Their phenotype was confirmed by immunofluorescence and PCR for both Sma and Sm22.

Immunofluorescence staining was performed as described above. Primary antibodies were used against smooth muscle actin (ab21027, Abcam) and sm22 (ab14106, Abcam), followed by the corresponding secondary antibody conjugated with AF488 or AF555 (Invitrogen).

PCR was performed as described above. The following primers were used: SMA forward: 5′-CGGCTTCGCTGGTGATGAT-3′, reverse: 5′-CATTCCAACCATTACTCCCTGAT-3′; SM22 forward: 5′-AACAGCCTGTACCCTGATGG-3′, reverse: 5′-CGGTAGTGCCCATCATTCTT-3′.

Derivation and characterization of miPSC-derived cardiomyocytes (miCMs). Before differentiation, miPSCs were passaged two times on gelatin coated flasks to remove the feeder cells. At day 0, differentiation was started with 80,000 cells per ml in IMEM/Ham's F12 (3/1, both Corning) +0.5% N2-Supplement, 1% B27 retinoic acid, 0.05% BSA, 1% pen-strep, 1% glutamine (Gibco), 5 mg ml^{-1} ascorbic acid and 40 ng ml^{-1} MTG (both Sigma-Aldrich) for 2 days in uncoated 10 cm plates At day 2, cells were transferred in IMEM/Ham's F12 (3/1, both Corning) with 0.5% N2-Supplement, 1% B27 retinoicacid, 0.05% BSA, 1% pen-strep, 1% glutamine (all Gibco), 5 mg ml^{-1} ascorbic acid and 40 ng ml^{-1} MTG (Sigma-Aldrich) for 2 days in uncoated 10 cm plates. On day 4, cells were plated in gelatin-coated six-well plates in SP34 media containing 1% glutamine, 50 µg ml^{-1} ascorbic acid, 5 ng ml^{-1} VEGF, 500 µg ml^{-1} hFGFb and 25 ng ml^{-1} hFGF10 (R&D Systems) Media was changed on day 7 to SP34 media containing 1% glutamine and 50 µg ml^{-1} ascorbic acid and was changed every other day. Beating of cells started around days 11–14 and demonstrated their function.

For enrichment, cells separated by MACS according the manufacturer's protocol using anti-CD15 mAb-coated magnetic microbeads (Miltenyi) for negative selection. The flow-through containing enriched miCMs were replated and used for different assays.

Immunofluorescence staining was performed as described above to confirm their phenotype. Primary antibodies were used against α-sarcomeric actinin (EA-53, Abcam) or troponin I (ab47003, Abcam) followed by the corresponding secondary antibody conjugated with AF488 or AF555 (Invitrogen).

PCR for Gata4 forward: 5′-CTGTCATCTCACTATGGGCA-3′, reverse: 5′-CCAAGTCCGAGCAGGAATTT-3′ and Mhy6 forward: 5′-ATCATTCCCAACGAGCGAAAG-3′, reverse: 5′-AAGTCCCCATAGAGAATGCGG-3′ was performed as described above.

Flow cytometry analysis. For the detection of MHC class I and II surface molecules on miPSCs, miECs, miSMCs and miCMs, cells were plated on gelatin-coated six-well plates in medium containing 100 ng ml^{-1} of IFN-γ. After collection, cells were labeled with antibodies. For MHC class I: PerCP-eFlour710-labeled anti-MHC class I antibody (clone AF6-88.5.5.3, eBioscience) or PerCP-eFlour710-labeled mouse IgG2b isotype-matched control antibody (clone eB149/10H5, eBioscience). The anti-MHC class I antibody reacts with the H-2K^{b} MHC class I alloantigen. For MHC class II: PerCP-eFlour710-labeled anti-MHC class II antibody (clone M5/114.15.2, eBioscience) or PerCP-eFlour710-labeled mouse IgG2a isotype-matched control antibody (clone eBM2a, eBioscience). The MHC class II antibody reacts with the mouse MHC class II, both I-A and I-E subregion encoded glycoproteins. Cd47: Alexa Fluor 647-labeled anti-mouse Cd47 antibody (clone miap301, BD Biosciences) or Alexa Fluor 647-labeled mouse IgG2a isotype-matched control antibody (clone R35-95, BD Biosciences). The anti-Cd47 antibody specifically binds to the extracellular domain of mouse Cd47, also known as Integrin-Associated Protein Cells were analyzed by flow cytometry (BD Bioscience) and results were expressed as fold change to isotype-matched control Ig staining.

For the assessment of purity of miPSC derivatives, antibodies against SSEA-1 (Thermo Fisher), VE-Cadherin (Sigma), SMA (Abcam) and Troponin I (Santa Cruz) were used. The miECs, miSMCs and miCMs were generated with a purity of >90%

Elispot assays. For uni-directional Elispot assays, recipient splenocytes were isolated from spleen 5 days after cell injection and used as responder cells. Donor cells were mitomycin-treated (50 µg ml^{-1} for 30 min) and used as stimulator cells. One hundred thousand stimulator cells were incubated with 1 × 10^{6} recipient responder splenocytes for 24h and IFN-γ and Il-4 spot frequencies were enumerated using an Elispot plate reader.

Donor-specific antibodies. Sera from recipient mice were de-complemented by heating to 56 °C for 30 min. Equal amounts of sera and cell suspensions (5 × 10^{6} ml) were incubated for 45 min at 4 °C. Cells were labeled with FITC-conjugated goat anti-mouse IgM (Sigma-Aldrich) and analyzed by flow cytometry (BD Bioscience).

Mouse NK cell Elispot assays in vitro. NK cells were isolated from fresh BALB/c spleen 18 h after poly I:C injection (150 ng poly I:C in 200 µl sterile saline, intraperitoneally, Sigma-Aldrich). After red cell lysis, cells were purified by anti-CD49b mAb-coated magnetic bead sorting and were used as responder cells. This cell population was >99% CD3- and contains NK cells (>90%) and other cells including myeloid cells (<10%). Using the Elispot principle, NK cells were co-cultured with $B2m^{-/-}Ciita^{-/-}$ or $B2m^{-/-}Ciita^{-/-}$ Cd47 tg miPSCs in the presence of IL-2 (1 ng ml^{-1}, Peprotech) and their IFN-γ release was measured. YAC-1 cells (Sigma-Aldrich) served as positive control. Mitomycin-treated (50 μg ml^{-1} for 30 min) stimulator cells were incubated with NK cells (1:1) for 24 h and IFN-γ spot frequencies were enumerated using an Elispot plate reader.

Mouse in vivo innate cytotoxicity assay. Five million WT miPSCs and 5×10^6 $B2m^{-/-}Ciita^{-/-}$ miPSCs or 5×10^6 $B2m^{-/-}Ciita^{-/-}$ Cd47 tg miPSCs were mixed and stained with 5 μM CFSE. Cells in saline with IL-2 (1 ngml^{-1}, Peprotech) were injected intraperitoneally into syngeneic C57BL/6 mice. After 48 h, cells were collected from the abdomen and stained with PerCP-eFlour710 labeled anti-MHC class I mAb for 45 min at 4 °C. The CFSE positive and MHC class 1-negative population was analyzed by flow cytometry (BD Bioscience) and compared between the WT and the engineered miPSC group. The assay was performed with miPSCs, miECs, miSMCs and miCMs. Some animals were pretreated with clodronate (200 μl intraperitoneally 3 days before the experiment; Liposoma) to eliminate macrophages and make the assay more specific for NK cells. Some animals were pretreated with in vivo Cd47 blocking antibody (BE0270, 100 μg intraperitoneally, 7 days and 3 days before the experiment; BioXCell) to eliminate Cd47.

NK cell stimulatory ligands. For the detection of NK cell stimulatory ligands on miPSCs, miECs, miSMCs and miCMs, cells were blocked with mouse FcR blocking reagent (Miltenyi) according to manufacturer's protocol. WT cells, $B2m^{-/-}Ciita^{-/-}$ cells and $B2m^{-/-}Ciita^{-/-}$ Cd47 tg cells were then incubated with the recombinant mouse NKp46 or NKG2D human Fc chimera protein or the recombinant control IgG1 Fc protein (R&D systems) for 45min at 4 °C. FITC-conjugated anti-human IgG1 antibody (Invitrogen) served as secondary antibody. YAC-1 cells were used as positive control. Data analysis was carried out using flow cytometry (BD Bioscience) and FlowJo software, and results were expressed as fold change to the isotype-matched control Fc fusion protein.

Survival analysis of differentiated derivatives using BLI. For BLI, D-luciferin firefly potassium salt (375mgkg^{-1}; Biosynth) was dissolved in PBS (pH7.4) (Gibco, Invitrogen) and was injected intraperitoneally (250μl per mouse) into anesthetized mice. Animals were imaged using the IVIS 200 system (Xenogen). Region of interest (ROI) bioluminescence was quantified in units of maximum photons per second per centimeter square per steradian (p s^{-1} cm^{-2} sr^{-1}). The maximum signal from an ROI was measured using Living Image software (MediaCybernetics). Mice were monitored on day 0, day 1 and every other day until day 30 and every 10 days afterwards.

Matrigel plugs: cell morphology for miECs, miSMCs or miCMs. Eight hundred thousand $B2m^{-/-}Ciita^{-/-}$ Cd47 tg miECs, miSMCs or miCMs in 1:1 diluted Matrigel (Corning) were injected into allogeneic BALB/c mice. Matrigel plugs were recovered after 1, 2, 3, 4, 5, 6 and 8 weeks and fixed in 4% paraformaldehyde in PBS with 1% glutaraldehyde for 24h. Samples were dehydrated, embedded in paraffin and cut into sections of 5 μm thickness. For histopathology, sections were stained with hematoxylin and eosin (Carl Roth) and images taken with an inverted light microscope. Origin of cells was demonstrated with immunofluorescence staining. Sections were rehydrated, and underwent antigen retrieval and blocking. Samples were incubated with antibodies against luciferase (ab21176), SMA (ab21027, Abcam), VE-Cadherin (SC-6458) or α-sarcomeric actinin (EA-53, Abcam) and a corresponding secondary antibody conjugated with AF488 or AF555 (Invitrogen). Cell nuclei were counterstained with DAPI and images taken with a Leica SP5 laser confocal microscope (Leica).

For co-staining experiments of miECs and immune cells, primary antibodies were used against VE-Cadherin (SC-6458, Sigma) and CD3 (ab16669, Abcam), followed by the corresponding secondary antibody conjugated with AF488 or AF555 (Invitrogen).

Generation of human iPSCs (hiPSCs). The Human Episomal iPSC Line was derived from CD34$^+$ cord blood using a three-plasmid, seven-factor (SOKMNLT; SOX2, OCT4 (POU5F1), KLF4, MYC, NANOG, LIN28 and SV40L T antigen) EBNA-based episomal system by Thermo Scientific. This cell line has been shown to be free of all reprogramming genes. These hiPSCs have a normal XX karyotype and endogenous expression of pluripotent markers including Oct4, SOX2 and NANOG (as shown by RT–PCR) and OCT4, SSEA4, TRA-1-60 and TRA-1-81 (as shown by immunofluorescence).

Gene editing of hiPSC. hiPSC underwent two gene-modification steps. In the first step, CRISPR technology was used for a combined targeting of the coding sequence of human *B2M* gene with the CRISPR sequence 5′-CGTGAGTAAACCTGAATCTT-3′ and the coding sequence of human *CIITA* gene with the CRISPR sequence 5′-GATATTGGCATAAGCCTCCC-3′. Linearized CRISPR sequence with T7 promoter were used to synthesize gRNA as per the kit's instructions (MEGAshortscript T7 Transcription Kit, Thermo Fisher). The obtained in vitro transcription (IVT) gRNA was then purified via the MEGAclear Transcription Clean-Up Kit. For IVT gRNA delivery, cells were electroporated with 300ng IVT gRNA using a Neon electroporation system and the conditions 1,200 V, 30 ms, 1 pulse into hiPSC stably expressing Cas9. After electroporation, edited hiPSC were expanded for single cell seeding: hiPSC cultures were dissociated into single cells using TrypLE Express (Gibco) and stained with Alexa Fluor 488-conjugated anti-TRA-160 mAb and propidium iodide. A FACSAria II cell sorter (BD Biosciences) was used for the sorting and doublets and debris were excluded from seeding by selective gating on forward and side light scatter properties. Viable pluripotent cells were selected on the absence of propidium iodide and presence of Tra1-60 staining. Single cells were then expanded into full-size colonies, after which the colonies were tested for CRISPR editing by sequencing. CRISPR-mediated cleavage was assessed using the GeneArt Genomic Cleavage Detection Kit (Thermo Fisher) for testing of the initial edited pools. For screening of the isolated clones, genomic DNA was isolated from 1×10^6 hiPSCs and the *B2M* and *CIITA* genomic DNA regions were PCR amplified using AmpliTaq Gold 360 Master Mix and the primer sets forward: 5′-TGGGGCCAAATCATGTAGACTC-3′ and reverse: 5′-TCAGTGGGGGTGAATTCAGTGT-3′ for *B2M* as well as forward: 5′-CTTAACAGCGATGCTGACCCC-3′ and reverse: 5′-TGGCCTCCATCTCCCCTCTCTT-3′ for *CIITA*. For TIDE analysis, the obtained PCR product was cleaned up (PureLink PCR Purification Kit, Thermo Fisher) and Sanger sequencing was performed for the prediction of indel frequency. After the confirmation of *B2M* and *CIITA* disruption, cells were further characterized through karyotype analysis and the TaqMan hiPSC Scorecard Panel (Thermo Fisher). The hiPSCs were found to be pluripotent and maintained a normal (46,XX) karyotype during the genome editing process.

In the second step, the CD47 cDNA was synthesized and the DNA was cloned into a lentiviral plasmid with an EFS promotor and puromycin resistance cassette. Cells were transduced with lentiviral stocks and 8 μgml^{-1} of Polybrene (Thermo Fisher). Media was changed daily after transduction. Three days after transduction, cells were expanded and selected with 0.5 μgml^{-1} of puromycin. After 5 days of antibiotic selection, antibiotic-resistant colonies emerged and were further expanded to generate stable pools. The expression of CD47 transcripts was confirmed by quantitative PCR. Pluripotency assay (TaqMan hPSC Scorecard Panel, Thermo Fisher) and karyotyping was performed again to verify the pluripotent status of the cells.

Teratoma assays to study iPSC survival in vivo. Six to eight week-old immunodeficient SCID-beige mice were used for transplantation of WT hiPSC or $B2M^{-/-}CIITA^{-/-}$ CD47 tg hiPSCs. Here 1×10^7 cells were resuspended in 100 μl saline solution and injected into the right thigh muscle of the mice. Teratomas were recovered, fixed in 4% paraformaldehyde, dehydrated, embedded in paraffin and cut into sections of 5 μm thickness. For histopathology, sections were rehydrated and stained with hematoxylin and eosin. Images were taken with an inverted light microscope. For immunofluorescence, slides underwent heat-induced antigen retrieval in a steamer with Dako antigen-retrieval solution (Dako), followed by antigen blocking with Image-iT FX signal enhancer solution (Invitrogen). Tissue sections were incubated with a primary antibody against brachyury (Ab20680, Abcam), followed by a goat anti-rabbit IgG secondary antibody conjugated with Alexa Fluor 555 (Invitrogen). Subsequently, sections were incubated with primary antibodies against cytokeratin 8 (EP1628Y, Abcam) and GFAP (GA5, Cell Signaling) conjugated with AF488 or AF647, respectively. DAPI was used to counterstain cell nuclei and images were acquired with a Leica SP5 laser confocal microscope (Leica).

Pluripotency analysis by RT–PCR and immunofluorescence. hiPSCs were plated in confocal dishes (MatTek) for immunofluorescence analysis 48 h after plating using the hiPSC Characterization Kit (Applied Stem Cell). Briefly, cells were fixed, permeabilized and stained overnight at 4 °C with the primary antibodies for OCT4, SOX2, SSEA4, TRA-1-60 and TRA-1-81 (Applied Stem Cell). After several washes, the cells were incubated with a secondary antibody and DNA staining solution. Alkaline phosphatase activity assay was performed (Applied Stem Cell). Stained cells were imaged using a fluorescent microscope.

For RT–PCR, RNA was extracted using the RNeasy Plus Mini Kit (Qiagen). Genomic DNA contamination was removed using the gDNA spin column. cDNA was generated using Applied Biosystems High-Capacity cDNA Reverse Transcription Kit. Gene-specific primers of the hiPSC Characterization Kit (Applied Stem Cell) were used to amplify target sequences. Actin was used as housekeeping gene. PCR reactions were performed on Mastercycler nexus (Eppendorf) and visualized on 2% agarose gels.

Humanized mice. Humanized NSG-SGM3 mice (18–30weeks) were purchased from Jackson Laboratories. Human CD34$^+$ hematopoietic stem cell-engrafted NSG-SGM3 mice develop multi-lineage human immune cells, and demonstrate a functional human immune system displaying T cell-dependent immune responses with no donor cell immune reactivity towards the host. Animals were randomly assigned to experimental groups. The percentage of CD3$^+$ cells among the human CD45$^+$ cell population was assessed in every animal and CD3 percentages were never significantly different between WT and $B2M^{-/-}CIITA^{-/-}$ CD47 tg groups (Supplementary Fig. 13a). The number of animals per experimental group is presented in each figure. All humanized NSG-SGM3 mice were HLA A typed and the number of mismatches to the cell graft calculated (Supplementary Fig 13b). In the Elispot assays with hiPSCs, there were 1.6 ± 0.5 and 1.7 ± 0.5 ($P = 0.61$), with hiCMs 1.3 ± 0.6 and 1.3 ± 0.6 ($P = 1$) mismatches for WT and $B2M^{-/-}CIITA^{-/-}$ CD47 tg, respectively, and in the hiEC groups there were always two mismatches. The mismatches for the BLI experiments are shown in Supplementary Fig. 10j.

All BLT mice were approved by the University of North Carolina at Chapel Hill Institutional Animal Care and Use Committee and were generated with the same human tissue using NSG mice (NOD Cg-$Prkdc^{scid}$ $Il2rg^{tm1Wjl}$/SzJ, Jackson Laboratories) and there were five out of six HLA class I and 4 out of 4 class II mismatches to the transplanted hiPSCs or derivatives. The percentage of CD3^{+} cells among the human CD45^{+} cell population was never significantly different between WT and $B2M^{-/-}CIITA^{-/-}$ CD47 tg groups (Supplementary Fig. 13c). The percentage of CD3^{+} cells among the human CD45^{+} cell population was typically in the 15–65% range

Human iPSC differentiation into hiECs. hiPSC were plated on diluted Matrigel (356231, Corning) in six-well plates and maintained in Essential 8 Flex media (Thermo Fisher). The differentiation was started at 60% confluency and media was changed to RPMI-1640 containing 2% B-27 minus insulin (both Gibco) and 5 μM CHIR 99021 (Selleckchem). On day 2, the media was changed to reduced media: RPMI-1640 containing 2% B-27 minus insulin (Gibco) and 2 μM CHIR 99021 (Selleckchem). From day 4 to 7, cells were exposed to RPMI-1640 EC media, RPMI-1640 containing 2% B-27 minus insulin plus 50 ng ml^{-1} human vascular endothelial growth factor (VEGF; R&D Systems), 10 ng ml^{-1} human fibroblast growth factor basic (FGFb; R&D Systems), 10 μM Y-27632 (Sigma-Aldrich), and 1 μM SB 431542 (Sigma Aldrich). Endothelial cell clusters were visible from day 7 and cells were maintained in EGM-2 SingleQuots media (Lonza) plus 10% FCS hi (Gibco), 25 ng ml^{-1} VEGF, 2 ng ml^{-1} FGFb, 10 μM Y-27632 (Sigma-Aldrich) and 1 μM SB 431542 (Sigma-Aldrich). The differentiation process was completed after 14 days und undifferentiated cells detached during the differentiation process. For purification, cells were treated with 20 μM PluriSIn 1 (StemCell Technologies) for 48 h. The highly purified ECs were cultured in EGM-2 SingleQuots media (Lonza) plus supplements and 10% FCS hi (Gibco). TrypLE Express was used for passaging the cells 1:3 every 3–4 days.

Immunofluorescence staining was performed as described above to confirm their phenotype. Primary antibodies were used against CD31 (ab28364, Abcam) and VE-Cadherin (sc-6458, Santa Cruz Biotechnology), followed by the corresponding secondary antibody conjugated with AF488 or AF555 (Invitrogen). Cell nuclei were stained with DAPI. Imaging was performed using a Leica SP5 laser confocal microscope (Leica).

PCR for VE-Cadherin (forward: 5′-AAGATGCAGAGGCTCATG 3′, reverse: 5′-CATGAGCCTCTGCATCTT-3′) was performed as described above.

Human iPSC differentiation into hiCMs. hiPSCs were plated on diluted Matrigel (356231, Corning) in six-well plates and maintained in Essential 8 Flex media (Thermo Fisher) Differentiation was started at 90% confluency and media was changed to 5 ml of RPMI-1640 containing 2% B 27 minus Insulin (Gibco) and 6 μM CHIR-99021 (Selleckchem). After 2 days, media was changed to RPMI-1640 containing 2% B 27 minus insulin without CHIR. On day 3, 5 μl IWR1 was added to the media for two further days. At day 5, the media was changed back to RPMI 1640 containing 2% B-27 minus insulin medium and left for 48 h. At day 7, media was changed to RPMI-1640 containing B27 plus insulin (Gibco) and replaced every 3 days thereafter with the same media. Spontaneous beating of cardiomyocytes was first visible around day 10. Purification of cardiomyocytes was performed on day 10 post differentiation. Briefly, media was changed to low glucose media and maintained for 3 days. At day 13, media was changed back to RPMI 1640 containing B27 plus insulin. This procedure was repeated on day 14

Immunofluorescence staining was performed as described above to confirm their phenotype. Primary antibodies were used against α-sarcomeric actinin (EA-53, Abcam) and troponin I (ab47003, Abcam), followed by the corresponding secondary antibody conjugated with AF488 or AF555 (Invitrogen). Cell nuclei were stained with DAPI. Imaging was performed using a Leica SP5 laser confocal microscope (Leica).

PCR for troponin (cTNT, forward: 5′-GAGGCACCAAGTTGGGCATGAACG A 3′, reverse: 5′-GGCAGCGGAAGAGGATGCTGAA′) was performed as described above.

Flow cytometry analysis. Human iPSCs, iCMs and iECs were plated in six well plates in medium containing 100 ng ml^{-1} of IFN γ. Cells were harvested and labeled with antibodies. APC conjugated anti-HLA-A,B,C antibody (clone G 46 2 6,BD Biosciences) or APC-conjugated IgG1 isotype-matched control antibody (clone MOPC-21,BD Biosciences). Alexa flour647-labeled anti-HLA DR,DP DQ antibody (clone Tu3a, BD Biosciences) or Alexa-flour647-labeled IgG2a isotype-matched control antibody (clone G155 178, BD Biosciences). PerCP-Cy5-conjugated anti CD47 (clone B6H12, BD Biosciences) or PerCPCy5-conjugated IgG1 isotype-matched control antibody (clone MOPC-21, BD Biosciences). Results were expressed as fold change to isotype-matched control Ig staining

For the assessment of purity of hiPSC derivatives, antibodies against TRA-1-60 (Thermo Fisher), VE-Cadherin (Santa Cruz) and Troponin I (Santa Cruz) were used. The hiECs and hiCMs were generated with a purity of >95%.

Human NK cell Elispot assays. Human NK cells were co cultured with $B2M^{-/-}CIITA^{-/-}$ or $B2M^{-/-}CIITA^{-/-}$ CD47 tg hiPSC and their IFN-γ release was measured. Human NK cells were purchased from StemCell Technologies and were >99% CD3- and 95% CD56^{+}. Flow cytometry revealed >95% NK cells and <5% other cells including myeloid cells Donor cells were mitomycin-treated and used as stimulator cells. K562 cells (Sigma-Aldrich) served as positive control. Stimulator cells were incubated with NK cells (1:1) in RPMI-1640 containing 1% pen-strep and 1 ng ml^{-1} human IL 2 (Peprotech) for 24 h and IFNγ spot frequencies were enumerated using an Elispot plate reader.

T cell Elispot using humanized mice. For uni-directional Elispot assays, recipient splenocytes were isolated from humanized mice 5 days after cell injection and used as responder cells. Cells were incubated for 24h in vitro with 1 μg ml^{-1} anti-CD3 and 1 μg ml^{-1} anti CD28 before plated for Elispot Assay Donor cells were mitomycin-treated (50 μg ml^{-1} for 30 min) and used as stimulator cells. One hundred thousand stimulator cells were incubated with 1 × 10^{6} recipient responder splenocytes for 48h and IFN γ and IL-5 spot frequencies were enumerated using an Elispot plate reader

DSA. Sera from recipient mice were de-complemented by heating to 56 °C for 30 min. Equal amounts of sera and cell suspensions (5 × 10^{6} per ml) were incubated for 45 min at 4 °C. Cells were labeled with FITC-conjugated goat anti-human IgM (BD Bioscience) and analyzed by flow cytometry (BD Bioscience)

Matrigel plugs: cell morphology. One million $B2M^{-/-}CIITA^{-/-}$ CD47 tg hiECs or hiCMs in 1:1 pro survival scaffold, consisting of 50% (vol/vol) Matrigel (Corning), 100 μM ZVAD (Millipore), 50 nM Bcl-XI BH4 (Millipore), 200 nM cyclosporine A (Sigma-Aldrich), 100 ng ml^{-1} IGF 1 (Peprotech) and 50 μM Pinacidil (Sigma-Aldrich) were injected into humanized NSG-SGM3 mice. Matrigel plugs were recovered after 2, 4, 6 and 8 weeks, fixed in 4% paraformaldehyde in PBS with 1% glutaraldehyde, dehydrated and embedded in paraffin. Sections of 5 μm thickness were cut. For immunofluorescence, sections were rehydrated and underwent antigen retrieval, followed by antigen blocking After incubation with a primary antibody against luciferase (ab21176), VE. Cadherin (SC 6458) or α sarcomeric actinin (EA 53, Abcam), sections were incubated with a corresponding secondary antibody conjugated with AF488 or AF555 (Invitrogen). DAPI was used to counterstain cell nuclei and images were obtained with a Leica SP5 laser confocal microscope (Leica).

BLI. For BLI, D-luciferin firefly potassium salt (375 mg kg^{-1}) (Biosynth) dissolved in sterile PBS (pH 7.4) (Gibco, Invitrogen) was injected intraperitoneally (250 μl per mouse) into anesthetized mice. Animals were imaged using the ami HT (Spectral Instruments Imaging) ROI bioluminescence was quantified in units of maximum photons per second per centimeter square per steradian (p s^{-1} cm^{-2} sr^{-1}). The maximum signal from an ROI was measured using Living Image software (MediaCybernetics). Humanized mice were injected with 5 × 10^{5} or 1 × 10^{6} cells in pro survival scaffold as described above. Mice were monitored on day 0, day 1 and every 4 days until cells were rejected or up to 50 days.

In vitro NK cell killing. Mouse NK cells were isolated from fresh BALB/c or C57BL/6 spleens 18h after poly I C injection (100 μg intraperitoneally). After red cell lysis, NK cells were purified with MagniSort Mouse NK cell Enrichment Kit (Invitrogen), followed by CD49b MACS sorting (Miltenyi). This cell population was highly selected for NK cells with a purity of >9%. Human NK cells from PBMCs were purchased from StemCell Technologies containing >99% NK cells.

NK cell killing assays were performed on the XCelligence SP platform (ACEA BioSciences). 96-well E-plates (ACEA BioSciences) were coated with collagen (Sigma-Aldrich) and 4 × 10^{5} WT, $B2m^{-/-}Ciita^{-/-}$, or $B2m^{-/-}Ciita^{-/-}$ Cd47 tg miECs or WT, $B2M^{-/-}CIITA^{-/-}$ or $B2M^{-/-}CIITA^{-/-}$ CD47 tg hiECs were plated in 100 μl cell-specific media containing 1 ng ml^{-1} mouse or human IL-2 (Peprotech). After the Cell Index value reached 0.7, NK cells were added with an effector cell / target cell (E/T) ratio of 0.5/1, 0.8/1 or 1/1. As a negative control, cell treated with 2% Triton X100 was used Some wells were pretreated with mouse Cd47 or human CD47-blocking antibody (BioXCell) with 10 μg ml^{-1} media for 2 h. Data were standardized and analyzed with the RTCA software (ACEA).

NK cell stimulatory ligands. For the detection of NKG2D, NKp80, NKp46, NKp44 and NKp30 on hiPSCs, hiECs and hiCMs, cells were plated on gelatin-coated six well plates. K562 cells were plated in six-well plates as suspension cells. After harvesting, cells were blocked with human FcR blocking reagent (Miltenyi) according to manufacturer's protocol. Cells were labeled with recombinant human NKG2D, Nkp80, Nkp46, Nkp44 or Nkp30 Fc chimera proteins or the recombinant control IgG1 Fc protein (all R&D Systems) for 45 min at 4 °C, followed by the secondary antibody IgG1 conjugated with FITC (Invitrogen). Data analysis was carried out by Flow Cytometry (BD Bioscience) and results were expressed as fold change to isotype control.

Statistics. All data are expressed as mean ± s.d. or in box blot graphs showing the median and the minimum to maximum range. Intergroup differences were appropriately assessed by either an unpaired Student's *t*-test or a one-way ANOVA with Bonferroni's post-hoc test. Further information on experimental design and reagents is available in the Nature Research Reporting Summary linked to this article.

Reporting Summary. Further information on research design is available in the Nature Research Reporting Summary linked to this article.

Data availability

All data supporting the findings of this study are available in the paper and its Supplementary Information files.

nature biotechnology

SUPPLEMENTARY INFORMATION

https://doi.org/10.1038/s41587-019-0016-3

In the format provided by the authors and unedited.

Hypoimmunogenic derivatives of induced pluripotent stem cells evade immune rejection in fully immunocompetent allogeneic recipients

Tobias Deuse[1,7], Xiaomeng Hu[1,2,3,7], Alessia Gravina[1], Dong Wang[1,2], Grigol Tediashvili[1,2,3], Chandrav De[4], William O. Thayer[4], Angela Wahl[4], J. Victor Garcia[4], Hermann Reichenspurner[2,3], Mark M. Davis[5], Lewis L. Lanier[6] and Sonja Schrepfer[1*]

[1]Department of Surgery, Division of Cardiothoracic Surgery, Transplant and Stem Cell Immunobiology Lab, University of California San Francisco, San Francisco, CA, USA. [2]Department of Cardiovascular Surgery, University Heart Center Hamburg, Hamburg, Germany. [3]Cardiovascular Research Center Hamburg and DZHK (German Center for Cardiovascular Research), Partner Site Hamburg/Kiel/Luebeck, Hamburg, Germany [4]Division of Infectious Diseases, UNC Center for AIDS Research, University of North Carolina School of Medicine, Chapel Hill, NC, USA. [5]Howard Hughes Medical Institute, Institute for Immunity, Transplantation and Infection, and Department of Microbiology and Immunology Stanford University School of Medicine, Stanford, CA, USA. [6]Department of Microbiology and Immunology and the Parker Institute for Cancer Immunotherapy, University of California San Francisco, San Francisco, California, USA. [7]These authors contributed equally: Tobias Deuse, Xiaomeng Hu. *e-mail: Sonja.Schrepfer@ucsf.edu

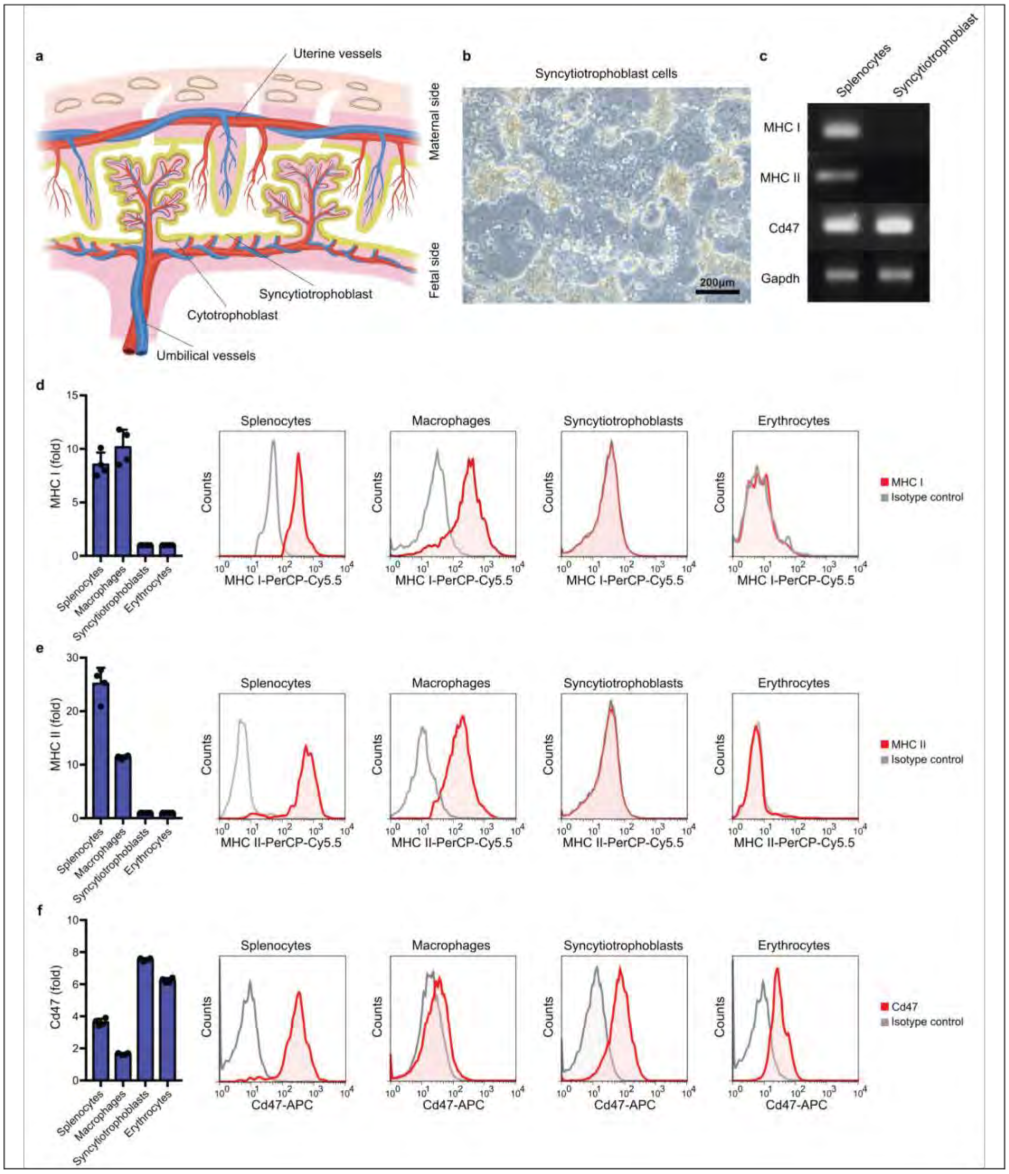
a
Uterine vessels
Maternal side
Fetal side
Syncytiotrophoblast
Cytotrophoblast
Umbilical vessels
b
Syncytiotrophoblast cells
200µm
c
Splenocytes
Syncytiotrophoblast
MHC I
MHC II
Cd47
Gapdh
d
MHC I (fold)
Splenocytes
Macrophages
Syncytiotrophoblasts
Erythrocytes
Counts
MHC I-PerCP-Cy5.5
MHC I
Isotype control
e
MHC II (fold)
MHC II-PerCP-Cy5.5
MHC II
Isotype control
f
Cd47 (fold)
Cd47-APC
Cd47
Isotype control

Supplementary Figure 1

The immune phenotype of syncytiotrophoblast cells.

a, The syncytiotrophoblast is the immediate interface between maternal blood and the fetal side of the placenta. **b**, Mouse syncytiotrophoblast cells were isolated and cultured (representative picture of two independent experiments). **c**, RT-PCR showed depleted MHC class I and II expression, but positive Cd47 expression (representative gel of three independent experiments). **d-f**, The surface expression of MHC class I (d), MHC class II (e), and Cd47 (f) was assessed by flow cytometry (mean ±s.d., 4 independent experiments per group). Representative histograms are shown.

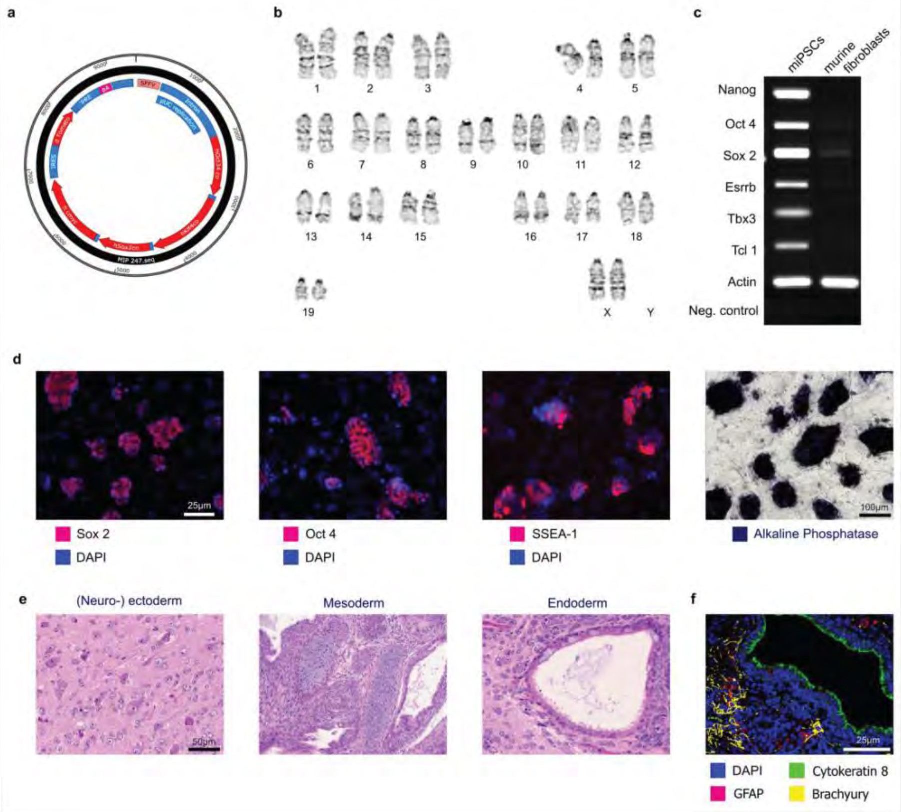
a
SFFV
Intron
pUC replication
pA
IRES
MIP 247.seq
1000
2000
3000
4000
5000
6000
7000
8000
9000
b
1
2
3
4
5
6
7
8
9
10
11
12
13
14
15
16
17
18
19
X
Y
c
miPSCs
murine fibroblasts
Nanog
Oct 4
Sox 2
Esrrb
Tbx3
Tcl 1
Actin
Neg. control
d
25µm
100µm
Sox 2
DAPI
Oct 4
DAPI
SSEA-1
DAPI
Alkaline Phosphatase
e
(Neuro-) ectoderm
Mesoderm
Endoderm
50µm
f
25µm
DAPI
Cytokeratin 8
GFAP
Brachyury

Supplementary Figure 2

The generation of miPSCs.

a, Mouse tail tip fibroblasts were re-programmed using a plasmid expressing the four re-programming factors Oct4, KLF4, Sox2, and c-Myc. **b**, The miPSCs showed a normal 40, XX mouse karyotype in one analysis. **c**, miPSCs showed the typical gene expression profile of pluripotent stem cells (representative gel of two independent experiments). **d**, In immunofluorescence, miPSC cultures were positive for Sox2, Oct4, SSEA-1, and alkaline phosphatase (representative pictures of three independent experiments). **e**, When transplanted into immunodeficient SCID-beige mice, they formed teratomas containing (neuro-) ectoderm, mesoderm, and endoderm (representative pictures of three independent experiments). **f**, Endodermal (cytokeratin 8), mesodermal (brachyury), and ectodermal (GFAP) lineages were demonstrated by confocal immunofluorescence microscopy (representative pictures of three independent experiments).

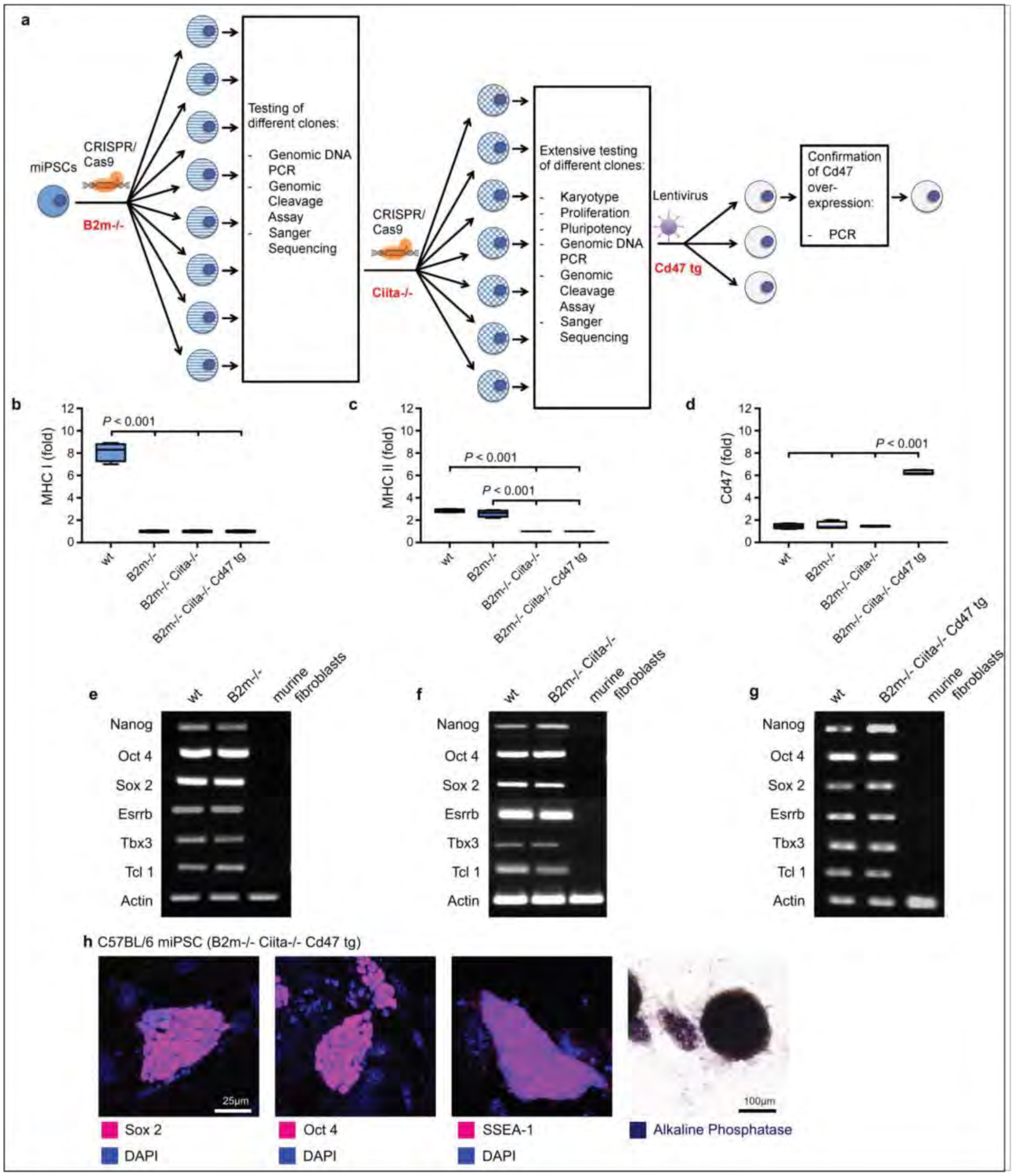
a
miPSCs
CRISPR/
Cas9
B2m-/-
Testing of different clones:
- Genomic DNA PCR
- Genomic Cleavage Assay
- Sanger Sequencing
CRISPR/
Cas9
Ciita-/-
Extensive testing of different clones:
- Karyotype
- Proliferation
- Pluripotency
- Genomic DNA PCR
- Genomic Cleavage Assay
- Sanger Sequencing
Lentivirus
Cd47 tg
Confirmation of Cd47 over-expression:
- PCR
b
MHC I (fold)
P < 0.001
0
2
4
6
8
10
12
wt
B2m-/-
B2m-/- Ciita-/-
B2m-/- Ciita-/- Cd47 tg
c
MHC II (fold)
P < 0.001
P < 0.001
0
2
4
6
8
10
12
wt
B2m-/-
B2m-/- Ciita-/-
B2m-/- Ciita-/- Cd47 tg
d
Cd47 (fold)
P < 0.001
0
2
4
6
8
10
12
wt
B2m-/-
B2m-/- Ciita-/-
B2m-/- Ciita-/- Cd47 tg
e
wt
B2m-/-
murine fibroblasts
Nanog
Oct 4
Sox 2
Esrrb
Tbx3
Tcl 1
Actin
f
wt
B2m-/- Ciita-/-
murine fibroblasts
Nanog
Oct 4
Sox 2
Esrrb
Tbx3
Tcl 1
Actin
g
wt
B2m-/- Ciita-/- Cd47 tg
murine fibroblasts
Nanog
Oct 4
Sox 2
Esrrb
Tbx3
Tcl 1
Actin
h C57BL/6 miPSC (B2m-/- Ciita-/- Cd47 tg)
25μm
100μm
Sox 2
DAPI
Oct 4
DAPI
SSEA-1
DAPI
Alkaline Phosphatase

Supplementary Figure 3

Immune phenotype and pluripotency of engineered miPSCs.

a, Mouse iPSCs underwent three editing steps to disrupt *B2m*, *Ciita*, and over-express Cd47 to achieve a hypo-immunogenic phenotype. Every step included rigorous testing for quality control. **b-d**, MHC class I (b), MHC class II (c), and Cd47 expression (d) by flow cytometry is shown for each engineering step, confirming successful gene editing (box 25th to 75th percentile with median, whiskers min-max, 4 independent experiments per graph, ANOVA with Bonferroni's post-hoc test). **e-g**, During the engineering process, all edited miPSCs maintained expression of the pluripotent gene expression signature (representative gel of two independent PCR experiments). **h**, *B2m*$^{-/-}$ *Ciita*$^{-/-}$ Cd47 tg miPSCs exhibited Sox2, Oct4, and SSEA-1 expression in confocal immunofluorescence stainings, as well as alkaline phosphatase in immunohistochemistry (representative pictures of three independent experiments).

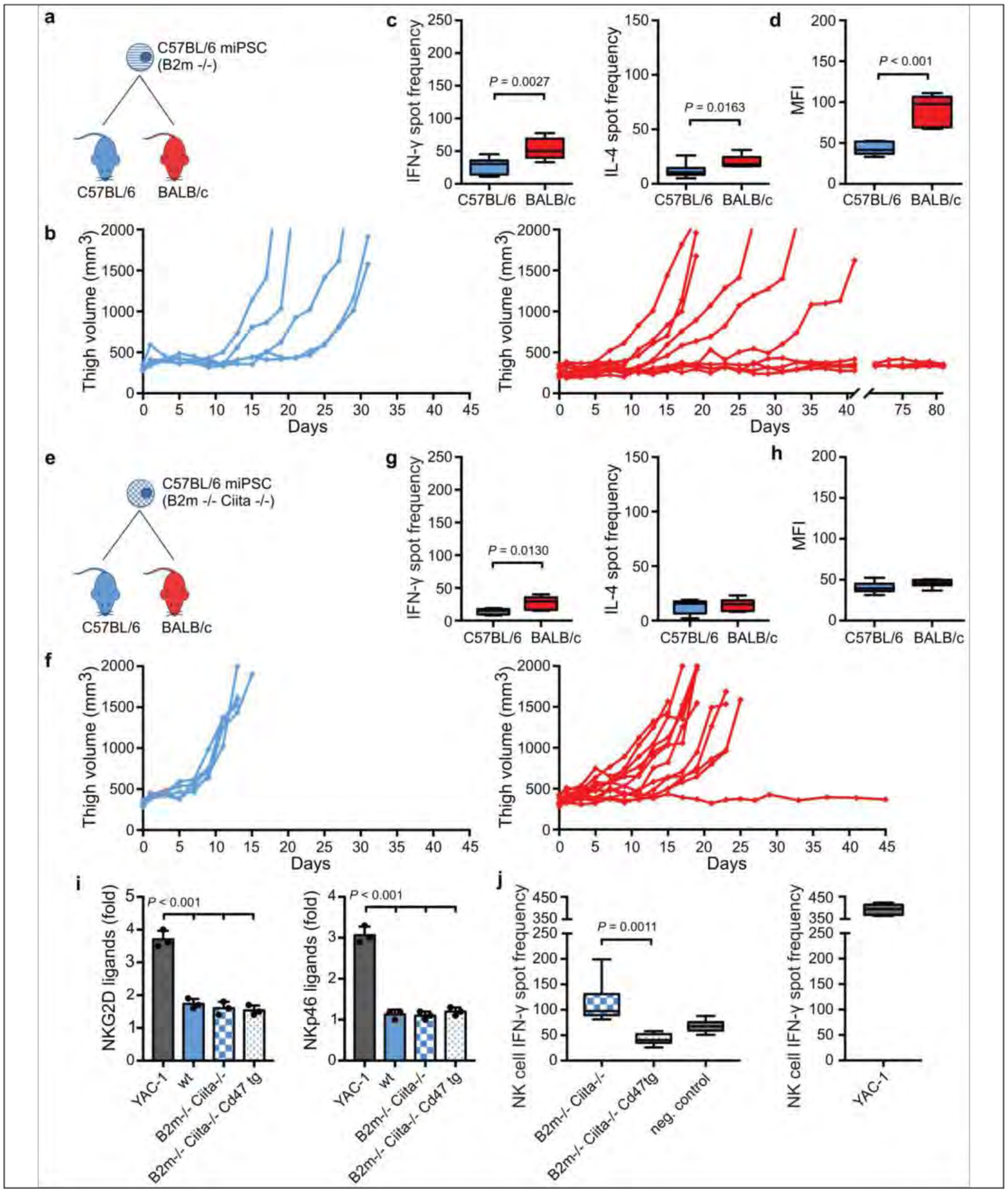
a
C57BL/6 miPSC
(B2m -/-)
C57BL/6
BALB/c
c
IFN-γ spot frequency
P = 0.0027
C57BL/6
BALB/c
IL-4 spot frequency
P = 0.0163
C57BL/6
BALB/c
d
MFI
P < 0.001
C57BL/6
BALB/c
b
Thigh volume (mm3)
Days
Thigh volume (mm3)
Days
e
C57BL/6 miPSC
(B2m -/- Ciita -/-)
C57BL/6
BALB/c
g
IFN-γ spot frequency
P = 0.0130
C57BL/6
BALB/c
IL-4 spot frequency
C57BL/6
BALB/c
h
MFI
C57BL/6
BALB/c
f
Thigh volume (mm3)
Days
Thigh volume (mm3)
Days
i
NKG2D ligands (fold)
P < 0.001
YAC-1
wt
B2m-/- Ciita-/-
B2m-/- Ciita-/- Cd47 tg
NKp46 ligands (fold)
P < 0.001
YAC-1
wt
B2m-/- Ciita-/-
B2m-/- Ciita-/- Cd47 tg
j
NK cell IFN-γ spot frequency
P = 0.0011
B2m-/- Ciita-/-
B2m-/- Ciita-/- Cd47tg
neg. control
NK cell IFN-γ spot frequency
YAC-1

Supplementary Figure 4

Survival of gene-engineered miPSCs.

a, C57BL/6 *B2m*$^{-/-}$ miPSCs were transplanted into either syngeneic C57BL/6 (blue) mice or allogeneic (red) BALB/c mice. **b,** The thigh volume of all five C57BL/6 and ten BALB/c animals is shown over time. The overall percentage of cell grafts that survived and formed teratomas in BALB/c was 60%. **c**, IFN-γ Elispots and IL-4 Elispots are shown with splenocytes recovered 5 days after the transplantation and *B2m*$^{-/-}$ miPSCs stimulator cells (box 25th to 75th percentile with median, whiskers min-max, 8 animals per group, two-tailed Student's t-test). d, Mean fluorescence (MFI) of IgM binding to *B2m*$^{-/-}$ miPSCs incubated with recipient serum after 5 days (box 25th to 75th percentile with median, whiskers min-max, 6 animals per group, two-tailed Student's t-test). **e**, C57BL/6 *B2m*$^{-/-}$*Ciita*$^{-/-}$ miPSCs were transplanted into syngeneic C57BL/6 or allogeneic BALB/c mice. **f**, The thigh volume of all 5 C57BL/6 and 12 BALB/c animals is shown over time. The overall percentage of cell grafts that survived and formed teratomas in BALB/c was 91.7%. **g**, IFN-γ Elispots and IL-4 Elispots are shown with splenocytes recovered 5 days after the transplantation and *B2m*$^{-/-}$*Ciita*$^{-/-}$ miPSCs stimulator cells (box 25th to 75th percentile with median, whiskers min-max, 6 animals per group, two-tailed Student's t-test). **h**, Mean fluorescence (MFI) of IgM binding to *B2m*$^{-/-}$*Ciita*$^{-/-}$ miPSCs incubated with recipient serum after 5 days (box 25th to 75th percentile with median, whiskers min-max, 6 animals per group, two-tailed Student's t-test). i, The expression of stimulatory NKG2D ligands and NKp46 ligands on miPSC lines and YAC-1 was assessed using receptor Fc chimera proteins in flow cytometry (mean ± s.d., 3 independent experiments per group, ANOVA with Bonferroni's post-hoc test). **j**, IFN-γ spot frequencies of miPSC lines and YAC-1 in Elispot assays with BALB/c NK cells (box 25th to 75th percentile with median, whiskers min-max, 6 independent experiments, ANOVA with Bonferroni's post-hoc test).

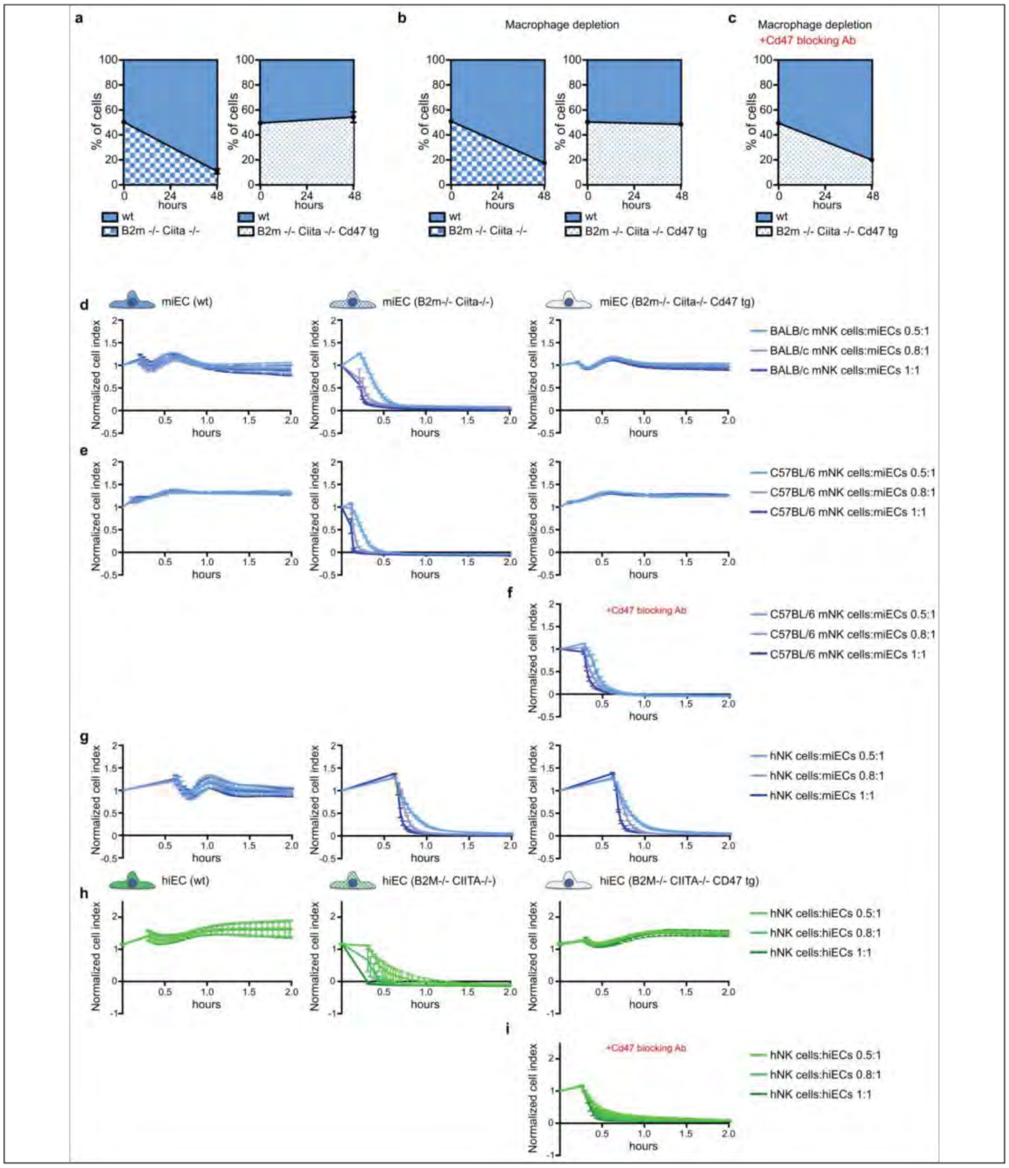
a
b
Macrophage depletion
c
Macrophage depletion
+Cd47 blocking Ab
% of cells
hours
wt
B2m -/- Ciita -/-
B2m -/- Ciita -/- Cd47 tg
d
miEC (wt)
miEC (B2m-/- Ciita-/-)
miEC (B2m-/- Ciita-/- Cd47 tg)
Normalized cell index
hours
BALB/c mNK cells:miECs 0.5:1
BALB/c mNK cells:miECs 0.8:1
BALB/c mNK cells:miECs 1:1
e
C57BL/6 mNK cells:miECs 0.5:1
C57BL/6 mNK cells:miECs 0.8:1
C57BL/6 mNK cells:miECs 1:1
f
+Cd47 blocking Ab
g
hNK cells:miECs 0.5:1
hNK cells:miECs 0.8:1
hNK cells:miECs 1:1
hiEC (wt)
hiEC (B2M-/- CIITA-/-)
hiEC (B2M-/- CIITA-/- CD47 tg)
h
hNK cells:hiECs 0.5:1
hNK cells:hiECs 0.8:1
hNK cells:hiECs 1:1
i
+Cd47 blocking Ab

Supplementary Figure 5

Interaction between CD47 and NK cells.

a, *In vivo* innate immune clearance was assessed by injecting a 1 : 1 mixture of CFSE-labeled wt miPSCs and either *B2m*$^{-/-}$*Ciita*$^{-/-}$ or *B2m*$^{-/-}$*Ciita*$^{-/-}$ Cd47 tg miPSCs into the peritoneum of syngeneic C57BL/6 mice. After 48 h, CSFE-labeled peritoneal miPSCs were recovered and the percentages of both fractions assessed by flow cytometry (mean ± s.d., 4 animals per group). While *B2m*$^{-/-}$*Ciita*$^{-/-}$ miPSCs were rapidly cleared, *B2m*$^{-/-}$*Ciita*$^{-/-}$ Cd47 tg miPSCs were spared. b, Mice were pre-treated with clodronate to deplete macrophages, making this model more specific to NK cell killing and again only *B2m*$^{-/-}$*Ciita*$^{-/-}$ Cd47 tg miPSCs were spared from NK cell killing (mean ± s.d., 4 animals per group). c, When a Cd47 blocking antibody was co-injected into the peritoneum, the protection was abolished and *B2m*$^{-/-}$*Ciita*$^{-/-}$ Cd47 tg miPSCs were killed (mean ± s.d., 4 animals per group). d, *In vitro* real-time NK cell killing was assessed on confluent wt, *B2m*$^{-/-}$*Ciita*$^{-/-}$, and *B2m*$^{-/-}$*Ciita*$^{-/-}$ Cd47 tg miECs in three different effector : target cell ratios. Using allogeneic BAL*B*/c mouse NK (mNK) cells, *B2m*$^{-/-}$*Ciita*$^{-/-}$ miECs were rapidly killed, and wt and *B2m*$^{-/-}$*Ciita*$^{-/-}$ Cd47 tg miECs permanently survived (mean ± s.d., 3 independent experiments per group). **e**, Similarly, using syngeneic C57*BL*/6 mNK cells, *B2m*$^{-/-}$*Ciita*$^{-/-}$ miECs were rapidly killed, and wt and *B2m*$^{-/-}$*Ciita*$^{-/-}$ Cd47 tg miECs permanently survived (mean ± s.d., 3 independent experiments per group). **f**, When a Cd47 blocking antibody was added to syngeneic C57*BL*/6 mNK cells, *B2m*$^{-/-}$*Ciita*$^{-/-}$ Cd47 tg miECs were swiftly killed (mean ± s.d., 3 independent experiments per group). **g**, When human NK (hNK) cells were used, both *B2m*$^{-/-}$*Ciita*$^{-/-}$ and *B2m*$^{-/-}$*Ciita*$^{-/-}$ Cd47 tg miECs were rapidly killed (mean ± s.d., 3 independent experiments per group). **h**, When hNK cells were used with human wt, *B2M*$^{-/-}$*CIITA*$^{-/-}$, and *B2M*$^{-/-}$*CIITA*$^{-/-}$ CD47 tg hiECs, only *B2M*$^{-/-}$*CIITA*$^{-/-}$ hiECs were rapidly killed and wt and *B2M*$^{-/-}$*CIITA*$^{-/-}$ CD47 tg hiECs were spared (mean ± s.d., 3 independent experiments per group). **i**, With a CD47 blocking antibody, *B2M*$^{-/-}$*CIITA*$^{-/-}$ CD47 tg hiECs were then swiftly killed (mean ± s.d., 3 independent experiments per group).

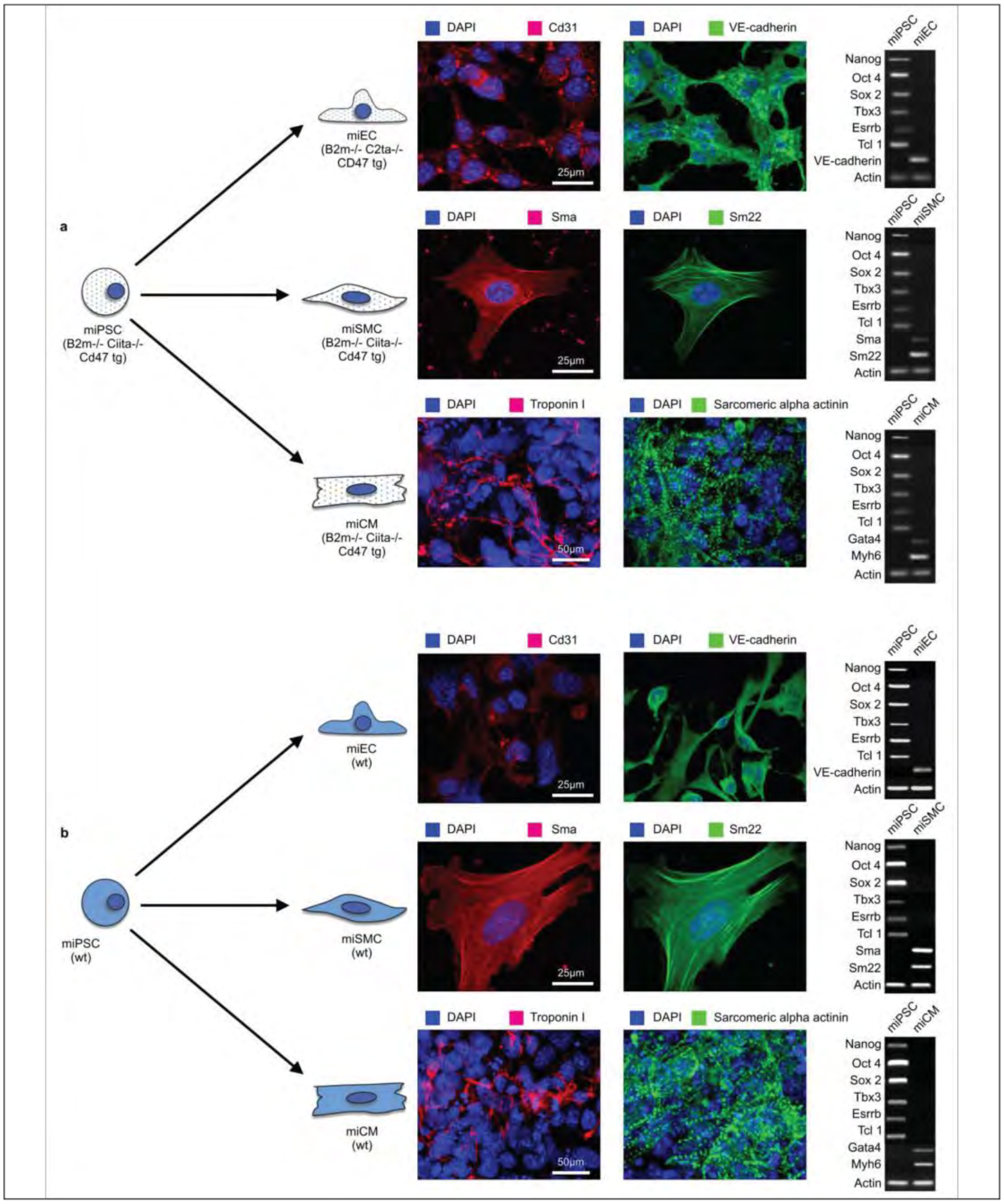
a
miPSC
(B2m-/- Ciita-/-
Cd47 tg)
miEC
(B2m-/- C2ta-/-
CD47 tg)
miSMC
(B2m-/- Ciita-/-
Cd47 tg)
miCM
(B2m-/- Ciita-/-
Cd47 tg)
DAPI
Cd31
25µm
DAPI
VE-cadherin
miPSC
miEC
Nanog
Oct 4
Sox 2
Tbx3
Esrrb
Tcl 1
VE-cadherin
Actin
DAPI
Sma
25µm
DAPI
Sm22
miPSC
miSMC
Nanog
Oct 4
Sox 2
Tbx3
Esrrb
Tcl 1
Sma
Sm22
Actin
DAPI
Troponin I
50µm
DAPI
Sarcomeric alpha actinin
miPSC
miCM
Nanog
Oct 4
Sox 2
Tbx3
Esrrb
Tcl 1
Gata4
Myh6
Actin
b
miPSC
(wt)
miEC
(wt)
miSMC
(wt)
miCM
(wt)
DAPI
Cd31
25µm
DAPI
VE-cadherin
miPSC
miEC
Nanog
Oct 4
Sox 2
Tbx3
Esrrb
Tcl 1
VE-cadherin
Actin
DAPI
Sma
25µm
DAPI
Sm22
miPSC
miSMC
Nanog
Oct 4
Sox 2
Tbx3
Esrrb
Tcl 1
Sma
Sm22
Actin
DAPI
Troponin I
50µm
DAPI
Sarcomeric alpha actinin
miPSC
miCM
Nanog
Oct 4
Sox 2
Tbx3
Esrrb
Tcl 1
Gata4
Myh6
Actin

Supplementary Figure 6

Differentiation of miPSCs into miECs, miSMCs and miCMs.

a b, *B2m*$^{-/-}$ *Ciita*$^{-/-}$ Cd47 tg miPSCs (a) and wt miPSCs (b) were successfully differentiated into corresponding miEC, miSMC, and miCM derivatives (representative pictures of three independent experiments). miECs were positive for Cd31 and VE-cadherin, miSMCs were positive for Sma and Sm22, miCMs were positive for Troponin I and Sarcomeric alpha-actinin by confocal immunofluorescence. All derivatives lost their expression of pluripotency genes (representative pictures of two independent PCR experiments).

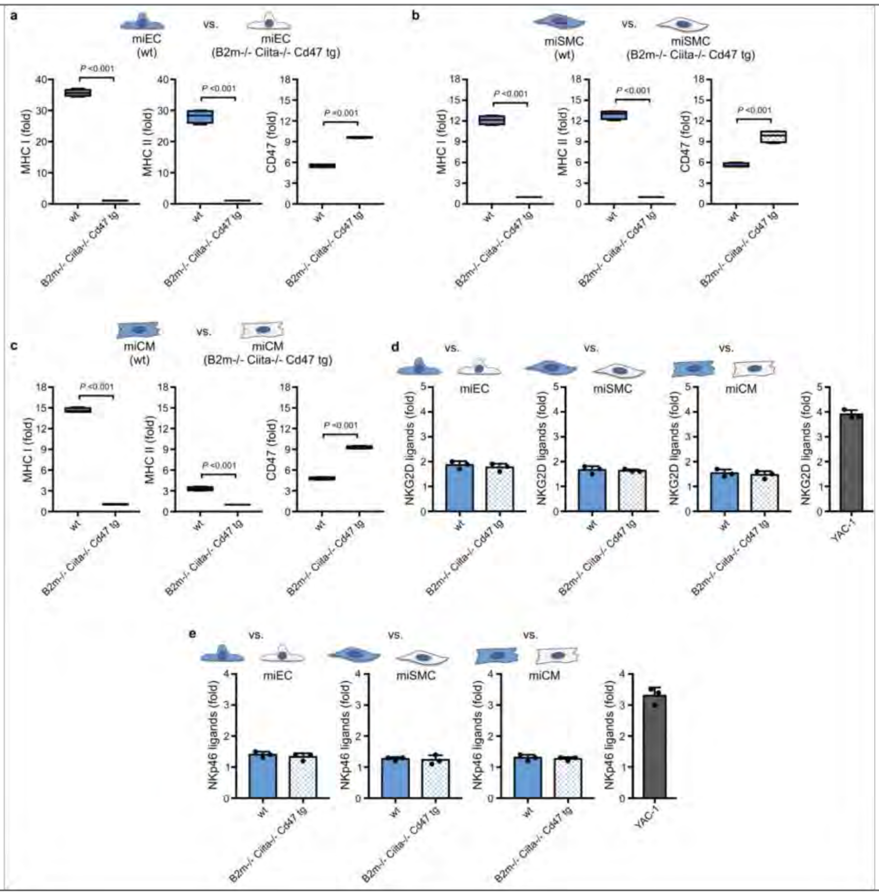

Supplementary Figure 7

Immune phenotype of wt and engineered miPSC derivatives.

a, wt miECs showed high MHC class I and MHC class II expression, while $B2m^{-/-}Ciita^{-/-}$ Cd47 tg miECs were MHC class I and MHC class II depleted and showed increased Cd47 expression (box 25th to 75th percentile with median, whiskers min-max, 4 independent experiments per graph, two-tailed Student's t-test). **b**, wt miSMCs showed moderate MHC class I and MHC class II expression, while $B2m^{-/-}Ciita^{-/-}$ Cd47 tg miSMCs were MHC class I and MHC class II depleted and showed increased Cd47 expression (box 25th to 75th percentile with median, whiskers min-max, 4 independent experiments per graph, two-tailed Student's t-test). **c**, wt miCMs showed moderate MHC class I and low MHC class II expression; $B2m^{-/-}Ciita^{-/-}$ Cd47 tg miCMs were MHC class I and MHC class II depleted and showed increased Cd47 expression (box 25th to 75th percentile with median, whiskers min-max, 4 independent experiments per graph, two-tailed Student's t-test). **d-e**, The expression of stimulatory NKG2D ligands (d) and NKp46 ligands (e) on wt and $B2m^{-/-}Ciita^{-/-}$ Cd47 tg miECs, miSMCs, miCMs, and YAC-1 was assessed using receptor Fc chimera proteins in flow cytometry (mean ± s.d., 3 independent experiments per group, two-tailed Student's t-test).

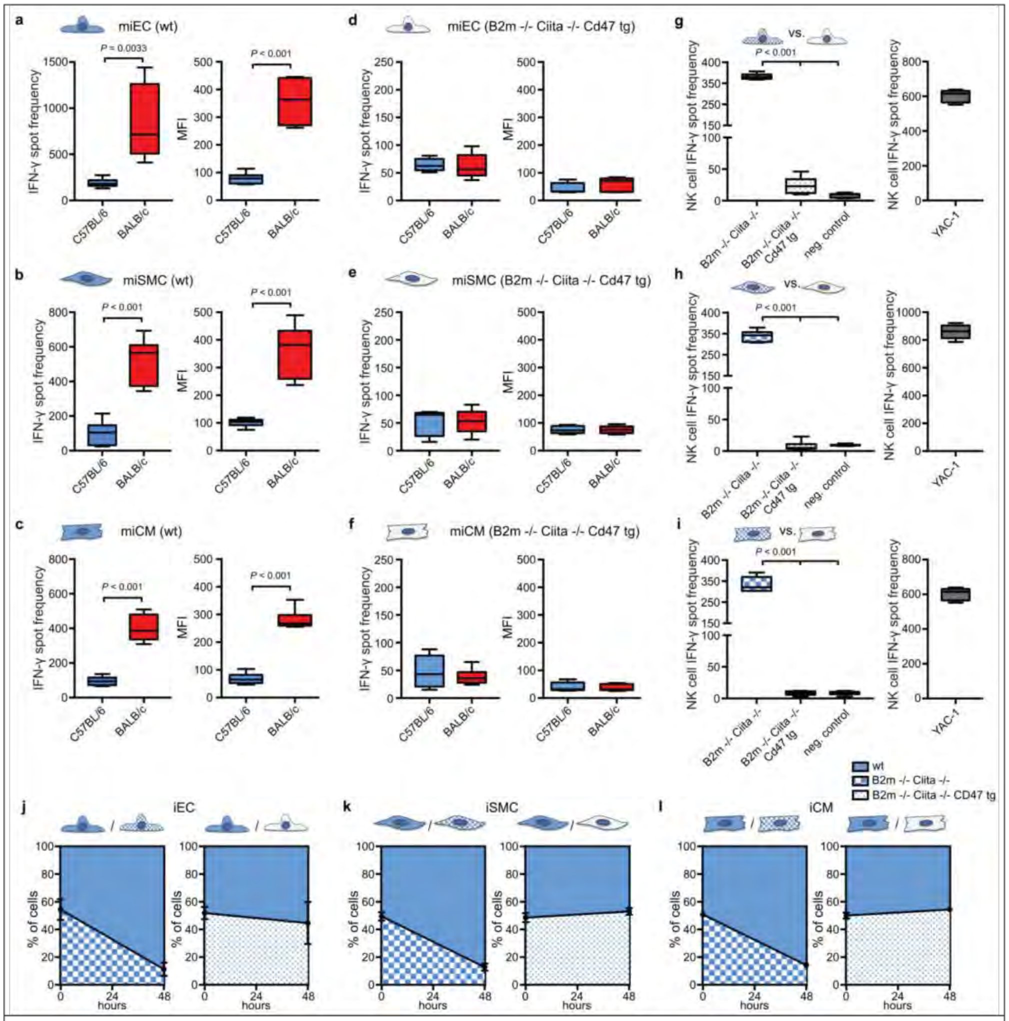

Supplementary Figure 8

Immune response against miPSC derivatives.

a-c, Five days after the injection of wt miPSC-derived miECs (a), miSMCs (b), or miCMs (c) into C57BL/6 or BALB/c recipients, splenocytes were recovered for IFN-γ Elispot assays (box 25th to 75th percentile with median, whiskers min-max, 6 animals per group, two-tailed Student's t-test). The IFN-γ response was vastly stronger in all allogeneic recipients. Mean fluorescence (MFI) of IgM binding to wt miPSC-derived miECs (a), miSMCs (b), and miCMs (c), incubated with recipient serum after 5 days (box 25th to 75th percentile

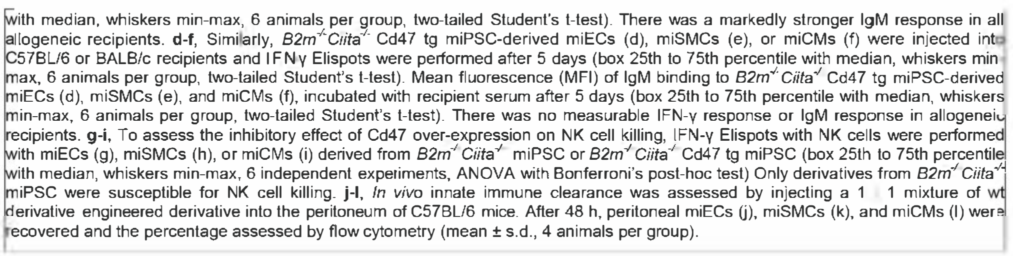

with median, whiskers min-max, 6 animals per group, two-tailed Student's t-test). There was a markedly stronger IgM response in all allogeneic recipients. **d-f**, Similarly, *B2m*$^{-/-}$*Ciita*$^{-/-}$ Cd47 tg miPSC-derived miECs (d), miSMCs (e), or miCMs (f) were injected into C57BL/6 or BALB/c recipients and IFN-γ Elispots were performed after 5 days (box 25th to 75th percentile with median, whiskers min-max, 6 animals per group, two-tailed Student's t-test). Mean fluorescence (MFI) of IgM binding to *B2m*$^{-/-}$*Ciita*$^{-/-}$ Cd47 tg miPSC-derived miECs (d), miSMCs (e), and miCMs (f), incubated with recipient serum after 5 days (box 25th to 75th percentile with median, whiskers min-max, 6 animals per group, two-tailed Student's t-test). There was no measurable IFN-γ response or IgM response in allogeneic recipients. **g-i**, To assess the inhibitory effect of Cd47 over-expression on NK cell killing, IFN-γ Elispots with NK cells were performed with miECs (g), miSMCs (h), or miCMs (i) derived from *B2m*$^{-/-}$*Ciita*$^{-/-}$ miPSC or *B2m*$^{-/-}$*Ciita*$^{-/-}$ Cd47 tg miPSC (box 25th to 75th percentile with median, whiskers min-max, 6 independent experiments, ANOVA with Bonferroni's post-hoc test) Only derivatives from *B2m*$^{-/-}$*Ciita*$^{-/-}$ miPSC were susceptible for NK cell killing. **j-l**, *In vivo* innate immune clearance was assessed by injecting a 1 : 1 mixture of wt derivative engineered derivative into the peritoneum of C57BL/6 mice. After 48 h, peritoneal miECs (j), miSMCs (k), and miCMs (l) were recovered and the percentage assessed by flow cytometry (mean ± s.d., 4 animals per group).

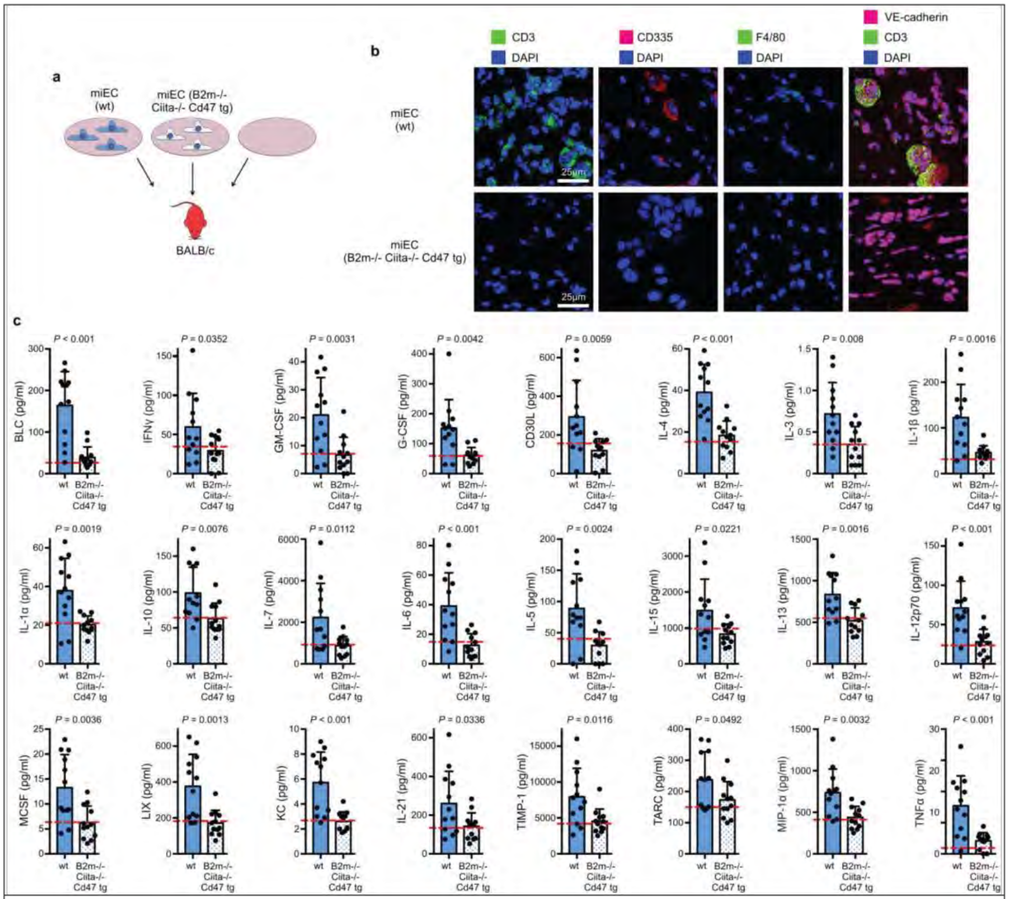

Supplementary Figure 9

Immune cell infiltration and cytokine expression in miEC grafts.

a, Matrigel plugs containing either wt miECs or $B2m^{-/-}Ciita^{-/-}$ Cd47 tg miECs were implanted in allogeneic BALB/c recipients. Cell-free matrigel plugs served as controls. **b**, Immunofluorescence stainings detected immune cell infiltration in wt iEC-plaques containing $CD3^{+}$ T lymphocytes, $CD335^{+}$ NK cells, and sparse $F4/80^{+}$ macrophages. Co-staining of CD3 and VE-cadherin confirmed $CD3^{+}$ lymphocyte infiltration in EC grafts in the wt group. Practically no immune cells were found in plugs containing $B2m^{-/-}Ciita^{-/-}$ Cd47 tg miECs (representative pictures of three independent experiments). **c**, The cytokine profile in wt miEC plugs was shifted towards a pro-inflammatory milieu. Multiple significantly up-regulated cytokines were typical of activated cytotoxic $CD8^{+}$ T cells, $CD4^{+}$ T helper-1 cells, and $CD4^{+}$ T helper-2 cells, as well as macrophages (mean ± s.d., 12 animals per group, two-tailed Student's t-test; dashed red lines show levels of cell-free matrigel).

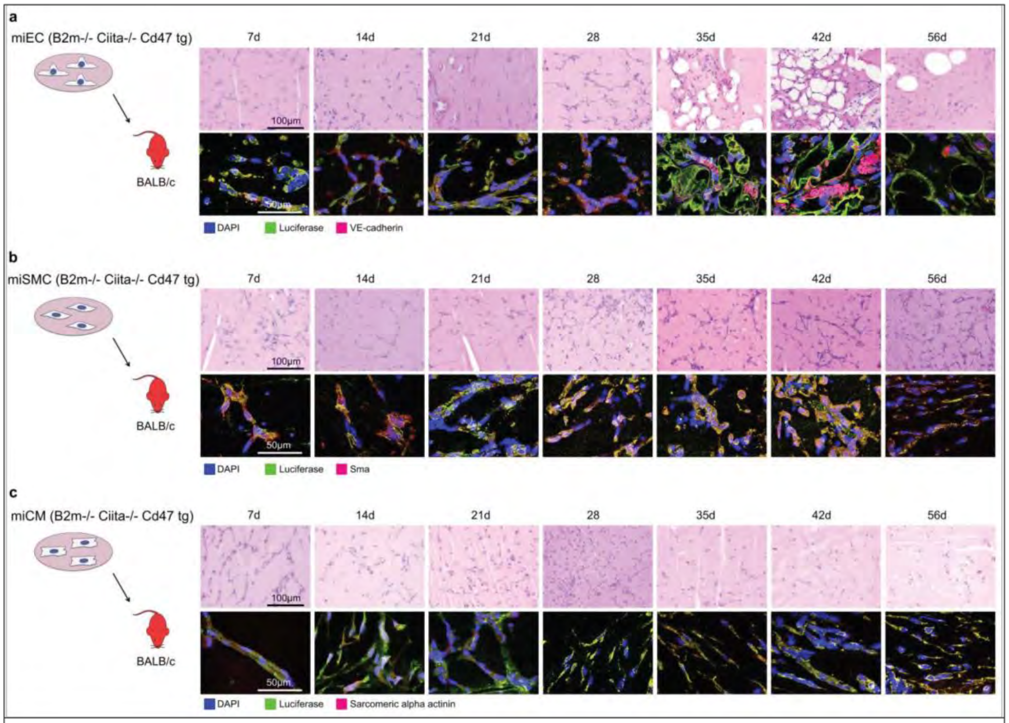
a
miEC (B2m-/- Ciita-/- Cd47 tg)
7d
14d
21d
28
35d
42d
56d
100µm
50µm
BALB/c
DAPI
Luciferase
VE-cadherin
b
miSMC (B2m-/- Ciita-/- Cd47 tg)
7d
14d
21d
28
35d
42d
56d
100µm
50µm
BALB/c
DAPI
Luciferase
Sma
c
miCM (B2m-/- Ciita-/- Cd47 tg)
7d
14d
21d
28
35d
42d
56d
100µm
50µm
BALB/c
DAPI
Luciferase
Sarcomeric alpha actinin

Supplementary Figure 10

Morphology of transplanted *B2m*$^{-/-}$*Ciita*$^{-/-}$ Cd47 tg miPSC derivatives in allogeneic hosts.

a-c, *B2m*$^{-/-}$*Ciita*$^{-/-}$ Cd47 tg miEC (a), miSMC (b), or miCM (c) grafts in matrigel were transplanted subcutaneously into allogeneic BALB/c mice to investigate whether these hypo-immunogenic derivatives further mature *in vivo* or change their morphology over time in allogeneic recipients. Matrigel plugs were recovered after different time points for hematoxylin and eosin and immunofluorescence stainings (representative pictures of two independent experiments). Transplanted miECs started to organize in circular structures around day 14 and formed primitive vessels that contained erythrocytes around day 35 (a). Transplanted miSMCs (b) maintained their typical spindle-shape appearance and loose arrangement, whereas miCMs retained their immature round progenitor morphology (c). Both latter cell types did not show a higher degree of three-dimensional organization, which may be attributed to the lack of mechanical stimulus necessary for maturation of any type of muscle cell.

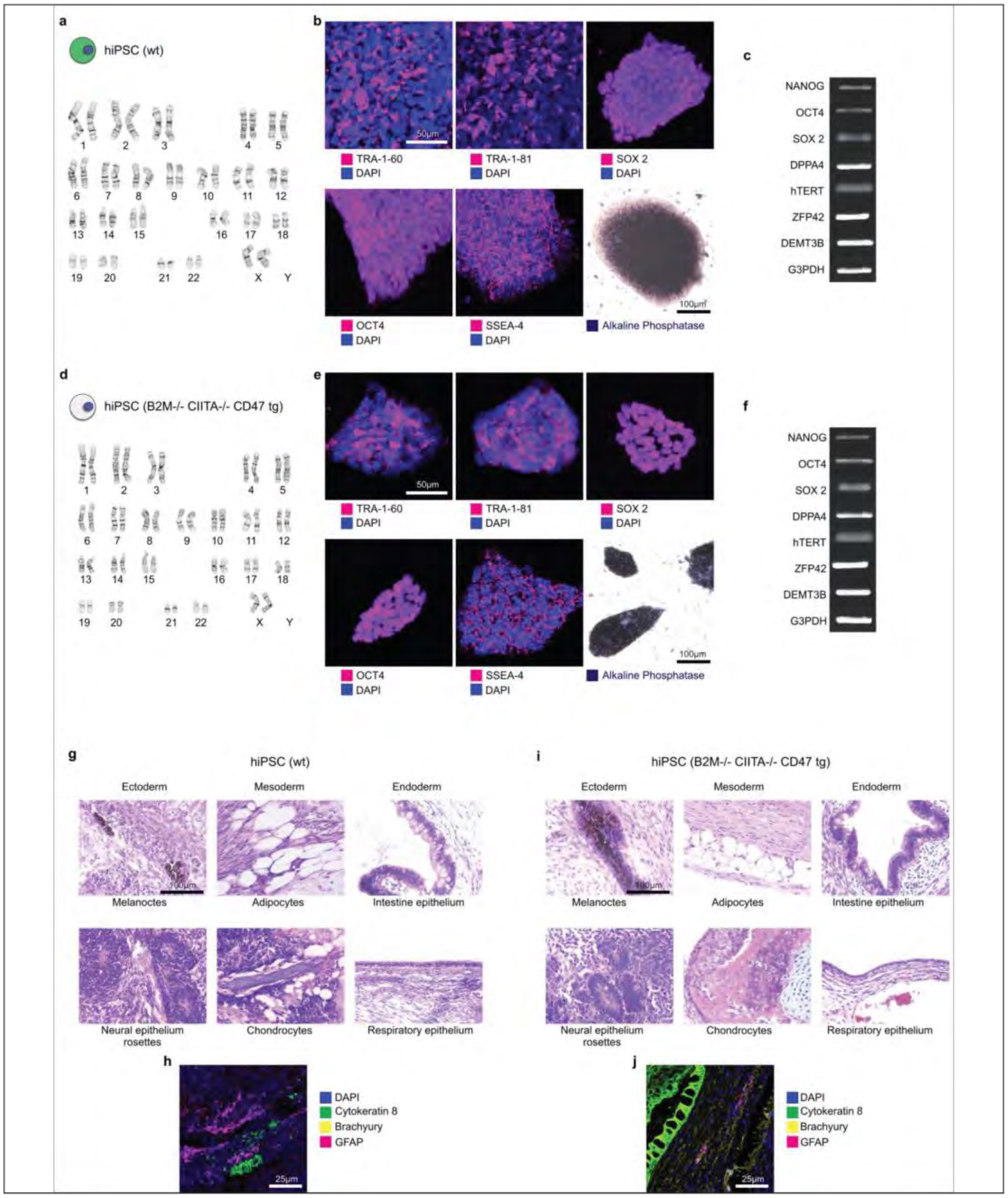
a
hiPSC (wt)
1
2
3
4
5
6
7
8
9
10
11
12
13
14
15
16
17
18
19
20
21
22
X
Y
b
50µm
TRA-1-60
DAPI
TRA-1-81
DAPI
SOX 2
DAPI
OCT4
DAPI
SSEA-4
DAPI
100µm
Alkaline Phosphatase
c
NANOG
OCT4
SOX 2
DPPA4
hTERT
ZFP42
DEMT3B
G3PDH
d
hiPSC (B2M-/- CIITA-/- CD47 tg)
1
2
3
4
5
6
7
8
9
10
11
12
13
14
15
16
17
18
19
20
21
22
X
Y
e
50µm
TRA-1-60
DAPI
TRA-1-81
DAPI
SOX 2
DAPI
OCT4
DAPI
SSEA-4
DAPI
100µm
Alkaline Phosphatase
f
NANOG
OCT4
SOX 2
DPPA4
hTERT
ZFP42
DEMT3B
G3PDH
g
hiPSC (wt)
Ectoderm
Mesoderm
Endoderm
100µm
Melanoctes
Adipocytes
Intestine epithelium
Neural epithelium rosettes
Chondrocytes
Respiratory epithelium
h
DAPI
Cytokeratin 8
Brachyury
GFAP
25µm
i
hiPSC (B2M-/- CIITA-/- CD47 tg)
Ectoderm
Mesoderm
Endoderm
100µm
Melanoctes
Adipocytes
Intestine epithelium
Neural epithelium rosettes
Chondrocytes
Respiratory epithelium
j
DAPI
Cytokeratin 8
Brachyury
GFAP
25µm

Supplementary Figure 11

Pluripotency of wt and *B2M*$^{-/-}$*CIITA*$^{-/-}$ CD47 tg hiPSCs.

a, wt hiPSCs showed a normal human 46, XX karyotype in one analysis. **b**, wt hiPSCs were positive for TRA-1-60, TRA-1-81, SOX 2, OCT4, and SSEA-4 in confocal immunofluorescence and positive for alkaline phosphatase in immunohistochemistry (representative pictures of three independent experiments). **c**, wt hiPSCs expressed typical pluripotency genes (representative gel of two independent PCR experiments). **d**, *B2M*$^{-/-}$*CIITA*$^{-/-}$ *CD47* tg hiPSCs maintained the normal human 46, XX karyotype in one analysis. e, *B2M*$^{-/-}$ *CIITA*$^{-/-}$ *CD47* tg hiPSCs were also positive for TRA-1-60, TRA-1-81, SOX 2, OCT4, and SSEA-4 in confocal immunofluorescence and positive for alkaline phosphatase in immunohistochemistry (representative pictures of three independent experiments). **f**, *B2M*$^{-/-}$ *CIITA*$^{-/-}$ *CD47* tg hiPSCs continued to express the typical pluripotency genes (representative gel of two independent PCR experiments). **g-j**, wt hiPSCs (g, h) and B2M$^{-/-}$ CIITA$^{-/-}$ CD47 tg hiPSCs (i, j) gave rise to cell types of all 3 germ layers after transplantation into SCID-beige mice. Endodermal (cytokeratin 8), mesodermal (brachyury), and ectodermal lineages (GFAP) were also demonstrated by confocal immunofluorescence microscopy (representative pictures of three independent experiments).

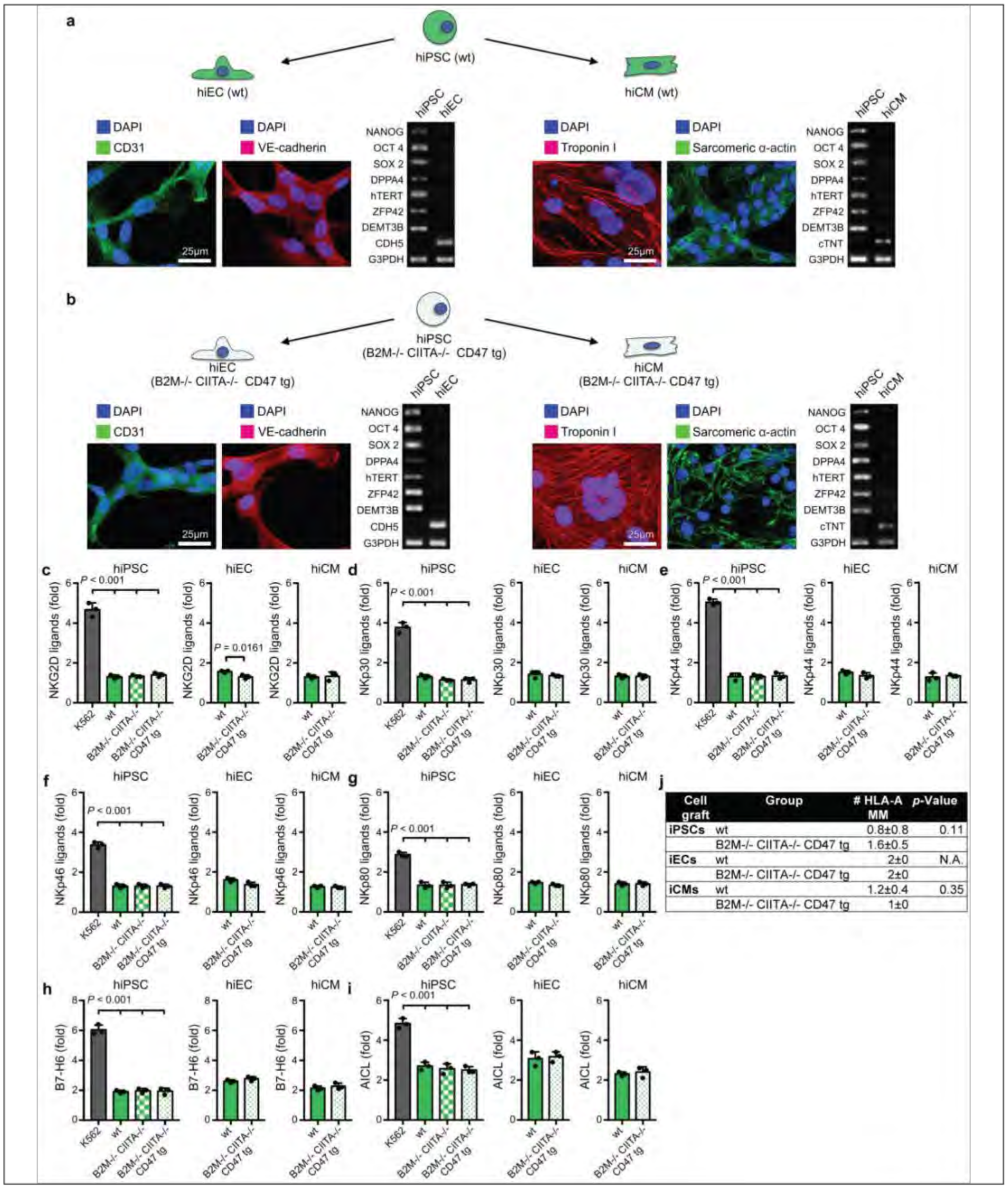

Cell graft	Group	# HLA-A MM	*p*-Value
iPSCs	wt	0.8±0.8	0.11
	B2M-/- CIITA-/- CD47 tg	1.6±0.5	
iECs	wt	2±0	N.A.
	B2M-/- CIITA-/- CD47 tg	2±0	
iCMs	wt	1.2±0.4	0.35
	B2M-/- CIITA-/- CD47 tg	1±0	

Supplementary Figure 12

Differentiation of hiPSCs into hiECs and hiCMs.

a-b, wt hiPSCs (a) and *B2M*$^{-/-}$ *CIITA*$^{-/-}$ *CD47* tg hiPSCs (b) were successfully differentiated into corresponding miEC and miCM derivatives (representative pictures of three independent experiments). miECs were positive for CD31 and VE-cadherin and miCMs were positive for Troponin I and Sarcomeric alpha-actinin by confocal immunofluorescence. All derivatives lost their expression of pluripotency genes (representative pictures of two independent experiments). **c-g**, The expression of stimulatory NK cell ligands was assessed on hiPSCs and their derivatives using receptor Fc chimera proteins in flow cytometry (mean ± s.d., 3 independent experiments per group, ANOVA with Bonferroni's post-hoc test (hiPSCs) or two-tailed Student's t-test (hiECs and hiCMs)). Ligands for NKG2D (c), NKp30 (d), NKp44 (e), NKp46 (f), and NKp80 (g) were compared between wt and engineered hiPSCs, hiECs, hiCMs, and K562. **h-i**, The expression of specific human natural cytotoxicity receptor ligands was evaluated by flow cytometry (mean ± s.d., 3 independent experiments per group, ANOVA with Bonferroni's post-hoc test (hiPSCs) or two-tailed Student's t-test (hiECs and hiCMs)). Surface expression of B7-H6 (h), and AICL (i) was compared between wt and engineered hiPSCs and derivatives, and K562. **i**, The HLA-A mismatches in transplant experiments with wt and *B2M*$^{-/-}$ *CIITA*$^{-/-}$ *CD47* tg hiPSCs, hiECs, and hiCMs in allogeneic humanized NSG-HGM3 recipients (mean ± s.d., 5 animals per group, two-tailed Student's t-test).

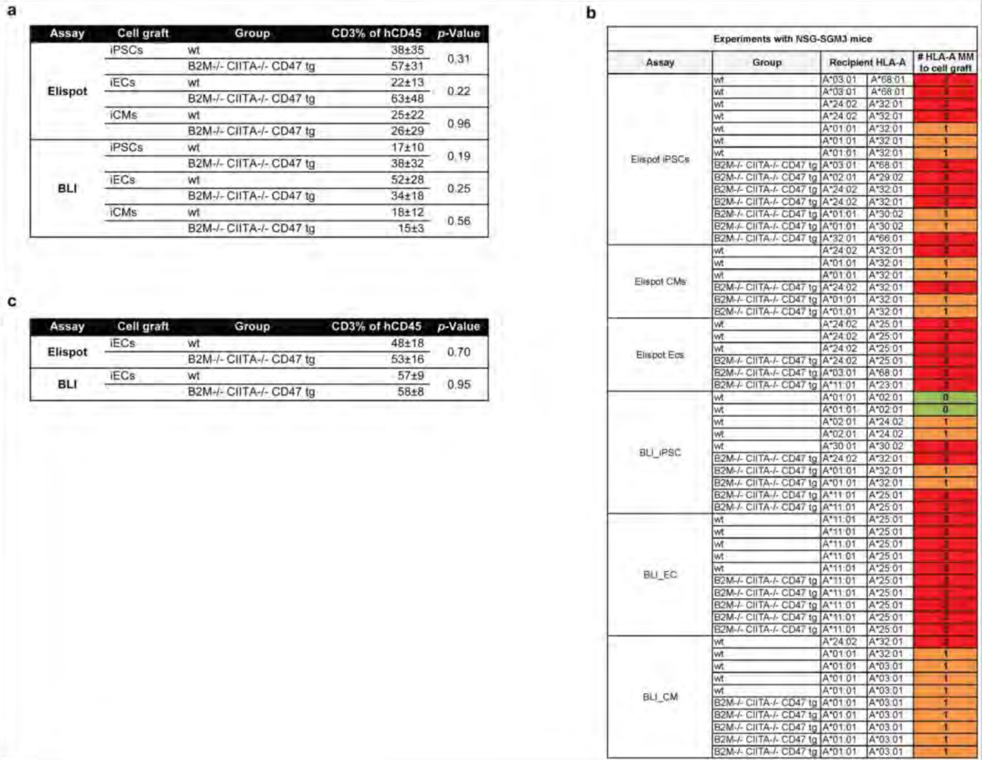

a

Assay	Cell graft	Group	CD3% of hCD45	*p*-Value
Elispot	iPSCs	wt	38±35	0.31
		B2M-/- CIITA-/- CD47 tg	57±31	
	iECs	wt	22±13	0.22
		B2M-/- CIITA-/- CD47 tg	63±48	
	iCMs	wt	25±22	0.96
		B2M-/- CIITA-/- CD47 tg	26±29	
BLI	iPSCs	wt	17±10	0.19
		B2M-/- CIITA-/- CD47 tg	38±32	
	iECs	wt	52±28	0.25
		B2M-/- CIITA-/- CD47 tg	34±18	
	iCMs	wt	18±12	0.56
		B2M-/- CIITA-/- CD47 tg	15±3	

b

Experiments with NSG-SGM3 mice

Assay	Group	Recipient HLA-A		# HLA-A MM to cell graft
Elispot iPSCs	wt	A*03:01	A*68:01	2
	wt	A*03:01	A*68:01	2
	wt	A*24:02	A*32:01	2
	wt	A*24:02	A*32:01	2
	wt	A*01:01	A*32:01	1
	wt	A*01:01	A*32:01	1
	wt	A*01:01	A*32:01	1
	B2M-/- CIITA-/- CD47 tg	A*03:01	A*68:01	2
	B2M-/- CIITA-/- CD47 tg	A*02:01	A*29:02	2
	B2M-/- CIITA-/- CD47 tg	A*24:02	A*32:01	2
	B2M-/- CIITA-/- CD47 tg	A*24:02	A*32:01	2
	B2M-/- CIITA-/- CD47 tg	A*01:01	A*30:02	1
	B2M-/- CIITA-/- CD47 tg	A*01:01	A*30:02	1
	B2M-/- CIITA-/- CD47 tg	A*32:01	A*66:01	2
Elispot CMs	wt	A*24:02	A*32:01	2
	wt	A*01:01	A*32:01	1
	wt	A*01:01	A*32:01	1
	B2M-/- CIITA-/- CD47 tg	A*24:02	A*32:01	2
	B2M-/- CIITA-/- CD47 tg	A*01:01	A*32:01	1
	B2M-/- CIITA-/- CD47 tg	A*01:01	A*32:01	1
Elispot Ecs	wt	A*24:02	A*25:01	2
	wt	A*24:02	A*25:01	2
	wt	A*24:02	A*25:01	2
	B2M-/- CIITA-/- CD47 tg	A*24:02	A*25:01	2
	B2M-/- CIITA-/- CD47 tg	A*03:01	A*68:01	2
	B2M-/- CIITA-/- CD47 tg	A*11:01	A*23:01	2
BLI_iPSC	wt	A*01:01	A*02:01	0
	wt	A*01:01	A*02:01	0
	wt	A*02:01	A*24:02	1
	wt	A*02:01	A*24:02	1
	wt	A*30:01	A*30:02	2
	B2M-/- CIITA-/- CD47 tg	A*24:02	A*32:01	2
	B2M-/- CIITA-/- CD47 tg	A*01:01	A*32:01	1
	B2M-/- CIITA-/- CD47 tg	A*01:01	A*32:01	1
	B2M-/- CIITA-/- CD47 tg	A*11:01	A*25:01	2
	B2M-/- CIITA-/- CD47 tg	A*11:01	A*25:01	2
BLI_EC	wt	A*11:01	A*25:01	2
	wt	A*11:01	A*25:01	2
	wt	A*11:01	A*25:01	2
	wt	A*11:01	A*25:01	2
	wt	A*11:01	A*25:01	2
	B2M-/- CIITA-/- CD47 tg	A*11:01	A*25:01	2
	B2M-/- CIITA-/- CD47 tg	A*11:01	A*25:01	2
	B2M-/- CIITA-/- CD47 tg	A*11:01	A*25:01	2
	B2M-/- CIITA-/- CD47 tg	A*11:01	A*25:01	2
	B2M-/- CIITA-/- CD47 tg	A*11:01	A*25:01	2
BLI_CM	wt	A*24:02	A*32:01	2
	wt	A*01:01	A*32:01	1
	wt	A*01:01	A*03:01	1
	wt	A*01:01	A*03:01	1
	wt	A*01:01	A*03:01	1
	B2M-/- CIITA-/- CD47 tg	A*01:01	A*03:01	1
	B2M-/- CIITA-/- CD47 tg	A*01:01	A*03:01	1
	B2M-/- CIITA-/- CD47 tg	A*01:01	A*03:01	1
	B2M-/- CIITA-/- CD47 tg	A*01:01	A*03:01	1
	B2M-/- CIITA-/- CD47 tg	A*01:01	A*03:01	1

c

Assay	Cell graft	Group	CD3% of hCD45	*p*-Value
Elispot	iECs	wt	48±18	0.70
		B2M-/- CIITA-/- CD47 tg	53±16	
BLI	iECs	wt	57±9	0.95
		B2M-/- CIITA-/- CD47 tg	58±8	

Supplementary Figure 13

CD3 reconstitution and HLA matching in humanized mice.

a, Percentage of CD3$^+$ cells among the reconstituted human CD45$^+$ cell population in NSG-SGM3 mice receiving hiPSC grafts (n=7 per group), hiEC grafts (n=3 per group), or hiCM grafts (n=3 per group) in the Elispot groups or hiPSC grafts, hiEC grafts, or hiCM grafts (n=5 per group) in the BLI groups (mean ± s.d., two-tailed Student's t-test). **b**, All NSG-SGM3 mice were typed for HLA-A and the number of HLA-A mismatches (MM) was calculated for every single animal used in this study. 2 MM are coded in red, 1 MM in orange, and zero MM in green. **c**, Percentage of CD3$^+$ cells among the reconstituted human CD45$^+$ cell population in BLT mice receiving iEC grafts in the Elispot groups (n=4 per group) or BLI groups (n=5) (mean ± s.d., two-tailed Student's t-test).

2.2 De novo mutations in mitochondrial DNA of iPSCs produce immunogenic neoepitopes in mice and humans

In diesem Kapitel wird die Publikation „De novo mutations in mitochondrial DNA of iPSCs produce immunogenic neoepitopes in mice and humans“ vorgestellt, welche im Jahr 2019 in Nature Biotechnology publiziert wurde. Mein Anteil der Publikation beinhaltete die Durchführung von immunologischen sowie molekularbiologischen Experimenten, die Zelldifferenzierung und Zellkultur, sowie *In-vivo* Imaging Studien und Datenanalysen. Meine Mitwirkung an dem Paper resultierte in einer Erstautorenschaft.

Titel: De novo mutations in mitochondrial DNA of iPSCs produce immunogenic neoepitopes in mice and humans

Autoren: Xiaomeng Hu*, Tobias Deuse*, Sean Agbor-Enoh, Martina Koch, Matthew H. Spitzer, Alessia Gravina, Malik Alawi, Argit Marishta, Bjoern Peters, Zeynep Kosaloglu-Yalcin, Yanqin Yang, Raja Rajalingam, Dong Wang, Bjoern Nashan, Rainer Kiefmann, Hermann Reichenspurner, Hannah Valantine, Irving L. Weissman, Sonja Schrepfer
*geteilte Erstautorenschaft

Journal: Nature Biotechnology, Volume 37, Pages 1137–1144

DOI: 10.1038/s41587-019-0227-7

nature biotechnology

LETTERS

https://doi.org/10.1038/s41587-019-0227-7

De novo mutations in mitochondrial DNA of iPSCs produce immunogenic neoepitopes in mice and humans

Tobias Deuse[1,16], Xiaomeng Hu[1,2,3,16], Sean Agbor-Enoh[4,5], Martina Koch[6], Matthew H. Spitzer[7,8,9], Alessia Gravina[1,3], Malik Alawi[10], Argit Marishta[5], Bjoern Peters[11], Zeynep Kosaloglu-Yalcin[11], Yanqin Yang[5], Raja Rajalingam[12], Dong Wang[1,2,3], Bjoern Nashan[6], Rainer Kiefmann[13], Hermann Reichenspurner[2,3], Hannah Valantine[5], Irving L. Weissman[14] and Sonja Schrepfer[1,2,3,15]*

The utility of autologous induced pluripotent stem cell (iPSC) therapies for tissue regeneration depends on reliable production of immunologically silent functional iPSC derivatives. However, rejection of autologous iPSC-derived cells has been reported, although the mechanism underlying rejection is largely unknown. We hypothesized that de novo mutations in mitochondrial DNA (mtDNA), which has far less reliable repair mechanisms than chromosomal DNA, might produce neoantigens capable of eliciting immune recognition and rejection. Here we present evidence in mice and humans that nonsynonymous mtDNA mutations can arise and become enriched during reprogramming to the iPSC stage, long-term culture and differentiation into target cells. These mtDNA mutations encode neoantigens that provoke an immune response that is highly specific and dependent on the host major histocompatibility complex genotype. Our results reveal that autologous iPSCs and their derivatives are not inherently immunologically inert for autologous transplantation and suggest that iPSC-derived products should be screened for mtDNA mutations.

iPSC-derived grafts can be immunogenic and rejected by the host even though they are derived from host cells. Several factors relating to the reprogramming of somatic cells, expansion of iPSCs in culture and differentiation of iPSCs into tissue cells are thought to contribute. Suppression[1] and overexpression[2] of pluripotency factors are known to establish de novo antigenicity that diminishes with differentiation[1,3,4]. However, differentiation of iPSCs can lead to the expression of immunogenic antigens not usually expressed in corresponding somatic cells causing rejection.[5] In addition, mutations acquired during reprogramming and expansion may generate mutant proteins that can act as neoantigens.

Mutation rates during reprogramming have been reported to be up to ninefold higher than the background mutation rate in culture.[6] Furthermore, the mutation rate for mtDNA is 10- to 20-fold higher than that of nuclear DNA[7–9]. Both mutated and wild-type mtDNA can coexist in the same cell, a phenomenon called heteroplasmy[10]. Nonsynonymous mtDNA mutations can impact both the function of proteins[11] and its antigenicity. mtDNA-encoded mitochondrial minor antigens[12] have been described as transplant barriers[13], and our group has shown that individual single nucleotide polymorphisms (SNPs) are sufficient to create immunogenic neoantigens[14]. However, the extent to which neoantigenic SNP enrichments affect autologous immune responses are not known. Here we sought to characterize the immunogenicity of mtDNA SNPs and assess their immunologic relevance for iPSC-based regenerative therapies.

First, we assessed the sensitivity and specificity of the mouse immune system to respond to isolated mtDNA SNPs. Using the technique of somatic cell nucleus transfer, embryonic stem cells (ESCs) with BALB/c (B/c) nuclear DNA and C57BL/6 (B6) mtDNA were generated (these cells are referred to as NT-ESCs throughout). In comparison to B/c, these NT-ESCs showed only two homoplasmic nonsynonymous SNPs in the *mt-Co3* and *mt-Cytb* genes, and generate cytochrome C oxidase III (Co3) or cytochrome b (Cytb) proteins with one amino acid substitution each (Supplementary Table 1). NT-ESCs were used for immunization against these two epitopes in B/c mice (Fig. 1a). To confirm that mitochondrial proteins with a single amino acid substitution can function as neoantigens, B/c fibroblasts were transfected to transiently overexpress either the B/c or B6 forms of Co3 or Cytb (Fig. 1a,b). Splenocytes recovered after 5d were used for enzyme-linked immunospot (ELISpot) assays against either of the four fibroblast preparations. ELISpot assays for interferon-γ (IFNγ) and interleukin-4 (IL-4) were performed. Spot

---

[1] Department of Surgery, Division of Cardiothoracic Surgery, Transplant and Stem Cell Immunobiology Lab, University of California, San Francisco, San Francisco, CA, USA. [2] Department of Cardiovascular Surgery, University Heart Center Hamburg, Hamburg, Germany. [3] Cardiovascular Research Center Hamburg and German Center for Cardiovascular Research, partner site Hamburg/Kiel/Luebeck, Hamburg, Germany. [4] Division of Pulmonary and Critical Care Medicine, The Johns Hopkins School of Medicine, Baltimore, MD, USA. [5] Laboratory of Transplantation Genomics, Division of Intramural Research, National Heart, Lung, and Blood Institute, Bethesda, MD, USA. [6] Department of Hepatobiliary and Transplant Surgery, University Medical Center Hamburg-Eppendorf, University Transplant Center, Hamburg, Germany. [7] Departments of Otolaryngology, Head and Neck Surgery and Microbiology and Immunology, Helen Diller Family Comprehensive Cancer Center, University of California, San Francisco, San Francisco, CA, USA. [8] Parker Institute for Cancer Immunotherapy, San Francisco, CA, USA. [9] Chan Zuckerberg Biohub, San Francisco, CA, USA. [10] Bioinformatics Core, University Medical Center Hamburg-Eppendorf, Hamburg, Germany. [11] Division of Vaccine Discovery, La Jolla Institute for Allergy and Immunology, La Jolla, CA, USA. [12] Immunogenetics and Transplantation Laboratory, Department of Surgery, University of California, San Francisco, San Francisco, CA, USA. [13] Department of Anaesthesia, University Medical Center Hamburg-Eppendorf, Hamburg, Germany. [14] Department of Developmental Biology, Stanford Institute for Stem Cell Biology and Regenerative Medicine, Stanford University School of Medicine, Stanford, CA, USA. [15] Sana Biotechnology Inc., South San Francisco, CA, USA. [16] These authors contributed equally: Tobias Deuse, Xiaomeng Hu. *e-mail: Sonja.Schrepfer@ucsf.edu

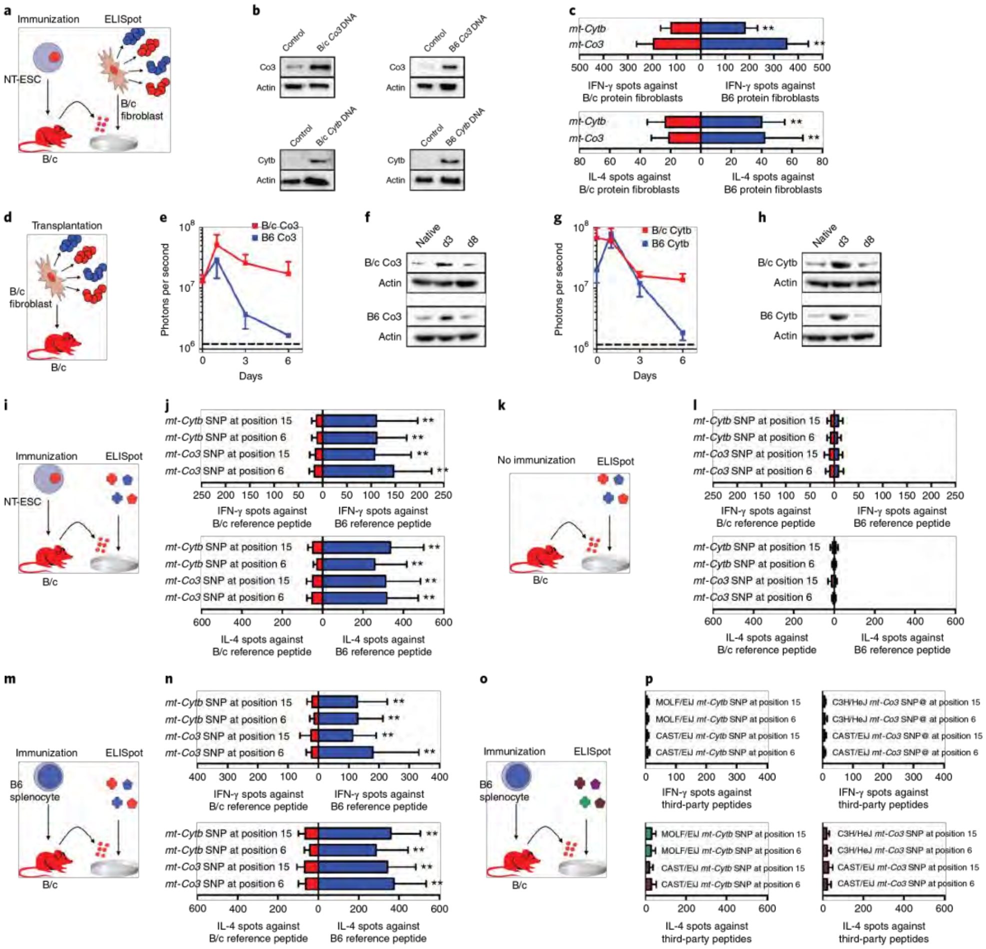

Fig. 1 | Immune response to allogeneic mtDNA-derived proteins in mice. a, B/c mice were immunized with NT-ESCs, which were generated by somatic cell nucleus transfer. NT-ESCs were suspended in saline and injected into the thigh muscle. NT-ESCs express two homoplasmic nonsynonymous mtDNA SNPs in the *mt-Co3* and *mt-Cytb* genes as compared to the B/c strain. **b**, We confirmed overexpression of the B/c or B6 forms of Co3 or Cytb protein in B/c fibroblasts using immunoblotting (pictures are representative of two replicates). **c**, Splenocytes were recovered after 5 d and their response against B/c fibroblasts expressing B/c (red) or B6 protein (blue) was assessed by IFN-γ and IL-4 ELISpot assay. Data are mean ± s.d. of quadruplicates from six animals per protein. **d**, B/c fibroblasts overexpressing B6 or B/c forms of Co3 or Cytb were suspended in saline and transplanted subcutaneously into B/c mice. **e–h**, Cell survival was assessed by bioluminescence imaging (BLI) and followed for 6 d. **e,g**, Cells were considered rejected when their BLI signals fell to background levels (dashed lines indicate background). Data are mean ± s.d. from five animals per group. **f,h**, Overexpression of B6 or B/c forms of Co3 or Cytb was confirmed over the 6-d study period by immunoblot. Blots are representative of two replicates. **i**, To confirm that the immunogenic epitope involves the SNP region, splenocytes of B/c mice immunized with NT-ESCs were tested against the B6-specific (blue) or B/c-specific (red) 20-residue oligomers with an amino acid variation at position 6 or 15. **j**, The immune responses were measured by ELISpot assay. Data are mean ± s.d. of quadruplicates from eight animals per 20-residue oligomer. **k,l**, The response of splenocytes derived from naive B/c mice and tested against the same B6-specific 20-residue oligmers (**k**) was assessed by ELISpot (**l**). Data are mean ± s.d. of quadruplicates from six (IFN-γ) or five (IL-4) animals per 20-residue oligomer. Significance was tested by two-tailed Student's *t* test. **m**, B/c mice were immunized with fully allogeneic B6 splenocytes that were MHC mismatched in addition to their mtDNA mismatch. **n**, IFN-γ and IL-4 spot frequencies were assessed in ELISpot assays. Data are mean ± s.d. of quadruplicates from eight animals per 20-residue oligomer. **o,p**, Splenocytes from B/c mice immunized with B6 cells (**o**) were tested against 20-residue oligomers derived from unconnected third-party strains (**p**). Data are mean ± s.d. of quadruplicates from five animals per 20-residue oligmer. Blue shades correspond to B6, red shades to B/c. **c,j,n**, $^{**}P < 0.01$, two-tailed Student's *t* test.

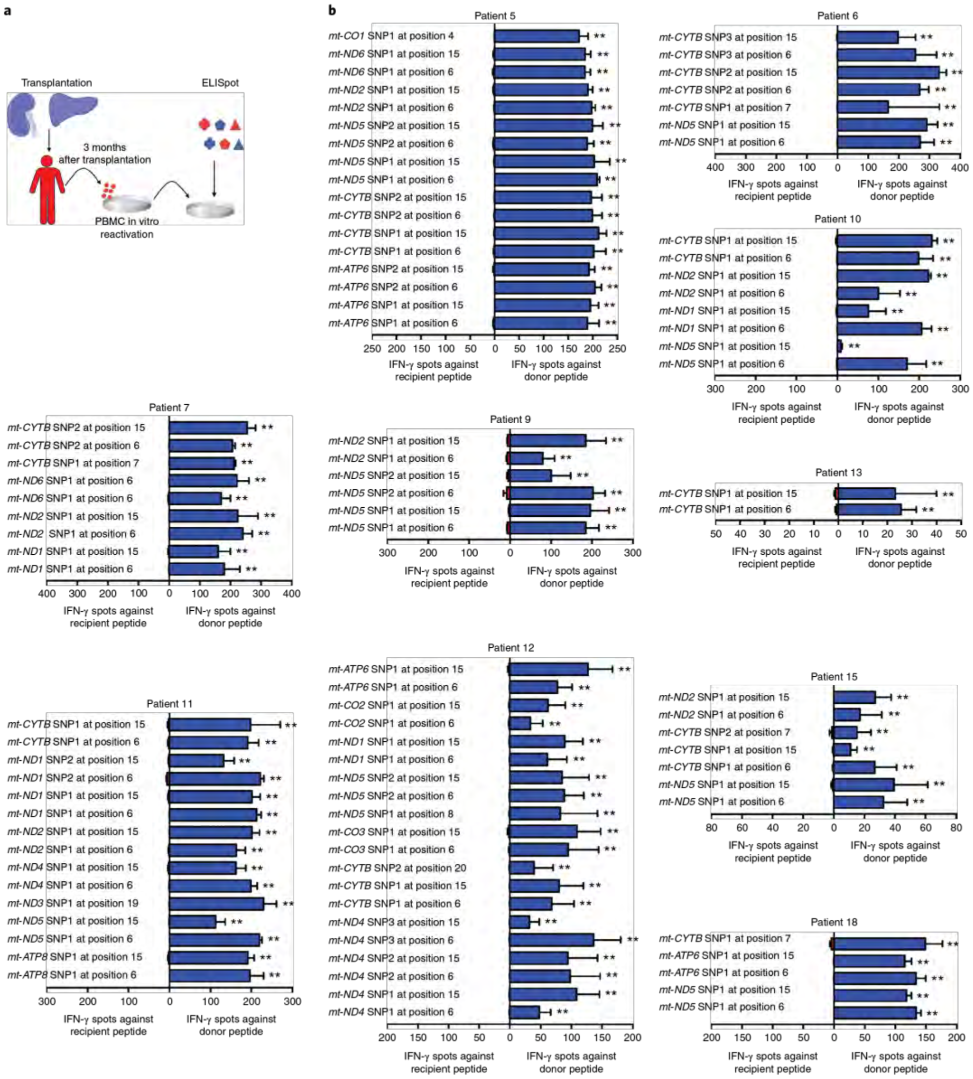

Fig. 2 | Immune response to allogeneic mtDNA-derived proteins in human transplant recipients. a, Patients underwent allogeneic kidney or liver transplantation. Donor–recipient pairs were screened for homoplasmic nonsynonymous mtDNA SNPs. After 3 months, recipient PBMCs were isolated, reactivated in vitro and incubated with 20-residue oligomer peptides covering the donor- or recipient-specific amino acid variation. **b**, PBMC responses were measured by ELISpot IFN-γ spot frequencies against the donor (blue) and recipient (red) 20-residue oligomers are shown for ten patients. Data are mean ± s.d. of quadruplicates per 20-residue oligomer and patient. Significance was assessed by two-tailed Student's *t* test, $^{**}P < 0.01$.

frequencies are presented to directly compare the immune response against the allogeneic B6 protein with that of the syngeneic B/c protein (Fig. 1c). Only the two fibroblasts overexpressing allogeneic B6 protein evoked a substantial T cell response. When transplanted into B/c recipients (Fig. 1d), only those two fibroblast grafts underwent rejection (Fig. 1e,g) during the time period of protein overexpression (Fig. 1f,h). Mass cytometry of splenocytes recovered after 5 d revealed remodeling of the T and B cell compartments as well as alterations to natural killer cells and dendritic cells in animals challenged with allogeneic Co3 or Cytb (Supplementary Figs. 1 and 2). Taken together, these results are consistent with the notion that single mtDNA SNPs are sufficient to trigger a broad systemic immune response.

To verify that the T cell epitopes span the SNP, B/c mice were again immunized with NT-ESC grafts, but this time, splenocytes were directly challenged with 20-residue oligomer peptides designed around the SNP (Fig. 1i). Two 20-residue oligomer peptides per epitope were generated with the amino acid variation from the SNP at position 6 or 15 (thus, overlapping by 11 residues; Supplementary Table 1). Splenocytes specifically recognized all four allogeneic 20-residue oligomers and showed marked IFN-γ and IL-4 release (Fig. 1j). No immune activation was observed in non-immunized B/c animals (Fig. 1k,l). To assess the possibility of cross-reactivity against fetal nuclear-gene-derived antigens present in ESCs, B/c mice were immunized with B/c ESCs (Supplementary Fig. 3). Splenocytes did not recognize any of the four allogeneic 20-residue oligomers, confirming the specificity of the immune response and identifying the sequence covering the SNP as minor histocompatibility antigens (MiHAs).

The relevance of MiHAs may weaken in the allogeneic transplant context in the presence of multiple major histocompatibility complex (MHC) antigens owing to antigen competition. To test this, we immunized B/c mice ($H2^d$) with fully allogeneic B6 splenocytes ($H2^b$), which carry the same B6 mitochondria as the NT-ESCs but are MHC mismatched. Recipient splenocytes were challenged with the same peptides representing the four syngeneic and allogeneic 20-residue oligomers (Fig. 1m), and the observed immune responses (Fig. 1n) were similar in intensity to those obtained after NT-ESC immunization (see Fig. 1j). Twenty-residue oligomers designed on the basis of allogeneic Co3 and Cytb from unconnected third-party strains (Supplementary Table 2 and Fig. 1o) did not evoke an immune response (Fig. 1p). This highlights the strong antigenicity of mitochondrial MiHAs, which elicited strong and specific immune activation despite abundant competing mismatched MHC burden.

We wanted to assess the immunologic relevance of mtDNA SNPs in human allogeneic transplantation. Patients undergoing allogeneic kidney or liver transplantation were screened for homoplasmic mtDNA differences to their donors (>99% heteroplasmy; Supplementary Fig. 4a). In 15 donor–recipient pairs, we found a total of 81 nonsynonymous SNPs, varying from 1–12 per pair with higher numbers between more distant ethnic groups (Supplementary Fig. 4b–d). Twenty-residue oligomer peptides were again designed around the autologous and allogeneic SNP (Supplementary Table 3). Three months after transplantation, blood was drawn from the 15 immunosuppressed recipients and peripheral blood mononuclear cells (PBMCs) were isolated and underwent in vitro reactivation (Supplementary Fig. 5). Thereby, PBMCs from recipients with adequate immunosuppression (mean tacrolimus trough level $= 9.6 \pm 2.7\,\text{ng}\,\text{ml}^{-1}$) regained their activity within 24 h. Reactivated PBMCs were challenged with autologous or allogeneic 20-residue oligomers (Fig. 2a) and immune responses were observed for every allogeneic 20-residue oligomer in all patients (Fig. 2b and Supplementary Fig. 6). To confirm the specificity of these results, we studied samples from patients ($n = 6$) with blood drawn 6 months after transplantation. Reactivated PBMCs were challenged with autologous and allogeneic 20-residue oligomers from both their organ donor and an unconnected donor (Supplementary Fig. 7 and Supplementary Table 4). Again, immune responses were observed against 20-residue oligomers from every donor. Immune responses were not observed against 20-residue oligomers from unconnected donors, but when SNPs were also present in the patient's donor immune responses were observed. However, despite the specificity, we noticed that the degree of immune activation varied between patients and between 20-residue oligomers.

We next assessed whether the strength of the immune response to mutated mtDNA-derived MiHAs depended on the ability of the mitochondrial epitope to bind to host human leukocyte antigens (HLAs). Two volunteers underwent four-digit HLA typing, and in silico antigenicity prediction was performed for proteins harboring one of 232 annotated human missense SNPs from Ensembl[15] (Supplementary Table 5). Twenty-residue oligomers were generated for the five top and the five bottom SNPs based on the HLA type of each individual, as well as for the corresponding autologous epitope (Supplementary Table 6). PBMCs from those volunteers were then used in extended 14-d naive in vitro immunization ELISpot assays, allowing in vitro antigen presentation and lymphocyte priming (Supplementary Fig. 8a). As predicted, the five top SNPs were markedly more immunogenic than the five bottom SNPs (Supplementary Fig. 8b), confirming that the antigenicity of mtDNA SNPs depends on the host HLA repertoire for presentation.

To screen for the occurrence of de novo mutations or SNP enrichments, we generated B6 and FVB iPSCs from fibroblasts and serially sequenced their mtDNA during culture (Fig. 3a,b and Supplementary Tables 7 and 8). On the basis of our sequencing depth of 4,000–10,000 per base pair, we defined the threshold for detection at 1% variant heteroplasmy. De novo mutations were regarded as candidates for neoantigens when the non-dominant SNP heteroplasmy increased from <1% to >5%, which corresponds to a drop from >99% to <95% in positions where the dominant SNP differs from the reference genome. SNP enrichments were regarded as potential neoantigens when low-level heteroplasmies of <5% in the source parental cell increased to >15% (or heteroplasmies >95% dropped below 85%) during cell culture. Both high-passage iPSC

Fig. 3 | Antigenicity of low- and high-passage iPSCs and their iEC derivatives in mice. **a**,**b**, B6 (**a**) and FVB (**b**) iPSCs were generated from fibroblasts and expanded in vitro. The source fibroblasts, low-passage iPSCs and high-passage iPSCs underwent mtDNA sequencing, and the variant SNP heteroplasmy according to the GRCm38 mouse reference genome is shown in heat maps. Automated clustering of nonsynonymous SNPs with >1% variation in heteroplasmy over time is shown with the corresponding amino acid substitutions. SNPs that increased in heteroplasmy from <1% in fibroblasts (below the detection threshold) to >1% in iPSCs were defined as de novo mutations and are marked in green. SNPs that were present in the parental fibroblast (>1% heteroplasmy) and were diluted or enriched over time are marked in black. Candidate SNPs for neoantigens are outlined (mutagenic SNPs increasing in heteroplasmy from <1% to >5% or enriched SNPs increasing from <5% to >15%; alternatively, SNPs decreasing in heteroplasmy from >99% to <95% or from >95% to <85% in positions where the dominant SNP differs from the reference genome). **c**–**e**, B6 mice received different amounts of autologous low-passage (P7) or high-passage (P37) iPSCs grafts injected into the thigh muscle and were followed for immune response and teratoma development (**c**). **d**, After 5d, splenocytes were recovered for ELISpot assays. Data are mean ± s.d. of quadruplicates from five animals per group, two-tailed Student's *t*-test. **e**, Teratoma growth is shown for every animal and the percentage of teratoma formation for each group is shown in a separate bar graph. Data are from five mice per cell amount and iPSC group. **f**–**h**, iECs derived from P7 or P37 iPSCs were transplanted into B6 mice and cell survival was followed by BLI (**f**). **g**, After 5d, splenocytes were recovered for ELISpot assays. Data are mean ± s.d. of quadruplicates from five animals per group. Significance was assessed by two-tailed Student's *t* test. **h**, The survival of iEC (P7) and iEC (P37) grafts was assessed by BLI and the percentage of graft survival for each group is shown in a separate bar graph. Cells were considered rejected when their BLI signals fell to background levels. Individual animals are shown, $n = 5$ per iEC group; dashed lines indicate background.

lines from B6 and FVB revealed potential neoantigens. Single-cell sequencing of B6 cells showed that the heteroplasmies obtained in bulk sequencing accurately reflected the average of more heterogeneous heteroplasmies in individual cells (Supplementary Table 9).

The MHC binding affinities of the B6 neoantigen candidates were modeled using in silico prediction (Supplementary Fig. 8c and Supplementary Table 10), which showed that the mutant SNP in *mt-Co1* generated peptides with decent MHC binding affinities whereas the affinity of the mutant Nd3 peptide was very low. Twenty-residue oligomers were synthesized from a sequence carrying the neoantigenic or reference SNP (Supplementary Table 11). Mice were immunized with low-passage or high-passage iPSCs and splenocytes were

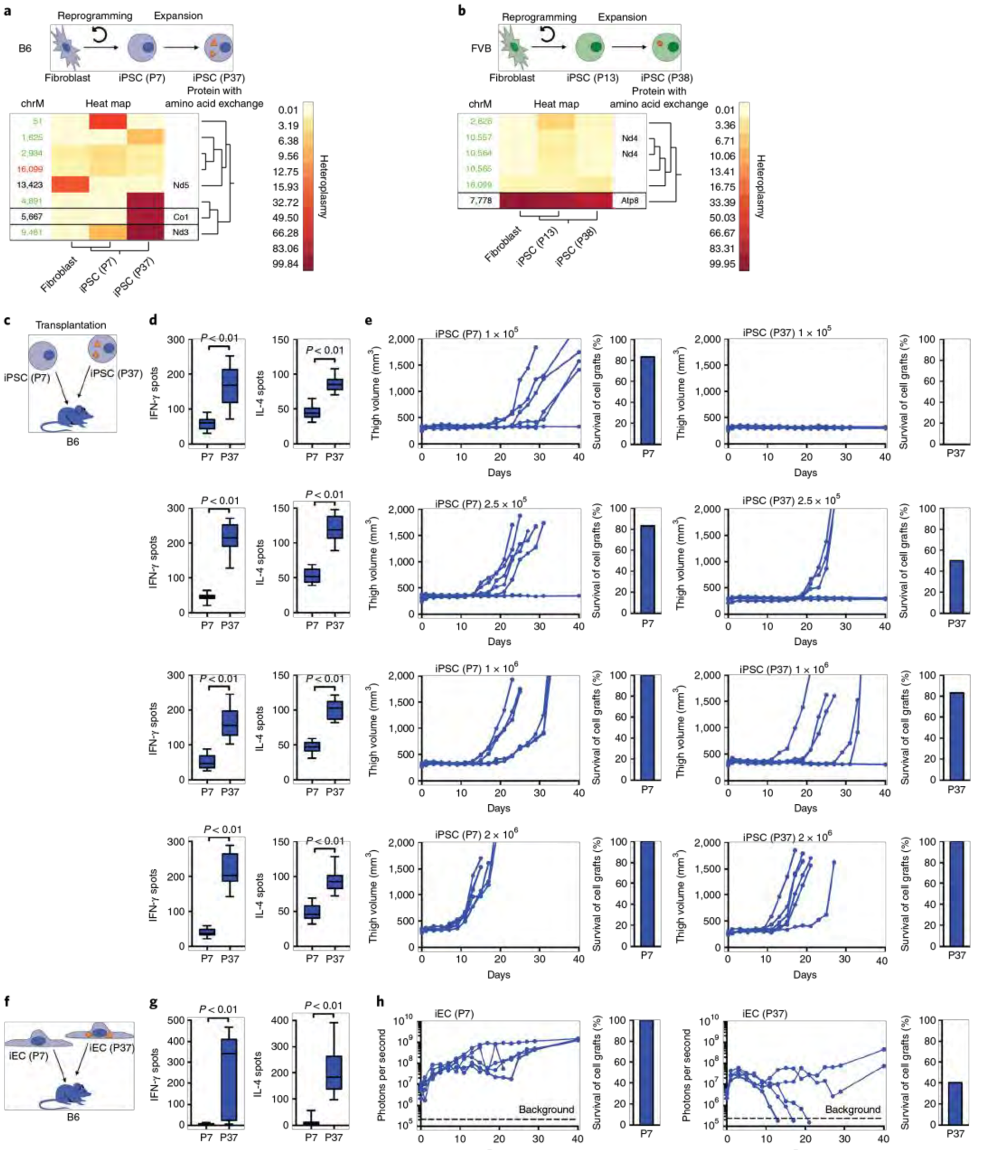

challenged with 20-residue oligomers 5 d later (Supplementary Fig. 8d–f). As predicted, in B6 mice we observed IFN-γ and IL-4 responses against the Co1 neoantigen but not the mutant Nd3. Immunogenicity was also demonstrated for the 20-residue oligomer of the Atp8 neoantigen in FVB (Supplementary Fig. 8g–i).

B6 (Fig. 3c–e) and FVB mice (Supplementary Fig. 9) then received subcutaneous grafts of either low-passage or high-passage iPSCs to assess whether the neoantigens could provoke an immune response and diminish cell survival in vivo. Varying cell numbers were used, as the survival and teratoma formation of pluripotent cell grafts depends on the overall cell load[16]. Across graft sizes, we observed an increased immune response and a correspondingly reduced survival of high-passage iPSC grafts.

Next, we sought to confirm the immunogenic nature of the reduced survival of B6 passage 37 (P37) iPSCs as compared to P7 iPSCs. Both P7 and P37 iPSCs showed similar proliferative capacity in vivo and in vitro (Supplementary Fig. 10 and Supplementary Video 1). P37 grafts showed more dense immune cell infiltrations than P7 in immunocompetent B6 mice (Supplementary Fig. 11a–d). Transplantation of low-dose P37 iPSCs in immunosuppressed or immunocompromised recipients did not cause substantial immune activation and resulted in 100% survival (Supplementary Fig. 11e–j). To assess whether this newly developed immunogenicity would persist after differentiation into functional tissue cells, B6 P7 and P37 iPSCs were differentiated into endothelial cells (iECs). We observed immune activation and markedly reduced survival of iEC P37 grafts, demonstrating that the acquired antigenicity persists after differentiation and is not associated with the pluripotency state (Fig. 3f–h).

We next aimed to assess whether MHC presentation of mtDNA neoantigens is required for T cell activation. We inactivated *B2m* and *Ciita* genes in P7 iPSCs using CRISPR–Cas9 and the derived MHC double knockout (dKO) iECs lacked expression of MHC class I and II, both of which were expressed in P7 iECs (Supplementary Fig. 12a–c). P7 and dKO iECs were then transfected to overexpress either B/c or B6 forms of Co3 and Cytb and used to immunize B6 mice (Supplementary Fig. 12d). Overexpression of syngeneic B6 Co3 and Cytb did not induce an IFN-γ response against either iEC population (Supplementary Fig. 12e). Overexpression of allogeneic B/c Co3 and Cytb induced an IFN-γ response in P7 iECs expressing MHC but did not induce a response in dKO iECs (Supplementary Fig. 12f). These results thus show that immunogenicity of mtDNA neoantigens requires MHC presentation.

Next, we evaluated the emergence of neoantigens during reprogramming and extended culture of human iPSCs (Fig. 4a). Four human iPSCs created from fibroblasts were sequentially sequenced up to ≥P60 (Fig. 4b–e and Supplementary Table 12). For nonsynonymous SNPs, the protein harboring the amino acid variation is listed. In all cases, unsupervised clustering automatically arranged the passages in the correct ascending order. The data show that, while the heteroplasmy of variant SNPs can drift in cell culture over time, the likelihood for de novo mutations and enrichment of rare SNPs increases with an increase in passages. The heteroplasmies quantified in bulk culture represent the mean of a more heterogeneic clonal distribution of cells with different degrees of heteroplasmy revealed by single cell sequencing (Supplementary Table 13). Applying our previous definition, two of the four cell lines developed candidates for neoantigens (boxed SNPs). To assess whether mtDNA neoantigens similarly occur in vivo, blood was taken from six healthy volunteers over a 6- to 12-month period and PBMCs, a cell type with high turnover, were sequenced (Supplementary Table 14). Of note, all heteroplasmic SNPs in protein-coding regions were maintained at a relatively constant level in vivo, and we did not find a single neoantigen candidate (Supplementary Fig. 13). We assume mechanisms to scavenge neoantigenic cells are effective in vivo but ineffective in vitro, potentially owing to the lack of immune surveillance in cell culture.

To assess whether neoantigens in autologous human iPSC derivatives could induce rejection, PBMCs from healthy volunteers were reprogrammed to iPSCs, differentiated into endothelial cells (iECs) and expanded in culture to P35 (Fig 4f). mtDNA sequencing revealed one neoantigen candidate mutation each in two of the three iECs (Fig 4g and Supplementary Table 15). Extended naive in vitro immunization ELISpot assays with 20-residue oligomers for the predominant and non-dominant proteins (Fig. 4h) showed a specific immune response against the two neoantigenic non-dominant peptides, but not any of the other peptides (Fig. 4i). To test whether these mtDNA neoantigens were immunogenic on a cellular level, parental PBMCs and iPSCs were differentiated into macrophages, a possible target cell type for both PBMCs and iPSCs (Fig. 4f). Autologous ELISpot assays (Fig. 4j) confirmed that only neoantigen-carrying iPSC-derived macrophages induced an immune response (Fig. 4k). To examine whether such an immune response would suffice to reject autologous iEC grafts, fresh volunteer PBMCs were primed with iECs in vitro for 7 d (Fig. 4l) and then transferred to iEC layers for real-time impedance measurements. Primed PBMCs killed neoantigen-expressing autologous iECs from volunteers 1 and 2, but not the iECs from volunteer 3 (Fig. 4m). This suggests that autologous iPSC-based cell products expressing mtDNA neoantigens can be subject to rejection.

Fig. 4 | Occurrence and antigenicity of mtDNA-derived neoantigens in human iPSCs and iECs. a, Human iPSCs were generated from adult fibroblasts and were culture expanded over >60 passages. **b–e**, During this process, serial mtDNA sequencing was performed and heat maps showing the heteroplasmies of the variant SNPs versus the Cambridge reference sequence are presented. SNPs in the non-coding D loop are marked in red. Non-dominant SNPs with <1% heteroplasmy in parental fibroblasts that increased to >1% in iPSCs were considered de novo mutations and are marked in green. SNPs that were present in the fibroblasts and changed their heteroplasmy >1% over time are marked in black. Candidate SNPs for neoantigens are boxed (mutagenic SNPs increasing in heteroplasmy from <1% to >5% or enriched SNPs increasing from <5% to >15%; alternatively, SNPs decreasing in heteroplasmy from >99% to <95% or from >95% to <85% in positions where the dominant SNP differs from the reference genome). For nonsynonymous SNPs, the protein with the amino acid substitution is listed. **f**, PBMCs from three volunteers were reprogrammed to iPSCs, differentiated to iECs and culture expanded to P35. PBMCs and iPSCs were also differentiated into macrophages (a cell type that both source cells can reliably be differentiated into) to assess the immunogenicity of mtDNA neoantigens on a cellular level. **g**, mtDNA from PBMCs, iPSCs and iECs was sequenced and in two of three volunteers iPSCs and iECs showed one neoantigenic SNP candidate. **h**, For all coding SNPs that changed their heteroplasmy by >1% over time, fresh PBMCs from volunteers were incubated with 20-residue oligomers from the volunteer's predominant (blue) or non-dominant mtDNA SNPs (yellow). **i**, IFN-γ and IL-5 responses were assessed in extended naive in vitro immunization ELISpot assays. Data are mean ± s.d. of quadruplicates per 20-residue oligomer. Significance was assessed by two-tailed Student's *t* test. **j**, Fresh PBMCs from volunteers were incubated with the autologous PBMC-derived macrophages (PBMC-Mac) or iPSC-derived macrophages (iPSC-Mac) generated in **f**. **k**, The autologous IFN-γ and IL-5 immune responses were assessed in extended in vitro immunization ELISpot assays. Data are mean ± s.d. from eight replicates per group. Significance was tested by two-tailed Student's *t* test. **l**, Fresh PBMCs from volunteers were incubated with the autologous P35 iECs generated in **f** to immunize T cells in vitro for 7 d. PBMCs were then collected and transferred to P35 iEC layers grown on electrodes for a real-time in vitro impedance cytotoxicity assay. **m**, The integrity of the autologous iEC layers over 48 h was expressed as normalized cell index. Data are mean ± s.d. from triplicates per group. Subsequently, the iECs were collected and the percentage of living cells was assessed by flow cytometry. Data are mean ± s.d. of quadruplicates per group. $^{**}P < 0.01$.

Although the compact circular 16,569-base-pair human mtDNA only encodes 13 protein subunits of the electron transport chain, it may contribute to almost 30% of total mRNA in certain tissues[17]. Nonsynonymous SNPs may thus generate a high amount of mutant peptide. In our study, the immune system of both mice and humans was able to recognize and respond to every mtDNA

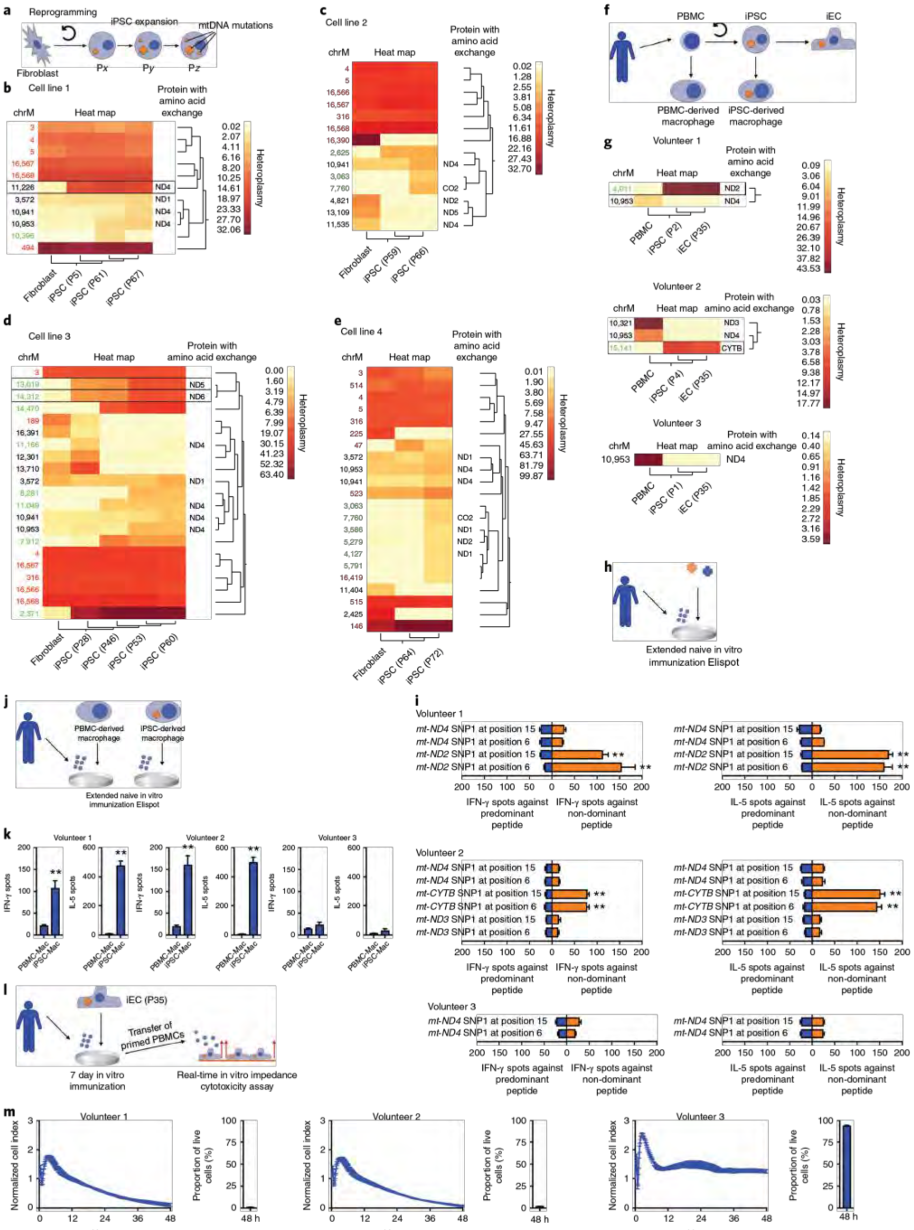

SNP-derived peptide (or the corresponding 20-residue oligomer) if it became sufficiently enriched to meet our definition of a neoantigen. Although the thresholds for changes in SNP heteroplasmy to qualify as neoantigen were set arbitrarily, we assumed the immune system would require a certain burden of mutant peptide to induce a response. A signaling threshold for the magnitude and duration of T cell-receptor signaling required for T cell activation has recently been described[18]. If an immune response was induced, it depended on MHC presentation, and we were able to predict immunogenicity on the basis of the host MHC genotype.

Presumably, most mtDNA heteroplasmies found in healthy tissue in vivo have been present since embryogenesis, and mtDNA SNP enrichments or de novo mutations are not regularly observed[10]. We believe that this phenomenon is due to constant immune surveillance. Malignant tumors, which evade immune clearance, show a much higher incidence of cancer-specific somatic mtDNA mutations in protein-coding or RNA-coding regions[10]. Long-term in vitro iPSC expansion resembles tumor growth, as it takes place in the absence of immune regulation and cell clones with growth advantage, whether attributed to their mtDNA or not, will promote their mtDNA composition within the overall expanding cell population. Reprogramming eliteness and clonal fitness have been shown to drive such cellular dynamics and poised clones are destined to dominate[19]. Most DNA[6,20–23], as well as mtDNA, mutations[11] found in iPSCs were shown to be derived from pre-existing mutations in donor cells, while de novo mutations were rather uncommon. However, no connection has so far been made with neoantigenicity of enriched SNPs. Extended iPSC culture, as shown herein, increases the risk of amplifying neoantigenic SNPs on a large scale. This acquired immunological barrier may become an inherent shortcoming of autologous iPSC-based regenerative strategies. Screening and assessment of neoantigenic mtDNA SNPs in industrial processes will be challenging. For the near future, unless such screening and assessments have been done, immunosuppression protocols for 'near match' iPSC products may be warranted.

Online content

Any methods, additional references, Nature Research reporting summaries, source data, statements of code and data availability and associated accession codes are available at https://doi.org/10.1038/s41587-019-0227-7.

Received: 13 November 2017; Accepted: 16 July 2019;
Published online: 19 August 2019

References

1. de Almeida, P. E. et al. Transplanted terminally differentiated induced pluripotent stem cells are accepted by immune mechanisms similar to selftolerance *Nat. Commun.* 5, 3903 (2014).
2. Zhao, T., Zhang, Z. N., Rong, Z. & Xu, Y. Immunogenicity of induced pluripotent stem cells. *Nature* 474, 212–215 (2011).
3. Araki, R. et al. Negligible immunogenicity of terminally differentiated cells derived from induced pluripotent or embryonic stem cells. *Nature* 494, 100–104 (2013).
4. Guha, P., Morgan, J. W., Mostoslavsky, G., Rodrigues, N. P. & Boyd, A. S. Lack of immune response to differentiated cells derived from syngeneic induced pluripotent stem cells. *Cell Stem Cell* 12, 407–412 (2013).
5. Zhao, T. et al. Humanized mice reveal differential immunogenicity of cells derived from autologous induced pluripotent stem cells. *Cell Stem Cell* 17, 353–359 (2015).
6. Ji, J. et al. Elevated coding mutation rate during the reprogramming of human somatic cells into induced pluripotent stem cells. *Stem Cells* 30, 435–440 (2012).
7. Brown, W. M., George, M. Jr. & Wilson, A. C. Rapid evolution of animal mitochondrial DNA. *Proc Natl Acad Sci. USA* 76, 1967-1971 (1979).
8. Yakes, F. M. & Van Houten, B. Mitochondrial DNA damage is more extensive and persists longer than nuclear DNA damage in human cells following oxidative stress. *Proc Natl Acad Sci USA* 94, 514–519 (1997)
9. Zastawny, T. H. et al. Comparison of oxidative base damage in mitochondrial and nuclear DNA. *Free Radic Biol Med.* 24, 722–725 (1998).
10. He, Y. et al. Heteroplasmic mitochondrial DNA mutations in normal and tumour cells. *Nature* 464, 610–614 (2010).
11. Kang, E. et al. Age-related accumulation of somatic mitochondrial DNA mutations in adult-derived human iPSCs *Cell Stem Cell* 18, 625-636 (2016).
12. Loveland, B., Wang, C. R., Yonekawa, H., Hermel, E. & Lindahl, K. F. Maternally transmitted histocompatibility antigen of mice: a hydrophobic peptide of a mitochondrially encoded protein. *Cell* 60, 971-980 (1990).
13. Hanekamp, J. S. et al. Cytoplasmic inheritance of transplantation antigens in animals produced by nuclear transfer. *Transplantation* 88, 30–37 (2009).
14. Deuse, T. et al. SCNT-derived ESCs with mismatched mitochondria trigger an immune response in allogeneic hosts. *Cell Stem Cell* 16, 33-38 (2015).
15. Yates, A. et al. Ensembl 2016. *Nucleic Acids Res* 44, D710–716 (2016).
16. Lee, A. S. et al. Effects of cell number on teratoma formation by human embryonic stem cells. *Cell Cycle* 8, 2608–2612 (2009).
17. Mercer, T. R. et al. The human mitochondrial transcriptome. *Cell* 146, 645–658 (2011).
18. Au-Yeung, B. B. et al. A sharp T cell antigen receptor signaling threshold for T cell proliferation. *Proc Natl Acad Sci USA* 111, E3679–3688 (2014).
19. Shakiba, N. et al. Cell competition during reprogramming gives rise to dominant clones. *Science* 364, eaan0925 (2019).
20. Young, M. A. et al. Background mutations in parental cells account for most of the genetic heterogeneity of induced pluripotent stem cells *Cell Stem Cell* 10, 570–582 (2012).
21. Quinlan, A. R. et al. Genome sequencing of mouse induced pluripotent stem cells reveals retroelement stability and infrequent DNA rearrangement during reprogramming. *Cell Stem Cell* 9, 366-373 (2011).
22. Laurent, L. C. et al. Dynamic changes in the copy number of pluripotency and cell proliferation genes in human ESCs and iPSCs during reprogramming and time in culture. *Cell Stem Cell* 8, 106–118 (2011).
23. Sugiura, M. et al. Induced pluripotent stem cell generation-associated point mutations arise during the initial stages of the conversion of these cells. *Stem Cell Reports* 2, 52-63 (2014).

Acknowledgements

We thank C. Pahrmann for cell culture work, assistance with experiments and immunoblots; G. Tediashvili for assistance with the in vivo experiments; and M.S. Mahadevan for computer assistance. Special thanks to R. Jaenisch (MIT Department of Biology, MIT, Cambridge, MA) for providing the NT ESCs and to J. Wu (Stanford Cardiovascular Institute, Stanford, CA) and P.-L. So (Stem Cell Core, Gladstone Institutes, San Francsico, CA) for providing the mouse and human iPSCs Special thanks to D. Sun and X. Wu for their help in developing the targeted mtDNA sequencing and droplet digital PCR assays. We thank R. Nelson and K. Copeland for their support with in vivo imaging and M. Lewis for his support with the Xcelligence experiments S.S. received research grants from the Deutsche Forschungsgemeinschaft (DFG; grants SCHR992/3-1, SCHR992/4-1), the Fondation Leducq (CDA 2013-2015) and the DZHK (German Center for Cardiovascular Research; grant FKZ 81Z2710105). D.W. was supported by the Max-Kade-Foundation (DFG). M.H.S. received an NIH shared instrumentation grant (1S10OD018040-01). B.P and Z.K.-Y were supported by the NIH (grant 1R21AI134127-01). S.A.-E., A.M., Y.Y. and H.V. were supported by National Heart Lung and Blood Institute (NHLBI) Intramural Research Program

Author contributions

T.D and S.S. designed the experiments, supervised the project and wrote the manuscript. X.H. performed the immunobiology experiments molecular biology, imaging studies, cell culture work and analyzed the data S.A.E., A.M., Y.Y and H.V performed the mtDNA sequencing and analysis. M.H.S. performed cytometry by time of flight experiments. A.G. did imaging studies and cell culture work. M.A. performed bioinformatics analyses. B.P and Z.K.-Y performed epitope predictions and designed 20-residue oligomers. R.R. performed HLA typing. D.W. performed the in vivo and immunofluorescence imaging studies (confocal microscopy). M.K., B.N. and R.K. performed the human kidney and liver transplant study. H.R and I.L.W gave technical support and conceptual advice All authors contributed to editing the manuscript.

Competing interests

The authors declare no competing interests

Additional information

Supplementary information is available for this paper at https://doi.org/10.1038/s41587-019-0227-7.

Reprints and permissions information is available at www.nature.com/reprints.

Correspondence and requests for materials should be addressed to S.S.

Publisher's note: Springer Nature remains neutral with regard to jurisdictional claims in published maps and institutional affiliations

© The Author(s), under exclusive licence to Springer Nature America, Inc 2019

Methods

Mice. Male 6- to 8-week-old BALB/c (BALB/c AnNCrl, H2^d), C57BL/6 (C57BL/6J, H2^b), FVB (FVB/NCrl), SCID-beige (CB17.Cg-*Prkdc*^{scid}*Lyst*$^{bg-J}$/Crl), and CD4-knockout (B6.129S2-*Cd4*^{tm1Mak}/J) mice were purchased from Charles River Laboratories or Jackson Laboratory, received humane care in compliance with the Guide for the Principles of Laboratory Animals, and experiments have complied with all relevant ethical regulations. Mouse studies were approved by the Hamburg Amt für Gesundheit und Verbraucherschutz or the University of California, San Francisco Institutional Animal Care and Use Committee. Some B6 animals were immunosuppressed with tacrolimus (Prograf, Astella Pharma) at a concentration of 0.5 mg kg^{-1} d^{-1}.

Generation and culture of ESCs. NT-ESCs were generated as previously described using F1 enucleated BDF1 oocytes (C57BL/6J × DBA/2NCrl) and somatic cell nucleus from BALB/c (B/c) fibroblasts[14]. NT-ESCs were cultured on γ-irradiated CF1 feeders (Millipore) using standard ESC medium (Gibco) containing leukemia inhibitory factor (LIF; Millipore). Before being used in experiments, NT-ESCs were cultured on gelatin (Millipore) without feeders using standard medium containing LIF. Cell cultures were regularly screened for mycoplasma infections (Lonza).

Mouse iPSC reprogramming and modification. FVB iPSCs were a gift from J. Wu (Stanford University, Stanford, CA). C57BL/6 iPSCs were generated by reprogramming mouse-tail-tip fibroblasts using a codon-optimized minicircle (CoMiC) construct as previously described[24]. CRISPR–Cas9 technology was used for the generation of B6 *B2m*$^{-/-}$*Ciita*$^{-/-}$ iPSCs[25]. Please see Supplementary Note 1 for details.

Mouse iPSC-derived iECs. For endothelial cell differentiation, mouse iPSCs were plated on gelatin in six-well plates. After the cells arrived at 60% confluence, the differentiation was started and medium was changed to RPMI-1640 containing 2% B-27 minus insulin (both Gibco) and 5 µM CHIR-99021 (Selleckchem). On day 2, the medium was changed to reduced RPMI-1640 containing 2% B-27 minus insulin and 2 µM CHIR-99021 (Selleckchem). From day 4 to day 7, cells were exposed to RPMI-1640 containing 2% B-27 minus insulin plus 50 ng ml^{-1} mouse vascular endothelial growth factor (mVEGF; R&D Systems), 10 ng ml^{-1} mouse fibroblast growth factor (mFGF; R&D Systems), 10 µM Y-27632 (Sigma Aldrich) and 1 µM SB 431542 (Sigma Aldrich). Endothelial cell clusters were visible from day 7 and cells were maintained in EGM-2 SingleQuots medium (Lonza) plus 10% heat-inactivated FCS (Gibco), 25 ng ml^{-1} mVEGF, 2 ng ml^{-1} mFGF, 10 µM Y-27632 (Sigma Aldrich) and 1 µM SB 431542. The differentiation process was completed after 21 d and undifferentiated cells detached during the differentiation process. For purification, cells went through MACS purification according to the manufactures' protocol using anti-CD15 monoclonal-antibody-coated magnetic microbeads (Miltenyi) for negative selection.

Human iPSC reprogramming. PBMCs were isolated from healthy volunteers and iPSCs were generated by the Yale University stem cell core laboratory using Sendai viral expression of *OCT4*, *SOX2*, *KLF4* and *MYC* genes. The experiments were approved by the University of California, San Francisco Institutional Review Board. Human iPSCs were plated on diluted Matrigel (356231, Corning) in six-well plates and maintained in Essential 8 Flex medium (Thermo Fisher Scientific). All human iPSC culture was feeder-layer free and cultures were clump passaged every 2–3 d. Cell cultures were regularly screened for mycoplasma infections (Lonza).

Human iPSC-derived iECs. For the differentiation to endothelial cells, iPSC cultures were grown to 60% confluence and medium was changed to RPMI-1640 containing 2% B-27 minus insulin and 5 µM CHIR-99021 (Selleckchem). On day 2 of the differentiation, the medium was changed to reduced RPMI-1640 containing 2% B-27 minus insulin and 2 µM CHIR-99021 (Selleckchem). From day 4 to day 7, cells were exposed to RPMI-1640 containing 2% B-27 minus insulin plus 50 ng ml^{-1} human vascular endothelial growth factor (VEGF; R&D Systems), 10 ng ml^{-1} human fibroblast growth factor (FGF; R&D Systems), 10 µM Y-27632 (Sigma Aldrich) and 1 µM SB 431542 (Sigma Aldrich). Endothelial cell clusters were visible from day 7 and cells were maintained in EGM-2 SingleQuots medium (Lonza) plus 10% heat-inactivated FCS (Gibco), 25 ng ml^{-1} VEGF, 2 ng ml^{-1} FGF, 10 µM Y-27632 (Sigma Aldrich) and 1 µM SB 431542 (Sigma Aldrich). The differentiation process was completed after 14 d and undifferentiated cells detached during the differentiation process. For purification, cells were treated with 20 µM PluriSIn-1 (StemCell Technologies) for 48 h. The highly enriched iECs were cultured in EGM-2 SingleQuots medium (Lonza) plus supplements and 10% heat-inactivated FCS (Gibco). TrypLE was used for passaging the cells at a 1:3 ratio every 3–4 d.

Human fibroblast-derived iPSCs. Human iPSCs and their parental fibroblasts from four different individuals were provided by the Cardiovascular Institute at Stanford School of Medicine and the Stem Cell Core at the Gladstone Institutes. HLA typing confirmed that the cell lines had no common origin.

Human iPSC-derived macrophages. To differentiate iPSC-derived macrophages, 2 × 10^6 iPSCs were resuspended in DMEM 11965, supplemented with 10% KO-serum, 1% glutamine, 0.1 mM 2-mercaptoethanol and 1% RevitaCells (all Gibco) and were cultured in six-well low-attachment plates (Corning) for 4 d for embryoid body formation. Embryoid bodies were transferred to gelatin-coated six-well plates in macrophage medium containing DMEM 11965, supplemented with 10% heat-inactivated FCS, 1% glutamine, 0.1 mM 2-mercaptoethanol (all Gibco), 50 ng ml^{-1} human macrophage colony stimulating factor (M-CSF) and 25 ng ml^{-1} human IL-3 (both Peprotech). Medium was changed every second day and non-adherent macrophages were collected on day 8. Macrophages were replated in macrophage medium with 100 ngml human M-CSF for another 24 h before the cells were used for assays.

Human PBMC-derived macrophages. PBMCs were isolated by Ficoll separation (GE Healthcare) from fresh blood from healthy volunteers and were resuspended in RPMI-1640 with 10% heat-inactivated FCS, 1% penicillin–streptomycin (all Gibco) and 10 ng ml^{-1} human M-CSF (Peprotech). Cells were plated in 24-well plates at a concentration of 1 × 10^6 cells per milliliter (1 milliliter per 24-well plate) and medium was changed every second day until day 6. Macrophages were stimulated from day 6 with 1 µg ml^{-1} human IL-2 (Peprotech) for 24 h before the cells were used for assays.

Protein overexpression in fibroblasts or endothelial cells for Co3 and Cytb. For transfection experiments, 1.5 × 10^5 B/c fibroblasts or B6 iECs were plated per well into six-well plates and incubated overnight at 37 °C in a cell incubator. Next day, transfection experiments were performed using Fugene (Promega) and 6.6 µg of *Co3* DNA or *Cytb* DNA (Eurofins) in a 3:2 ratio. The transfection reagent solution was pipetted to OptiMEM (Gibco), mixed and incubated for 10 min at room temperature. The DNA transfection complex was added to 2 ml of cell medium. After 24 h, the transfection was stopped and cells were grown for another 48 h in cell-specific medium until they were used for experiments. Successful transfection was confirmed by immunoblots. Proteins were separated on SDS–PAGE gels (Invitrogen) and immunoblots were conducted with specific antibodies to Cytb (ab81215, Abcam), Co3 (ABIN223366, antikoerper-online.de) or actin (ab3280, Abcam). Membranes were digitized using BLI and quantified using the NIH ImageJ software v.1.46r. Actin served as a housekeeping control.

Human transplant study. Patients listed for kidney or liver transplantation gave consent to participate in this study. The study was approved by the External Review Board of the Ärztekammer Hamburg (PV5100) and complied with all relevant ethical regulations. A total of nine patients underwent kidney transplantation (patients 4, 7, 9, 10, 12, 13, 14, 15 and 16) and six patients underwent liver transplantation (patients 5, 6, 11, 17, 18 and 21). During the transplant operation, a blood sample from the recipient and some discarded fat tissue from the donor organ was collected and mtDNA sequencing was performed. Homoplasmic mismatches (heteroplasmy >99%) were identified. Twenty-residue oligomer peptides were designed and generated to cover the donor SNP and the recipient's own autologous SNP, respectively. Patients received standard immunosuppression, which included tacrolimus, cyclosporine A or co-stimulation blockers according to center-specific protocols. At 3 and 6 months after the transplantation (only at 6 months for patient 4), blood was drawn from the recipients during regular follow-up visits.

Ethylenediaminetetraacetic-acid-treated blood was drawn and tacrolimus was quantified using liquid chromatography–mass spectrometry (AescuLabor).

To verify the in vitro PBMC reactivation protocol, PBMCs from kidney or liver transplant recipients were isolated with Ficoll centrifugation (GE Healthcare). These PBMCs then served as responder cells either directly after cell isolation or after 24 h of in vitro cell culture with 1 µg ml^{-1} anti-CD3 and anti-CD28 antibodies (Sanquin) in IMEM medium supplemented with 1% penicillin–streptomycin (all Gibco) (Supplementary Fig. 4). Recipient responder PBMCs (5 × 10^5 cells) were incubated with phorbol myristate acetate (PMA; 1 ng ml^{-1}) and ionomycin (500 ng ml^{-1}) (both Sigma Aldrich) for 24 h and IFN-γ spot frequencies were automatically enumerated using an ELISpot plate reader (AID).

For quantitative PCR analysis of IL-2, PBMCs from patients after kidney or liver transplantation were isolated as described above and were stimulated either directly after cell isolation or after 24 h in vitro culture with 1 µg ml^{-1} anti-CD3 and anti-CD28 antibodies (Sanquin) with PMA (1 ng ml^{-1}) and ionomycin (500 ng ml^{-1}) (both Sigma Aldrich) for 4 h (Supplementary Fig. 4). Total RNA was isolated with a TRIzol-based RNA isolation protocol (Invitrogen). RNA was quantified by NanoDrop (Agilent Technologies). Samples required 260/280 ratios of >1.8. RNA was reverse-transcribed with the high-capacity cDNA reverse transcription kit (Applied Biosystems) according to the manufacturer's instructions. Quantitative determination of cDNA was performed by quantitative PCR with reverse transcription with SYBR Premix Ex taq II (Takara Bio), according to the manufacturer's instructions. IL-2 RNA was amplified using the following primers: forward, 5′-GTCACAAACAGTGCACCTAC-3′; and reverse, 5′-CCCTGGGTCTTAAGTGAAAG-3′. Experiments were performed on the Mx3000p (Agilent Technologies). The RNA amount was estimated according to the comparative C_t method using the $2^{-\Delta\Delta C_t}$ formula.

For the human ELISpot assays, PBMCs were isolated using Ficoll centrifugation (GE Healthcare), washed to eliminate immunosuppressive agents and cultured in the presence of anti CD3 and anti-CD28 antibodies (Sanquin) in IMEM medium supplemented with 1% penicillin–streptomycin (all Gibco) to reactivate their responsiveness. IFN-γ ELISpot assays were performed against the recipient and donor 20-residue oligomers. One hundred thousand responder PBMCs were incubated with each peptide at a concentration of 40μg ml^{-1} for 48h and IFN-γ spot frequencies were automatically enumerated as described before.

mtDNA sequencing and analysis. For human kidney or liver transplant donor–recipient pairs, genomic DNA was extracted from adipose tissue or 1 × 10^6 cells (Qiagen DNeasy Blood and Tissue kit, Qiagen). mtDNA was enriched by depletion of nuclear genomic DNA (depiction of methylated genomic DNA using anti-methylated-DNA-coated beads (Next Microbiome DNA Enrichment kit, New England Biolabs) and exonuclease digestion to remove the linear genomic DNA (New England Biolabs)) and targeted amplification of mtDNA sequences using mtDNA-specific primers and multiple-displacement technology (REPLIg Mitochondrial DNA kit, Qiagen). Enzymatic fragmentation and tagmentation were used to prepare the mtDNA libraries (Nextera XT DNA Library Prep kit, Illumina). The quality of mtDNA libraries was analyzed by electrophoresis (Bioanalyzer 2100 High Sensitivity DNA, Agilent) before sequencing (HiSeq 2500, 2 × 50, Illumina). Raw sequencing data were cleaned up by Trimmomatic[26] (v0.36) to remove Illumina adaptor sequences and unpaired reads. The trimmed paired reads were aligned to the revised Cambridge reference sequence (rCRS; accession number NC_012920)[27] using Bowtie2 (v2.2.9)[28]. After marking PCR duplication reads in Picard (v.2.9.0; http://broadinstitute.github.io/picard/), the paired donor and recipient mapped reads were piled up by Samtools (v1.4)[29]. The variants between each pair of donor and recipient samples were called in Varscan (v2.4.3)[30] with the following customized parameters: --min coverage 500 --min reads 10 --min avg qual 26 --min var freq 0.02 --min freq for hom 0.95. The differences in mutation frequency between donor and recipient were computed for selection. A mismatched homoplasmy was selected if the difference in paired frequencies was greater than 95%. Differences in the frequencies in the range of 5% to 95% were grouped as mismatched heteroplasmy mutations. The annotation of variants was performed using ANNOVAR[31] and the UniProt IDs of nonsynonymous mutations were input into the UniProtKB database[32] to retrieve their amino acid sequence in fasta format.

The same pipeline and parameter settings were applied for analyzing mouse iPSC mitochondrial sequencing data referencing the chrMT genome retrieved from the GRCm38 mouse genome. Residual genetic material originating from mouse embryonic feeder cells (Supplementary Table 16) was excluded from further analysis. For sequential sequencing data of human and mouse mtDNA, SNPs were filtered out if their change in heteroplasmy was < 1%. Heat maps showing the heteroplasmy of the variant SNP were generated. Our mtDNA sequencing method was confirmed using two established techniques (targeted sequencing and digital droplet quantitative PCR) focusing on individual SNP positions (Supplementary Table 17). For targeted sequencing, we designed primer sets to amplify both alleles of the SNP of interest. Using DNA from iPSC passages, the region of interest was amplified by PCR. Amplified sequences were used to make DNA libraries that were then pooled and sequenced on the Illumina MiSeq platform. Sequence reads were then aligned to the reference genome sequence to identify individual alleles. The percentage of the alleles were then computed and compared to the percentage derived from unbiased mtDNA sequencing. For single-cell targeted mtDNA sequencing, please see Supplementary Note 2.

Design of 20-residue oligomers. The amino acid sequences around the SNPs were obtained from the NCBI protein database (https://blast.ncbi.nlm.nih.gov/Blast.cgi). Peptides were synthesized as crude material on a small (1-mg) scale (A and A) and were prepared at 20 mg ml^{-1} in 100% DMSO for assays. Two 20-residue oligomer peptides per epitope were generated with the amino acid variation of the SNP at position 6 or 15, thus overlapping by 11 residues. If the amino acid corresponding to the SNP was located 8–14 positions from the start or end of the peptide, then the SNP in one of the 20-residue oligomers was displaced accordingly. If it was located less than 8 positions from the start or end of the peptide, then only one 20-residue or 21-residue oligomer was generated. The peptide sequences are provided in Supplementary Tables 1–4, 6, 11 and 15.

ELISpot assays. Human IFN-γ ELISpot assays (BD Bioscience) were performed against 20-residue oligomers using 10^5 responder PBMCs incubated with 40 μg ml^{-1} peptide for 48 h and IFN-γ spot frequencies were automatically enumerated using an ELISpot plate reader (AID).

When using non-stimulated responder cells, extended naive in vitro immunization ELISpot assays were performed. One hundred thousand PBMCs from human volunteers were incubated in vitro for 14d in IMEM medium supplemented with 10% heat-inactivated FCS with 40 μg ml^{-1} of peptide and 1 μl ml^{-1} of anti CD3 and anti-CD28 antibodies (Sanquin). If macrophages were used as stimulator cells, 10^5 responder PBMCs were incubated with 10^5 macrophages in RPMI medium containing 10% heat inactivated FCS (Gibco). Macrophages were inhibited with mitomycin. Medium was changed on days 3, 7 and 10. IFN-γ (BD Bioscience) and IL-5 (Mabtech) spot frequencies were analyzed as described before.

For mouse ELISpot assays, recipient splenocytes were isolated from fresh spleen 5 d after cell injection and used as responder cells. When cells were used as stimulators, they were mitomycin-inhibited. One hundred thousand stimulator cells were incubated with 5 × 10^5 recipient responder splenocytes for 24 h and IFN-γ and IL-4 spot frequencies (both BD Bioscience) were automatically enumerated using an ELISpot plate reader (AID). When peptides were used as stimulators, isolated splenocytes from fresh spleen 5d after cell injection or from untreated mice were preincubated in vitro for 24 h with 40 μg ml^{-1} peptide in RPMI medium containing 10% heat-inactivated FCS (all Gibco). Peptide (40 μg ml^{-1}) was incubated with 10^6 recipient responder splenocytes for 48h and IFN-γ spot frequencies were automatically analyzed using an ELISpot plate reader (AID).

When using non-stimulated responder cells, extended naive in vitro immunization ELISpot assays were performed. One million splenocytes were incubated in vitro for 14d in RPMI-1640 medium supplemented with 10% heat-inactivated FCS with 40 μg ml^{-1} peptide or 10^6 cells. Medium was changed on days 3, 7 and 10. IFN-γ spot frequencies were analyzed as described before.

ELISpot frequencies are displayed in bar graphs directly comparing two experimental conditions. The positive *x* axis shows the allogeneic or neoantigenic condition and the negative *x* axis shows the autologous, reference or control condition.

In vitro T cell-mediated rejection. T cell-mediated rejection was assessed with the real-time in vitro impedance XCelligence SP platform (ACEA BioSciences). Fresh PBMCs from volunteers and autologous iECs derived from the same volunteer were co-cultured with 1 μl ml^{-1} anti-CD3 and anti-CD28 antibodies (Sanquin) in six-well plates at a 1:1 ratio for 7 d. PBMCs were collected while iECs were discarded. In parallel, 96-well E-plates (ACEA BioSciences) were coated with gelatin (Millipore) and 4 × 10^5 iECs were plated in 100 μl of cell-specific medium. After the cell index value reached 0.7, PBMCs were transferred to the E-plates at an effector cell:target cell ratio of 1:1. As a control, iECs were grown in the absence of PBMCs. Data were standardized and analyzed with the RTCA software (ACEA).

After 90h, iECs were collected and stained for the live/dead assay (LifeTechnologies). In brief, cells were stained with 2μl of 50 μM calcein AM and 4 μl of 2 mM ethidium homodimer 1 for 45 min at 4 °C. The analysis was performed by flow cytometry (BD Bioscience) and results were expressed as a percentage of live cells. Please see Supplementary Note 3 for details on gating.

Mass cytometry (cytometry by time of flight). A summary of all mass cytometry antibodies, reporter isotopes and concentrations used for analysis can be found in Supplementary Table 18. Please see Supplementary Note 4 for details.

Teratoma development of mouse iPSCs in vivo. Before transplantation, iPSCs were cultured off feeder for two passages to avoid contamination with feeder cells. Cells were trypsinated, resuspended in sterile saline and directly injected into the thigh muscles using a 27-gauge syringe (cell numbers as indicated in the figures). Cell survival leading to teratoma formation was monitored using a digimatic caliper (Mitutoyo). Animals were killed once the thigh volume exceeded 1,500 mm^3.

Bioluminescence imaging of iECs and fibroblasts. Luciferase-expressing iECs (5 × 10^5) were injected into the right thigh muscle of B6 animals using a 27-gauge syringe. Imaging was performed on days 0 and 1, every second day until day 30 and on day 40. Luciferase expressing fibroblasts (5 × 10^5) overexpressing Co3 and Cytb were mixed at a 1:1 ratio with BD Matrigel high concentration (BD Biosciences) and 500 μl was injected subcutaneously into the right lower abdomen of B/c mice using a 23-gauge syringe. Imaging of the animals was performed on days 0, 3 and 6. BLI was performed on the amiHT bioimaging platform (Spectral Instruments Imaging). D-Luciferin potassium salt (Biosynth AG) dissolved in PBS, pH 7.4 (Gibco) was injected intraperitoneally (375 mg kg^{-1}) into anesthetized mice (2% isoflurane). Region of interest (ROI) bioluminescence was quantified in units of maximum photons per second per square centimeter per steradian. The maximum ROI signal was measured using AmiView Image Analysis Software (Spectral Instruments).

iPSC graft infiltration. A total of 1 × 10^6 B6 P7 or P37 iPSCs were injected below the kidney capsule of syngeneic B6 mice. After 5 d, the kidneys were recovered, embedded in paraffin and the injection sites were sectioned at 5-μm thickness. Slides were stained with antibodies against CD3 (Ab16669, Abcam), CD335 (16-3351-81, Thermo Fisher Scientific) and F4/80 (ab6640, Abcam) and were counterstained with DAPI (Thermo Fisher Scientific).

Epitope prediction. The Immune Epitope Database (IEDB) analysis resource[33,34], was used to perform predictions of MHC class I and MHC class II binding. We used the standalone versions of the MHC class I and MHC class II predictors with the default setting 'IEDB_recommended', which is usually a consensus method combining different prediction methods[33], and performed predictions for each MHC–peptide combination.

For the human prediction based on the volunteers' HLA type (see Supplementary Note 5), only the 232 annotated human missense SNPs with SIFT prediction listed as 'tolerated' in Ensembl were used. For HLA class I peptides, we took lengths 8–11 into account, while for HLA class II peptides we considered 15-residue oligomers. The predicted percentile ranks were used to rank and select peptides for further evaluation. Based on the predicted percentile ranks, five peptides with the highest predicted immunogenicity and five peptides with the lowest predicted immunogenicity were picked for testing.

Mouse predictions are possible for B6, which express H-2 K^b and H-2 D^b for MHC class I and H2 IAb for MHC class II. For MHC class I, we considered less than second percentile rank a possible binder, less than first percentile a likely binder, and less than a half percentile a likely high-affinity binder. For MHC class II, we considered less than 20th percentile rank a reasonable threshold to identify candidates.

Statistics. In box plots, the median is shown, the edges of the box are the 25th and 75th percentiles and the whiskers extend to the most extreme data points. Bar graphs show the mean ± s.d. Intergroup differences were appropriately assessed by either unpaired Student's *t* test or one-way analysis of variance (ANOVA) with Bonferroni's post hoc test. $P < 0.01$ is represented by asterisks if space is restricted.

Reporting Summary. Further information on research design is available in the Nature Research Reporting Summary linked to this article.

Data availability

All epitope sequences and 20-residue oligomer sequences are presented in the paper. All data supporting the findings of this study are available in the paper and its supplementary information files. Sequencing data are available from the Sequence Read Archive under accession code PRJNA544330.

References

24. Diecke, S. et al. Novel codon-optimized mini-intronic plasmid for efficient, inexpensive, and xeno-free induction of pluripotency. *Sci. Rep.* **5**, 8081 (2015).
25. Deuse, T. et al. Hypoimmunogenic derivatives of induced pluripotent stem cells evade immune rejection in fully immunocompetent allogeneic recipients. *Nat. Biotechnol.* **37**, 252–258 (2019).
26. Bolger, A. M., Lohse, M. & Usadel, B. Trimmomatic: a flexible trimmer for Illumina sequence data. *Bioinformatics* **30**, 2114–2120 (2014).
27. Andrews, R. M. et al. Reanalysis and revision of the Cambridge reference sequence for human mitochondrial DNA. *Nat. Genet.* **23**, 147 (1999).
28. Langmead, B. & Salzberg, S. L. Fast gapped-read alignment with Bowtie 2. *Nat. Methods* **9**, 357–359 (2012).
29. Li, H. et al. The Sequence Alignment/Map format and SAMtools. *Bioinformatics* **25**, 2078–2079 (2009).
30. Koboldt, D. C. et al. VarScan 2: somatic mutation and copy number alteration discovery in cancer by exome sequencing. *Genome Res.* **22**, 568–576 (2012).
31. Wang, K., Li, M. & Hakonarson, H. ANNOVAR: functional annotation of genetic variants from high-throughput sequencing data. *Nucleic Acids Res.* **38**, e164 (2010).
32. The UniProt Consortium UniProt: the universal protein knowledgebase. *Nucleic Acids Res.* **45**, D158–D169 (2017).
33. Fleri, W. et al. The immune epitope database and analysis resource in epitope discovery and synthetic vaccine design. *Front. Immunol.* **8**, 278 (2017).
34. Kim, Y. et al. Immune epitope database analysis resource. *Nucleic Acids Res.* **40**, W525–530 (2012).

nature biotechnology

SUPPLEMENTARY INFORMATION

https://doi.org/10.1038/s41587-019-0227-7

In the format provided by the authors and unedited.

De novo mutations in mitochondrial DNA of iPSCs produce immunogenic neoepitopes in mice and humans

Tobias Deuse[1,16], Xiaomeng Hu[1,2,3,16], Sean Agbor-Enoh[4,5], Martina Koch[6], Matthew H. Spitzer[7,8,9], Alessia Gravina[1,3], Malik Alawi[10], Argit Marishta[5], Bjoern Peters[11], Zeynep Kosaloglu-Yalcin[11], Yanqin Yang[5], Raja Rajalingam[12], Dong Wang[1,2,3], Bjoern Nashan[6], Rainer Kiefmann[13], Hermann Reichenspurner[2,3], Hannah Valantine[5], Irving L. Weissman[14] and Sonja Schrepfer[1,2,3,15*]

[1]Department of Surgery, Division of Cardiothoracic Surgery, Transplant and Stem Cell Immunobiology Lab, University of California, San Francisco, San Francisco, CA, USA. [2]Department of Cardiovascular Surgery, University Heart Center Hamburg, Hamburg, Germany [3]Cardiovascular Research Center Hamburg and German Center for Cardiovascular Research, partner site Hamburg/Kiel/Luebeck, Hamburg, Germany [4]Division of Pulmonary and Critical Care Medicine, The Johns Hopkins School of Medicine, Baltimore, MD, USA. [5]Laboratory of Transplantation Genomics, Division of Intramural Research, National Heart, Lung, and Blood Institute, Bethesda, MD, USA. [6]Department of Hepatobiliary and Transplant Surgery, University Medical Center Hamburg-Eppendorf, University Transplant Center, Hamburg, Germany. [7]Departments of Otolaryngology, Head and Neck Surgery and Microbiology and Immunology, Helen Diller Family Comprehensive Cancer Center, University of California, San Francisco, San Francisco, CA, USA. [8]Parker Institute for Cancer Immunotherapy, San Francisco, CA, USA. [9]Chan Zuckerberg Biohub, San Francisco, CA, USA. [10]Bioinformatics Core, University Medical Center Hamburg-Eppendorf, Hamburg, Germany. [11]Division of Vaccine Discovery, La Jolla Institute for Allergy and Immunology, La Jolla, CA, USA. [12]Immunogenetics and Transplantation Laboratory, Department of Surgery, University of California, San Francisco, San Francisco, CA, USA. [13]Department of Anaesthesia, University Medical Center Hamburg-Eppendorf, Hamburg, Germany. [14]Department of Developmental Biology, Stanford Institute for Stem Cell Biology and Regenerative Medicine, Stanford University School of Medicine, Stanford, CA, USA. [15]Sana Biotechnology Inc., South San Francisco, CA, USA. [16]These authors contributed equally: Tobias Deuse, Xiaomeng Hu. *e-mail: Sonja.Schrepfer@ucsf.edu

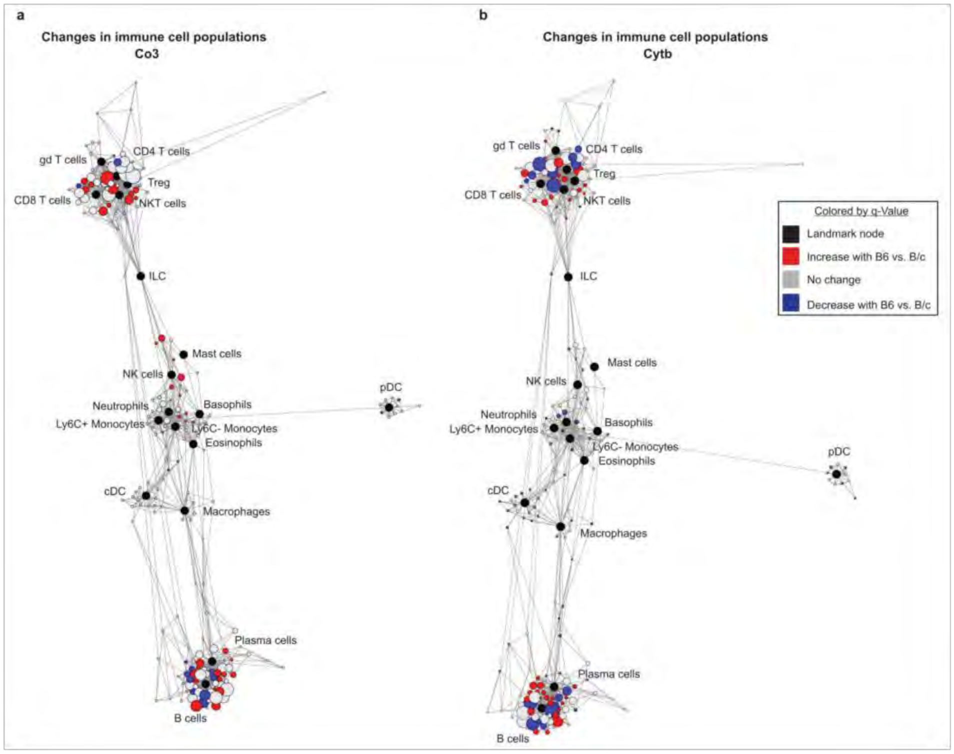
a
Changes in immune cell populations
Co3
gd T cells
CD4 T cells
Treg
CD8 T cells
NKT cells
ILC
Mast cells
NK cells
Neutrophils
Basophils
pDC
Ly6C+ Monocytes
Ly6C- Monocytes
Eosinophils
cDC
Macrophages
Plasma cells
B cells
b
Changes in immune cell populations
Cytb
gd T cells
CD4 T cells
Treg
CD8 T cells
NKT cells
Colored by q-Value
Landmark node
Increase with B6 vs. B/c
No change
Decrease with B6 vs. B/c
ILC
Mast cells
NK cells
Neutrophils
Basophils
Ly6C+ Monocytes
Ly6C- Monocytes
Eosinophils
pDC
cDC
Macrophages
Plasma cells
B cells

Supplementary Figure 1

System-wide analysis of the immune response by mass cytometry.

a-b, B/c splenocytes from animals receiving syngeneic fibroblasts overexpressing syngeneic B/c or allogeneic B6 Co3 (a) or Cytb proteins (b) were harvested and analyzed by mass cytometry (representative pictures of 6 animals per group). Statistical scaffold analysis was performed on the resulting data to identify immune cell populations of differing frequencies. Immune cell subsets that are significantly increased or decreased in animals receiving B6-overexpressing cells are shown in red and blue, respectively. Landmark cell populations manually identified in the data are shown in black and facilitate interpretation of the map.

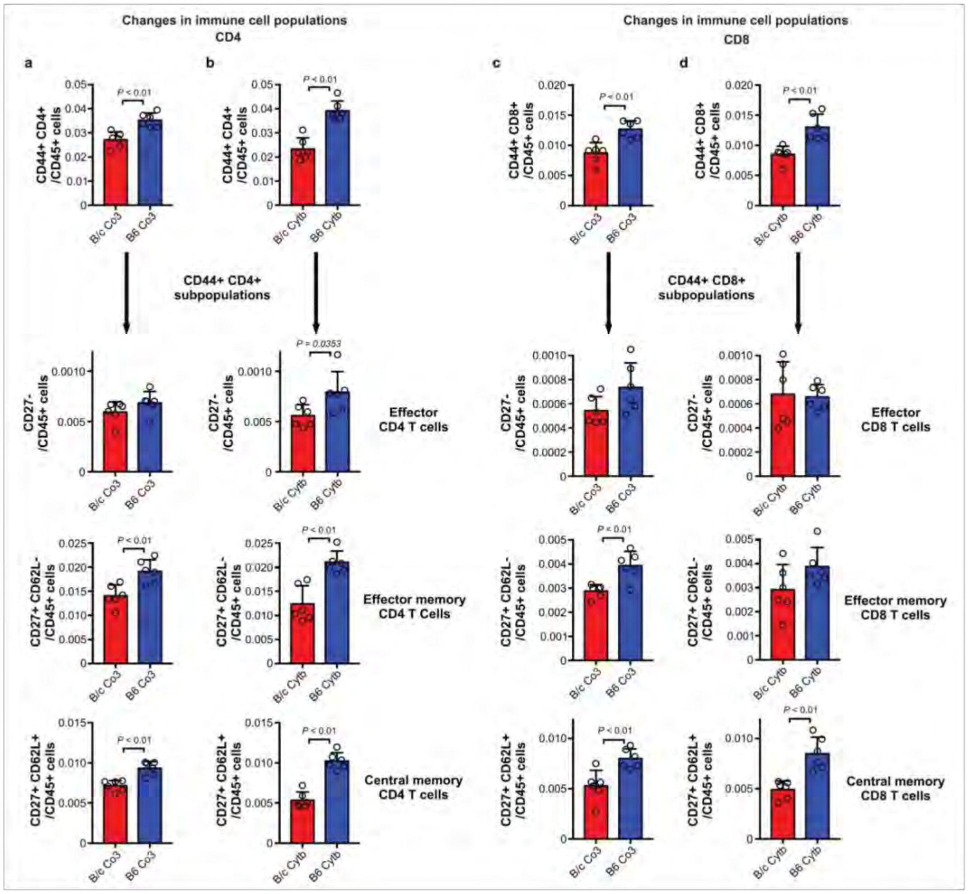

Supplementary Figure 2

Animals challenged with allogeneic proteins have expanded effector / memory T cell populations.

a-d, Animals were immunized with B/c or B6 Co3 proteins (a, c) or Cytb (b, d). Mass cytometry data were analyzed for the frequency of effector / memory CD4 (a, b) and CD8 (c, d) T cell subsets in the spleen (mean ± s.d., 6 animals per group, two-tailed Student's *t*-test). Frequencies of total antigen experienced ($CD44^+$), short-lived effector ($CD45^+CD27^-$), effector memory ($CD45^+CD27^+CD62L^-$), and central memory ($CD45^+CD27^+CD62L^+$) CD4 or CD8 T cells are shown.

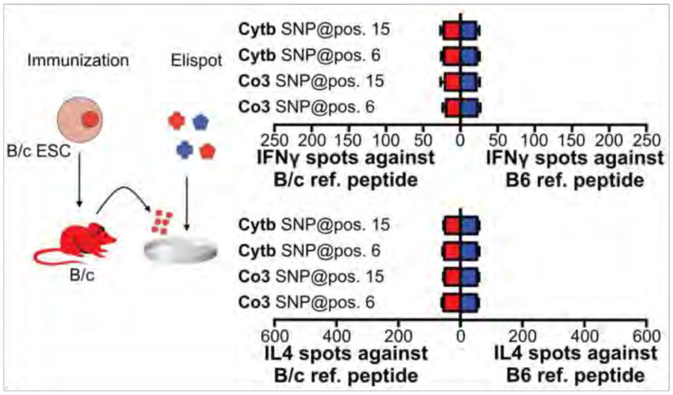

Supplementary Figure 3

There is no cross-reactivity between fetal nuclear gene-derived antigens and the Co3 and Cytb 20mers.

B/c mice were immunized with B/c ESCs, which were suspended in saline and injected into the thigh muscle. After 5 days, Elispot assays were performed with recipient splenocytes to test reactivity against 20mers carrying the B6-specific (blue) or B/c-specific (red) amino acid of the SNP at position 6 or 15 (mean ± s.d., quadruplicates of 4 animals per protein, two-tailed Student's *t*-test).

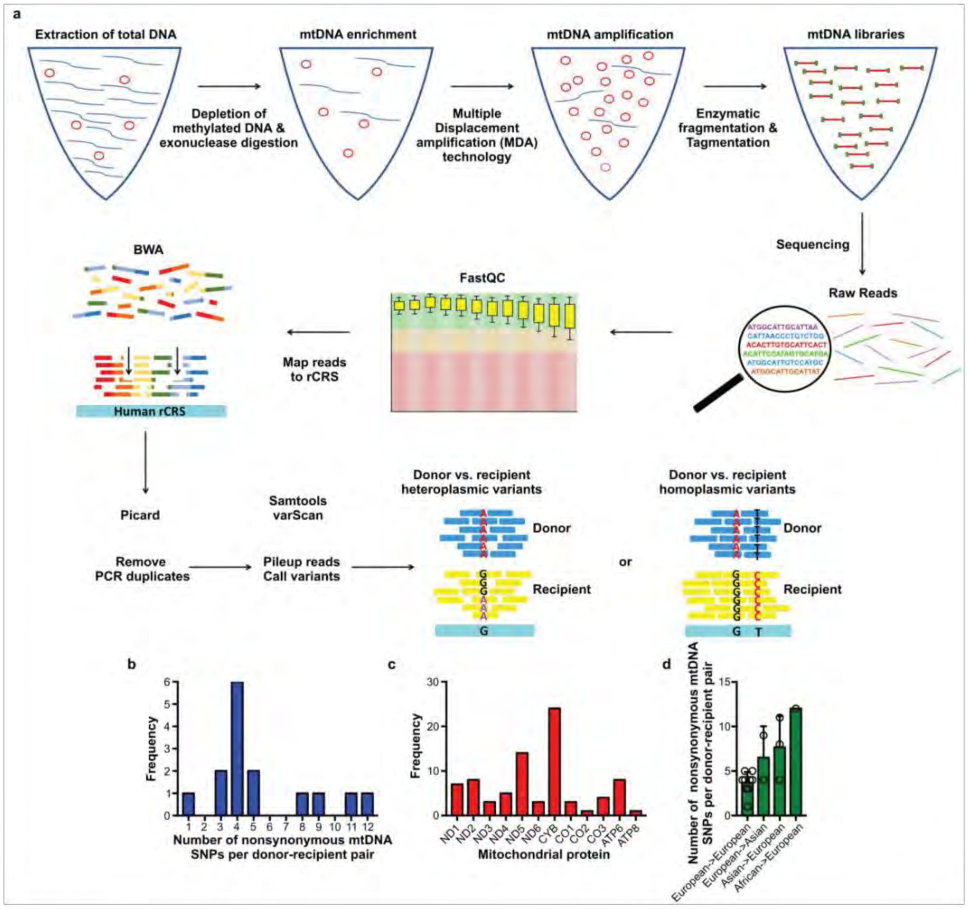

Supplementary Figure 4

mtDNA sequencing of human donor-recipient pairs.

a, Total DNA was extracted from donor tissue and recipient blood. mtDNA was enriched and amplified and mtDNA libraries were created. After sequencing, raw reads underwent quality control and map reads were aligned to human rCRS. After removal of duplicates and pileup of variants, either heteroplasmic or homoplasmic donor-recipient SNP variants were identified. **b**, Of 15 patient pairs, the number of homoplasmic nonsynonymous mtDNA SNPs is shown. **c**, Nonsynonymous homoplasmic SNPs were found at different frequencies in 12 mitochondrial proteins. **d**, The number of nonsynonymous mtDNA SNPs in donor-recipient pairs by ethnic background is shown.

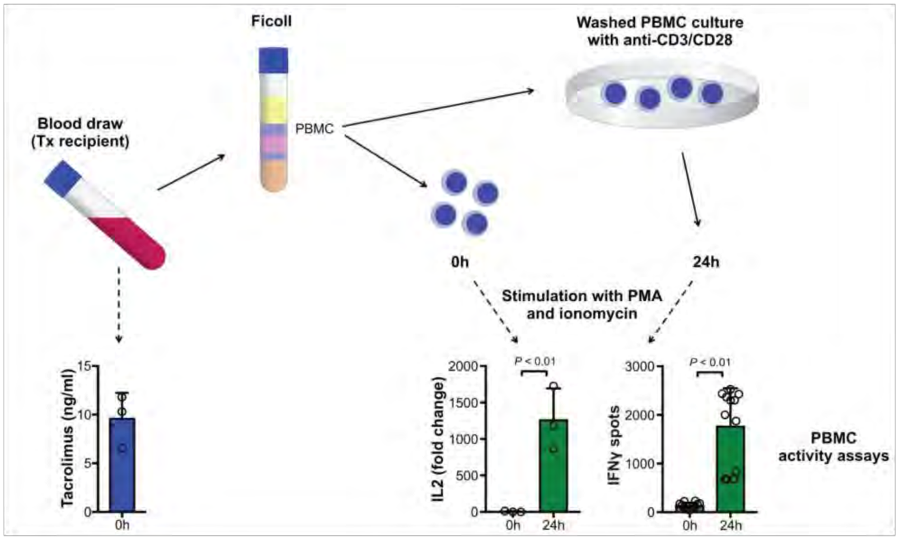

Supplementary Figure 5

In vitro reactivation of PBMCs of immunosuppressed organ recipients.

Blood was drawn from three organ recipients 3 weeks after transplantation. All patients were on a regimen including tacrolimus, mycophenolate mofetil, and steroids with therapeutic tacrolimus trough levels (mean ± s.d., n = 3 patients). PBMCs were isolated using Ficoll gradient centrifugation and one fraction was immediately tested for their immune responsiveness (0 h). Another fraction of PBMCs was washed and cultured in the presence of anti-CD3 and anti-CD28 for 24 h before being tested (24 h). PBMCs were unspecifically stimulated with PMA and ionomycin and their IL2 expression was quantified by PCR (mean ± s.d., n = 3 patients, two-tailed Student's *t*-test) and their IFNγ release by Elispot assays (mean ± s.d., quadruplicates of n = 3 patients, two-tailed Student's *t*-test).

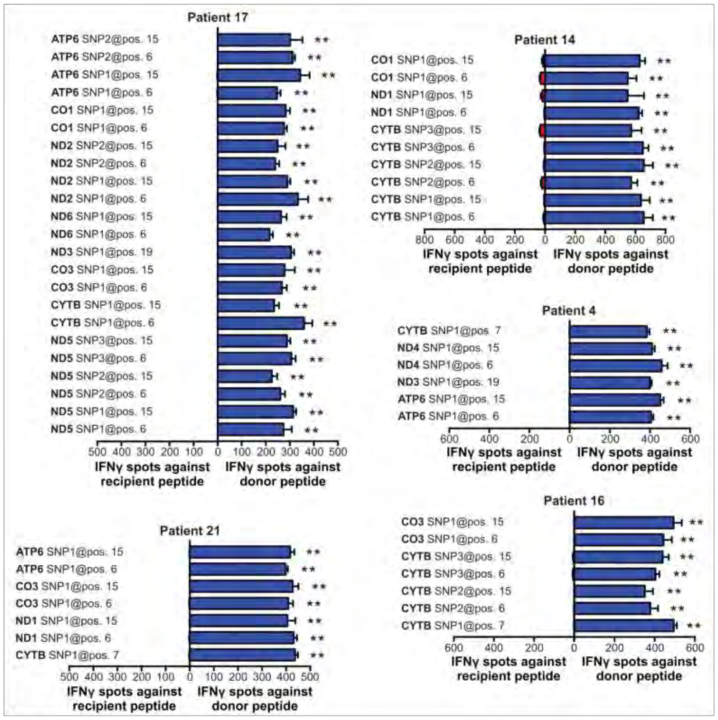

Supplementary Figure 6

Additional patients for the human transplant study.

Five more patients are displayed from the human transplant study outlined in Figure 2 (mean ± s.d., quadruplicates per 20mer and patient, two-tailed Student's *t*-test). Blue shades correspond to donor, red shades to recipient 20mers. ** $P < 0.01$.

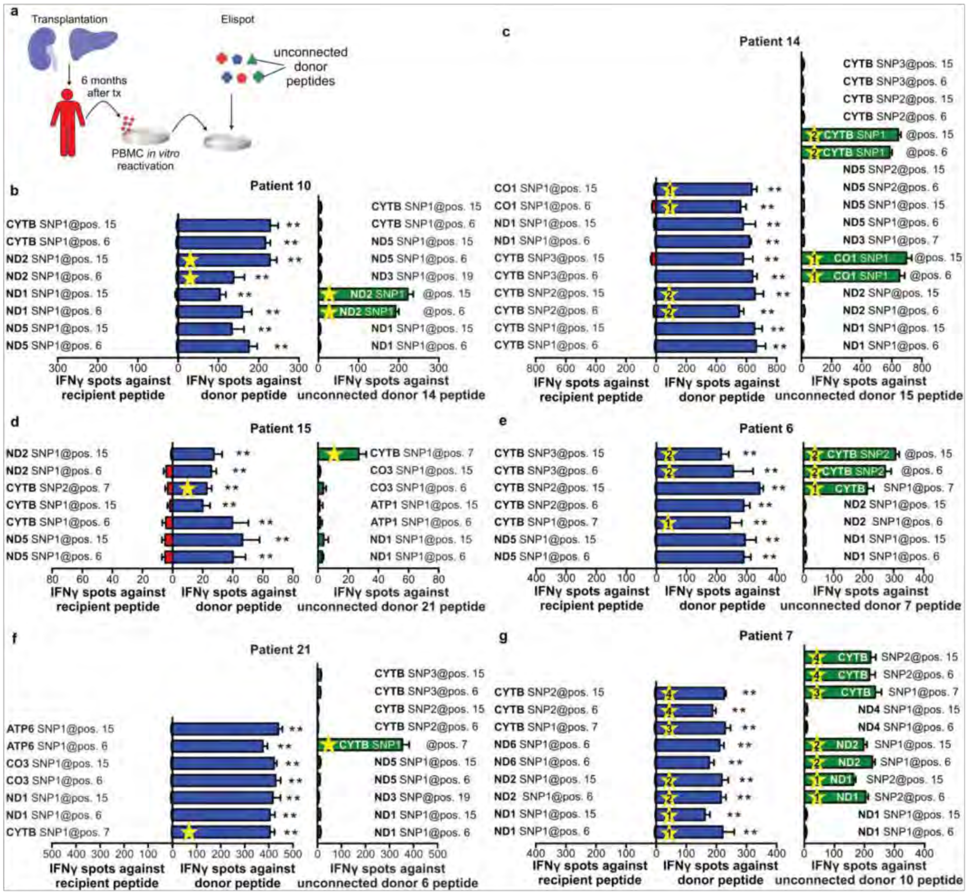

Supplementary Figure 7

Confirmatory patient study on the specificity of the immune response.

Six patients with 4-5 nonsynonymous mtDNA SNPs to their donor were chosen for this study. Blood was drawn 6 months after liver or kidney transplantation and PBMCs underwent *in vitro* reactivation. In Elispot assays, PBMCs were challenged with autologous (red) or two sets of allogeneic 20mers reflecting mtDNA SNPs of their donor (blue) or another unconnected donor (green; mean ± s.d., quadruplicates per 20mer and patient, two-tailed Student's *t*-test). Among the depicted SNPs, yellow asterisks mark SNPs that are identical between the patient's donor and the unconnected donor. ** $P < 0.01$.

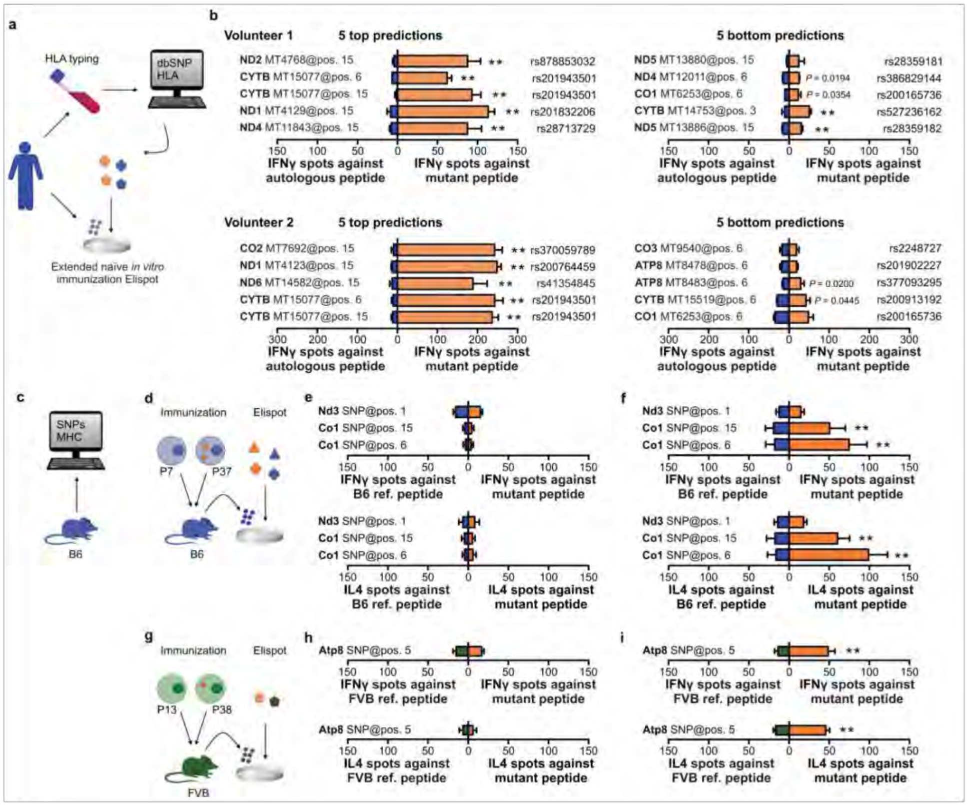

Supplementary Figure 8

In silico antigenicity predictions of human and mouse SNPs.

a, Blood was drawn from two volunteers for 4-digit HLA typing. Using *in silico* prediction models, the top 5 peptides with the highest predicted immunogenicity and bottom 5 SNPs with the lowest predicted immunogenicity from the annotated human SNP library were identified for each volunteer. **b**, 20mers were generated to cover either the mutant or autologous SNP and used in extended naïve *in vitro* immunization Elispot assays with volunteer PBMCs (Volunteer 1: mean ± s.d., triplicates per 20mer, two-tailed Student's *t*-test; Volunteer 2: mean ± s.d., quadruplicates per 20mer, two-tailed Student's *t*-test). Blue shades correspond to autologous, yellow shades to mutant 20mers. **c**, *In silico* predictions for B6 MHC binding was performed for the 3 neoantigenic SNP candidates identified in P37 iPSCs. **d**, B6 mice were immunized with autologous P7 or P37 iPSCs and after 5 days, splenocytes were incubated in Elispot assays with 20mers from the 2 neoantigen candidate SNPs or the B6 reference SNPs. **e**, Elispot assays from mice immunized with P7 iPSCs (mean ± s.d., quadruplicates of 6 animals per 20mer, two-tailed Student's *t*-test). **f**, Elispot assays from mice immunized with P37 iPSCs (mean ± s.d., quadruplicates of 6 animals per 20mer, two-tailed Student's *t*-test). **g**, FVB mice were immunized with autologous P13 or P38 iPSCs and after 5 days, splenocytes were incubated in Elispot assays with 20mers from the neoantigen candidate SNP or the FVB reference SNP. **h**, Elispot assays from mice immunized with P13 iPSCs (mean ± s.d., quadruplicates of 6 animals per 20mer, two-tailed Student's *t*-test). **i**, Elispot assays from mice immunized with P38 iPSCs (mean ± s.d., quadruplicates of 6 animals per 20mer, two-tailed Student's *t*-test). Blue shades correspond to the B6 reference 20mer, green to the FVB reference 20mer, and yellow shades to the neoantigenic 20mer. ** $P < 0.01$.

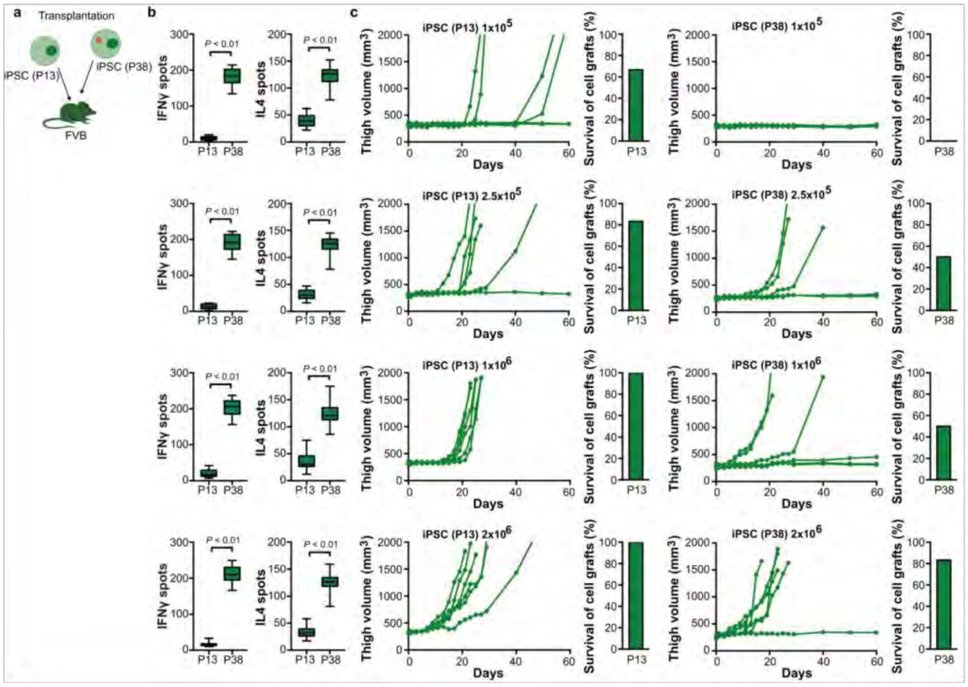

Supplementary Figure 9

Survival of low- and high-passage FVB iPSCs.

a, FVB mice received different cell amounts of autologous low-passage (P13) or high-passage (P38) iPSCs grafts injected into the thigh muscle and were followed for immune response and teratoma development. **b**, After 5 days, splenocytes were recovered for Elispot assays (mean ± s.d., quadruplicates of 6 animals per group, two-tailed Student's *t*-test). **c**, Teratoma growth is depicted for every animal and the percentage of teratoma formation for each group is shown in a separate bar graph (n = 6 per cell amount and iPSC group).

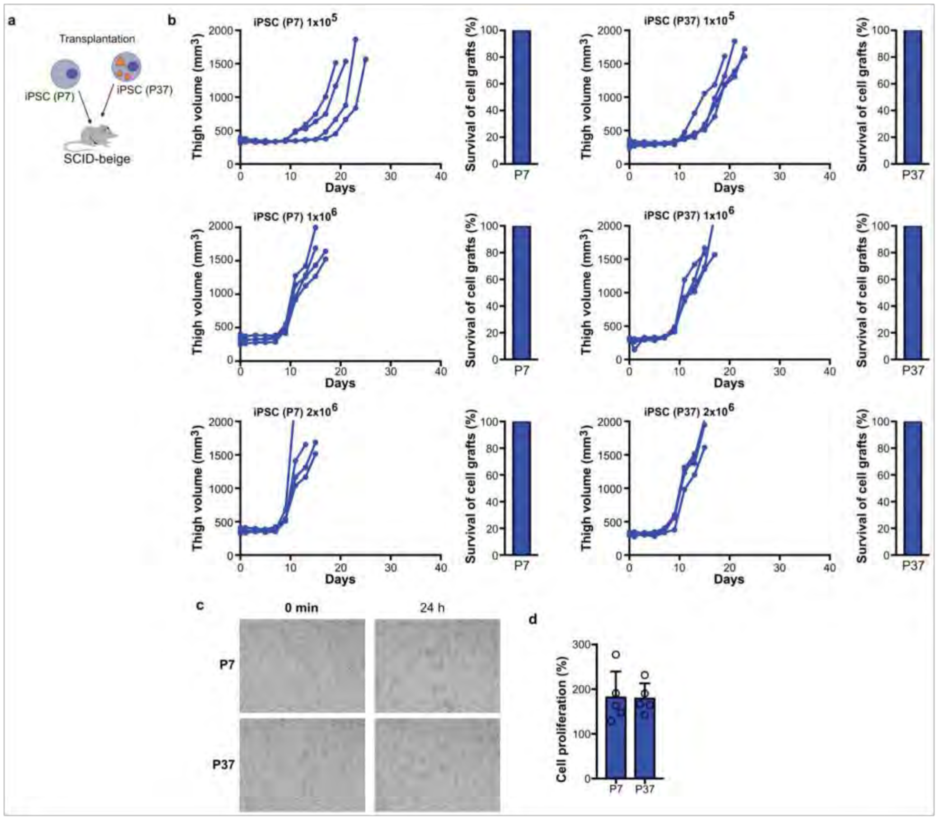

Supplementary Figure 10

Proliferative capacity of B6 iPSCs P7 and P37 *in vivo* and *in vitro*.

a, B6 iPSC grafts from P7 and P37 were injected into the thigh muscle of immunodeficient SCID-beige mice. **b**, Teratoma growth of iPSCs P7 and P37 was followed and the percentage of teratoma formation for each group is shown in a separate bar graph (Individual animals are shown, n = 4 per group). **c**, *In vitro* growth of P7 and P37 iPSC cultures was captured with time-laps life cell imaging and the confluency at 0 min and 24 h is shown (representative pictures of two independent experiments). **d**, The calculated cell proliferation after 24 h is shown (mean ± s.d., 5 replicates per group, two-tailed Student's *t*-test).

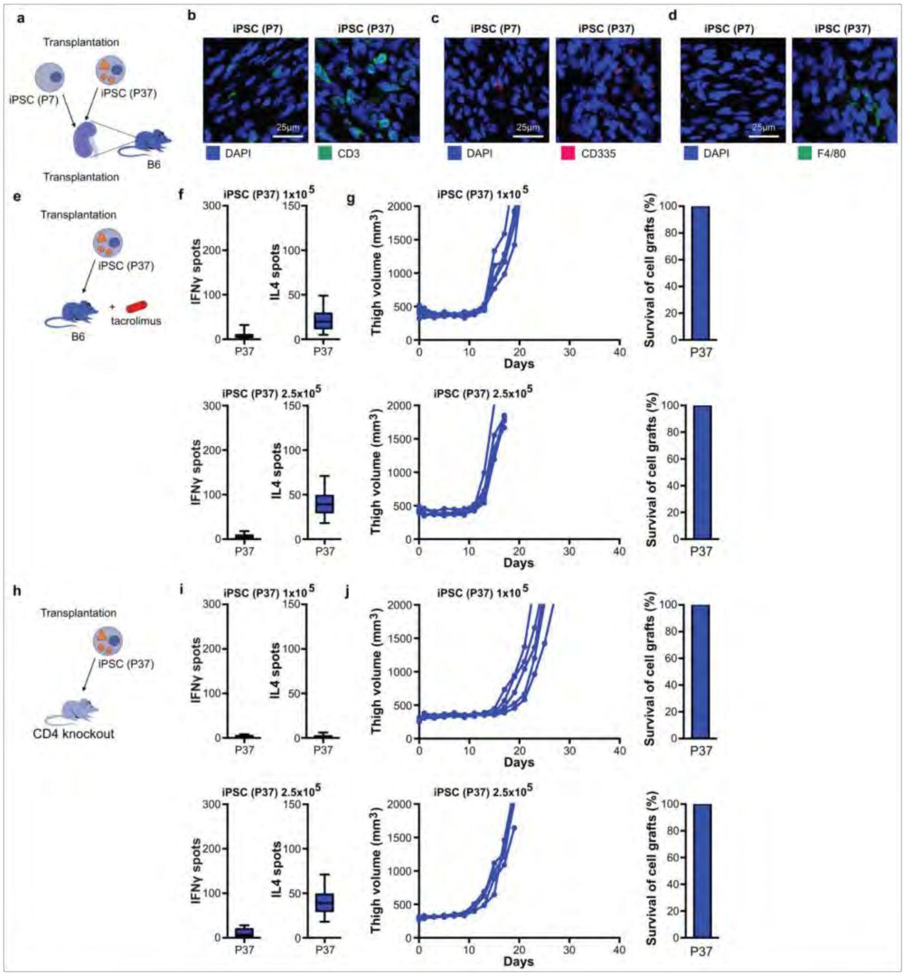

Supplementary Figure 11

The immunogenic nature of B6 iPSC P37 fate after transplantation.

a, iPSC grafts from P7 and P37 were injected below the kidney capsule of syngeneic B6 recipients. **b-d**, Infiltration of P7 and P37 iPSC grafts with CD3$^+$ lymphocytes (b), CD335$^+$ natural killer cells (c), and F4/80$^+$ macrophages (d) by immunofluorescence staining is shown. Scale bar 25 µm. **e**, P37 iPSC grafts at two low cell amounts, which were completely or mostly rejected in immunocompetent B6 mice in Figure 3, were injected into the thigh muscle of B6 recipients immunosuppressed with tacrolimus. **f**, Elispot assays with splenocytes recovered after 5 days are shown (mean ± s.d., quadruplicates of 5 animals per group). **g**, Teratoma growth is depicted for every animal and the percentage of teratoma formation for each group is shown in a separate bar graph (n = 5 animals per group). **h**, P37 iPSC grafts at the same two low cell amounts were then transplanted into immunocompromized CD4 knockout recipients on B6 background. **i**, Elispot assays with splenocytes recovered after 5 days are shown (mean ± s.d., quadruplicates of 5 animals per group). **j**, Teratoma growth is depicted for every animal and the percentage of teratoma formation for each group is shown in a separate bar graph (n = 5 animals per group).

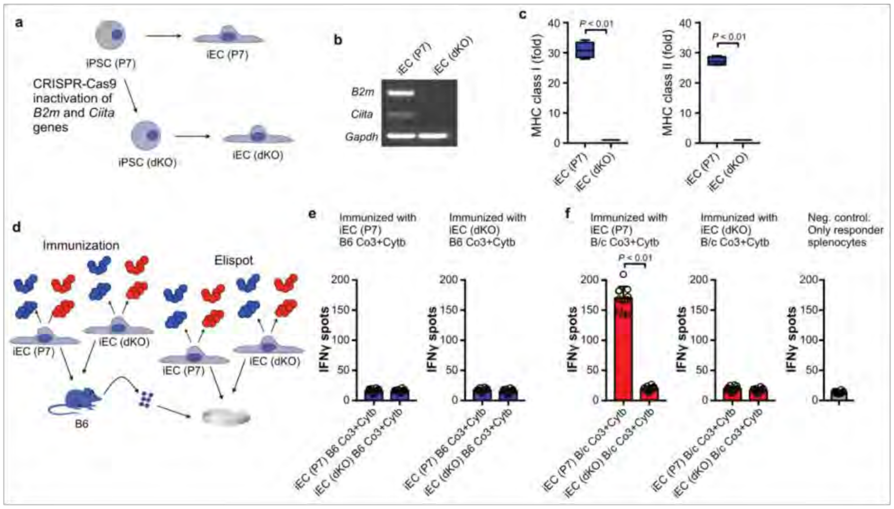

Supplementary Figure 12

Presentation of mtDNA neoantigens via MHC.

a, iPSCs (P7) underwent CRISPR-Cas9 inactivation of the *B2m* and *Ciita* genes to generate double MHC knockout (dKO) iPSCs and iEC (dKO) were differentiated. **b**, The knockouts of *B2m* and *Ciita* in iEC (dKO) were confirmed by PCR (representative gel of two independent experiments). **c**, Surface expression of MHC class I and II was assessed by flow cytometry (mean ± s.d., 4 independent experiments per group, two-tailed Student's *t*-test). **d**, B/6 mice were immunized with either iEC (P7) or iEC (dKO) overexpressing B/c (red) or B6 (blue) Co3 and Cytb. The splenocyte response after 5 days against the same overexpressed proteins in either iEC (P7) or iEC (dKO) was assessed in Elispot assays to determine the mechanistic role of MHC. **e**, Elispot assays of B/6 mice immunized with iEC (P7) or iEC (dKO) overexpressing syngeneic B/6 proteins are shown (mean ± s.d., quadruplicates of 3 animals per group, two-tailed Student's *t*-test). **f**, Elispot assays of B/6 mice immunized with iEC (P7) or iEC (dKO) overexpressing allogeneic B/c proteins are shown. Unstimulated responder splenocytes served a control (mean ± s.d., quadruplicates of 3 animals per group, two-tailed Student's *t*-test).

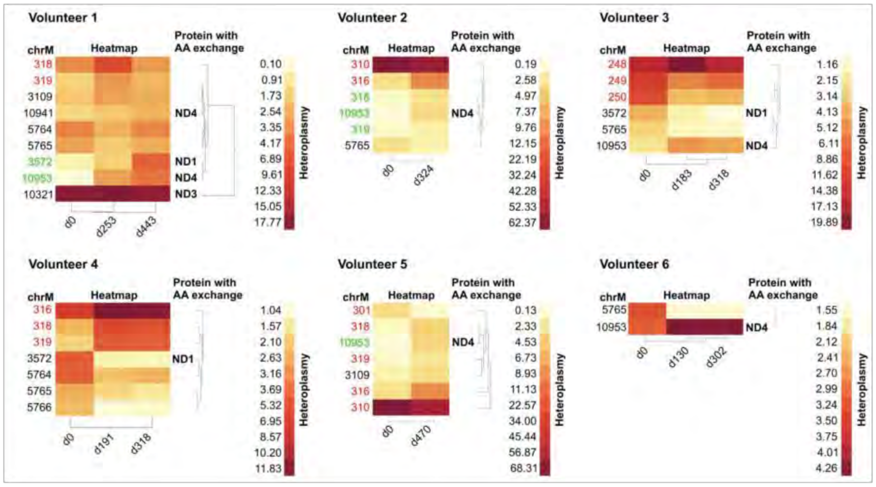

Supplementary Figure 13

Longitudinal mtDNA sequencing of human PBMC SNPs *in vivo*.

PBMCs were repeatedly isolated from 6 volunteers over a minimum of 6 months and mtDNA sequencing was performed. SNPs in the non-coding D-loop are marked in red. SNPs with < 1% heteroplasmy in the first specimen that increased to > 1% in subsequent specimens were considered de novo mutations and are marked in green. SNPs that have been present in the first PBMC specimen and changed their heteroplasmy >1% over time are marked in black. None of the volunteers developed candidate SNPs for neoantigens *in vivo*.

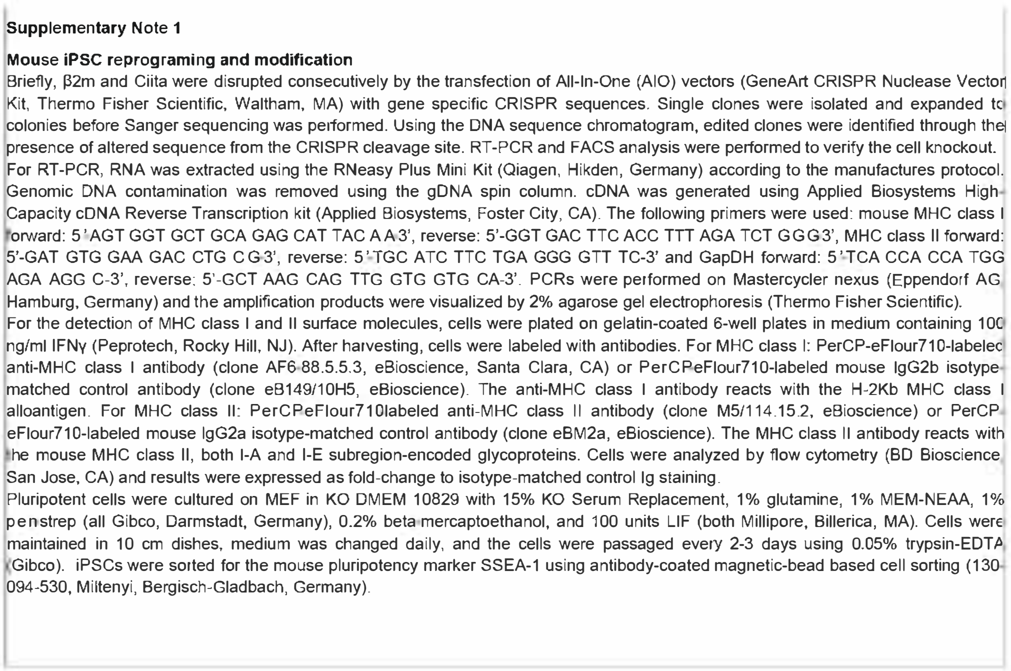

Supplementary Note 1

Mouse iPSC reprograming and modification

Briefly, β2m and Ciita were disrupted consecutively by the transfection of All-In-One (AIO) vectors (GeneArt CRISPR Nuclease Vector Kit, Thermo Fisher Scientific, Waltham, MA) with gene specific CRISPR sequences. Single clones were isolated and expanded to colonies before Sanger sequencing was performed. Using the DNA sequence chromatogram, edited clones were identified through the presence of altered sequence from the CRISPR cleavage site. RT-PCR and FACS analysis were performed to verify the cell knockout.

For RT-PCR, RNA was extracted using the RNeasy Plus Mini Kit (Qiagen, Hikden, Germany) according to the manufactures protocol. Genomic DNA contamination was removed using the gDNA spin column. cDNA was generated using Applied Biosystems High-Capacity cDNA Reverse Transcription kit (Applied Biosystems, Foster City, CA). The following primers were used: mouse MHC class I forward: 5’-AGT GGT GCT GCA GAG CAT TAC AA-3’, reverse: 5’-GGT GAC TTC ACC TTT AGA TCT GGG-3’, MHC class II forward: 5’-GAT GTG GAA GAC CTG CG-3’, reverse: 5’-TGC ATC TTC TGA GGG GTT TC-3’ and GapDH forward: 5’-TCA CCA CCA TGG AGA AGG C-3’, reverse: 5’-GCT AAG CAG TTG GTG GTG CA-3’. PCRs were performed on Mastercycler nexus (Eppendorf AG, Hamburg, Germany) and the amplification products were visualized by 2% agarose gel electrophoresis (Thermo Fisher Scientific).

For the detection of MHC class I and II surface molecules, cells were plated on gelatin-coated 6-well plates in medium containing 100 ng/ml IFNγ (Peprotech, Rocky Hill, NJ). After harvesting, cells were labeled with antibodies. For MHC class I: PerCP-eFlour710-labeled anti-MHC class I antibody (clone AF6-88.5.5.3, eBioscience, Santa Clara, CA) or PerCP-eFlour710-labeled mouse IgG2b isotype-matched control antibody (clone eB149/10H5, eBioscience). The anti-MHC class I antibody reacts with the H-2Kb MHC class I alloantigen. For MHC class II: PerCP-eFlour710labeled anti-MHC class II antibody (clone M5/114.15.2, eBioscience) or PerCP-eFlour710-labeled mouse IgG2a isotype-matched control antibody (clone eBM2a, eBioscience). The MHC class II antibody reacts with the mouse MHC class II, both I-A and I-E subregion-encoded glycoproteins. Cells were analyzed by flow cytometry (BD Bioscience, San Jose, CA) and results were expressed as fold-change to isotype-matched control Ig staining.

Pluripotent cells were cultured on MEF in KO DMEM 10829 with 15% KO Serum Replacement, 1% glutamine, 1% MEM-NEAA, 1% penstrep (all Gibco, Darmstadt, Germany), 0.2% beta-mercaptoethanol, and 100 units LIF (both Millipore, Billerica, MA). Cells were maintained in 10 cm dishes, medium was changed daily, and the cells were passaged every 2-3 days using 0.05% trypsin-EDTA (Gibco). iPSCs were sorted for the mouse pluripotency marker SSEA-1 using antibody-coated magnetic-bead based cell sorting (130-094-530, Miltenyi, Bergisch-Gladbach, Germany).

Supplementary Note 2

Single cell targeted mtDNA sequencing

Single cell analysis was done to determine the distribution of heteroplasmy frequencies at a single cell resolution. We analyzed this in cell line 1 P61 and in one mtDNA position (mtDNA11226). For controls, several positions that showed homoplasmy in bulk culture were added. To validate the PCR primers, we aliquoted known quantities of DNA from bulk iPSC culture and used quantitative PCR to quantitate the DNA of interest; the expected and measured DNA were similar. We then sorted individual cells into individual wells and used the designed PCR primers to amplify both variants of the SNP by PCR. The amplified sequences were used to make libraries that were then sequenced and analyzed. Sequences were aligned to the reference sequence to identify the SNP and the frequency of heteroplasmy was then computed. We only analyzed single cell data in experiments that showed adequate amplification defined as coverage at the position of interest of >150× accompanied by >150× coverage on the bulk DNA sample.

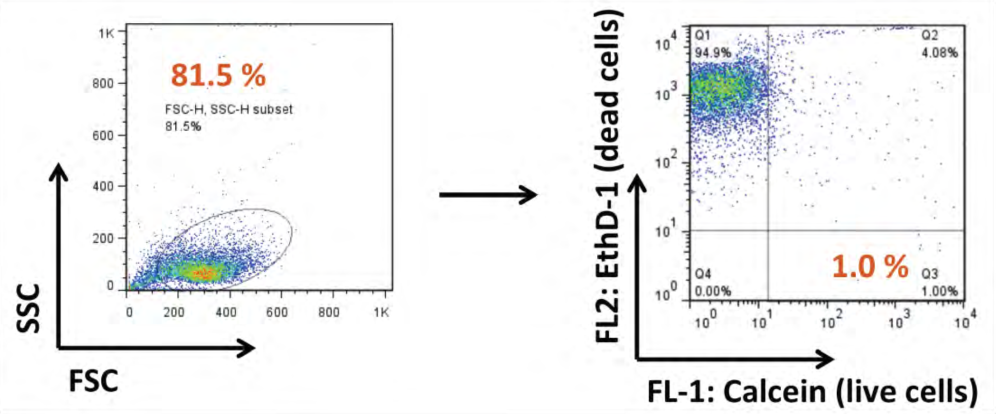

Supplementary Note 3

Example of the flow cytometry gating strategy for the Live/Dead assay.

First gating shows the FSC (forward scatter) and SSC (side scatter) to exclude cellular debris. Cells in FSC-SSC subset were investigated for calcein in channel FL-1 (staining for live cells) and EthD-1 in channel FL-2 (staining for dead cells). Live cells were defined as calcein positive and EthD-1 negative cells. Results were expressed as percentage of live cells.

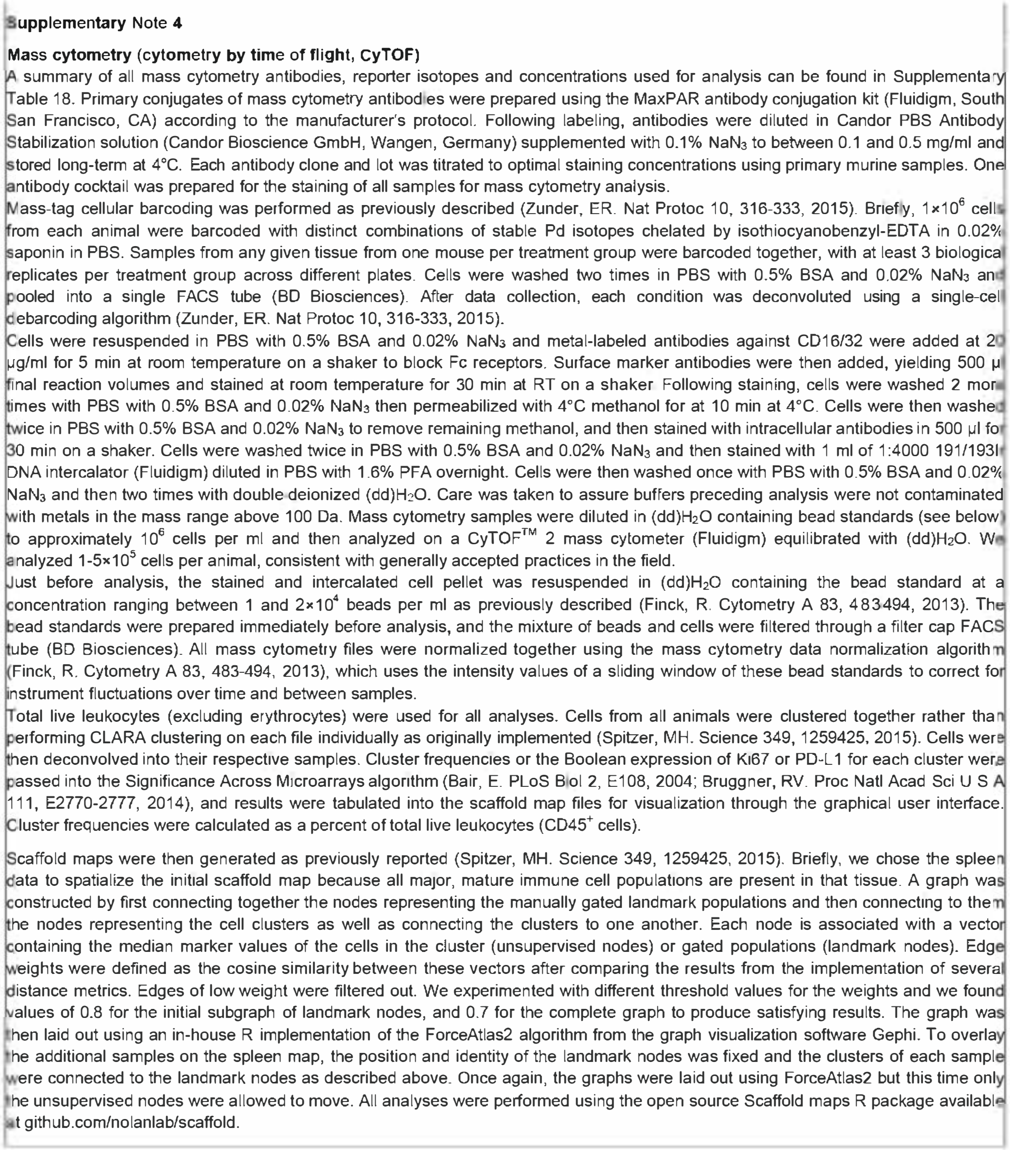

Supplementary Note 4

Mass cytometry (cytometry by time of flight, CyTOF)

A summary of all mass cytometry antibodies, reporter isotopes and concentrations used for analysis can be found in Supplementary Table 18. Primary conjugates of mass cytometry antibodies were prepared using the MaxPAR antibody conjugation kit (Fluidigm, South San Francisco, CA) according to the manufacturer's protocol. Following labeling, antibodies were diluted in Candor PBS Antibody Stabilization solution (Candor Bioscience GmbH, Wangen, Germany) supplemented with 0.1% NaN_3 to between 0.1 and 0.5 mg/ml and stored long-term at 4°C. Each antibody clone and lot was titrated to optimal staining concentrations using primary murine samples. One antibody cocktail was prepared for the staining of all samples for mass cytometry analysis.

Mass-tag cellular barcoding was performed as previously described (Zunder, ER. Nat Protoc 10, 316-333, 2015). Briefly, 1×10^6 cells from each animal were barcoded with distinct combinations of stable Pd isotopes chelated by isothiocyanobenzyl-EDTA in 0.02% saponin in PBS. Samples from any given tissue from one mouse per treatment group were barcoded together, with at least 3 biological replicates per treatment group across different plates. Cells were washed two times in PBS with 0.5% BSA and 0.02% NaN_3 and pooled into a single FACS tube (BD Biosciences). After data collection, each condition was deconvoluted using a single-cell debarcoding algorithm (Zunder, ER. Nat Protoc 10, 316-333, 2015).

Cells were resuspended in PBS with 0.5% BSA and 0.02% NaN_3 and metal-labeled antibodies against CD16/32 were added at 20 µg/ml for 5 min at room temperature on a shaker to block Fc receptors. Surface marker antibodies were then added, yielding 500 µl final reaction volumes and stained at room temperature for 30 min at RT on a shaker. Following staining, cells were washed 2 more times with PBS with 0.5% BSA and 0.02% NaN_3 then permeabilized with 4°C methanol for at 10 min at 4°C. Cells were then washed twice in PBS with 0.5% BSA and 0.02% NaN_3 to remove remaining methanol, and then stained with intracellular antibodies in 500 µl for 30 min on a shaker. Cells were washed twice in PBS with 0.5% BSA and 0.02% NaN_3 and then stained with 1 ml of 1:4000 191/193Ir DNA intercalator (Fluidigm) diluted in PBS with 1.6% PFA overnight. Cells were then washed once with PBS with 0.5% BSA and 0.02% NaN_3 and then two times with double-deionized $(dd)H_2O$. Care was taken to assure buffers preceding analysis were not contaminated with metals in the mass range above 100 Da. Mass cytometry samples were diluted in $(dd)H_2O$ containing bead standards (see below) to approximately 10^6 cells per ml and then analyzed on a CyTOF™ 2 mass cytometer (Fluidigm) equilibrated with $(dd)H_2O$. We analyzed $1\text{-}5\times10^5$ cells per animal, consistent with generally accepted practices in the field.

Just before analysis, the stained and intercalated cell pellet was resuspended in $(dd)H_2O$ containing the bead standard at a concentration ranging between 1 and 2×10^4 beads per ml as previously described (Finck, R. Cytometry A 83, 483-494, 2013). The bead standards were prepared immediately before analysis, and the mixture of beads and cells were filtered through a filter cap FACS tube (BD Biosciences). All mass cytometry files were normalized together using the mass cytometry data normalization algorithm (Finck, R. Cytometry A 83, 483-494, 2013), which uses the intensity values of a sliding window of these bead standards to correct for instrument fluctuations over time and between samples.

Total live leukocytes (excluding erythrocytes) were used for all analyses. Cells from all animals were clustered together rather than performing CLARA clustering on each file individually as originally implemented (Spitzer, MH. Science 349, 1259425, 2015). Cells were then deconvolved into their respective samples. Cluster frequencies or the Boolean expression of Ki67 or PD-L1 for each cluster were passed into the Significance Across Microarrays algorithm (Bair, E. PLoS Biol 2, E108, 2004; Bruggner, RV. Proc Natl Acad Sci U S A 111, E2770-2777, 2014), and results were tabulated into the scaffold map files for visualization through the graphical user interface. Cluster frequencies were calculated as a percent of total live leukocytes ($CD45^+$ cells).

Scaffold maps were then generated as previously reported (Spitzer, MH. Science 349, 1259425, 2015). Briefly, we chose the spleen data to spatialize the initial scaffold map because all major, mature immune cell populations are present in that tissue. A graph was constructed by first connecting together the nodes representing the manually gated landmark populations and then connecting to them the nodes representing the cell clusters as well as connecting the clusters to one another. Each node is associated with a vector containing the median marker values of the cells in the cluster (unsupervised nodes) or gated populations (landmark nodes). Edge weights were defined as the cosine similarity between these vectors after comparing the results from the implementation of several distance metrics. Edges of low weight were filtered out. We experimented with different threshold values for the weights and we found values of 0.8 for the initial subgraph of landmark nodes, and 0.7 for the complete graph to produce satisfying results. The graph was then laid out using an in-house R implementation of the ForceAtlas2 algorithm from the graph visualization software Gephi. To overlay the additional samples on the spleen map, the position and identity of the landmark nodes was fixed and the clusters of each sample were connected to the landmark nodes as described above. Once again, the graphs were laid out using ForceAtlas2 but this time only the unsupervised nodes were allowed to move. All analyses were performed using the open source Scaffold maps R package available at github.com/nolanlab/scaffold.

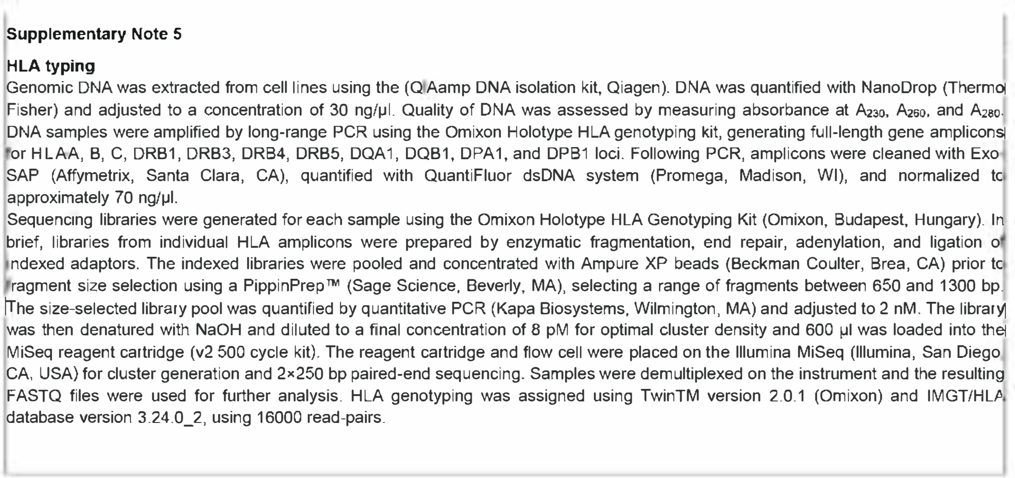

Supplementary Note 5

HLA typing

Genomic DNA was extracted from cell lines using the (QIAamp DNA isolation kit, Qiagen). DNA was quantified with NanoDrop (Thermo Fisher) and adjusted to a concentration of 30 ng/µl. Quality of DNA was assessed by measuring absorbance at A_{230}, A_{260}, and A_{280}. DNA samples were amplified by long-range PCR using the Omixon Holotype HLA genotyping kit, generating full-length gene amplicons for HLA-A, B, C, DRB1, DRB3, DRB4, DRB5, DQA1, DQB1, DPA1, and DPB1 loci. Following PCR, amplicons were cleaned with ExoSAP (Affymetrix, Santa Clara, CA), quantified with QuantiFluor dsDNA system (Promega, Madison, WI), and normalized to approximately 70 ng/µl.

Sequencing libraries were generated for each sample using the Omixon Holotype HLA Genotyping Kit (Omixon, Budapest, Hungary). In brief, libraries from individual HLA amplicons were prepared by enzymatic fragmentation, end repair, adenylation, and ligation of indexed adaptors. The indexed libraries were pooled and concentrated with Ampure XP beads (Beckman Coulter, Brea, CA) prior to fragment size selection using a PippinPrep™ (Sage Science, Beverly, MA), selecting a range of fragments between 650 and 1300 bp. The size-selected library pool was quantified by quantitative PCR (Kapa Biosystems, Wilmington, MA) and adjusted to 2 nM. The library was then denatured with NaOH and diluted to a final concentration of 8 pM for optimal cluster density and 600 µl was loaded into the MiSeq reagent cartridge (v2 500 cycle kit). The reagent cartridge and flow cell were placed on the Illumina MiSeq (Illumina, San Diego, CA, USA) for cluster generation and 2×250 bp paired-end sequencing. Samples were demultiplexed on the instrument and the resulting FASTQ files were used for further analysis. HLA genotyping was assigned using TwinTM version 2.0.1 (Omixon) and IMGT/HLA database version 3.24.0_2, using 16000 read-pairs.

3. Diskussion

Im Laufe der Jahre wurden verschiedene Strategien untersucht, um die Aktivierung des Immunsystems nach einer Transplantation zu verhindern und somit die Abstoßung des Transplantats zu vermeiden. Um die beste Stammzelle für die Anwendung in der Stammzelltherapie zu bestimmen, wurden sie auf ihre Eigenschaften und Immunogenität untersucht. Basierend auf den Ergebnissen von vorherigen Studien wurden zunächst adulte Stammzellen ausgeschlossen (Biehl and Russell, 2009). Diese Zellen sind multipotent und bieten daher nicht die gewünschte Palette an Zellderivaten, welche für den Einsatz der Stammzelltherapie für unterschiedliche Anwendungen notwendig wäre. Embryonale Stammzellen (ESC) sind zwar pluripotent, jedoch ethisch bedenklich und ihr Einsatz in der Medizin bleibt kontrovers. Anfängliche Vermutungen, welche den ESCs eine immunotolerante Eigenschaft zusprechen, wurden schnell widerlegt (Deuse et al., 2011). Ihre Anwendung ist mit der Gabe von Immunsuppressiva begleitet, was mit starken Risiken und Nebenwirkungen verbunden ist. Patientenspezifische Stammzellen, hergestellt durch den somatischen Nukleustransfer (SCNT), tragen zwar die gleichen genetischen Informationen wie der Patient, jedoch führen darin enthaltene allogene Mitochondrien-Proteine zu einer Abstoßung des Transplantats durch die Nebenhistokompatibilitätsmerkmale (miHA). Induzierte pluripotente Stammzellen (iPS-Zellen) sind zwar autologe Stammzellen, jedoch ist ihre Reprogrammierung nicht bei jedem Patienten zu gewährleisten. Bis zum fertigen Endprodukt dauert die Generierung mehrere Wochen bis Monate, was für eine akute Anwendung, zum Beispiel nach einem Myokardinfarkt, nicht praktikabel ist. In dieser Arbeit wurde zudem gezeigt, dass autologe iPS-Zellen auch das eigene Immunsystem durch eventuelle Mutationen in der mtDNA aktivieren können.

Trotz dieser Herausforderungen gab es bereits mehrere klinischen Pilotstudien, in denen allogene pluripotente Stammzell-Derivate (PSC-Derivate) transplantiert wurden. Dies umfasst unter anderem retinale Pigmentepithelzellen bei Makuladegeneration (Mandai et al., 2017; Schwartz et al., 2012; Schwartz et al., 2015), sowie kardiale Vorläuferzelle bei Herzerkrankungen (Miller, 2018). Die Transplantationen verliefen in den meisten Fällen in Begleitung mit einer immunsuppressiven Therapie, welche das Überleben der allogenen Zelltransplantate zwar fördert, jedoch in lebensbedrohlichen

Folgen für den Patienten resultieren kann (Gorantla et al., 2000). Aus diesem Grund ist verheißungsvoll, universelle hypoimmunogene Spenderzellen herzustellen, die nach einer Transplantation nicht abgestoßen werden und keine immunsuppressive Therapie benötigen. Die genetische Modifizierung ist eine vielversprechende Strategie zur Erstellung dieser universeller Spenderzellen.

Die vorliegende Arbeit vorfolgte das Ziel der Generierung einer hypoimmunogenen Stammzelllinie, die für eine klinische Anwendung in der Zelltherapie in Betracht gezogen werden kann. Damit soll die Stammzelltherapie als Option für die Regenerierung von Zellen und Gewebe gefördert werden. Sie kann als Alternative zu einer Organtransplantation angewendet werden und somit den Mangel an Spenderorganen kompensieren.

3.1 Die Immunogenität von iPS-Zellen

Induzierte pluripotente Stammzellen werden von körpereigenen somatischen Zellen, wie z.B. Fibroblasten, durch die Rückprogrammierung *ex vivo* generiert und sind „ethisch korrekte“ Stammzellen (Moradi et al., 2019). Dabei wird die Expression von Pluripotenzgenen in der Zelle künstlich eingeleitet. Sie scheinen das Problem der Transplantatabstoßung zu lösen durch die Generierung autologer Transplantate, welche Patienten-spezifisch hergestellt werden können. iPS-Zellen werden nicht dieselben Eigenschaften wie embryonalen Stammzellen zugesprochen, stattdessen werden sie nur als „embryonic stem cell–like“ bezeichnet.

Erste Erfahrungen mit Transplantationen autologer Epithelzellen in der Netzhaut zeigten die technischen Schwierigkeiten bei der Erzeugung autologer Transplantatzellen (Mandai et al., 2017). Es erfordert eine umfangreiche und langwierige Generierung der iPS-Zellen und in vielen Fällen erfüllen sie nicht die definierte Qualitätskontrolle, welche für eine erfolgreiche Differenzierung dieser pluripotenten Zellen in ihre Derivate gewährleistet. Während die Standards noch angepasst werden könnten, berichteten viele Studien über den Verlust von transplantierten Zellen aus dem Gewebe, womit diese Therapie wirkungslos bleibt (Todorova et al., 2016). Die genauen Mechanismen dafür sind bis dato weitgehend ungeklärt. Zhao et al. beschrieb im Jahr 2011, dass während des Rückprogrammierungsprozesses autologer iPS-Zellen die Expression bestimmter Gene hoch- bzw. herunterreguliert wird. Diese Änderungen könnten vom Immunsystem des Empfängers erkannt und die Zellen als körperfremd markiert werden, so dass es zur Abstoßung des Transplantats kommt (Zhao et al., 2011). Andere Studien berichteten von Teratomformationen nach einer Injektion humaner iPSCs in humanisierten Mäusen, die von T-Zell-Infiltraten und Gewebenekrose begleitet wurden (Zhao et al., 2015).

Auch der Zelltyp der Ausgangszelle für die Generierung von iPS-Zellen scheint ihre einhergehende Abstoßung zu beeinflussen (Zhao et al., 2015). Zudem wurde auch berichtet, dass sich die Immunogenität pluripotenter Stammzellen mit der Differenzierung in ihre Zellderivate verringert (Araki et al., 2013; de Almeida et al., 2014; Guha et al., 2013).

Während der Rückprogrammierung entstehen neue Mutationen bis zu neun Mal häufiger als in Zellkulturen und könnten dabei als Neoantigene fungieren (Ji et al., 2012). In den codierenden DNA-Sequenzen können Spontanmutationen durch den Austausch einzelner Nukleinbasen zwar stumm verlaufen, jedoch auch zu „nonsense“, „missense“ und „readthrough“ Mutationen führen. Die Funktion des Proteins und auch dessen Antigenität kann demnach verändert werden. Die mitochondrielle DNA (mtDNA) ist mit einer 10- bis 20-fach erhöhten Mutationssrate noch anfälliger als die genomische DNA, bei der sie nur 7- bis 9-fach erhöht ist (Brown et al., 1979; Yakes and Van Houten, 1997; Zastawny et al., 1998).

In dieser Arbeit wurde die Integrität der mtDNA in iPS-Zellen als möglicher Auslöser für die Abstoßung von autologen Transplantaten untersucht. Die Gründe einer erhöhten Mutationsrate in der mtDNA könnten unter anderem durch eine geringere Funktion der mtDNA-Reparaturmechanismen, das Fehlen von Histonen, welche die chromosomale DNA schützen, die Schädigung der mtDNA durch Sauerstoffintermediate oder auch die hohe Replikationsgeschwindigkeit der mtDNA begründet sein (Croteau et al., 1999). Obwohl die 16.569-Basenpaare umfassende humane mtDNA nur für 13 Proteinuntereinheiten der Elektronentransportkette codiert, kann sie in bestimmten Geweben zu fast 30% der gesamten mRNA beitragen (Mercer et al., 2011). Die Entstehung von Heteroplasmie in der mtDNA und ihre Anreicherung kann die zellulären Eigenschaften der iPS-Zellen stark verändern und somit eine Immunbarriere für die autologe iPS-Transplantation bilden. mtDNA codierte Minor-Antigene sind bereits als Transplantationsbarrieren bekannt (Deuse et al., 2015), wobei das Auftreten eines einzelnen Einzelnukleotidpolymorphismus (engl. Single Nucleotide Polymorphismus, SNP) für die Immunaktivierung ausreichend ist.

Für die Untersuchung der Ergebnisse wurden mtDNA Sequenzierungen von murinen und humanen iPS-Zellen durchgeführt. Das Auftreten von Neoantigenen, ausgelöst durch SNPs, wurde dabei häufig beobachtet. Basierend auf mtDNA-Mutationen und Heteroplasmie-Anreicherung, validiert in unterschiedlichen Versuchen, konnte ein Schwellenwert für Neoantigene definiert werden. Das Erreichen dieser Schwelle an prozentualem Heteroplasmie-Anteil scheint essenziell für das Auslösen einer Immunantwort zu sein. Diese Neoantigene, die durch die Amplifikation von Zellen entstehen, würden normalerweise *in vivo* eine „immune clearance“ untergehen (He et al., 2010). Da bei der Reprogrammierung und Kulturexpansion keine Immunüberwachung stattfindet, kommt es zu einer „künstlichen“ Anreichung der Heteroplasmie. Ob ein Neoantigen, das ausschließlich auf der mtDNA-Veränderung basiert, zu einem immunologisch relevanten Antigen wird, hängt davon ab, wie gut die MHC/HLA Proteine des Empfängers dieses Epitop präsentieren können.

Anhand von unterschiedlichen Immunassays wurde validiert, dass das humane und murine Immunsystem bestimmte Neoantigene erkennt, die durch die SNPs in der mtDNA hervorgerufen wurden. Dabei ist es unerheblich, ob diese durch allogene Transplantation eingeführt wurden oder ob sie in autologen Zellen während der Reprogrammierung und der *in vitro* Kulturexpansion aufgetreten sind.

3.2 Die hypoimmunogene Stammzelle

Die Natur gibt uns mit dem Beispiel der fetomaternalen Toleranz während der Schwangerschaft ein gutes Vorbild, wie das Immunsystem zwar allogene Zellen als fremd erkennt, jedoch diese nicht aktiv abstößt. Um eine hypoimmunogene Zelle zu konzipieren ist es wichtig, dass sie sowohl gegen die adaptiven als auch gegen die angeborenen Abwehrmechanismen geschützt ist bzw. der Immunabwehr des Empfängers aktiv entgegensteuern kann. Die Generierung einer solchen hypoimmunogenen Stammzelle kann als eine universell kompatible Zellquelle dienen. Die Differenzierung zu unterschiedlichen Zellderivaten kann direkt von Forschern *ex vivo* in großen Mengen und standardisiert durchgeführt werden. Somit werden nicht nur Kosten gespart, sondern auch eine bessere Qualität gewährleistet. Für akute Krankheiten können diese „gebrauchsfertigen“ Zellderivate direkt, ohne die Zugabe von Immunsuppression, eingesetzt werden.

In dieser Arbeit wurde die Generierung einer solchen hypoimmunogenen Stammzelle durch das Knockout von MHCI (*B2m*-/-) und MHCII (*Ciita*-/-) mittels der CRISPR/Cas9 Technologie, sowie die lentivirale Überexpression des Oberflächenmoleküls Cd47, durchgeführt. Als Ausgangszelle im Mausmodell diente zunächst eine C57BL/6 iPS-Zelle (miPSC). Die Modifizierung der miPSC verlief dabei schrittweise und ihre Immunogenität wurde nach jedem Modifikationsschritt überprüft. Die miPSCs wurden syngen in C57BL/6 (H2b-Haplotyp) oder allogen in BALB/c (H2d-Haplotyp) transplantiert. Wie erwartet wurden die unmodifizierten miPSCs in BALB/c Mäusen abgestoßen und zeigten 100% Überleben im syngenen Modell. Zudem wurde im allogenen BALB/c Modell eine starke Immunaktivierung beobachtet und keine Immunaktivierung im syngenen C57BL/6 Modell. Mit jedem Modifikationsschritt wurde das Überleben der miPSC im allogenen Setting gesteigert mit einer gleichzeitigen Verminderung der Immunantwort Die hypoimmunogene Zelle mit allen drei Modifikationen zeigte keine Immunaktivierung *in vitro* und 100% Langzeitüberleben *in vivo*.

Mit dem ersten Modifikationsschritt wurde die MHCI vermittelte T-Zell Immunantwort durch das Knockout von beta-2 Microglobulin (B2m) schon deutlich geschwächt. Das

Langzeitüberleben der *B2m-/-* miPS-Zellen *in vivo* in allogenen BALB/c Mäusen ist von 0% auf 60% gestiegen. Dennoch wurden fünf Tage nach der Zelltransplantation Donor-spezifische IgM-Antikörper im Serum nachgewiesen, welche hochsignifikant zu der syngenen Kontrolle angestiegen sind. Dieser Anstieg wurde mit der zweiten Modifizierung, dem Knockout von Ciita, deutlich reduziert. Auch das *in vivo* Überleben der *B2m-/-Ciita-/-* miPSCs in den BALB/c Mäusen ist auf 90% angestiegen. Die dritte Modifikation mit der Überexpression von Cd47 verfolgte das Ziel, die Zelle gegen die unspezifische Immunantwort durch die NK-Zellen und Makrophagen zu schützen. Um die NK-Zellen vermittelte Immunantwort zu erforschen, wurden *B2m-/-Ciita-/-* und *B2m-/-Ciita-/-Cd47tg* miPSCs vergleichend in spezifischen Assays untersucht. Während die *B2m-/-Ciita-/-* miPSC eine NK-Zellaktivierung zeigten, konnte bei der *B2m-/-Ciita-/-Cd47tg* miPSC keine Aktivierung der NK-Zellen festgestellt werden.

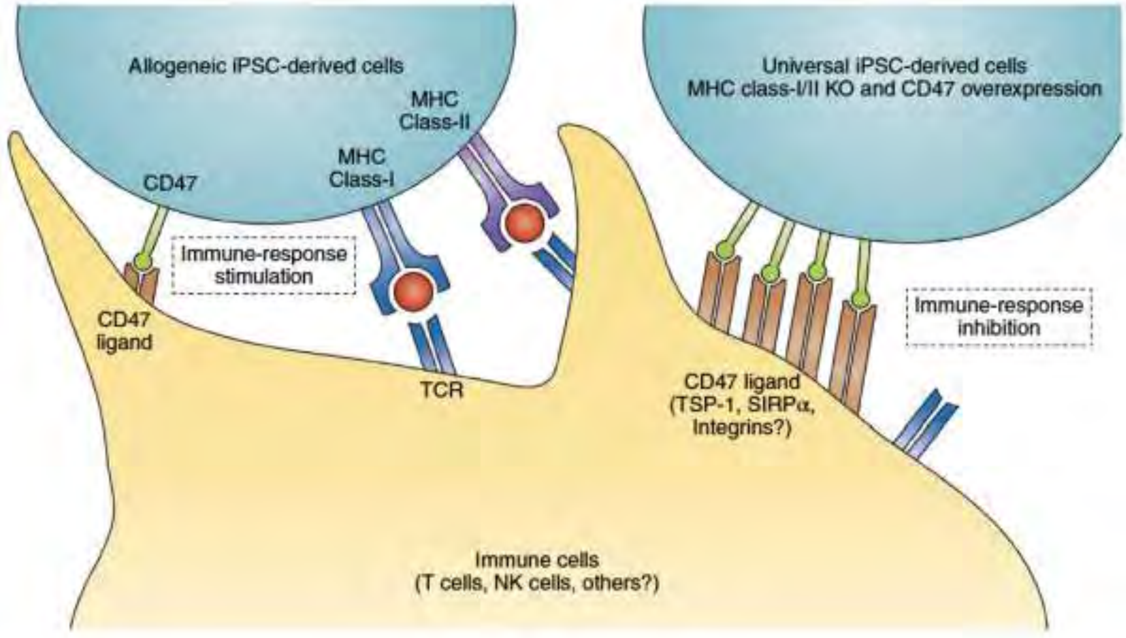
Allogeneic iPSC-derived cells
MHC Class-II
MHC Class-I
CD47
Immune-response stimulation
CD47 ligand
TCR
Universal iPSC-derived cells MHC class-I/II KO and CD47 overexpression
Immune-response inhibition
CD47 ligand (TSP-1, SIRPα, Integrins?)
Immune cells (T cells, NK cells, others?)

Abbildung 3.1: **Die Immunaktivierung durch Immunzellen einer unmodifizierten iPSC versus der hypoimmunogenen iPSC** durch das Knockout von MHC Klasse I und Klasse II sowie die Überexpression von CD47 (Shani and Hanna, 2019).

Die Modifikationsstrategien wurden danach auf humane iPS-Zellen (hiPSCs) übertragen, wobei die hypoimmunogenen hiPSCs in zwei Schritten generiert wurden: Im ersten Schritt wurden die Gene für B2M und CIITA gleichzeitig ausgeknockt und in einem zweiten Schritt das Oberflächenmolekül CD47 überexprimiert. Die

Immunogenität von *B2M-/-CIITA-/-CD47tg* hiPSCs wurde anschließend in humanisierten Mäusen untersucht. Die *B2M-/-CIITA-/-CD47tg* hiPSC zeigte dabei *in vivo* eine hundertprozentige Überlebensrate und auch *in vitro* keine Aktivierung des Immunsystems.

In der Zelltherapie ist die Verwendung von Stammzellen aufgrund des Risikos einer Teratombildung nicht möglich. Daher ist es notwendig, diese pluripotenten Zellen in ihre Zellderivate, die benötigten Zelltypen, zu differenzieren. Sowohl miPSCs als auch hiPSCs wurden in Zellen der mesodermen Zelllinie differenziert, unter anderem in Endothelzellen, glatte Muskelzellen und Herzmuskelzellen. Die differenzierten Zellen aus unmodifizierten iPS-Zellen zeigten in der Durchflusszytometrie eine erhöhte Expression von MHCI und MHCII, was auf einer Steigerung der Immunogenität gegenüber ihrer Ausgangszelle hinweist. Zusammenfassend kann die Aussage getroffen werden, dass alle drei Modifikationsschritte notwendig sind, um eine allogene Immunantwort zu inhibieren.

3.3 Risiken und Nebenwirkungen

Das Verwenden von Zellen ohne die Expression von MHC-Molekülen auf ihrer Zelloberfläche ist in vielerlei Hinsicht bedenklich. Ein großes Problem könnte die maligne Transformation darstellen (Hicklin et al., 1998). Studien belegen, dass MHCI und MHCII Knockouts bei Mäusen an sich zwar nicht die Onkogenese fördern, jedoch könnte die Transplantation von Zellen ohne MHC Expression, welche von der malignen Transformation betroffen sind, die Bekämpfung durch das Immunsystem des Empfängers erschweren. In der Theorie ist es sogar möglich, dass Tumorzelllinien unter verschiedenen Individuen übertragbar wären. Ein extremes Beispiel bieten Tumorzelllinien, die bei Hunden oder auch bei den Beutelteufeln auftreten und die Übertragung dieser Zellen z.B. über Geschlechtskontakt ermöglichen (Pearse and Swift, 2006). Charakteristisch für diese Tumorzelllinien ist die reduzierte Expression von MHCI und MHCII, welche unter anderem durch TAP2 und RFXAP reguliert werden (Decker et al., 2015).

Für die klinische Anwendung sollte daher die zu transplantierende Zellpopulation auf onkogenetische Mutationen gescreent werden, um das Risiko der malignen Transformation zu minimieren. Dennoch wird immer ein Restrisiko verbleiben: onkogenetische Zellen, die nicht durch das Screening identifiziert wurden, oder Tumorzellen, die nach der Transplantation entstehen. Als zusätzlichen Mechanismus wäre der Einbau eines Suizidgens in die hypoimmunogenen Zellen denkbar, dessen Expression bei Bedarf induziert werden kann (Gargett and Brown, 2014).

Die Wirkungsweise eines solchen Sicherheitssystems ist unterschiedlich und hängt von vielen Faktoren ab, letztlich auch davon, wie das Suizidgen in das Genom integriert ist. In den meisten Anwendungen, wie der „induzierbaren Caspase 9 (iCasp9)“ oder der „Herpes simplex virus thymidine kinase“, wurden die Genkopien zufällig im Genom integriert (Straathof et al., 2005). Die Expression und somit auch die Wirksamkeit des Suizidgens ist stark von den integrierten Kopienzahl abhängig (Ramos et al., 2010). Bei der iCasp9 wird die Zellapoptose durch eine Dimerisation mithilfe von small molecules wie AP1903 oder AP20187 eingeleitet. Zellen, die dagegen das Protein „Herpes simplex virus thymidine kinase“ exprimieren, gehen durch die Zugabe von Ganciclovir, einem Virostatikum, in die Apoptose.

Die Suizidgene können auch in den hypoimmunogenen Zellen so transkribiert sein, dass sie nur in sich schnell teilenden Zellen aktiviert werden. Dies würde eine selektive Eliminierung von Zellen ermöglichen, die eventuell von der malignen Transformation betroffen sind.

Ein anderes Bedenken ist die virale Infektion von MHC negativen Zellen, die normalerweise vom Immunsystem erkannt und eliminiert werden. Dennoch haben Studien gezeigt, dass MHC-defiziente Mäuse die Inokulation mit vielen Pathogenen durch die Aktivierung des unspezifischen Immunsystem umgehen und eine mögliche Infektion durch MHC-unabhängige Mechanismen limitieren (Hou et al., 1992; Spriggs et al., 1992).

3.4 Strategien zur Generierung von hypoimmunogenen Zellen

Die Anwendung einer hypoimmunogenen Zelllinie für die klinische Zelltherapie erfordert, dass sie als Spenderzellen das Immunsystem des Patienten autonom manipulieren. Ein entscheidendes Element wird daher die Fähigkeit sein, bestimmte Gene, die eine Abstoßung hervorrufen, auszuschalten und gleichzeitig immunmodulatorische Gene zu überexprimieren.

3.4.1 Modifizierung von MHC I

Das MHCI-Molekül besteht aus einer polymorphen, schweren Kette, die mit einer Mikroglobulin (β2M) Untereinheit verbunden ist. Es ist seit langem bekannt, dass MHC-Moleküle eine entscheidende Rolle bei der Abstoßung allogener Zellen und Gewebe durch die T-Zellaktivierung spielen. Während bei der hämatopoetischen Zelltransplantation die Übereinstimmung der HLA Merkmale zwischen dem Spender und dem Empfänger besonders wichtig ist (Petersdorf, 2008), können Patienten bei einer soliden Organtransplantation einen HLA-Mismatch besser tolerieren (Zachary and Leffell, 2016).

Das B2m-Gen war eines der ersten Gene, die in der Maus ausgeschaltet wurden. Bei diesen Mäusen fehlt die Oberflächenexpression von MHC I-Molekülen. Sie zeigen keine groben Anomalien, außer einem Mangel an CD8+ T-Zellen (Koller et al., 1990; Zijlstra et al., 1990). Ebenso weisen Menschen mit Mutationen in den Transporter-Molekülen TAP1 oder TAP2 eine geringe Oberflächenexpression von HLA-Klasse-I-Molekülen auf und sind nahezu gesund (Zimmer et al., 2005). Auch in humanen Zellen führt das Knockout von B2M zu einer fehlenden Expression von HLA-I auf der Zelloberfläche (Mattapally et al., 2018). Einige Studien berichteten von einer Chromosomenanomalie, welche durch das Knockout von B2M hervorgerufen wurde und sich somit letztendlich auf den therapeutischen Nutzen dieser Strategie auswirken könnte (Gornalusse et al., 2017). Eine der möglichen Ursachen für die Chromosomenanomalie könnte die Technik zur Generierung der Knockout-Zelle sein. Dieses Phänomen konnten wir in unserer Arbeit nicht bestätigen.

Der B2m-/- Mausstamm stellte die ersten universellen Spenderorgane bereit für allogene Transplantationen im Mausmodell. In einigen Studien war ein signifikant besseres Überleben des Spendergewebes gezeigt worden (Coffman et al., 1993; Prange et al., 2001; Qian et al., 1996). Knochenmarktransplantationen mit Zellen der B2m-/- Mäuse zeigten, dass die fehlende MHCI Expression das Killing durch die NK-Zellen förderte und es zu einer Abstoßung der Spenderzellen kam (Bix et al., 1991). Es ist ebenso bekannt, dass NK-Zellen beim Menschen eine komplexe Rolle bei allogenen Organtransplantation spielen (Benichou et al., 2011). Man spricht dabei von der sogenannten „missing-self“ Theorie (Karre et al., 1986), welche besagt, dass MHCI auf NK-Zellen eine inhibierende Wirkung haben und im Umkehrschluss somit die Zellen ohne MHCI durch NK-Zellen lysiert werden.

Ein möglicher Ansatz zur Generierung universeller hypoimmunogener Stammzellen könnte auch die Modifikation von HLAI-Molekülen darstellen, wie die Moleküle der Klasse Ib HLA-E und HLA-G. Wird nur die Expression dieser nicht polymorphen Oberflächenmoleküle gefördert, kann die NK-Zell-abhängige Lyse inhibiert werden, ohne dabei eine allogene Immunantwort zu triggern (Navarro et al., 1999).

HLA-E ist ein Ligand für den CD94 / NKG2A-Rezeptor und hat einen inhibierenden Effekt auf NK-Zellen (Braud et al., 1998; Lee et al., 1998). HLA-G wird normalerweise auf der Oberfläche von Zellen in den Trophoblasten der Plazenta exprimiert, die kein HLA-A, HLA-B oder HLA-C aufweisen, und schützt sie somit vor der NK-Zell-vermittelten Lyse durch die Wechselwirkung mit den inhibierenden Rezeptoren KIR2DL4 und ILT2. In einigen Studien wurde auch gezeigt, dass HLA-I negative Tumorzellen HLA-G exprimieren, um sich vor der NK-Zell Lyse zu schützen (Gonen-Gross et al., 2010; Pazmany et al., 1996; Rajagopalan and Long, 1999). Über die Funktion ist weniger bekannt.

Die Überexpression von HLA-E und HLA-G führte zu einer reduzierten Immunogenität von humanen Stammzellen und ihren Zellderivaten, einschließlich einer verminderten NK-Zell Aktivierung (Zhao et al., 2017; Zhao et al., 2014). Gornalusse et al. berichteten von der Überexpression eines Fusionsproteins aus B2M und HLA-E auf einer ansonsten B2M-/- ESC-Linie. HLA-E war somit das einzig exprimierte HLA-I Molekül auf der Zelloberfläche (Gornalusse et al., 2017). *In vitro* Experimente wiesen eine signifikante Reduzierung von CD8+ T-Zellen, NK-Zellen und B-Zellen auf. Letztlich ist es unwahrscheinlich, dass die alleinige Überexpression von HLA-E eine allogene Immunantwort komplett inhibieren kann, da humane NK-Zellen ein besonders diverses Rezeptorrepertoire aufweisen (Horowitz et al., 2013).

3.4.2 Modifizierung von MHC II

HLA Klasse II Proteine (HLA-DP, HLA-DQ und HLA-DR) sind Heterodimere mit polymorphen α -Ketten und β -Ketten, die auf Antigen-präsentierenden Zellen, wie z. B. B-Zellen, Makrophagen und dendritischen Zellen exprimiert werden. Therapien, die auf diesen Zelltypen basieren, erfordern ein kombiniertes Engineering von HLA Klasse I und Klasse II, um eine allogene Abstoßung zu verhindern. Da HLA-II Proteine nicht wie HLA-I Proteine auf fast jeder Zelle exprimiert sind, wurde das Engineering von HLA-II oft als optional angesehen. Die vorliegende Arbeit zeigt jedoch, dass durch eine Stimulierung durch TNFα sowohl die iPSCs als auch ihre Zellderivate (Kardiomyozyten, glatte Muskelzellen und Endothelzellen) MHC-II als Oberflächenmolekül exprimieren. Andere Studien belegen ebenfalls die HLA-II Expression nach Zytokinstimulierung bei Stromazellen und β-Islet-Zellen (Hematti, 2008; Soldevila et al., 1990; Sugimoto et al., 1989).

Im Gegensatz zum HLA-I Knockout, führt ein Knockout von HLA-II nicht zur Aktivierung von NK-Zellen. Anstatt einzelne polymorphe HLA-Klasse-II-Gene auszuschalten, ist es deutlich einfacher, einen der Transkriptionsfaktoren zu modifizieren, der für die Expression aller HLA-II Gene erforderlich ist. Bei Menschen mit „bare lymphocyte“ Syndrom fehlt die HLA-II Expression aufgrund von Mutationen in einem von vier verschiedenen Transkriptionsfaktor-Genen: CIITA, RFX5, RFXAP oder RFXANK (DeSandro et al., 1999). Ciita-/- Mäuse wurden bereits erfolgreich auf die Abwesenheit der MHC-II Oberflächenmoleküle getestet und das Mausmodell wurde bereits etabliert (Chang et al., 1996). Trotz fehlender Expression von HLA-II beim Menschen und MHC-II bei der Maus zeigen Betroffene eine nahezu normale Entwicklung mit der Ausnahme von einer T-Zell-Defizienz und Immunschwäche (Cosgrove et al., 1991; Ouederni et al., 2011). Sowohl CIITA als auch RFXANK konnten in humanen pluripotenten Stammzellen ausgeknockt werden und zeigten kein

HLA-II auf der Zelloberfläche (Chen et al., 2015). Mattapally et al. haben bereits im Jahr 2018 ein kombiniertes Knockout von B2M und CIITA beschrieben (Mattapally et al., 2018).

3.4.3 Weitere Strategien

Neben dem gezielten Knockout der polymorphen HLA-Expression bietet die Natur vielerlei Strategien von „immune cloaking“, welche eventuell für das Design weiterer Versionen von Universalzellen herangezogen werden können. Krebszellen sind ein gutes Beispiel dafür: Sie exprimieren einzigartige Antigene, die von T-Zellen erkannt werden können, und müssen daher Wege finden, um das Immunsystem zu umgehen (Coulie et al., 2014).

Ähnlich wie die Plazenta während einer Schwangerschaft, haben einige Krebszellen die Fähigkeit entwickelt, die Expansion und Aktivität von Effektor-T-Zellen durch die Induktion und Aktivierung regulatorischer T-Zellen (Tregs) zu verhindern. Klinische Daten zeigen, dass ein geringer Anteil von Tregs unter den tumorinfiltrierenden Lymphozyten bei Krebserkrankungen entscheidend ist und sich positiv auf die Heilungschancen auswirkt (Gooden et al., 2011). Tumorzellen haben ebenfalls ein sehr hohes Expressionslevel der Checkpoint-Moleküle PDL1 (engl. programmed cell death ligand 1) und CTLA4 (engl. cytotoxic T-lymphocyte-associated protein 4), welche T-Zellen und kostimulatorische Zellen hemmen (Pardoll, 2012). Andere T-Zell-Inhibitoren wie das Enzym IDO (Indoleamin-Pyrrol-2,3-Dioxygenase) oder das Oberflächenmolekül FASL27 werden ebenfalls exprimiert (Balachandran et al., 2011; Peter et al., 2015).

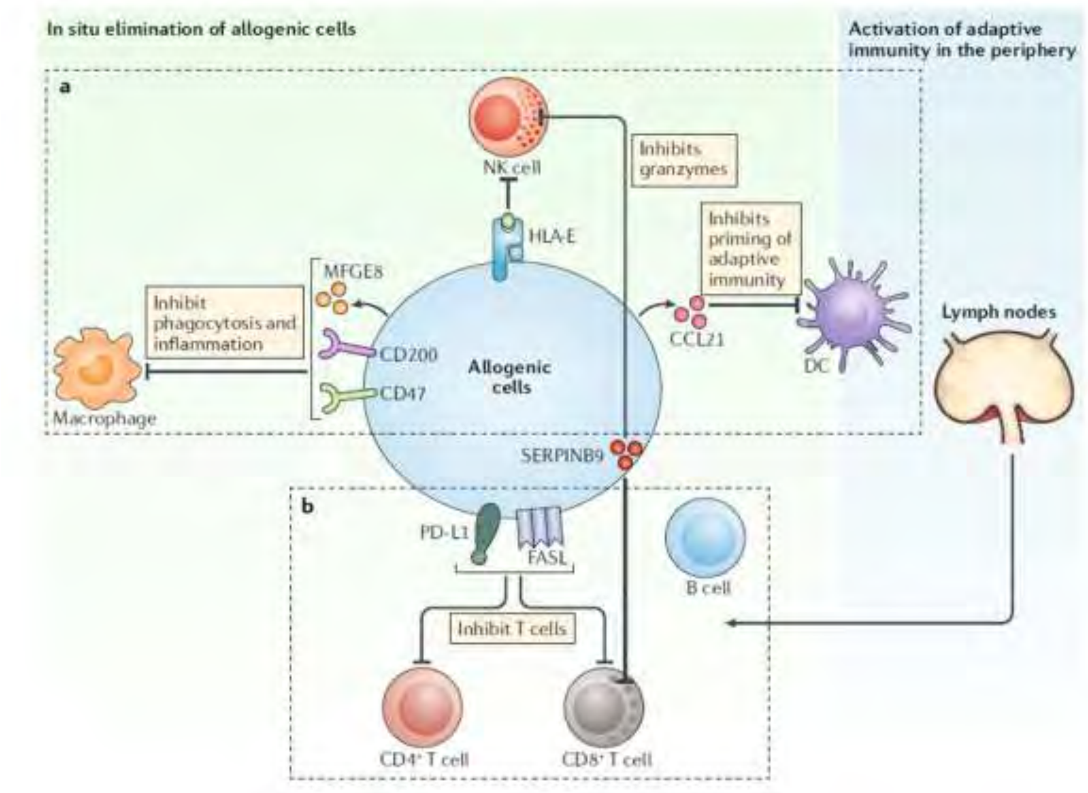
In situ elimination of allogenic cells
Activation of adaptive immunity in the periphery
a
NK cell
Inhibits granzymes
HLA-E
Inhibits priming of adaptive immunity
MFGE8
Inhibit phagocytosis and inflammation
CD200
CD47
Allogenic cells
CCL21
DC
Lymph nodes
Macrophage
SERPINB9
b
PD-L1
FASL
B cell
Inhibit T cells
CD4+ T cell
CD8+ T cell

Abbildung 3.2: Mechanismen zur Unterdrückung der Immunaktivierung. Die Abstoßung von allogenen Zellen durch das angeborene Immunsystem (a) und durch das adaptive Immunsystem (b) (Lanza et al., 2019)

Es wurde auch gezeigt, dass Krebszellen die Fähigkeit besitzen, die von NK- und T-Zellen produzierten Granzyme zu inhibieren durch die Expression von Protease-Inhibitoren wie SERPINB9 (Medema et al., 2001), weiterhin den Angriff von Makrophagen durch die Expression von CD47 zu inhibieren (Matlung et al., 2017) und ebenso die Differenzierung der Monozyten zu entzündungshemmenden M2 Phänotypen zu fördern (Gajewski et al., 2013). Diese Signalwege werden vor allem durch immunsuppressive Zytokine wie CCL21 (engl. CC-chemokine ligand 21), oder auch TGFβ (engl. transforming growth factor beta) unterstützt (Bierie and Moses, 2006; Shields et al., 2010). Eine weitere Studie zeigte, dass die Überexpression von acht lokal wirkenden immunmodulatorischen Transgenen, einschließlich Pdl1, FasL, Cd47, Cd200, Ccl21, Mfge8, H2-M3 und Spi6 in C57BL/6 ESCs, das Langzeitüberleben dieser Zellen in diversen allogenen Mausmodellen bewirkt (Harding et al., 2020).

3.5 Ausblick

Die Ergebnisse dieser Doktorarbeit haben gezeigt, dass autologe iPSC und iPSC-abgeleitete Zellprodukte nicht automatisch immunologisch inert sind. Für die autologe Zelltransplantation sollten Mutationen in der mtDNA unbedingt als Ursache für eine mögliche Immunaktivierung in Betracht gezogen werden.

Das allogene Überleben der hypoimmunogenen Zellen und ihrer Zellderivate konnte sowohl im Mausmodell für Mauszellen als auch im humanisierten Mausmodell für humanen Zellen gezeigt werden. Die Kombination der drei beschriebenen Moleküle scheint vielversprechend zu sein um universale iPSCs zu generieren die jederzeit für allogene Transplantationen in der regenerative Medizin verwendet werden können.

4. Referenz

Aasen, T., Raya, A., Barrero, M.J., Garreta, E., Consiglio, A., Gonzalez, F., Vassena, R., Bilic, J., Pekarik, V., Tiscornia, G.*, et al.* (2008). Efficient and rapid generation of induced pluripotent stem cells from human keratinocytes. Nat Biotechnol *26*, 1276-1284.

Abbas, A.K., Lichtman, A.H., and Pillai, S. (2012). Cellular and molecular immunology, 7th edn (Philadelphia: Elsevier/Saunders).

Aluvihare, V.R., Kallikourdis, M., and Betz, A.G. (2004). Regulatory T cells mediate maternal tolerance to the fetus. Nat Immunol *5*, 266-271.

Araki, R., Uda, M., Hoki, Y., Sunayama, M., Nakamura, M., Ando, S., Sugiura, M., Ideno, H., Shimada, A., Nifuji, A.*, et al.* (2013). Negligible immunogenicity of terminally differentiated cells derived from induced pluripotent or embryonic stem cells. Nature *494*, 100-104.

Arck, P.C., and Hecher, K. (2013). Fetomaternal immune cross-talk and its consequences for maternal and offspring's health. Nat Med *19*, 548-556.

Balachandran, V.P., Cavnar, M.J., Zeng, S., Bamboat, Z.M., Ocuin, L.M., Obaid, H., Sorenson, E.C., Popow, R., Ariyan, C., Rossi, F.*, et al.* (2011). Imatinib potentiates antitumor T cell responses in gastrointestinal stromal tumor through the inhibition of Ido. Nat Med *17*, 1094-1100.

Benichou, G., Yamada, Y., Aoyama, A., and Madsen, J.C. (2011). Natural killer cells in rejection and tolerance of solid organ allografts. Curr Opin Organ Transplant *16*, 47-53.

Biehl, J.K., and Russell, B. (2009). Introduction to stem cell therapy. J Cardiovasc Nurs *24*, 98-103; quiz 104-105.

Bierie, B., and Moses, H.L. (2006). Tumour microenvironment: TGFbeta: the molecular Jekyll and Hyde of cancer. Nat Rev Cancer *6*, 506-520.

Bix, M., Liao, N.S., Zijlstra, M., Loring, J., Jaenisch, R., and Raulet, D. (1991). Rejection of class I MHC-deficient haemopoietic cells by irradiated MHC-matched mice. Nature *349*, 329-331.

Blesch, A. (2004). Lentiviral and MLV based retroviral vectors for ex vivo and in vivo gene transfer. Methods *33*, 164-172.

Boch, J. (2011). TALEs of genome targeting. Nat Biotechnol *29*, 135-136.

Borghans, J.A., Noest, A.J., and De Boer, R.J. (1999). How specific should immunological memory be? J Immunol *163*, 569-575.

Bortin, M.M., Horowitz, M.M., Mrsic, M., Rimm, A.A., and Sobocinski, K.A. (1991). Progress in bone marrow transplantation for leukemia: a preliminary report from the Advisory Committee of the International Bone Marrow Transplant Registry. Transplant Proc *23*, 61-62.

Braud, V.M., Allan, D.S., O'Callaghan, C.A., Soderstrom, K., D'Andrea, A., Ogg, G.S., Lazetic, S., Young, N.T., Bell, J.I., Phillips, J.H., *et al.* (1998). HLA-E binds to natural killer cell receptors CD94/NKG2A, B and C. Nature *391*, 795-799.

Brown, W.M., George, M., Jr., and Wilson, A.C. (1979). Rapid evolution of animal mitochondrial DNA. Proc Natl Acad Sci U S A *76*, 1967-1971.

Capecchi, M.R. (2005). Gene targeting in mice: functional analysis of the mammalian genome for the twenty-first century. Nat Rev Genet *6*, 507-512.

Chang, C.H., Guerder, S., Hong, S.C., van Ewijk, W., and Flavell, R.A. (1996). Mice lacking the MHC class II transactivator (CIITA) show tissue-specific impairment of MHC class II expression. Immunity *4*, 167-178.

Chen, H., Li, Y., Lin, X., Cui, D., Cui, C., Li, H., and Xiao, L. (2015). Functional disruption of human leukocyte antigen II in human embryonic stem cell. Biol Res *48*, 59.

Clark, D.A., Chaouat, G., Wong, K., Gorczynski, R.M., and Kinsky, R. (2010). Tolerance mechanisms in pregnancy: a reappraisal of the role of class I paternal MHC antigens. Am J Reprod Immunol *63*, 93-103.

Coffman, T., Geier, S., Ibrahim, S., Griffiths, R., Spurney, R., Smithies, O., Koller, B., and Sanfilippo, F. (1993). Improved renal function in mouse kidney allografts lacking MHC class I antigens. J Immunol *151*, 425-435.

Cong, L., Ran, F.A., Cox, D., Lin, S., Barretto, R., Habib, N., Hsu, P.D., Wu, X., Jiang, W., Marraffini, L.A., *et al.* (2013). Multiplex genome engineering using CRISPR/Cas systems. Science *339*, 819-823.

Cosgrove, D., Gray, D., Dierich, A., Kaufman, J., Lemeur, M., Benoist, C., and Mathis, D. (1991). Mice lacking MHC class II molecules. Cell *66*, 1051-1066.

Coulie, P.G., Van den Eynde, B.J., van der Bruggen, P., and Boon, T. (2014). Tumour antigens recognized by T lymphocytes: at the core of cancer immunotherapy. Nat Rev Cancer *14*, 135-146.

Croteau, D.L., Stierum, R.H., and Bohr, V.A. (1999). Mitochondrial DNA repair pathways. Mutat Res *434*, 137-148.

Cui, X., Ji, D., Fisher, D.A., Wu, Y., Briner, D.M., and Weinstein, E.J. (2011). Targeted integration in rat and mouse embryos with zinc-finger nucleases. Nat Biotechnol *29*, 64-67.

de Almeida, P.E., Meyer, E.H., Kooreman, N.G., Diecke, S., Dey, D., Sanchez-Freire, V., Hu, S., Ebert, A., Odegaard, J., Mordwinkin, N.M.*, et al.* (2014). Transplanted terminally differentiated induced pluripotent stem cells are accepted by immune mechanisms similar to self-tolerance. Nat Commun *5*, 3903.

Decker, B., Davis, B.W., Rimbault, M., Long, A.H., Karlins, E., Jagannathan, V., Reiman, R., Parker, H.G., Drogemuller, C., Corneveaux, J.J.*, et al.* (2015). Comparison against 186 canid whole-genome sequences reveals survival strategies of an ancient clonally transmissible canine tumor. Genome Res *25*, 1646-1655.

DeSandro, A., Nagarajan, U.M., and Boss, J.M. (1999). The bare lymphocyte syndrome: molecular clues to the transcriptional regulation of major histocompatibility complex class II genes. Am J Hum Genet *65*, 279-286.

Deuse, T., Seifert, M., Phillips, N., Fire, A., Tyan, D., Kay, M., Tsao, P.S., Hua, X., Velden, J., Eiermann, T.*, et al.* (2011). Human leukocyte antigen I knockdown human embryonic stem cells induce host ignorance and achieve prolonged xenogeneic survival. Circulation *124*, S3-9.

Deuse, T., Wang, D., Stubbendorff, M., Itagaki, R., Grabosch, A., Greaves, L.C., Alawi, M., Grunewald, A., Hu, X., Hua, X.*, et al.* (2015). SCNT-derived ESCs with mismatched mitochondria trigger an immune response in allogeneic hosts. Cell Stem Cell *16*, 33-38.

Doss, M.X., and Sachinidis, A. (2019). Current Challenges of iPSC-Based Disease Modeling and Therapeutic Implications. Cells *8*.

Drukker, M., Katz, G., Urbach, A., Schuldiner, M., Markel, G., Itskovitz-Eldor, J., Reubinoff, B., Mandelboim, O., and Benvenisty, N. (2002). Characterization of the expression of MHC proteins in human embryonic stem cells. Proc Natl Acad Sci U S A *99*, 9864-9869.

Evans, M.J., and Kaufman, M.H. (1981). Establishment in culture of pluripotential cells from mouse embryos. Nature *292*, 154-156.

Finkenzeller, D., Fischer, B., McLaughlin, J., Schrewe, H., Ledermann, B., and Zimmermann, W. (2000). Trophoblast cell-specific carcinoembryonic antigen cell adhesion molecule 9 is not required for placental development or a positive outcome of allotypic pregnancies. Mol Cell Biol *20*, 7140-7145.

Gajewski, T.F., Schreiber, H., and Fu, Y.X. (2013). Innate and adaptive immune cells in the tumor microenvironment. Nat Immunol *14*, 1014-1022.

Gammage, P.A., and Frezza, C. (2019). Mitochondrial DNA: the overlooked oncogenome? BMC Biol *17*, 53.

Gargett, T., and Brown, M.P. (2014). The inducible caspase-9 suicide gene system as a "safety switch" to limit on-target, off-tumor toxicities of chimeric antigen receptor T cells. Front Pharmacol *5*, 235.

Gonen-Gross, T., Goldman-Wohl, D., Huppertz, B., Lankry, D., Greenfield, C., Natanson-Yaron, S., Hamani, Y., Gilad, R., Yagel, S., and Mandelboim, O. (2010). Inhibitory NK receptor recognition of HLA-G: regulation by contact residues and by cell specific expression at the fetal-maternal interface. PLoS One *5*, e8941.

Gooden, M.J., de Bock, G.H., Leffers, N., Daemen, T., and Nijman, H.W. (2011). The prognostic influence of tumour-infiltrating lymphocytes in cancer: a systematic review with meta-analysis. Br J Cancer *105*, 93-103.

Gorantla, V.S., Barker, J.H., Jones, J.W., Jr., Prabhune, K., Maldonado, C., and Granger, D.K. (2000). Immunosuppressive agents in transplantation: mechanisms of action and current anti-rejection strategies. Microsurgery *20*, 420-429.

Gornalusse, G.G., Hirata, R.K., Funk, S.E., Riolobos, L., Lopes, V.S., Manske, G., Prunkard, D., Colunga, A.G., Hanafi, L.A., Clegg, D.O*., et al.* (2017). HLA-E-expressing pluripotent stem cells escape allogeneic responses and lysis by NK cells. Nat Biotechnol *35*, 765-772.

Guha, P., Morgan, J.W., Mostoslavsky, G., Rodrigues, N.P., and Boyd, A.S. (2013). Lack of immune response to differentiated cells derived from syngeneic induced pluripotent stem cells. Cell Stem Cell *12*, 407-412.

Guleria, I., and Sayegh, M.H. (2007). Maternal acceptance of the fetus: true human tolerance. J Immunol *178*, 3345-3351.

Hale, G., Cobbold, S., and Waldmann, H. (1988). T cell depletion with CAMPATH-1 in allogeneic bone marrow transplantation. Transplantation *45*, 753-759.

Harding, J., Vintersten-Nagy, K., Shutova M., Y., H., Tang J.K., M., M., Izaidfar, Z., Zhang, P., Li, C., and Nagy, A. (2020). Induction of long-term allogeneic cell acceptance and formation of immune privileged tissue in immunocompetent hosts.

He, Y., Wu, J., Dressman, D.C., Iacobuzio-Donahue, C., Markowitz, S.D., Velculescu, V.E., Diaz, L.A., Jr., Kinzler, K.W., Vogelstein, B., and Papadopoulos, N. (2010). Heteroplasmic mitochondrial DNA mutations in normal and tumour cells. Nature *464*, 610-614.

Hematti, P. (2008). Role of mesenchymal stromal cells in solid organ transplantation. Transplant Rev (Orlando) *22*, 262-273.

Hicklin, D.J., Wang, Z., Arienti, F., Rivoltini, L., Parmiani, G., and Ferrone, S. (1998). beta2-Microglobulin mutations, HLA class I antigen loss, and tumor progression in melanoma. J Clin Invest *101*, 2720-2729.

Hirayama, M., Azuma, E., and Komada, Y. (2012). Tolerogenic effect of non-inherited maternal antigens in hematopoietic stem cell transplantation. Front Immunol *3*, 135.

Horowitz, A., Strauss-Albee, D.M., Leipold, M., Kubo, J., Nemat-Gorgani, N., Dogan, O.C., Dekker, C.L., Mackey, S., Maecker, H., Swan, G.E*., et al.* (2013). Genetic and environmental determinants of human NK cell diversity revealed by mass cytometry. Sci Transl Med *5*, 208ra145.

Hou, S., Doherty, P.C., Zijlstra, M., Jaenisch, R., and Katz, J.M. (1992). Delayed clearance of Sendai virus in mice lacking class I MHC-restricted CD8+ T cells. J Immunol *149*, 1319-1325.

Ji, J., Ng, S.H., Sharma, V., Neculai, D., Hussein, S., Sam, M., Trinh, Q., Church, G.M., McPherson, J.D., Nagy, A.*, et al.* (2012). Elevated coding mutation rate during the reprogramming of human somatic cells into induced pluripotent stem cells. Stem Cells *30*, 435-440.

Jinek, M., Chylinski, K., Fonfara, I., Hauer, M., Doudna, J.A., and Charpentier, E. (2012). A programmable dual-RNA-guided DNA endonuclease in adaptive bacterial immunity. Science *337*, 816-821.

Karre, K. (2002). NK cells, MHC class I molecules and the missing self. Scand J Immunol *55*, 221-228.

Karre, K., Ljunggren, H.G., Piontek, G., and Kiessling, R. (1986). Selective rejection of H-2-deficient lymphoma variants suggests alternative immune defence strategy. Nature *319*, 675-678.

Kelley, J., Walter, L., and Trowsdale, J. (2005). Comparative genomics of major histocompatibility complexes. Immunogenetics *56*, 683-695.

Kim, Y.G., Cha, J., and Chandrasegaran, S. (1996). Hybrid restriction enzymes: zinc finger fusions to Fok I cleavage domain. Proc Natl Acad Sci U S A *93*, 1156-1160.

Koller, B.H., Marrack, P., Kappler, J.W., and Smithies, O. (1990). Normal development of mice deficient in beta 2M, MHC class I proteins, and CD8+ T cells. Science *248*, 1227-1230.

Lanza, R., Russell, D.W., and Nagy, A. (2019). Engineering universal cells that evade immune detection. Nat Rev Immunol *19*, 723-733.

Lee, N., Llano, M., Carretero, M., Ishitani, A., Navarro, F., Lopez-Botet, M., and Geraghty, D.E. (1998). HLA-E is a major ligand for the natural killer inhibitory receptor CD94/NKG2A. Proc Natl Acad Sci U S A *95*, 5199-5204.

Lieber, M.R. (2008). The mechanism of human nonhomologous DNA end joining. J Biol Chem *283*, 1-5.

Mackay, C.R., Marston, W.L., and Dudler, L. (1990). Naive and memory T cells show distinct pathways of lymphocyte recirculation. J Exp Med *171*, 801-817.

Mali, P., Esvelt, K.M., and Church, G.M. (2013). Cas9 as a versatile tool for engineering biology. Nat Methods *10*, 957-963.

Mandai, M., Watanabe, A., Kurimoto, Y., Hirami, Y., Morinaga, C., Daimon, T., Fujihara, M., Akimaru, H., Sakai, N., Shibata, Y.*, et al.* (2017). Autologous Induced Stem-Cell-Derived Retinal Cells for Macular Degeneration. N Engl J Med *376*, 1038-1046.

Martin, G.R. (1981). Isolation of a pluripotent cell line from early mouse embryos cultured in medium conditioned by teratocarcinoma stem cells. Proc Natl Acad Sci U S A *78*, 7634-7638.

Matlung, H.L., Szilagyi, K., Barclay, N.A., and van den Berg, T.K. (2017). The CD47-SIRPalpha signaling axis as an innate immune checkpoint in cancer. Immunol Rev *276*, 145-164.

Mattapally, S., Pawlik, K.M., Fast, V.G., Zumaquero, E., Lund, F.E., Randall, T.D., Townes, T.M., and Zhang, J. (2018). Human Leukocyte Antigen Class I and II Knockout Human Induced Pluripotent Stem Cell-Derived Cells: Universal Donor for Cell Therapy. J Am Heart Assoc *7*, e010239.

Mawby, W.J., Holmes, C.H., Anstee, D.J., Spring, F.A., and Tanner, M.J. (1994). Isolation and characterization of CD47 glycoprotein: a multispanning membrane protein which is the same as integrin-associated protein (IAP) and the ovarian tumour marker OA3. Biochem J *304 (Pt 2)*, 525-530.

Medema, J.P., de Jong, J., Peltenburg, L.T., Verdegaal, E.M., Gorter, A., Bres, S.A., Franken, K.L., Hahne, M., Albar, J.P., Melief, C.J.*, et al.* (2001). Blockade of the granzyme B/perforin pathway through overexpression of the serine protease inhibitor PI-9/SPI-6 constitutes a mechanism for immune escape by tumors. Proc Natl Acad Sci U S A *98*, 11515-11520.

Medvedev, S.P., Shevchenko, A.I., and Zakian, S.M. (2010). Induced Pluripotent Stem Cells: Problems and Advantages when Applying them in Regenerative Medicine. Acta Naturae *2*, 18-28.

Mercer, T.R., Neph, S., Dinger, M.E., Crawford, J., Smith, M.A., Shearwood, A.M., Haugen, E., Bracken, C.P., Rackham, O., Stamatoyannopoulos, J.A.*, et al.* (2011). The human mitochondrial transcriptome. Cell *146*, 645-658.

Miller, L.W. (2018). Trial of Embryonic Stem Cell-Derived Cardiac Progenitor Cells: An Encouraging Start. J Am Coll Cardiol *71*, 439-442.

Moradi, S., Mahdizadeh, H., Saric, T., Kim, J., Harati, J., Shahsavarani, H., Greber, B., and Moore, J.B.t. (2019). Research and therapy with induced pluripotent stem cells (iPSCs): social, legal, and ethical considerations. Stem Cell Res Ther *10*, 341.

Muhlethaler-Mottet, A., Otten, L.A., Steimle, V., and Mach, B. (1997). Expression of MHC class II molecules in different cellular and functional compartments is controlled by differential usage of multiple promoters of the transactivator CIITA. EMBO J *16*, 2851-2860.

Murphy, K., Travers, P., Walport, M., and Janeway, C. (2012). Janeway's immunobiology, 8th edn (New York: Garland Science).

Nass, S., and Nass, M.M. (1963). Intramitochondrial Fibers with DNA Characteristics. Ii. Enzymatic and Other Hydrolytic Treatments. J Cell Biol *19*, 613-629.

Navarro, F., Llano, M., Bellon, T., Colonna, M., Geraghty, D.E., and Lopez-Botet, M. (1999). The ILT2(LIR1) and CD94/NKG2A NK cell receptors respectively recognize HLA-G1 and HLA-E molecules co-expressed on target cells. Eur J Immunol *29*, 277-283.

Ouederni, M., Vincent, Q.B., Frange, P., Touzot, F., Scerra, S., Bejaoui, M., Bousfiha, A., Levy, Y., Lisowska-Grospierre, B., Canioni, D*., et al.* (2011). Major histocompatibility complex class II expression deficiency caused by a RFXANK founder mutation: a survey of 35 patients. Blood *118*, 5108-5118.

Pardoll, D.M. (2012). The blockade of immune checkpoints in cancer immunotherapy. Nat Rev Cancer *12*, 252-264.

Patel, M.S., and Abt, P.L. (2019). Current practices in deceased organ donor management. Curr Opin Organ Transplant *24*, 343-350.

Pazmany, L., Mandelboim, O., Vales-Gomez, M., Davis, D.M., Reyburn, H.T., and Strominger, J.L. (1996). Protection from natural killer cell-mediated lysis by HLA-G expression on target cells. Science *274*, 792-795.

Pearse, A.M., and Swift, K. (2006). Allograft theory: transmission of devil facial-tumour disease. Nature *439*, 549.

Peter, M.E., Hadji, A., Murmann, A.E., Brockway, S., Putzbach, W., Pattanayak, A., and Ceppi, P. (2015). The role of CD95 and CD95 ligand in cancer. Cell Death Differ *22*, 549-559.

Petersdorf, E.W. (2008). Optimal HLA matching in hematopoietic cell transplantation. Curr Opin Immunol *20*, 588-593.

Piquereau, J., Caffin, F., Novotova, M., Lemaire, C., Veksler, V., Garnier, A., Ventura-Clapier, R., and Joubert, F. (2013). Mitochondrial dynamics in the adult cardiomyocytes: which roles for a highly specialized cell? Front Physiol *4*, 102.

Prange, S., Zucker, P., Jevnikar, A.M., and Singh, B. (2001). Transplanted MHC class I-deficient nonobese diabetic mouse islets are protected from autoimmune injury in diabetic nonobese recipients. Transplantation *71*, 982-985.

Qian, S., Fu, F., Li, Y., Lu, L., Rao, A.S., Starzl, T.E., Thomson, A.W., and Fung, J.J. (1996). Impact of donor MHC class I or class II antigen deficiency on first- and second-set rejection of mouse heart or liver allografts. Immunology *88*, 124-129.

Rajagopalan, S., and Long, E.O. (1999). A human histocompatibility leukocyte antigen (HLA)-G-specific receptor expressed on all natural killer cells. J Exp Med *189*, 1093-1100.

Ramos, C.A., Asgari, Z., Liu, E., Yvon, E., Heslop, H.E., Rooney, C.M., Brenner, M.K., and Dotti, G. (2010). An inducible caspase 9 suicide gene to improve the safety of mesenchymal stromal cell therapies. Stem Cells *28*, 1107-1115.

Rapacz-Leonard, A., Dabrowska, M., and Janowski, T. (2014). Major histocompatibility complex I mediates immunological tolerance of the trophoblast during pregnancy and may mediate rejection during parturition. Mediators Inflamm *2014*, 579279.

Sander, J.D., and Joung, J.K. (2014). CRISPR-Cas systems for editing, regulating and targeting genomes. Nat Biotechnol *32*, 347-355.

Schwartz, S.D., Hubschman, J.P., Heilwell, G., Franco-Cardenas, V., Pan, C.K., Ostrick, R.M., Mickunas, E., Gay, R., Klimanskaya, I., and Lanza, R. (2012). Embryonic stem cell trials for macular degeneration: a preliminary report. Lancet *379*, 713-720.

Schwartz, S.D., Regillo, C.D., Lam, B.L., Eliott, D., Rosenfeld, P.J., Gregori, N.Z., Hubschman, J.P., Davis, J.L., Heilwell, G., Spirn, M.*, et al.* (2015). Human embryonic stem cell-derived retinal pigment epithelium in patients with age-related macular degeneration and Stargardt's macular dystrophy: follow-up of two open-label phase 1/2 studies. Lancet *385*, 509-516.

Shani, T., and Hanna, J.H. (2019). Universally non-immunogenic iPSCs. Nat Biomed Eng *3*, 337-338.

Shields, J.D., Kourtis, I.C., Tomei, A.A., Roberts, J.M., and Swartz, M.A. (2010). Induction of lymphoidlike stroma and immune escape by tumors that express the chemokine CCL21. Science *328*, 749-752.

Shigenaga, M.K., Hagen, T.M., and Ames, B.N. (1994). Oxidative damage and mitochondrial decay in aging. Proc Natl Acad Sci U S A *91*, 10771-10778.

Shoffner, J.M., Lott, M.T., Voljavec, A.S., Soueidan, S.A., Costigan, D.A., and Wallace, D.C. (1989). Spontaneous Kearns-Sayre/chronic external ophthalmoplegia plus syndrome associated with a mitochondrial DNA deletion: a slip-replication model and metabolic therapy. Proc Natl Acad Sci U S A *86*, 7952-7956.

Sijpkens, Y.W., Doxiadis, II, De Fijter, J.W., Mallat, M.J., van Es, L.A., De Lange, P., Zwinderman, A.H., Westendorp, R.G., van Kemenade, F.J., Bruijn, J.A.*, et al.* (1999). Sharing cross-reactive groups of MHC class I improves long-term graft survival. Kidney Int *56*, 1920-1927.

Snell, G.D. (1948). Methods for the study of histocompatibility genes. J Genet *49*, 87-108.

Soldevila, G., Doshi, M., James, R., Lake, S.P., Sutton, R., Gray, D., Bottazzo, G.F., and Pujol-Borrell, R. (1990). HLA DR, DP, DQ induction in human islet beta cells by the cytokine combination IFN-gamma + TNF-alpha. Autoimmunity *6*, 307-317.

Spinelli, P., Latchney, S.E., Reed, J.M., Fields, A., Baier, B.S., Lu, X., McCall, M.N., Murphy, S.P., Mak, W., and Susiarjo, M. (2019). Identification of the novel Ido1 imprinted locus and its potential epigenetic role in pregnancy loss. Hum Mol Genet *28*, 662-674.

Spriggs, M.K., Koller, B.H., Sato, T., Morrissey, P.J., Fanslow, W.C., Smithies, O., Voice, R.F., Widmer, M.B., and Maliszewski, C.R. (1992). Beta 2-microglobulin-, CD8+ T-cell-deficient mice survive inoculation with high doses of vaccinia virus and exhibit altered IgG responses. Proc Natl Acad Sci U S A *89*, 6070-6074.

Stewart, J.B., and Chinnery, P.F. (2015). The dynamics of mitochondrial DNA heteroplasmy: implications for human health and disease. Nat Rev Genet *16*, 530-542. Straathof, K.C., Pule, M.A., Yotnda, P., Dotti, G., Vanin, E.F., Brenner, M.K., Heslop, H.E., Spencer, D.M., and Rooney, C.M. (2005). An inducible caspase 9 safety switch for T-cell therapy. Blood *105*, 4247-4254.

Sugimoto, T., Horii, Y., Hino, T., Kemshead, J.T., Kuroda, H., Sawada, T., Morioka, H., Imanishi, J., and Inoko, H. (1989). Differential susceptibility of HLA class II antigens induced by gamma-interferon in human neuroblastoma cell lines. Cancer Res *49*, 1824-1828.

Susal, C., Dohler, B., and Opelz, G. (2009). Presensitized kidney graft recipients with HLA class I and II antibodies are at increased risk for graft failure: a Collaborative Transplant Study report. Hum Immunol *70*, 569-573.

Taanman, J.W. (1999). The mitochondrial genome: structure, transcription, translation and replication. Biochim Biophys Acta *1410*, 103-123.

Tachibana, M., Amato, P., Sparman, M., Gutierrez, N.M., Tippner-Hedges, R., Ma, H., Kang, E., Fulati, A., Lee, H.S., Sritanaudomchai, H.*, et al.* (2013). Human embryonic stem cells derived by somatic cell nuclear transfer. Cell *153*, 1228-1238.

Takahashi, K., Tanabe, K., Ohnuki, M., Narita, M., Ichisaka, T., Tomoda, K., and Yamanaka, S. (2007). Induction of pluripotent stem cells from adult human fibroblasts by defined factors. Cell *131*, 861-872.

Terasaki, P.I. (2003). Humoral theory of transplantation. Am J Transplant *3*, 665-673. Thomson, J.A., Itskovitz-Eldor, J., Shapiro, S.S., Waknitz, M.A., Swiergiel, J.J., Marshall, V.S., and Jones, J.M. (1998). Embryonic stem cell lines derived from human blastocysts. Science *282*, 1145-1147.

Todorova, D., Kim, J., Hamzeinejad, S., He, J., and Xu, Y. (2016). Brief Report: Immune Microenvironment Determines the Immunogenicity of Induced Pluripotent Stem Cell Derivatives. Stem Cells *34*, 510-515.

van der Bogt, K.E., Schrepfer, S., Yu, J., Sheikh, A.Y., Hoyt, G., Govaert, J.A., Velotta, J.B., Contag, C.H., Robbins, R.C., and Wu, J.C. (2009). Comparison of transplantation of adipose tissue- and bone marrow-derived mesenchymal stem cells in the infarcted heart. Transplantation *87*, 642-652.

Vento-Tormo, R., Efremova, M., Botting, R.A., Turco, M.Y., Vento-Tormo, M., Meyer, K.B., Park, J.E., Stephenson, E., Polanski, K., Goncalves, A.*, et al.* (2018). Single-cell reconstruction of the early maternal-fetal interface in humans. Nature *563*, 347-353.

Yakes, F.M., and Van Houten, B. (1997). Mitochondrial DNA damage is more extensive and persists longer than nuclear DNA damage in human cells following oxidative stress. Proc Natl Acad Sci U S A *94*, 514-519.

Yu, J., and Thomson, J.A. (2008). Pluripotent stem cell lines. Genes Dev *22*, 1987-1997.

Yu, J., Vodyanik, M.A., Smuga-Otto, K., Antosiewicz-Bourget, J., Frane, J.L., Tian, S., Nie, J., Jonsdottir, G.A., Ruotti, V., Stewart, R*., et al.* (2007). Induced pluripotent stem cell lines derived from human somatic cells. Science *318*, 1917-1920.

Zachary, A.A., and Leffell, M.S. (2016). HLA Mismatching Strategies for Solid Organ Transplantation - A Balancing Act. Front Immunol *7*, 575.

Zastawny, T.H., Dabrowska, M., Jaskolski, T., Klimarczyk, M., Kulinski, L., Koszela, A., Szczesniewicz, M., Sliwinska, M., Witkowski, P., and Olinski, R. (1998). Comparison of oxidative base damage in mitochondrial and nuclear DNA. Free Radic Biol Med *24*, 722-725.

Zenclussen, A.C., Gerlof, K., Zenclussen, M.L., Sollwedel, A., Bertoja, A.Z., Ritter, T., Kotsch, K., Leber, J., and Volk, H.D. (2005). Abnormal T-cell reactivity against paternal antigens in spontaneous abortion: adoptive transfer of pregnancy-induced CD4+CD25+ T regulatory cells prevents fetal rejection in a murine abortion model. Am J Pathol *166*, 811-822.

Zhao, H.X., Jiang, F., Zhu, Y.J., Wang, L., Li, K., Li, Y., Wang, X.H., Li, L.S., and Yao, Y.Q. (2017). Enhanced Immunological Tolerance by HLA-G1 from Neural Progenitor Cells (NPCs) Derived from Human Embryonic Stem Cells (hESCs). Cell Physiol Biochem *44*, 1435-1444.

Zhao, L., Teklemariam, T., and Hantash, B.M. (2014). Heterelogous expression of mutated HLA-G decreases immunogenicity of human embryonic stem cells and their epidermal derivatives. Stem Cell Res *13*, 342-354.

Zhao, T., Zhang, Z.N., Rong, Z., and Xu, Y. (2011). Immunogenicity of induced pluripotent stem cells. Nature *474*, 212-215.

Zhao, T., Zhang, Z.N., Westenskow, P.D., Todorova, D., Hu, Z., Lin, T., Rong, Z., Kim, J., He, J., Wang, M*., et al.* (2015). Humanized Mice Reveal Differential Immunogenicity of Cells Derived from Autologous Induced Pluripotent Stem Cells. Cell Stem Cell *17*, 353-359.

Zijlstra, M., Bix, M., Simister, N.E., Loring, J.M., Raulet, D.H., and Jaenisch, R. (1990). Beta 2-microglobulin deficient mice lack CD4-8+ cytolytic T cells. Nature *344*, 742-746.
Zimmer, J., Andres, E., Donato, L., Hanau, D., Hentges, F., and de la Salle, H. (2005). Clinical and immunological aspects of HLA class I deficiency. QJM *98*, 719-727.

Autorenschaft Beitrag

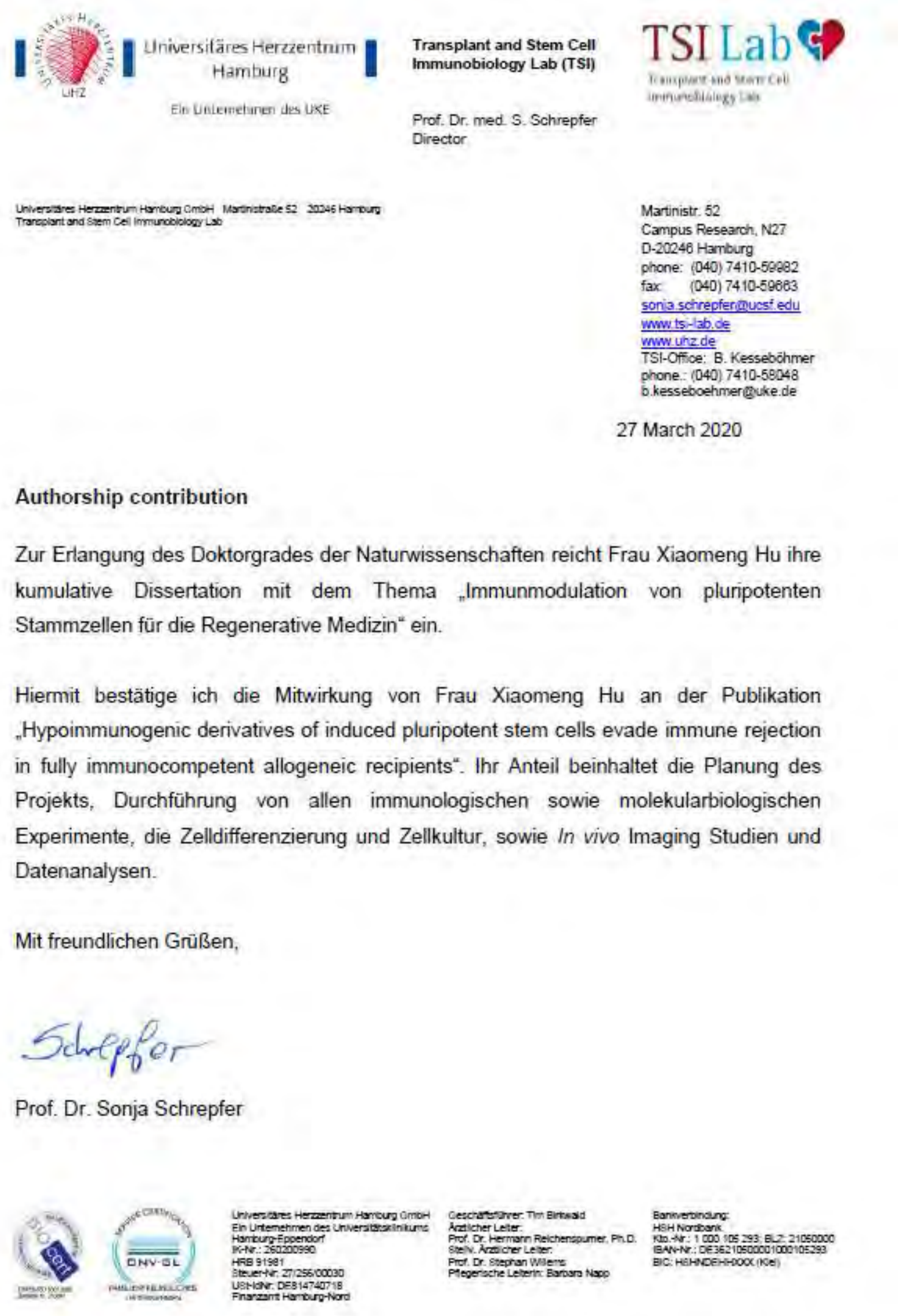

Universitäres Herzzentrum Hamburg
Ein Unternehmen des UKE

Transplant and Stem Cell Immunobiology Lab (TSI)

Prof. Dr. med. S. Schrepfer
Director

TSI Lab
Transplant and Stem Cell Immunobiology Lab

Universitäres Herzzentrum Hamburg GmbH Martinistraße 52 20246 Hamburg
Transplant and Stem Cell Immunobiology Lab

Martinistr. 52
Campus Research, N27
D-20246 Hamburg
phone: (040) 7410-59982
fax: (040) 7410-59663
sonja.schrepfer@ucsf.edu
www.tsi-lab.de
www.uhz.de
TSI-Office: B. Kesseböhmer
phone.: (040) 7410-58048
b.kesseboehmer@uke.de

27 March 2020

Authorship contribution

Zur Erlangung des Doktorgrades der Naturwissenschaften reicht Frau Xiaomeng Hu ihre kumulative Dissertation mit dem Thema „Immunmodulation von pluripotenten Stammzellen für die Regenerative Medizin“ ein.

Hiermit bestätige ich die Mitwirkung von Frau Xiaomeng Hu an der Publikation „Hypoimmunogenic derivatives of induced pluripotent stem cells evade immune rejection in fully immunocompetent allogeneic recipients“. Ihr Anteil beinhaltet die Planung des Projekts, Durchführung von allen immunologischen sowie molekularbiologischen Experimente, die Zelldifferenzierung und Zellkultur, sowie *In vivo* Imaging Studien und Datenanalysen.

Mit freundlichen Grüßen,

Schrepfer

Prof. Dr. Sonja Schrepfer

Universitäres Herzzentrum Hamburg GmbH
Ein Unternehmen des Universitätsklinikums Hamburg-Eppendorf
IK-Nr.: 260200990
HRB 91981
Steuer-Nr. 27/256/00030
USt-IdNr. DE814740718
Finanzamt Hamburg-Nord

Geschäftsführer: Tim Birkwald
Ärztlicher Leiter:
Prof. Dr. Hermann Reichenspurner, Ph.D.
Stellv. Ärztlicher Leiter:
Prof. Dr. Stephan Willems
Pflegerische Leiterin: Barbara Napp

Bankverbindung:
HSH Nordbank
Kto.-Nr.: 1 000 105 293; BLZ: 21050000
IBAN-Nr.: DE36210500001000105293
BIC: HSHNDEHHXXX (Kiel)

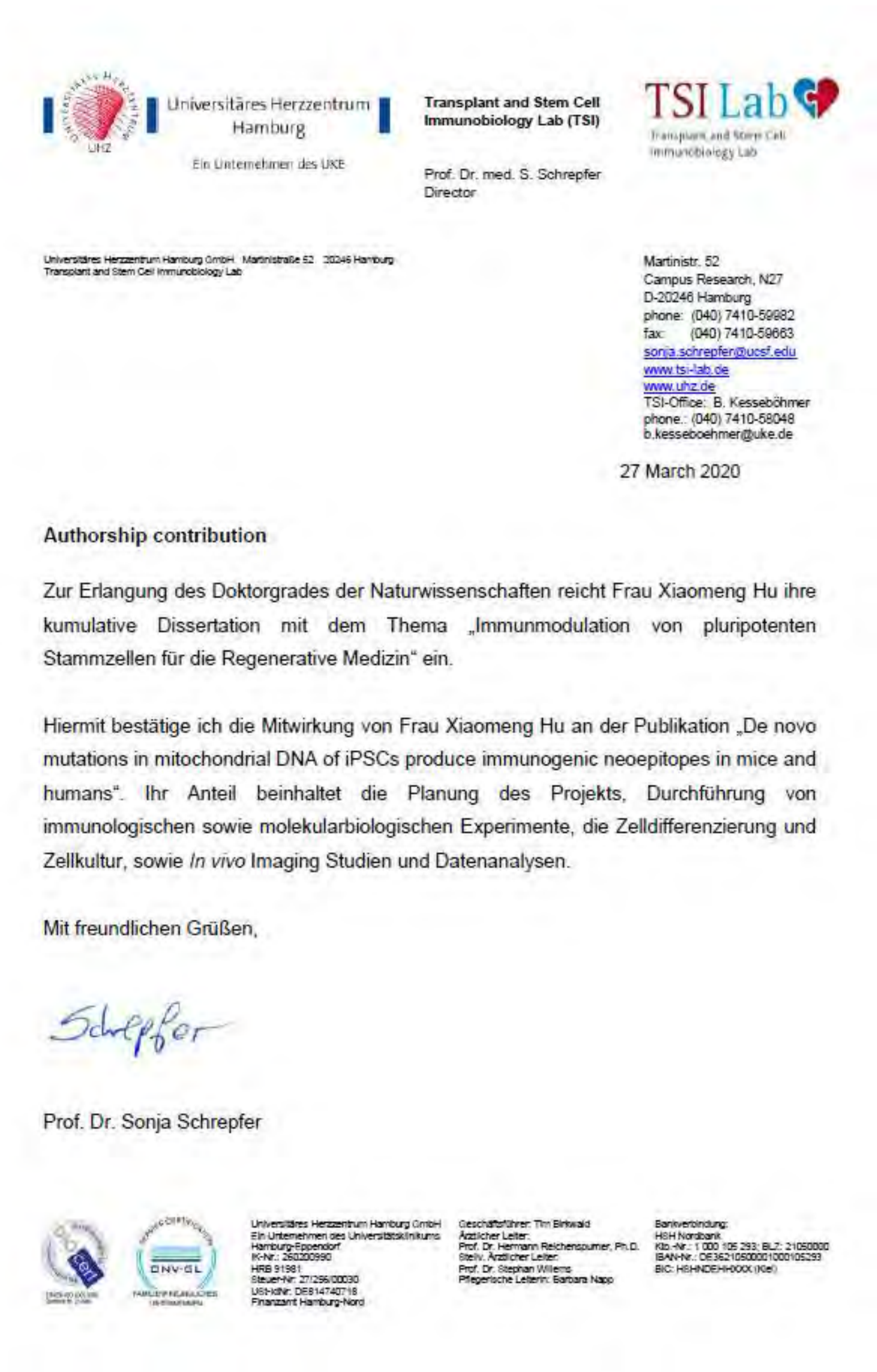

Universitäres Herzzentrum Hamburg
Ein Unternehmen des UKE

Transplant and Stem Cell Immunobiology Lab (TSI)

Prof. Dr. med. S. Schrepfer
Director

TSI Lab
Transplant and Stem Cell Immunobiology Lab

Universitäres Herzzentrum Hamburg GmbH Martinistraße 52 20246 Hamburg
Transplant and Stem Cell Immunobiology Lab

Martinistr. 52
Campus Research, N27
D-20246 Hamburg
phone: (040) 7410-59982
fax: (040) 7410-59663
sonja.schrepfer@ucsf.edu
www.tsi-lab.de
www.uhz.de
TSI-Office: B. Kessebõhmer
phone.: (040) 7410-58048
b.kesseboehmer@uke.de

27 March 2020

Authorship contribution

Zur Erlangung des Doktorgrades der Naturwissenschaften reicht Frau Xiaomeng Hu ihre kumulative Dissertation mit dem Thema „Immunmodulation von pluripotenten Stammzellen für die Regenerative Medizin“ ein.

Hiermit bestätige ich die Mitwirkung von Frau Xiaomeng Hu an der Publikation „De novo mutations in mitochondrial DNA of iPSCs produce immunogenic neoepitopes in mice and humans“. Ihr Anteil beinhaltet die Planung des Projekts, Durchführung von immunologischen sowie molekularbiologischen Experimente, die Zelldifferenzierung und Zellkultur, sowie *In vivo* Imaging Studien und Datenanalysen.

Mit freundlichen Grüßen,

Schrepfer

Prof. Dr. Sonja Schrepfer

Universitäres Herzzentrum Hamburg GmbH
Ein Unternehmen des Universitätsklinikums Hamburg-Eppendorf
IK-Nr.: 260200990
HRB 91981
Steuer-Nr. 27/296/00030
USt-IdNr. DE814740718
Finanzamt Hamburg-Nord

Geschäftsführer: Tim Birkwald
Ärztlicher Leiter:
Prof. Dr. Hermann Reichenspurner, Ph.D.
Stellv. Ärztlicher Leiter:
Prof. Dr. Stephan Willems
Pflegerische Leiterin: Barbara Napp

Bankverbindung:
HSH Nordbank
Kto.-Nr.: 1 000 105 293; BLZ: 21050000
IBAN-Nr.: DE36210500001000105293
BIC: HSHNDEHHXXX (Kiel)

Lebenslauf

Name	Xiaomeng Hu
Geburtstag	20. Juni 1988
Geburtsort	Tianjin, Volksrepublik China
Nationalität	Deutsch

Akademischer Werdegang

Seit 03/2014	Universität Hamburg Universitäres Herz- und Gefäßzentrum UKE Hamburg Abteilung Herz- und Gefäßchirurgie, TSI-Lab *Doktorandin*
10/2016 – 10/2019	University of California, San Francisco (UCSF) Department of Surgery *Assistant Specialist*
10/2010 – 10/2013	Universität Hamburg *Master of Science (M.Sc.), Biologie*
10/2007 – 10/2010	Universität Hamburg *Bachelor of Science (B.Sc), Biologie*

Auszeichnungen

05/2017	The Transplant Society (TTS) Mentee/Mentor Award Projekt: Generation of hypoimmunogenic induced pluripotent stem cells for allogeneic cell and tissue transplantation
03/2016	Deutsches Zentrum für Herz-Kreislauf-Forschung (DZHK) Reisestipendium Projekt: Learning the Methods of Acquired tolerance and Luminex assay at the University of California, San Francisco (UCSF)
01/2016	Universitätsklinikum Hamburg-Eppendorf (UKE) Reisestipendium Projekt: Embryonic Stem Cell Derived Cardiomyocytes for Myocardial Restoration at the University of California, San Francisco (UCSF)

Mitgliedschaften:

Seit 06/2019	International Society for Stem Cell Research (ISSCR)
Seit 04/2017	The Transplantation Society (TTS)
Seit 01/2017	International Society for Heart and Lung Transplantation (ISHLT)
Seit 07/2016	American Heart Association (AHA)
Seit 05/2015	German Centre for Cardiovascular Research (DZHK)

Konferenzen:

14-15. Okt. 2019	The Space Summit 2019, Coronado Island/San Diego, CA, USA Oral presentation: Immunological Senescence in Space Affects Stem Cell Behavior and Function
26-29. Jun. 2019	International Society for Stem Cell Research (ISSCR), Annual Meeting 2019, Los Angeles, CA, USA Poster presentation: Murine SCNT-derived ESCs and iPSCs with mismatched mitochondria trigger an immune response *in vivo* Poster presentation: H-Y-Incompatible Stem Cell Transplantation Causes Rejection of Nucleus Matched Cells
10-11. Mrz. 2019	NIH Tissue Chips Consortium Rockville, MD, USA Oral presentation: Launch experience from SpX-CRS16 – highlights and lessons learned
24-26. Mai 2017	Transplantation Science Symposium (TSS) 2017 Victoria, BC, Canada Oral presentation: Generation of hypoimmunogenic induced pluripotent stem cells for allogeneic cell and tissue transplantation *Gewinnerin des „Mentee/Mentor Awards“*
28-29. Apr. 2017	Northern California Chapter of the American College of Surgeons (NCCACS) Annual Meeting 2017, Berkeley, CA, USA Oral presentation: Generating Hypoimmunogenic Induced Pluipotent Stem Cell for Allogeneic Cell and Tissue Transplantation *Finalistin der "Trainee Research Competition"*

05-08. Apr. 2017 International Society for Heart and Lung Transplantation (ISHLT) Annual Meeting 2017, San Diego, CA, USA

Oral presentation: Generating Hypoimmunogenic Murine Induced Pluripotent Stem Cells by the Disruption of beta-2-Microglobulin

Poster presentation: H-Y-Incompatible Stem Cell Transplantation Causes Rejection of Nucleus Matched Cells

Publikationen

1. **Hu X***, Deuse T*, Gravina A, Wang D, Tediashvili G, De C, Thayer WO, Wahl A, Garcia JV, Reichenspurner H, Davis MM, Lanier LL, Schrepfer S. Hypoimmunogenic derivatives of induced pluripotent stem cells evade immune rejection in fully immunocompetent allogeneic recipients. **Nat Biotechnol 2019** Mar;37(3):252-258.

2. **Hu X***, Deuse T*, Agbor-Enoh S, Koch M, Spritzer M, Gravina A, Alawi M, Marishta A, Peters B, Kosaloglu-Yalcin Z, Yang Y, Rajalingam R, Wang D, Nashan B, Kiefman R, Reichenspurner H, Valentine H, Weissman I, Schrepfer S. De novo mutations in mitochondrial DNA of iPSCs produce immunogenic neoepitopes in mice and humans. **Nat Biotechnol 2019** Oct;37(10):1137-1144.

3. Wang D*, Tediashvili G*, **Hu X**, Gravina A, Marcus SG, Zhang H, Olgin JE, Deuse T, Schrepfer S. A Cryoinjury Model to Study Myocardial Infarction in the Mouse. **J Vis Exp 2019** (151), e59958.

4. Miller KK, Wang D, **Hu X**, Hua X, Deuse T, Neofytou E, Renne T, Velden J, Reichenspurner H, Schrepfer S, Bernstein D. Thalidomide treatment prevents chronic graft rejection after aortic transplantation in rats. **Transpl Int 2017**;30(11):1181-1189.

5. Deuse T, Wang D, Stubbendorff M, Itagaki R, Grabosch A, Greaves LC, Alawi M, Grünewald A, **Hu X**, Hua X, Velden J, Reichenspurner H, Robbins RC, Jaenisch R, Weissman IL, Schrepfer S. SCNT-Derived ESCs with Mismatched Mitochondria Trigger an Immune Response in Allogeneic Hosts**. Cell Stem Cell 2015**; 16(1):33-8. Report in the Research Highlights in Nature. “Matched stem cells still rejected”. Nature 2014; 516, 11 doi:10.1038/516011c.

6. Koch M, Lehnhardt A, **Hu X**, Brunswig-Spickenheier B, Stolk M, Bröcker V, Noriega M, Seifert M, Lange C. Isogeneic MSC application in a rat model of acute renal allograft rejection modulates immune response but does not prolong allograft survival. **Transpl Immunol 2013;** 29(1-4):43-50.

7. **Hu X***, Deuse T*, Tarantal A, Saygi C, Alawi M, Liu Y, Lanier LL, Schrepfer S. The SIRPα-CD47 immune checkpoint in NK cells. **Nat Immunol 2020** (under review)

8. **Hu X***, Kueppers S*, Kooreman NG*, Gravina A, Wang D, Tediashvili G, Marcus SG, Fuchs S, Velden J, Reichenspurner H, Volk HD, Deuse T, Schrepfer S. The Immunobiology of the Y-Chromosome in Embryonic Stem Cell Transplantation for Tissue and Organ Regeneration. **Stem Cells and Development 2020** (under review).

9. Deuse T, Tediashvili G, **Hu X**, Gravina A, Wang D, Tamenang AN, Mueller C, Alawi M, Lanier LL, Schrepfer S. Hypoimmunogenic iPSC-derived cell products treat cardiovascular and pulmonary diseases in immunocompetent allogeneic mice. **Nat Med 2020** (under review)

10. Deuse T, Wang D, **Hu X**, Bolandos JP, Tediashvili G, Reichenspurner H, Tsao PS, Schrepfer S. Mitochondrial superoxide inhibits vascular smooth muscle cell proliferation and restenosis. **Nat Metab 2019** (under review).

Eidesstattliche Erklärung

Hiermit bestätige ich, Xiaomeng Hu, dass die vorliegende Arbeit von mir selbständig verfasst wurde und ich keine anderen als die angegebenen Hilfsmittel – insbesondere keine im Quellenverzeichnis nicht benannten Internetquellen – benutzt habe und die Arbeit von mir vorher nicht einem anderen Prüfungsverfahren eingereicht wurde.

San Francisco, den 23.03.2020

Xiaomeng Hu

Xiaomeng Hu

Danksagung

Ich möchte mich an dieser Stelle ganz herzlich bei den Menschen bedanken, die mich bei der Fertigstellung dieser Arbeit unterstützt haben.

Zuerst möchte ich meiner Doktormutter, Prof. Dr. Sonja Schrepfer für die Bereitstellung dieses spannenden Themas, sowie die Betreuung und Unterstützung zu jeder Zeit herzlich danken. Mir wurde die Möglichkeit geboten, selbstständig zu forschen und eigene Ideen zu realisieren. Sie hatte mich immer durch ihrer Art stets motiviert und immer an mich geglaubt. Ich danke Dr. Tobias Deuse für die großartige Betreuung und die vielen spannenden Diskussionen zu jeder Tages und Nachtzeit.

Herrn Prof. Dr. Dr. Hermann Reichenspurner danke ich für die Möglichkeit, meine Doktorarbeit in der Abteilung Herz- und Gefäßchirurgie des Universitätsklinikums Hamburg-Eppendorf durchführen zu können. Herrn Prof. Dr. Friedrich Koch-Nolte danke ich für die Übernahme des Zweitgutachtens.

Insbesondere möchte ich mich bei Grigol Tediashvili für die schöne gemeinsame Zeit bedanken. Bei Dr. Dong Wang, Alessia Gravina, Annika Tamenang, Simon Küppers und Christiane Pahrmann bedanke ich mich für die außerordentliche Hilfsbereitschaft, das entspannte Arbeitsklima, den Spaß im Laboralltag und die vielen schönen Stunden außerhalb des Labors in Hamburg und in San Francisco.

Ebenfalls bedanke ich mich bei meinen ehemaligen Kommilitoninnen Dr. Susann Burow, Dr. Christine Mentges, Dr. Denise Palm und Dr. Annika Stubbe für ihren moralischen Beistand und unsere gegenseitigen Hilfestellungen.

Ein ganz besonderer Dank geht an meinen Eltern, die mir das Studium ermöglicht haben und mich immer seelisch unterstützt haben. Meinem weiteren Freundeskreis danke ich für ihr Verständnis für meinen Mangel an Zeit und Unterstützung in allen Phasen dieser Arbeit.